# ELECTROCHEMICAL DEGRADATION AND DETECTION METHODS OF PHARMACEUTICALS FROM WATER USING CARBON BASED ELECTRODES

Teză destinată obţinerii
titlului ştiinţific de doctor inginer
la
Universitatea "Politehnica" din Timişoara
în domeniul Inginerie Chimică
de către

**Ing. Sorina MOȚOC**

| | |
|---|---|
| Conducător ştiinţific: | prof.univ.dr.ing Georgeta BURTICĂ |
| Referenţi ştiinţifici: | prof.dr.h. h.c. Joop SCHOONMAN |
| | prof.univ.dr.ing. Carmen TEODOSIU |
| | prof.univ.dr.ing. Rodica PODE |

Ziua susţinerii tezei: 07 decembrie 2012

Seriile Teze de doctorat ale UPT sunt:

1. Automatică
2. Chimie
3. Energetică
4. Ingineria Chimică
5. Inginerie Civilă
6. Inginerie Electrică
7. Inginerie Electronică şi Telecomunicaţii
8. Inginerie Industrială
9. Inginerie Mecanică
10. Ştiinţa Calculatoarelor
11. Ştiinţa şi Ingineria Materialelor

Universitatea „Politehnica" din Timişoara a iniţiat seriile de mai sus în scopul diseminării expertizei, cunoştinţelor şi rezultatelor cercetărilor întreprinse în cadrul şcolii doctorale a universităţii. Seriile conţin, potrivit H.B.Ex.S Nr. 14 / 14.07.2006, tezele de doctorat susţinute în universitate începând cu 1 octombrie 2006.



România, 300159 Timişoara, Bd. Republicii 9,
tel. 0256 403823, fax. 0256 403221
e-mail: editura@edipol.upt.ro

# Foreword

This thesis was performed during doctoral internship with frequency at "Politehnica" University of Timisoara, Faculty of Industrial Chemistry and Environmental Engineering.

A major research project like this is never the work of anyone alone. The contributions of many different people, in their different ways, have made this possible. I would like to extend my appreciation especially to the following.

First of all, I would like to express my deepest sense of gratitude to my supervisor Prof. univ. dr. ing. **Georgeta BURTICĂ**, who offered her continuous advice and encouragement during this thesis.

I would like to express my heartfelt gratitude to Ass.prof. **Florica MANEA** who is more than a mentor for me, whose patience and kindness, as well as her academic experience, have been invaluable to me. I could not have asked for better role model, who taught me what research and life is.

I would like to express my profound gratitude to Prof. univ. dr. ing **Rodica PODE** for her constant supervision and availability, her useful comments and her positive attitude and help.

I acknowledge my thesis committee, ***Prof.univ.dr.ing. Nicolae VASZILCSIN***, ***Joop SCHOONMAN***, ***Prof.univ.dr.ing, Carmen TEODOSIU, Prof.univ.dr.ing. Rodica PODE,*** for finding time to read through the manuscript of the present thesis, and for their valuable and precious comments and suggestions.

The informal support and encouragement of many colleagues and friends has been indispensable, and I would like particularly to acknowledge the contribution of **Anamaria Baciu, Aniela Pop, Corina Orha, Adriana Remeș, Liliana Colar, Agnes Jakab, Magda Ardeleanu, Laura Cocheci, and not the last, Sue and Chris Hibbert.**

I gratefully acknowledge to my sister **Anamaria Moțoc**, my brother-in-law **Alin Neș**, my aunt and uncle **Ana and Emil Mircea**, and to very special man in my life **Petre Ilieș**, for all the love, support and understanding and for making the impossible wherever it was necessary.

This research would not have been possible without the financial support of the strategic grant **POSDRU/88/1.5/S/50783** of the Ministry of Labour, Family and Social Protection, Romania, co-financed by the European Social Funds-Investing in People and **PN II Ideas 165/ 2011**.

At the end of my thesis, it is a pleasant task to express my thanks to all those who contributed in many ways to the success of this study and made it an unforgettable experience for me.

But not least, I want to acknowledge to **GOD** for this success.

Timişoara, December 2012 Sorina MOȚOC

MOȚOC, Sorina

**ELECTROCHEMICAL DEGRADATION AND DETECTION METHODS OF PHARMACEUTICALS FROM WATER USING CARBON BASED ELECTRODES**

Teze de doctorat ale UPT, Seria 4, Nr. 64, Editura Politehnica, 2012, 208 pagini, 84 figuri, 30 tabele.

ISSN: 1842-8223

ISBN: 978-606-554-583-0

Cuvinte cheie: dual electrochemical techniques, pharmaceutical pollutants, wastewater treatment, wastewater quality monitoring, carbon-based composite electrodes.

Rezumat:
The aim of this study is to explore the dual character of the electrochemical techniques and electrode materials for the application in pharmaceuticals-containing water treatment and control. It is noteworthy that electrode materials for water quality monitoring are conceptually very similar to those used in the degradation of pollutants from water. Thus, the development of suitable electrode materials and electrochemical techniques involves actually relatively easy adaptation from a field to another, taking into account the specific application peculiarities (*e.g.,* electrode geometry, design and operating conditions for degradation application).

# TABLE OF CONTENTS

# LIST OF ABBREVIATION

AA - ascorbic acid;
AO - anodic oxidation;
AOPs - advanced oxidation processes;
AgZCNT - silver-doped zeolite-carbon nanotubes-epoxy composite;
AgZCNF - silver-doped zeolite-carbon nanofiber-epoxy composite;
AgCNF - silver-decorated carbon-nanofiber-epoxy composite;
AgZEG -silver-doped zeolite-expanded-graphite-epoxy composite;
AgZ - silver-modified zeolite;
BDD - boron-doped diamond;
BSA - batch system analysis;
CA - chronoamperometry;
CNF - carbon nanofibers;
CNT - carbon nanotubes-epoxy composite;
COD - chemical oxygen demand;
CP - carbon pastes;
CV - cyclic voltammetry;
DA - dopamine;
DCF - Sodium diclofenac;
DMF - N,N-dimethylformamide;
DO - dissolved oxygen;
DPV - differential-pulse voltammetry;
EC - electrocoagulation;
EG - expanded-graphite;
ELSD - evaporative light scattering detection;
EO - electrooxidation;
EOD - electrochemical oxygen demand;
EOI - electrochemical oxidability index;
FPP - four-point probe resistance measurements;
GC - glassy carbon;
GC-MS - gas chromatography with mass spectrometry detection;

GC-MS/MS - gas chromatography mass spectrometry detection;

GC-NCI-MS - gas chromatography-negative chemical ionization-mass spectrometry;

GDEs - gas diffusion electrodes;

HPLC-MS/MS - high performance liquid chromatography with tandem mass spectrometry;

IBP - ibuprofen;

ICE - instantaneous current efficiency;

LC-FD - liquid chromatography with fluorescence detection;

LC-MS - liquid chromatography with mass spectrometry detection;

LC-MS/MS - liquid chromatography with tandem mass spectrometry Detection;

LC-QqLIT-MS - liquid chromatography-quadruple-linear ion trap-mass spectrometry detection;

LOD - limit of detection;

LQ - limit of quantification;

LSV - linear-scan voltammetry;

MA - modulation amplitudes;

MCE - mineralization current efficiency;

MPA - multiple-pulsed amperometry techniques;

NOM - natural organic matter;

NZ - natural zeolite;

PAD - amperometric detection as an electroanalytical technique;

PCP - pentachlorophenol;

PEC - photoelectrocatalysis;

RSD - relative standard deviation;

SCE - saturated calomel;

SEM - Scanning electron microscopy;

SP - step potentials;

SWV - Square-wave voltammetry;

TOC - total organic carbon;

TRM - two-roll mill;

UA - uric acid;

WWTP - wastewater treatment plant.

# LIST OF TABLES

# LIST OF FIGURES

# CHAPTER 1. OCCURRENCE OF PHARMACEUTICALS IN ENVIRONMENT

Water being an essential resource for life in all ecosystems, a great effort has been made in the past decades to modify the water sector technologies in order to improve the water quality [1].

During the last three decades, the impact of chemical pollution has focused almost exclusively on the conventional "priority" pollutants, especially those acutely toxic/ carcinogenic pesticides and industrial intermediates displaying persistence in the environment. This spectrum of chemicals, however, is only one piece of the larger puzzle in "holistic" risk assessment. Another diverse group of bioactive chemicals which have been received comparatively little attention as potential environmental pollutants includes the pharmaceuticals [1-4].

Pharmaceuticals are designed to have a physiological effect on humans and animals in trace concentrations. Persistence against biological degradation and their biological activity are key proprieties of these pollutants. They retain their chemical structure long enough to do their therapeutic work and because of their continuous input they could persist in the environment for a long time and their presence is considered dangerous in both low and high concentrations. Their active ingredients are selected or designed because of their activity for organisms. It's expected to have effect against bacteria, fungi and possible non target higher organisms [4, 5].

The presence of pharmaceuticals in water is not a new issue, the occurrence of pharmaceuticals as trace environmental pollutants, originating primarily from consumer use and actions rather than manufacturer effluents, continues to become more firmly established.

The growing, worldwide importance of freshwater resources underscores the need for ensuring that any aggregate or cumulative impacts on (or from) water supplies are minimized [5-8]. In the 1970's, several researchers reported the presence in wastewater of chlofibric acids, a breakdown product of several blood lipid regulators, and salicylic acid as a breakdown product of aspirin. However, based on importance of the sensitivity for the analytical techniques over the years, many more pharmaceuticals have been detected in ambient water, wastewater, and drinking water. One problem with assessing risk of pharmaceuticals in drinking water is the very large number of pharmaceuticals in use today. Information on the occurrence of pharmaceuticals in drinking water is available only for a limited number of compounds. In addition, many pharmaceuticals are biologically degraded to active metabolites that have not been evaluated [8].

Since pharmaceuticals may have long half-lives in the environment, they can be accumulated to reach detectable and biologically active levels, much scientific attention being devoted to the occurrence of pharmaceuticals in the environment. Small amounts of pharmaceutical chemicals may be released into the environment during manufacture use and disposal of pharmaceuticals [9].

In the manufacture of many pharmaceuticals, use of particulate raw materials is a common stage. More than 70 % of pharmaceutical drugs consumed are by type of solid oral dosage type (*e.g.*, tablets, capsules), and the majority of the constituents of a dosage form are particulate, being released in the environment as particulate form [8, 9].

Figure 1.1 shows a schematic flow of pharmaceuticals in the environment. As can be seen from Figure 1.1, Wastewater Treatment Plant (WWTP) represents one of the most major sink for pharmaceuticals. Because of an incomplete removal in WWTP, residues of many toxic organic compounds, including pharmaceutical products, are also found in surface waters [10]. The drug residues from farms usage reach the terrestrial environmental compartment. Unused, expired, or rejected drug products are disposed by manufacturers, pharmacies, hospitals, clinics, and the patient population. Pharmacies, hospitals, and clinics, which may buy the drugs from distributors or manufacturers in bulk, return the expired or unused drugs to the respective suppliers, who may dispose them in certified landfills or incinerate them [11].

Pharmaceuticals enter both the soil and aquatic environments through a variety of routes, including, but not limited to, wastewater effluent, treated sewage sludge, landfill leachate, industrial effluent, combined sewer overflows, aquaculture, and animal feed lots. Contributions to the environment from these sources remain poorly characterized. Specific examples of releases of pharmaceuticals to the environment include [8-13]:

— People excreting un-metabolized medications into septic or wastewater collection systems.

— People flushing unused or expired pharmaceuticals down the toilet or sink.

— People washing cosmetics, antibiotic soap, perfumes and sunscreens into water while bathing or swimming.

— Veterinary drugs, including hormones and antibiotics, excreted by farm animals into fields where they run off into surface water or infiltrate to groundwater.

— Pharmaceuticals that are discharged from manufacturing processes or improper commercial disposal methods.

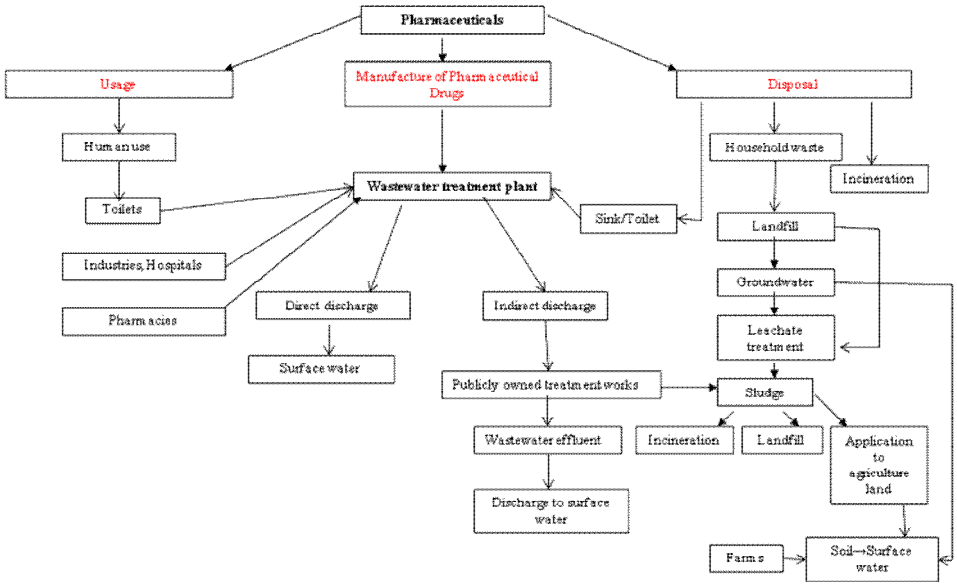


**Figure 1.1.** Source and occurrence of pharmaceuticals in the environment.

Information about the fate of pharmaceuticals in the environment is limited [9]. The possible fates of pharmaceuticals, as all other xenobiotics once they enter the aquatic environment are mainly:

1. the compound is ultimately mineralized to carbon dioxide and water;
2. the compound does not degrade readily because it is lipophilic and is partially retained in the sludge;
3. the compound metabolizes to a more hydrophilic molecule, passes through the wastewater treatment plant and ends up in the receiving waters (surface waters, mainly rivers). These compounds exhibit the highest persistence in the environment;
4. the volume of the water body.

The low volatility of pharmaceutical products indicates that distribution in the environment will occur primarily by aqueous transport, but also by food-chain dispersal. Although the persistence of pharmaceutical products is low, they are ubiquitous in the environment because rates of release are greater than their rates of transformation. Sulfonamides and fluoroquinolones are the most persistent, then macrolides, tetracyclines, aminoglycosides, and β- lactam antibiotics. The most easily absorbed by soils and sediments are tetracyclines and fluoroquinolones, then macrolides, sulfonamides, aminoglycosides, and β-lactams [8, 11]. Transformation of active pharmaceutical compounds also occurs in wastewater-treatment plants, and depends on the composition of the sewage, weather conditions, and the design and operation of the treatment process. The fate of pharmaceutical products and their metabolites in such plants may be mineralization to carbon dioxide and water, adsorption on suspended solids (if the compound is lipophilic), or release in the effluent either as the original compound or as a degradation product. Adsorption of some pharmaceuticals in digested sludge has been reported to be relatively low [8].

The easily adsorbed pharmaceuticals can reach the terrestrial environment when sludge is used as an agricultural fertilizer. They can also enter agricultural land from manure from medicated, in-house reared, animals and from animals raised on pastures. From the terrestrial environment the pharmaceuticals can subsequently be transported to surface water and groundwater. Pharmaceuticals used in aquaculture are released directly into surface water [9]. Acidic pharmaceuticals, for example acetylsalicylic acid, ibuprofen, fenoprofen, ketoprofen, naproxen, diclofenac, and indomethacin, with pKa values from 4.9 to 4.1, and chlofibric acid, bezafibrate (pKa 3.6) and gemfibrozil occur as ions at neutral pH, and are, therefore, not readily absorbed by sludge, and remain in the aqueous phase. Limited adsorption may occur at lower pH [12, 13].

The consumption of pharmaceuticals is substantial. Recent studies reported concentrations of a wide range of about 80–100 pharmaceuticals from many classes of drugs and some of their metabolites in many countries in treated sewage, rivers and creeks, seawater, groundwater and even drinking water. In the European Union (EU) about 3000 different substances are used in human medicine such as analgesics and anti-inflammatory drugs, contraceptives, antibiotics, beta-blockers, lipid regulators, neuroactive compounds and many others [8]. In England, Germany and Australia, the amounts for the most frequently used drugs are in the hundreds of tons per year. A list of "top" pharmaceuticals for human use, excreted unmetabolized in substantial amounts, with estimated environmental loads (amoxycillin, atenolol, ranitidine, ceftazidime, lincomycin, erythromycin, ceftriaxone, furosemide, salbutamol) [9]. A second group of pharmaceuticals was selected because they had already been measured in the environment in previous occasional surveys (ibuprofen, diazepam, bezafibrate, cyclophosphamide, clofibric acid). The pattern of consumed pharmaceuticals for the different countries is not identical and some drugs may be forbidden or replaced by related drugs. Some drugs are regularly documented within the most frequently applied range: the class of non-steroidal anti-inflammatory drugs (NSAID) including acetylsalicylic acid (*e.g*. 836 t in Germany in 2001), paracetamol (*e.g*. 622 t in Germany in 2001), ibuprofen (*e.g*. 345 t in Germany in 2001), naproxen (*e.g*. 35 t in England in 2000) and diclofenac (86 t in Germany in 2001), the oral antidiabetic metformin (*e.g*. 517 t in Germany 2001) and the antiepileptic carbamazepine (*e.g*. 88 t in Germany 2001) [9, 13].

Everyday, an increasing number of pharmaceuticals reach the environment all over the world. However, there is a gap in legislation regarding environmental contamination by pharmaceuticals. This probably arises because available data is insufficient to quantify a precise contamination profile. Abundant conclusive studies concerning chronic toxicity are also lacking so that it becomes impossible to infer the risks of long-term exposure of pharmaceuticals and their metabolites on fauna and flora. EU and US laws concerning the necessity of environmental risk assessment studies to obtain a marketing authorization for pharmaceuticals is approached [5, 9, 13]. The European Union Directive 92/18/EEC introduced for the first time the requirement for an environmental risk assessment, as a prerequisite to obtain marketing authorization for veterinary pharmaceuticals [14]. For this purpose, the European Agency for the Evaluation of Medicinal Products (EMEA) published a "Note for Guidance" where guidelines to assess the environmental risk of veterinary medicinal products are established [15]. The European Commission extended its concerns to pharmaceuticals for human use by publishing Directive 2001/83/EC which was subsequently amended by Directive 2004/27/EC [16]. These directives established that marketing authorization for new medical products for human use should be accompanied by an environmental risk assessment, whose

guidelines were set out by EMEA [17]. Nevertheless, the environmental impact does not provide sufficient grounds for a refusal. Environmental risk assessment of both veterinary and human pharmaceuticals is assessed in a step-wise approach, divided into two phases. In Phase I, environmental exposure to the pharmaceutical or its metabolites is estimated. Phase II comprises its fate and effects in the environment. For this reason, Phase II is sub-divided into two parts: Tier A, in which possible fate and effects of the pharmaceutical and/ or its major metabolites are evaluated; and Tier B, which focuses on the effects on fauna and flora within environmental compartments that are likely to be affected. However, medicinal products for human use only require Phase II studies if the predicted environmental concentration in surface water is equal to or above 0.01 $\mu gL^{-1}$.

In the US, issues concerning pharmaceuticals in the environment are regulated by the U.S. Food and Drug Administration (FDA) [18]. This institution requires environmental assessments to obtain marketing authorizations which are specified in the "Guidance for Industry-Environmental Assessment of Human Drug and Biologic Applications". However, an environmental assessment is required only if the estimated environmental concentration of the pharmaceutical at the point of the entry is above 1 $\mu gL^{-1}$. As EMEA, the FDA also requires environmental assessments for veterinary medicinal products, using a tiered approach. With a view to harmonizing the guidelines that govern these environmental impact assessments, the EU, US and Japan elaborated two guidelines: "Environmental Impact Assessment (EIAs) for Veterinary Medicinal Products (VMPs)—Phase I" [19] and "Environmental Impact Assessment for Veterinary Medicinal Products—Phase II Guidance" [20] so that environmental fate and toxicity data obtained could be used to obtain marketing authorization in all these regions.

## 1.1. References

[1] A.B.A. Boxall, EMBO reports 5 12 (2004).
[2] T. Heberer, Toxicol. Lett. 131 (2002) 5.
[3] W.V. Collentro, J. Val. Technol. 16 2 (2010) 37.
[4] C.G. Daughton, T.A. Ternes, Environ. Health Persp. 107 6 (1999) 907.
[5] T.L. ter Laak, M. van der A,C. J. Houtman, P.G. Stoks, A.P. van Wezel, Environ. Int. 36 (2010) 403.
[6] A.S. Mestre, J. Pires, J.M.F. Nogueira, J.B. Parra, A.P. Carvalho, C.O. Ania, Bioresource Technol. 100 (2009) 1720.
[7] S. Weigel, U. Berger, E. Jensen, R. Kallenborn, H. Thoresen, H Huhnerfuss, Chemosphere 56 (2004) 583.
[8] C. Miege, J.M. Choubert, L. Ribeiro, M. Eusebe, M. Coquery, Environ. Pollut. 157 (2009) 1721.
[9] K. Fent, A.A. Weston, D. Caminada, Aquat. Toxicol. 76 (2006) 122.
[10] M.D. Hernando, A.R. Fernandez-Alba, R. Tauler, D. Barcelo, Talanta 65 (2005) 358.
[11] E. Zuccato, S. Castiglioni, R. Fanelli, G. Reitano, R. Bagnati, C. Chiabrando, F. Pomati, C. Rossetti, D. Calamari, Environ. Pollut. 131 (2006) 15.
[12] C. Holloway, P. Rush, New York City Environmental protection (2006).
[13] K. Kummerer, J. Environ. Manage. 90 (2009) 2354.
[14] Commission Directive 92/18/EEC, 1992.
[15] EMEA, Note for Guidance: Environmental Risk Assessment for Veterinary Medicinal Products Other Than GMO-Containing and Immunological Products, The

European Agency for the Evaluation of Medicinal Products: Veterinary Medicines Evaluation Unit, EMEA/CVMP/055/96-FINAL, 1998.
[16] EudraLex- Volume 1- Pharmaceutical Legislation Medicinal Products for Human Use, Online at: http://ec.europa.eu/ enterprise/ pharmaceuticals/ eudralex/ vol1 en.htm.
[17] EMEA, Guideline on the Environmental Risk Assessment of Medicinal Products for Human Use, The European Agency for the Evaluation of Medicinal Products: Committee for Medicinal Products for Human Use, EMEA/CHMP/SWP/4447/00, 2006.
[18] FDA, Guidance for Industry: Environmental Assessment of Human Drug and Biologics Applications, Food and Drug Administration (Centre for Drug Evaluation and Research), CMC 6, Revision 1, 1998.
[19] EMEA, Guideline on Environmental Impact Assessment (EIAs) for Veterinary Medicinal Products- Phase I, The European Agency for the Evaluation of Medicinal Products: Committee for Medicinal Products for Veterinary Use, CVMP/VICH/592/98-FINAL, 2000.
[20] EMEA, Guideline on Environmental Impact Assessment for Veterinary Medicinal Products- Phase II, The European Agency for the Evaluation of Medicinal Products: Committee for Medicinal Products for Veterinary Use, CVMP/VICH/790/03-FINAL, 2005.

# CHAPTER 2. QUANTITATIVE DETERMINATION METHODS OF PHARMACEUTICALS IN WATER.

The analytical method requirements differ in direct relation to the concentration range of interest. In therapeutic drug monitoring, their quantitative determinations are usually performed with higher drug concentrations than in pharmacokinetic studies, where extreme sensitivity is needed for the terminal phase of their removal.

Literature reveals various methods available for the determination of pharmaceuticals like, *e.g.*, HPLC, capillary electrophoresis, mass spectrometry, liquid chromatography/ mass spectrometry and spectrophotometric methods. However, most pharmaceuticals can be analyzed by following:

(1) Liquid/ Gas Chromatography/ Mass Spectrometry;

(2) High Performance Liquid Chromatography/ Mass Spectrometry.

Most spectrophotometric methods suffer from low sensitivity, high detection limits, tedious experimental conditions and complex procedures for the preparation of samples or standard solutions. In general, HPLC and LC based techniques are expensive, but rapid analysis and a high degree of resolution make them choice of the researchers. Table 2.1 presents the analytical methods reported for the detection of several pharmaceuticals.

**Table 2.1.** The analytical methods for the detection of pharmaceuticals.

| Analytical Method | Pharmaceutical compound | LOD ($\mu gL^{-1}$) | Concentration ($\mu gL^{-1}$) | References |
|---|---|---|---|---|
| SPE-GC-MS | Acetylsalicylic acid | $1.0*10^{-2}$-$3.0*10^{-2}$ | $3.0*10^{-2}$-19.4 | [1, 2] |
| | Salicylic acid | $1.0*10^{-2}$ | 2.8-12.7 | [3] |
| | Diclofenac | $8.0*10^{-4}$-$1.0*10^{-1}$ | $1.2*10^{-3}$-2.9 | [3-11] |
| | Fenofren | $1.0*10^{-3}$-$2.3*10^{-2}$ | $9.5*10^{-3}$-168.0 | [2, 4] |
| | Ibuprofen | $5.0*10^{-4}$-$3.0*10^{-2}$ | $<1.0*10^{-3}$-6.7 | [1-5, 7, 8, 11-14] |
| | Mefenamic acid | $1.0*10^{-3}$ | $4.4*10^{-3}$-$3.9*10^{-1}$ | [2] |
| | Naproxen | $1.0*10^{-2}$ | $<1.0*10^{-3}$-$5.0*10^{-3}$ | [8] |
| | Paracetamol | $3.2*10^{-2}$ | 29.0-246.0 | [4] |
| | Carbamazepine | $2.0*10^{-3}$-$7.0*10^{-2}$ | $6.0*10^{-3}$-$9.0*10^{-1}$ | [1, 2, 4, 6, 9] |

| Analytical Method | Pharmaceutical compound | LOD ($\mu gL^{-1}$) | Concentration ($\mu gL^{-1}$) | References |
|---|---|---|---|---|
| SPE-LC-MS | Ibuprofen | $1.8*10^{-2}$ | $3.1*10^{-3}$ | [13] |
| | Paracetamol | $5.0*10^{-3}$-$9.0*10^{-3}$ | $3.8*10^{-1}$-56.9 | [13, 15] |
| | Ciprofloxacin | $6.0*10^{-3}$-$5.0*10^{-2}$ | $2.0*10^{-2}$-$3.0*10^{-1}$ | [16-18] |
| | Enrofloxacin | $5.0*10^{-2}$ | $2.5*10^{-1}$ | [17] |
| | Norfloxacin | $7.0*10^{-3}$-$2.0*10^{-2}$ | $4.0*10^{-2}$-$2.0*10^{-1}$ | [16, 18] |
| | Ofloxacin | $6.0*10^{-3}$ | $<6.0*10^{-3}$-$2.8*10^{-1}$ | [18] |
| | Penicillin G | $9.3*10^{-1}$ | 153.0 | [19] |
| | Lincomycin | $5.0*10^{-2}$ | $3.2*10^{-1}$ | [13] |
| | Sulfachloropyridazine | $3.0*10^{-2}$ | $<3.0*10^{-2}$-$4.7*10^{-1}$ | [15] |
| | Sulfadiazine | $2.1*10^{-2}$ | $2.3*10^{-1}$ | [20] |
| | Sulfadimethoxine | $8.0*10^{-3}$-$5.0*10^{-2}$ | $<1.0*10^{-3}$-$2.1*10^{-1}$ | [15, 16, 20] |
| | Sulfamethazine | $2.0*10^{-2}$ | $1.6*10^{-1}$-$3.6*10^{-1}$ | [13, 17] |
| | Sulfamethoxazole | $9.0*10^{-3}$-$8.0*10^{-2}$ | $1.5*10^{-1}$-1.1 | [4, 12, 15-18, 20] |
| | Sulfapyride | $1.2*10^{-2}$ | $<1.2*10^{-2}$-$1.2*10^{-1}$ | [20] |
| | Sulfathiazole | 0.03 | <0.03-0.531 | [15] |
| | Oxytetracycline | 0.1 | 0.340 | [16] |
| | Tylosin | $5.0*10^{-2}$ | $4.0*10^{-1}$ | [16] |
| | Trimethoprim | $1.0*10^{-2}$-$5.0*10^{-2}$ | $<1.0*10^{-2}$-$4.9*10^{-1}$ | [15, 17] |
| | Carbamezepine | $2.4*10^{-4}$-$5.0*10^{-3}$ | $<5.0*10^{-3}$-$4.5*10^{-1}$ | [15] |
| SPE-LC-FD | Ciprofloxacin | $2.5*10^{-2}$ | $1.9*10^{-2}$-$6.6*10^{-1}$ | [21, 22] |
| | Enrofloxacin | $2.5*10^{-2}$-$5.0*10^{-2}$ | $6.7*10^{-1}$-$4.4*10^{-1}$ | [21, 22] |
| | Norfloxacin | $2.5*10^{-2}$ | $4.0*10^{-1}$ | [21, 22] |
| | Ofloxacin | $2.5*10^{-1}$ | - | [21] |
| SPE-GC-MS/MS | Salicylic acid | $1.0*10^{-4}$ | $5.5*10^{-1}$-2.2 | [12] |
| | Diclofenac | $1.0*10^{-3}$ | $3.2*10^{-3}$-$4.5*10^{-1}$ | [12] |
| | Naproxen | 5.0*10-$^{4}$ | $2.7*10^{-1}$-7.9 | [12] |

| | | | | |
|---|---|---|---|---|
| SPE-LC-MS/MS | Diclofenac | $2.5*10^{-4}$-$1.0*10^{-3}$ | $<2.5*10^{-4}$-$1.2*10^{-1}$ | [23-25] |
| | Ibuprofen | $3.0*10^{-4}$-$1.0*10^{-3}$ | $1.0*10^{-3}$-3.1 | [24, 25] |
| | Mefenamic acid | $1.0*10^{-2}$ | $<1.0*10^{-3}$-$3.2*10^{-1}$ | [26] |
| | Naproxen | $5.0*10^{-4}$-$1.0*10^{-3}$ | $5.0*10^{-4}$-$4.8*10^{-1}$ | [23, 25] |
| | Paracetamol | $5.0*10^{-4}$-$1.0*10^{-3}$ | $1.8*10^{-3}$-78.2 | [27] |
| | Carbamazepine | $2.7*10^{-4}$-$1.0*10^{-3}$ | $8.0*10^{-3}$-$5.9*10^{-1}$ | [25-27] |
| | Atenolol | $2.5*10^{-4}$-$3.0*10^{-2}$ | $4.7*10^{-4}$-$6.9*10^{-1}$ | [7, 26, 28] |
| | Metoprolol | - | $1.6*10^{-1}$ | [7] |
| | Propranolol | $1.0*10^{-2}$ | $04.0*10^{-2}$-$5.0*10^{-3}$ | [7, 26] |
| SPE-HPLC-MS/MS | Diclofenac | $7.0*10^{-3}$-$3.0*10^{-2}$ | $3.0*10^{-2}$-1.9 | [10, 29-33] |
| | Ibuprofen | $4.2*10^{-3}$-$3.10^{-2}$ | $3.7*10^{-3}$-151.0 | [10, 28-32] |
| | Ketorolac | $2.6*10^{-2}$ | $2.0*10^{-1}$-59.5 | [31] |
| | Mefenamic acid | $5.0*10^{-2}$ | $1.3*10^{-1}$-1.1 | [29, 33] |
| | Naproxen | $1.0*10^{-1}$-$2.6*10^{-2}$ | $1.0*10^{-1}$-$6.9*10^{-1}$ | [10, 30] |
| | Paracetamol | $2.0*10^{-3}$-$5.0*10^{-2}$ | $<5.0*10^{-3}$-69.6 | [10, 29, 31, 33] |
| | Ciprofloxacin | $3.0*10^{-4}$-$2.0*10^{-2}$ | 0-1.0 | [28, 34] |
| | Nalidixic acid | - | $2.3*10^{-3}$-$3.7*10^{-1}$ | [32] |
| | Norfloxacin | $1.3*10^{-2}$ | $<1.3*10^{-2}$ | [35] |
| | Ofloxacin | $1.0*10^{-2}$ | $1.2*10^{-3}$-$3.9*10^{-1}$ | [32, 34] |
| | Ampicilin | $01.0*10^{-2}$ | $2.1*10^{-2}$ | [10] |
| | Cephalexin | $1.3*10^{-2}$ | $1.0*10^{-2}$-4.4 | [32, 35] |
| | Lincomycin | $3.0*10^{-4}$-$1.0*10^{-2}$ | 0-2.0 | [28, 34] |
| | Clarithromycin | 0- $3.0*10^{-4}$ | $4.9*10^{-4}$-1.43 | [28, 32] |
| | Erythromycin | $3.0*10^{-4}$ | $1.4*10^{-3}$-$1.6*10^{-3}$ | [28] |

| Analytical Method | Pharmaceutical compound | LOD ($\mu gL^{-1}$) | Concentration ($\mu gL^{-1}$) | References |
|---|---|---|---|---|
| SPE-HPLC-MS/MS | Erythromycin-H2O | $1.3*10^{-2}$ | $2.2*10^{-1}$-1.5 | [10, 32, 35] |
| | Roxithromycin | $2.0*10^{-3}$ | $5.0*10^{-3}$-$6.0*10^{-3}$ | [36] |
| | Spiramycin | $3.0*10^{-3}$ | $<8.0*10^{-3}$-$4.3*10^{-2}$ | [28] |
| | Tylosin | $3.0*10^{-4}$ | $<3.0*10^{-3}$ | [28] |
| | Sulfamethazine | $5.0*10^{-4}$ | - | [10] |
| | Sulfamethoxazole | $1.2*10^{-2}$ | $1.8*10^{-1}$-1.3 | [10, 32, 34] |
| | Chlortetracycline | $5.0*10^{-3}$ | $5.7*10^{-3}$ | [10] |
| | Oxytetracycline | $3.0*10^{-4}$-$2.0*10^{-3}$ | $2.3*10^{-2}$ | [10, 28] |
| | Tetracycline | $2.0*10^{-3}$-$1.3*10^{-2}$ | $<1.3*10^{-2}$-$2.3*10^{-1}$ | [24, 28, 35] |
| | Metronidazole | - | $1.0*10^{-3}$-$2.9*10^{-1}$ | [32] |
| | Trimethoprim | $1.0*10^{-2}$-$1.3*10^{-2}$ | $1.7*10^{-1}$-1.4 | [32, 34, 35] |
| | Carbamazepine | $2.7*10^{-4}$-$1.4*10^{-2}$ | $3.0*10^{-2}$-1.3 | [31, 32] |
| | Propanolol | $5.0*10^{-4}$-$1.0*10^{-3}$ | $5.4*10^{-2}$-6.5 | [10, 29, 31, 33] |
| | Acebutolol | $8.0*10^{-4}$ | $3.9*10^{-1}$-$5.1*10^{-1}$ | [5] |
| | Atenolol | $3.0*10^{-4}$-$2.8*10^{-2}$ | $3.4*10^{-3}$-122.0 | [28, 31, 32] |
| | Metoprolol | - | $1.4*10^{-2}$-$6.0*10^{-1}$ | [32] |
| | Sotalol | $3.9*10^{-3}$-$8.0*10^{-3}$ | $5.6*10^{-1}$-$8.3*10^{-1}$ | [9] |
| SPE-HPLC-MS | Ofloxacin | $2.6*10^{-3}$ | $1.0*10^{-2}$-$5.2*10^{-2}$ | [36] |
| | Erithromycin-H2O | $2.0*10^{-3}$ | $3.3*10^{-3}$-$3.4*10^{-3}$ | [36] |
| | Roxithromycin | $3.0*10^{-2}$ | $5.0*10^{-2}$ | [16] |
| | Sulfadiazine | $5.0*10^{-4}$ | - | [36] |
| | Sulfamethoxazole | $8.0*10^{-4}$ | - | [36] |
| | Chloramphenicol | $4.1*10^{-3}$ | - | [36] |

| Analytical Method | Pharmaceutical compound | LOD ($\mu gL^{-1}$) | Concentration ($\mu gL^{-1}$) | References |
|---|---|---|---|---|
| GC-NCI-MS | Diclofenac | $1.1*10^{-3}$ | $1.5*10^{-1}$ | [37] |
| | Mefenamic Acid | $2.2*10^{-3}$ | $2.2*10^{-2}$ | [37] |
| | Naproxen | $1.3*10^{-3}$ | $1.1*10^{-1}$ | [37] |
| SPE-LC-QqLIT-MS | Diclofenac | $4.0*10^{-3}$ | $08.9*10^{-1}$-1.4 | [38] |
| | Mefenamic acid | $3.0*10^{-3}$ | $4.0*10^{-2}$-$6.0*10^{-2}$ | [38] |

GC–MS—Gas Chromatography with Mass Spectrometry Detection; GC–MS/MS—Gas Chromatography Mass Spectrometry Detection; GC-NCI-MS—Gas Chromatography-Negative Chemical Ionization-Mass Spectrometry; LC-QqLIT-MS—Liquid chromatography-quadrupole-linear ion trap-mass spectrometry detection. LC-FD—Liquid Chromatography with Fluorescence Detection; LC–MS—Liquid Chromatography with Mass Spectrometry Detection; LC–MS/MS—Liquid Chromatography with Tandem Mass Spectrometry Detection; HPLC–MS/MS—High Performance Liquid Chromatography with Tandem Mass Spectrometry.

## 2.1. References

[1] Z. Moldovan, Chemosphere 64 (2006) 1808.
[2] N. Nakada, T. Tanishima, H. Shinohara, K. Kiri, H. Takada, Water Res. 40 (2006) 3297.
[3] H.B. Lee, T.E. Peart, M.L. Svoboda, J. Chromatogr. A 1094 (2005) 122.
[4] M.J. Gomez, M.J. Martinez Bueno, S. Lacorte, A.R. Fernandez-Alba, A. Aguera, Chemosphere 66 (2007) 993.
[5] A. Tauxe-Wuersch, L.F. De Alencastro, D. Grandjean, J. Tarradellas, Water Res. 39 (2005) 1761.
[6] V. Koutsouba, T. Heberer, B. Fuhrmann, K. Schmidt-Baumler, D. Tsipi, A. Hiskia, Chemosphere 51 (2003) 69.
[7] D. Bendz, N.A. Paxeus, T.R. Ginn, F.J. Loge, J. Hazard. Mater. 122 (2005) 195.
[8] M. Stumpf, T.A. Ternes, R.D. Wilken, S.V. Rodrigues, W. Baumann, Sci. Total Environ. 225 (1999) 135.
[9] F. Sacher, F.T. Lange, H.J. Brauch, I. Blankenhorn, J. Chromatogr. A 938 (2001) 199.
[10] A.Y.C. Lin, Y.T. Tsai, Sci. Total Environ. 407 (2009) 3793.
[11] S. Weigel, R. Kallenborn, H. Huhnerfuss, J. Chromatogr. A 1023 (2004) 183.
[12] S.S. Verenitch, C.J. Lowe, A. Mazumder, J. Chromatogr. A 1116 (2006) 193.
[13] K.K. Barnes, D.W. Kolpin, E.T. Furlong, S.D. Zaugg, M.T. Meyer, L.B. Barber, Sci. Total Environ. 402 (2008) 192.
[14] P.M. Thomas, G.D. Foster, J. Environ. Sci. Heal. A Toxic/Hazard A39 (2004) 1969.
[15] K. Choi, Y. Kim, J. Park, C.K. Park, M. Kim, H.S. Kim, P. Kim, Sci. Total Environ. 405 (2008) 120.
[16] D.W. Kolpin, E.T. Furlong, M.T. Meyer, E.M. Thurman, S.D. Zaugg, L.B. Barber, H.T. Buxton, Environ. Sci. Technol. 36 (2002) 1202.

[17] K.G. Karthikeyan, M.T. Meyer, Sci. Total Environ. 361 (2006) 196.
[18] R.H. Lindberg, P. Wennberg, M.I. Johansson, M. Tysklind, B.A.V. Andersson, Environ. Sci. Technol. 39 (2005) 3421.
[19] D. Li, M. Yang, J. Hu, Y. Zhang, H. Chang, F. Jin, Water Res. 42 (2008) 307.
[20] D. Perret, A. Gentili, S. Marchese, A. Greco, R. Curini, Chromatographia 63 (2006) 225.
[21] M. Seifrtova, A. Pena, C.M. Lino, P. Solich, Anal. Bioanal. Chem. 391 (2008) 799.
[22] A. Pena, D. Chmielova, C.M. Lino, P. Solich, J. Sep. Sci. 30 (2007) 2924.
[23] M.J. Benotti, R.A. Trenholm, B.J. Vanderford, J.C. Holady, B.D. Stanford, S.A. Snyder, Environ. Sci. Technol. 43 (2009) 597.
[24] J.Y. Pailler, K.L. Pfister, L. Hoffmann, C. Guignard, Sci. Total Environ. 407 (2009) 4736.
[25] S.D. Kim, J. Cho, I.S. Kim, B.J. Vanderford, S.A. Snyder, Water Res. 41 (2007) 1013.
[26] J.W. Kim, H.S. Jang, J.G. Kim, H. Ishibashi, M. Hirano, K. Nasu, N. Ichikawa, Y. Takao, R. Shinohara, K. Arizono, J. Health Sci. 55 (2009) 249.
[27] S. Grujic, T. Vasiljevic, M. Lausevic, J. Chromatogr. A 1216 (2009) 4989.
[28] D. Calamari, E. Zuccato, S. Castiglioni, R. Bagnati, R. Fanelli, Environ. Sci. Technol. 37 (2003) 1241.
[29] P.H. Roberts, K.V. Thomas, Sci. Total Environ. 356 (2006) 143–153.
[30] M.D. Hernando, E. Heath, M. Petrovic, D. Barcelo, Anal. Bioanal. Chem. 385 (2006) 985.
[31] M.J. Gomez, M. Petrovic, A.R. Fernandez-Alba, D. Barcelo, J. Chromatogr. A 1114 (2006) 224.
[32] M.J. Hilton, K.V. Thomas, J. Chromatogr. A 1015 (2003) 129.
[33] A.Y.C. Lin, T.H. Yu, S.K. Lateef, J. Hazard. Mater. 167 (2009) 1163.
[34] K.D. Brown, J. Kulis, B. Thomson, T.H. Chapman, D.B. Mawhinney, Sci. Total Environ. 366 (2006) 772.
[35] A. Gulkowska, Y. He, M.K. So, L.W.Y. Yeung, H.W. Leung, J.P. Giesy, P.K.S. Lam, M. Martin, B.J. Richardson, Pollut. Bull. 54 (2007) 1287.
[36] W.H. Xu, G. Zhang, S.C. Zou, X.D. Li, Y.C. Liu, Environ. Pollut. 145 (2007) 672.
[37] J.L. Zhao, G.G. Ying, L. Wang, J.F. Yang, X.B. Yang, L.H. Yang, X. Li, Sci. Total Environ. 407 (2009) 962.
[38] M.J.M. Bueno, A. Aguera, M.D. Hernando, M.J. Gomez, A.R. Fernandez-Alba, J. Chromatogr. A 1216 (2009) 5995.

# CHAPTER 3. DEGRADATION METHODS OF PHARMACEUTICAL COMPOUNDS FROM WATER

The high usage of drugs throughout the world, their partial metabolism after ingestion, and inconsistencies in their disposed way, make their presence in the aquatic environment inevitable. Their sources in natural waters are not limited to excretion of parent compounds and their metabolites by individuals and pets but also, include disposal of unused medications to sewage systems, underground leakage from sewage system infrastructures, release of treated or untreated hospital wastes, disposal by pharmacies and physicians, and humanitarian drug surplus to domestic sewage systems. There are several transmission route of drugs to the environment *e.g.*, their release to the private septic fields, the treated effluent from domestic sewage treatment plants discharged to surface waters; overflow of untreated sewage from storm events and system failures directly to surface waters, transfer of sewage solids to land, droppings from medicated domestic animals and confined animal feeding operations; direct release via washing, bathing, or swimming; discharges from industrial manufacturing and clandestine drug laboratories, as well as illicit drug usage, leaching from defective landfills; and release from aquaculture. After release into the environment, most pharmaceutically compounds are eventually transported to the aqueous domain and are expected to be only partially degraded and transformed into other products by phototransformative, physicochemical and biological degradation processes.

The environmental impact and public health effects of long-term, low-level exposure and combinatory effects of these compounds require their removal/ degradation. Particular concern should be raised over those compounds that resist to the conventional wastewater and drinking water treatment.

Providing sufficiently clean water to the public has become a challenging issue worldwide as the quality of water sources are increasingly deteriorates [1]. As a consequence, treated wastewater has attracted attention as an alternative water resource, provided appropriate treatment [2]. Therefore, the removal of microcontaminants, such as pharmaceuticals, in wastewater is critical because many of these compounds survive conventional treatment [3]. Although these concentrations are much lower than the levels of traditionally known organic pollutants, the potential long-term effects of these compounds to humans and wildlife cannot be neglected [4, 5].

## 3.1. Conventional treatment methods

### *3.1.1. Biological treatment*

The pharmaceutical compounds in wastewater can be reduced or eliminated in biological wastewater treatment systems using the activated sludge process, which is the most commonly used wastewater treatment process in the world. Wastewater treatment process generally consists of a primary, secondary, and sometimes an advanced treatment stage, with different biological, physical, and chemical processes available for each stage of treatment [6].

The removal mechanisms in conventional biological wastewater treatment processes are biodegradation and sorption by microorganisms. They may be subdivided into aerobic and anaerobic processes. Aerobic applications include activated sludge, membrane batch reactors and sequence batch reactors [7-10]. Anaerobic methods include anaerobic sludge reactors, anaerobic film reactors and anaerobic filters [11]. The key component in biological WWTPs responsible for the removal of pharmaceutical pollutants is the aeration basin containing the microorganisms (activated sludge). Activated sludge (AS) treatment is unsuitable for the treatment of wastewater where the COD levels are greater than 4000 $mgL^{-1}$ [8]. Conventional activated sludge with a long hydraulic retention time (HRT) was the treatment selected for the pharmaceutical industry wastewater [12, 13]. It has a lower capital cost than more advanced treatment methods and a limited operational requirement, and it is generally more environmentally friendly than chlorination. However, high energy consumption, the production of large amounts of sludge [14] and operational problems including colour, foaming and bulking in secondary clarifiers are associated with activated sludge plants [13]. Factors which affect the efficiency of activated sludge facilities for the treatment of pharmaceutical wastewater include HRT, temperature, pH, dissolved oxygen (DO), organic load, microbial community, presence of toxic or recalcitrant substances and the batch operation of pharmaceutical production facilities [8, 15, 16]. These variables require modification for adaptation to pharmaceutical industry wastewater. Temperature is a key factor in the efficiency of activated sludge facilities. It has an important role in selecting individual microbial species and overall microbial diversity in the activated sludge. This is where industrial wastewater can be very different from municipal wastewater. Therefore, water from high temperature processes must be cooled prior to treatment by AS, which increases the time and cost of treatment. The impact of pharmaceuticals on the AS process appears to be negligible under normal operating conditions [17].

Biodegradation and sorption also could take place in other unit processes, such as primary settling, but removal efficiencies at this stage are difficult to control [18]. The wastewater characteristics play a key role in the selection of biological treatments. Solvents, pharmaceutical compounds, intermediates and raw materials represent biologically recalcitrant substances which affect the efficiency of the biological treatment systems [13]. Other removal mechanisms such as volatilization (due to aeration) or photodegradation (due to sunlight) are either negligible or nonexistent [19].

The advantages of anaerobic treatment over aerobic processes are its ability to deal with high strength wastewater, with lower energy inputs, sludge yield, nutrient requirements, operating cost, space requirement and improved biogas recovery. However, because a wide range of natural and xenobiotic organic chemicals in pharmaceutical wastewaters are recalcitrant and nonbiodegradable to the microbial mass within the conventional treatment system, anaerobic processes are not always effective in removing these substances. Not all WWTPs include a disinfection step, many facilities only disinfect treated effluents seasonally, and several studies reported that disinfection does not effectively remove a wide range of antibiotics [20].

### *3.1.2. Membrane processes*

Membrane filtration processes are used for water treatment and various industrial applications when production and distribution of water with high chemical

and microbiological quality is required. The applications of several membranes were evaluated for the removal of pharmaceuticals including microfiltration, ultra filtration, nanofiltration, reverse osmosis, electro dialysis reversal, membrane bioreactors and combinations of membranes in series [21, 22].

Microfiltration and ultra filtration are generally not fully effective in removing organic contaminants as pore sizes vary from 100-1000 times larger than the micro pollutants which can slip through the membranes. Reverse osmosis (RO) in different configurations showed efficient removal of pharmaceutical compounds including antibiotics, lipid regulators, hormones and oral contraceptives, antiepileptics and analgesics [22, 23]. RO membranes removed the majority of compounds investigated to levels below the limit of detection. However, pentoxifylline, iodopromide, dimethyltoluamide (DEET), meprobamate, phosphanetriyltripropanoic acid (TCEP), gemfibrozil, ketone and oxybenzone were detected in a variety of the configurations [21-23].

Both nanofiltration (NF) and RO treatment shows potential as an efficient method for removing pharmaceuticals from the wastewater, but pharmaceuticals can be rejected by one or a combination of three basic mechanisms: size exclusion (sieving, steric effect), charge exclusion (electrical) and physico-chemical interactions between solute, solvent and membrane. The disposal of the sludge which could contain the pollutant in a more concentrated form remains. However, a major disadvantage of using any of these filtration processes is that the removal of pharmaceutical compounds is accompanied by production of a rejection concentrate that will be much more concentrated than the feed water and will consequently require additional treatment and disposal [24, 25].

### *3.1.3. Activated carbon (AC)*

A conventional technology is activated carbon (AC) sorption/ filtration applied for the removal of both natural and synthetic organic contaminants [26, 27]. It is most commonly applied as a powdered feed or in granular form in packed bed filters. Granular activated carbon (GAC) can be used as a replacement for anthracite media in conventional filters, providing both adsorption and filtration. It can be applied after to the conventional active sludge (AS) treatment as an adsorbent. Carbon regeneration and disposal represent environmental and economical questions [22].

Also, powered activated carbon (PAC) can be used as sorbent for the removal of pharmaceuticals. PAC performance can also be improved by increasing the retention time [28, 29].

The general difficulty with powdered activated carbon (PAC) treatment lies in separating the carbon from the water. Various options are available: it can be done either via sedimentation, which necessitates the use of precipitants, or via (membrane) filtration, which requires additional energy. The filtration step reduces the carbon demand of the wastewater due to reduced blocking of the micropores by high molecular weight compounds. Consequently PAC is only suitable for the treatment of pre-treated wastewaters or wastewaters with a low organic loading.

### *3.1.4. Chlorination*

Chlorination has been shown to be effective for the removal of pharmaceuticals including 17α- ethinylestradiol and 17 β- estradiol, and sulfonamides [30, 31]. Chlorine dioxide is also effective for the removal of

acetaminophen, sulfamethoxazole, roxithromycin, trimethoprim, ciprofloxacin, enrofloxacin, metoprolol, flumequine, carbadox and diclofenac [24, 25, 32-39]. Acetaminophen, diclofenac, sulfamethoxazole and fluoroquinlone are oxidised during chlorination. By-products of acetaminophen include the toxic byproducts *N*-acetyl-*p*-benzoquinine imine and 1,4 benzoquinone. Both metoprolol and sulfamethoxazole form carcinogens, such as chloramines as one of their oxidation products and this may be due to the fact that ammonia chlorination was about one thousand times faster than phenol chlorination [39].

Recent reports demonstrate that conventional WWTPs are not able to remove pharmaceutical contaminants under typical operating conditions, which results in a discharge of these compounds into surface waters [20, 40-43].

## 3.2. Advanced oxidation processes

Advanced oxidation processes (AOPs) can be broadly defined as oxidation methods based on highly reactive species, such as (primarily but not entirely) hydroxyl radicals in the mechanisms leading to the destruction of the target pollutant. Hydroxyl radical is the active main species responsible for the destruction of pollutants [44]. It is a powerful, non-selective oxidant, which acts very rapidly with most organic compounds oxidizing them into carbon dioxide and water thanks to its high standard reduction potential (Table 3.1).

**Table 3.1.** Relative oxidation power of some oxidizing species [45].

| Oxidizing species | Relative oxidation power |
|---|---|
| Chlorine | 1.00 |
| Hypochlorous acid | 1.10 |
| Permanganate | 1.24 |
| Hydrogen peroxide | 1.31 |
| Ozone | 1.52 |
| Atomic oxygen | 1.78 |
| Hydroxyl radicals | 2.05 |
| Positively charged hole on titanium dioxide | 2.35 |

Once the hydroxyl radicals are generated, they virtually attack all organic compounds. Depending on the nature of the organic species, two types of initial attack are possible. In the first one, the radical remotes a hydrogen atom to form water (in the case of alkanes or alcohols). The second possibility consists of an electrophylic addition of the radical to double bonds, as in the case of olefins or aromatic compounds [44, 45]. After the addition of the radical, free organic radicals are generated (R•) that react with oxygen molecules generating a peroxiradical and allowing the initiation of a chain reaction system that ends in the complete mineralization of the contaminant [46].

Over the past 30 years, research and development concerning AOPs has been immense particularly for two reasons, namely (a) the diversity of technologies involved and (b) the areas of potential application. Although water and wastewater treatment is by far the most common area for research and development, AOPs have also found applications as diverse as groundwater treatment, soil remediation,

municipal wastewater sludge conditioning, production of ultrapure water and volatile organic compounds treatment and odour control.

AOPs are suited for destroying dissolved organic contaminants, such as: halogenated hydrocarbons (trichloroethane, trichloroethylene), aromatic compounds (benzene, toluene, ethylenzene, xylene), pentachlorophenol (PCP), nitrophenols, detergents, pesticides. They can be also used to oxidize inorganic contaminants, such as: cyanide, sulphide and nitrite [45].

There are several technologies included in the AOPs and each one is at a different level of development and commercialization. Figure 3.1 shows the application range of some wastewater treatments depending on the flow rate and organic matter content of the effluent to be treated. Technologies based on UV radiation and ozonation should be preferred at low flow rates and low organic loads in the incoming effluent. When the incoming effluent contains a high organic load, processes such as incineration and wet oxidation should be employed depending on the flow rate of the effluent [45].

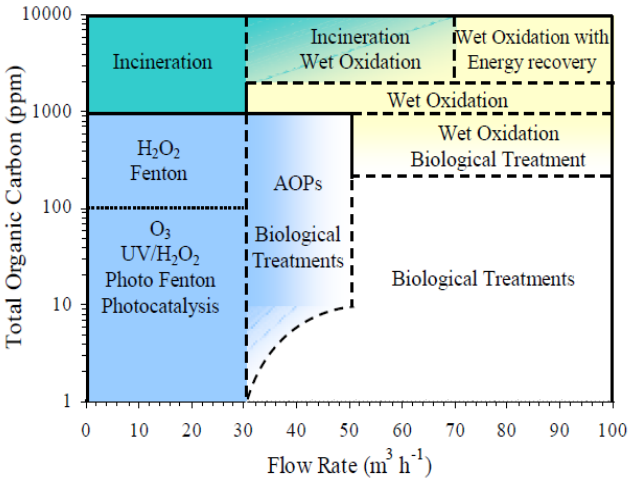


**Figure 3.1.** Application range of different oxidation technologies [47, 48].

Depending on the properties of the waste stream to be treated and the treatment objective itself, AOPs can be employed either alone or coupled with other physicochemical and biological processes. Process coupling is conceptually beneficial usually leading to improved treatment efficiencies [47, 48].

### *3.2.1. Photolysis*

Photolysis process involves the interaction of artificial or natural light with the target molecule and the induction of photochemical reactions, which can lead to its direct degradation to intermediate products, which further decomposition eventually yields mineral end-products [49]. UV treatment has traditionally been employed for the disinfection of drinking water with the advantage, compared to chlorination, of minimizing the formation of any regulated disinfection by-products [50]. For a compound to be photolabile, it needs to have the capacity to absorb

light. As a consequence of that light absorption, it will undergo transformation. It can also undergo degradation by receiving energy from other excited species (sensitized photolysis) or by chemical reactions involving very reactive and short-lived species such as hydroxyl-radicals, peroxy-radicals, or singlet oxygen [51]. The most extensively studied of these compounds is the analgesic/ anti-inflammatory drug diclofenac, which has been shown to degrade in the aquatic environment due to ultraviolet (UV) light. Other compounds such as the topical antimycotic drugs naftifine, sulbentine, cloxiquin, tolnaftate, and chlorphenesin have also been shown to be light sensitive [52].

The efficiency of direct photolysis is usually enhanced when irradiation is combined with hydrogen peroxide, a strong oxidant, whose photolytic dissociation yields hydroxyl radicals, thus facilitating the degradation process. This advanced oxidation process involve the formation of hydroxyl radicals generated by the photolysis of $H_2O_2$ and the corresponding propagation reactions. The photolysis of hydrogen peroxide occurs when UV radiation (*hv*) is applied, as shown in the following reaction (Equation 1) [53]:

$$H_2O_2 \xrightarrow{hv} 2OH\bullet \qquad (1)$$

This photolysis rate is not dependent on the pH and increases under more alkaline conditions.

When the water to be treated has a higher absorbance, it may compete for the radiation with the hydrogen peroxide. This is one of the greatest disadvantages of this method. An $H_2O_2$/ UV system can totally mineralize any organic compound, reducing it to $CO_2$ and water. The toxicity of oxidation products is not a problem since they are easily degraded [53].

It has been demonstrated at bench scale experiments the beneficial role of hydrogen peroxide that promote photolysis (indirect photolysis) [54-56]. The efficiency of photolytic degradation depends on several factors, such as: the absorbance spectrum of the pharmaceutical, the quantum yield of photolysis, the concentration of hydrogen peroxide employed, the molar absorption coefficient (the molar extinction coefficient is a measure of the capacity of a compound to absorb light). For example ibuprofen, diphenhydramine, phenazone, and phenytoin are some examples of pharmaceuticals degraded by photolytic reactions [57]. The water matrix plays an important role as the presence of natural organic matter (NOM) in waters, that may induce radicals scavenging, thus decreasing degradation [56]. Indirect photolysis is caused when photosensitizes, such as nitrate and dissolved organic matter, absorb light and generate reactive oxygenated radicals that subsequently degrade other compounds [58].

UV radiation can be generated using low pressure (LP) lamps that emit monochromatic light at 254 nm or medium pressure (MP) lamps that emit a broadband ranging from 205 to above 500 nm [59]. MP lamps were found to achieve a more effective degradation of bisphenol A, ethinyl estradiol, 2-chloropyridine, mefenamic, carbazepine, clofibic acid, sulfamethoxazole, diclofenac, ofloxacin, propanolol and estradiol as compared to direct photolysis using LP lamps [60].

### *3.2.2. Photocatalysis*

Photocatalysis is the acceleration of a photochemical transformation by the action of a catalyst such semiconductor like $TiO_2$, ZnO or CdS, and aims to promote

electrons from the valence to the conduction band, forming oxidant and reductive sites able of creating the conditions for the degradation of pollutants. From a mechanistic point of view, illumination of an aqueous $TiO_2$ suspension with irradiation with energy greater than the band gap energy of the semiconductor generates valence band holes and conduction band electrons. Holes and electrons may either undesirably recombine liberating heat or make their separate ways to the surface of $TiO_2$, where they can react with species adsorbed on the catalyst surface [61-63]. Valence band holes can react with water and the hydroxide ion (*i.e.* under alkaline conditions) to generate hydroxyl radicals, while electrons can react with adsorbed molecular oxygen reducing it to superoxide radical anion which, in turn, reacts with protons to form peroxide radicals [61-63].

The heterogeneous photocatalysis systems are based on the absorption of photons with energy greater than 3.2 eV (which corresponds to wavelengths lower than 390 nm) to initiate the excitation, related to a charge separation event (gap band), *i.e.*, one electron promotion at the conductive band ($e_{CB-}$) and a positive hole at valence band ($h_{VB}^+$), as represented in Equation 2 (bands formed by the evolvement of molecular orbital of $TiO_2$ as it is packed into a lattice). The $h_{VB}^+$ can oxidize $H_2O$ molecules and $OH^-$ ions adsorbed at the particle surface ($TiO_2$) producing •OH radicals (Equations 3 and 4) [61]. The hydroxyl radical is a short-lived and extremely powerful agent in the organic substances oxidation, degrading and mineralizing them to $CO_2$, $H_2O$ and inorganic ions [62, 63].

$$TiO_2 + hv \rightarrow e_{CB}^- + h_{VB}^+ \quad (2)$$

$$H_2O_{(ads)} + h_{VB}^+ \rightarrow \bullet OH + H^+ \quad (3)$$

$$OH_{(ads)}^- + h_{VB}^+ \rightarrow \bullet OH \quad (4)$$

On the other hand, $e_{CB}^-$ can react with $O_2$ forming the anion radical superoxide as represented in Equation 5 [61]. Subsequent reactions can lead to hydrogen peroxide and, once again, to the hydroxyl radical [64].

$$O_2 + e_{CB}^- \rightarrow O_2\bullet^- \quad (5)$$

The presence of such dissolved oxygen is very important for heterogeneous photocatalysis because it can make the recombination process on $TiO_2$ ($h_{VB}^+$/ $e_{CB}^-$) more difficult and maintain the electroneutrality of the $TiO_2$ particles. This condition makes the treatment practicable for industrial scale application in the environment conditions [61]. However, according to literature [64], for the $TiO_2$ photocatalysis process to succeed, the chemical oxygen demand (COD) must be lower than 800 $mgL^{-1}$.

Regarding the degradation of pharmaceuticals, heterogeneous photocatalysis is, without doubt, the most investigated photochemical AOP. In the literature, there is a series of investigations regarding the relevance of process variables, different types of catalysts, or simply, better ways to know the response of pharmaceuticals facing these processes. Studies involving the photocatalytic degradation of furosemide, ranitidine, ofloxacine, phenazone, naproxen, carbamazepine, clofibric acid, iomeprol and iopromide have proven the efficiency of the process and confirmed that it is a suitable alternative [61, 62, 65].

Heterogeneous semiconductor photocatalysis using $TiO_2$ as the photocatalyst is an emerging technology with key advantages including operation at ambient conditions as well as the fact that the catalyst itself is inexpensive, commercially available at various crystalline forms and particle characteristics, non-toxic and photochemically stable, which characteristically possess a narrow band gap [64].

Although available at various crystalline forms, a commercially available product containing 80:20 anatase:rutile shows exceptional activity and its superiority against other grades of $TiO_2$. Its superiority is attributed to the morphology of its crystallites [66]. This morphology allows an easy electron transfer from rutile to anatase, thus stabilizing charge separation and, therefore, lowering the recombination of photogenerated carriers. Besides $TiO_2$, ZnO and CdS have also been employed as photocatalysts in water treatment containing pharmaceutical compounds. Radicals formed degrade impurities in the water relatively unselectively, reacting with impurities in the wastewater as well as the target pharmaceuticals [67]. Photocatalytic reactions typically involve $TiO_2$ suspensions with the catalyst concentration being an important parameter that affects performance. Among this, the light wavelength and intensity, the solution pH which dictates the ionization state of the catalyst surface and consequently affects the extent of organics adsorption and degradation, the addition of $H_2O_2$ as an extra oxidant to promote reactions, and the water matrix (*i.e.* the presence of humic substances, bicarbonates or dissolved gases) represent important parameters which influences process performance. Photocatalytic reactions usually obey to Langmuir–Hinshelwood kinetic model which is reduced to pseudo-first or zero-order kinetics depending on the operating conditions. From an engineering point of view, the use of catalyst in slurry form requires an additional treatment step to remove it from the treated effluent. Investigations into the removal of the pharmaceuticals using $TiO_2$, include but are not limited to antibiotics, lipid regulators, x-ray contrast media, antiepileptics and antiphlogistics [68, 69]. Removal rates have been reported at 98 % for antibiotics when used in combination with UV [70]. The removal rates for carbamazepine are under 10 % [68]. Furthermore, solar studies have proved effective for a wide range of pharmaceuticals replacing the expense of generating UV light. There are difficulties in implementation on a commercial scale due to the number of operating parameters, *e.g.,* type and geometry of reactor, the photocatalyst, optimum energy use and wavelength of radiation. Moreover, it is difficult to assess the true success of the photocatalytic process in the absence of identified intermediate compounds and end products.

### *3.2.3. Ozonation*

Ozone has been applied to the treatment of waters primarily due to its strong disinfection and sterilization properties [71].

Ozone is a strong oxidant that either decomposes in water to form hydroxyl radicals, which are stronger oxidizing agents than ozone itself, thus inducing the so-called indirect oxidation or attacks selectively certain functional groups of organic molecules through an electrophilic mechanism [72]. Ozone is a very selective oxidant that will react with double bonds, activated aromatic compounds, and deprotonated amines, whereas hydroxyl radicals (OH•) generated when ozone is employed in advanced oxidation mode react with most water constituents with nearly diffusion controlled rates. Depending on the type of the substrate and the operating conditions, ozone oxidation is usually favoured at increased pH values due to the increased production of hydroxyl radicals. Moreover, treatment performance

is enhanced if ozone is combined with light irradiation [73], hydrogen peroxide [74] or with iron or copper complexes that act as catalysts [75]. Ozonization has been traditionally employed in drinking water treatment for odour and taste control and disinfection, as well as for wastewater disinfection [76]. The amount of ozone required depends on various parameters, such as: the level of background dissolved organic matter and wastewater pH and alkalinity, as well as the desired elimination performance [77]. The results of the various studies indicate that ozonization of pharmaceuticals depends on their chemical structure. While compounds with a C=C bond or aromatic structures seem to be susceptible to ozonization, compounds with amide structures are resistant to it [78]. Recent kinetic studies on pharmaceuticals including amoxicillin, lincomycin, clofibric acid, acetaminophen, bisphenol A, 17-estradiol, and 17-ethinylestradiol have shown ozone attacks aromatic rings and amino groups [54, 79]. Also, direct attack on the phenolic ring leading to the formation of hydroxyl derivative intermediates, without evidence of oxidation of the sulphur atom was reported for amoxicillin oxidation [80]. The reaction of the aromatic structure is independent of solution pH. However, amine groups do not react directly with ozone and the reactivity of amines strongly depends on the pKa of the amine and the pH of the solution. It must be considered that other compounds in the waste stream may produce more harmful byproducts as a consequence of the ozonization process. The main disadvantage of ozonization is incomplete mineralization and more harmful substances can be produced as a result. The degradation products must be analyzed as they may be more toxic than the parent compound [81].

The combination of hydrogen peroxide and ozone has been successfully used to degrade penicillin formulation effluent [74, 82]. Combination of UV, $O_3$ and $H_2O_2$ treatment was applied to a municipal wastewater treatment plant effluent containing pharmaceuticals including antibiotics, β-blockers, antiepileptics, antiphlogistics and lipid lowering agents [83]. Removal of all target analytes below detection limits was noted with the exception of the diatrizoate, iopamidol, iopromide and iomeprol which showed removal efficiencies of maximum 14 %. The oxidation studies of pharmaceuticals using hydrogen peroxide show efficiencies ranging from 40 % for Acetaminophen [79] to >95 % for some hormones by combination with UV [80].

When hydrogen peroxide is used in an $O_3$/ UV process, it accelerates the decomposition of ozone and increases the generation of OH· radicals, but the cost is very high. $O_3$/ $H_2O_2$/ UV processes are the most expensive because of the use of two types of reagents as compared to processes that use only one. This process is the result of the combination of two binary systems, $O_3$/ UV and $O_3$/ $H_2O_2$, in such a way that the resulting action is the following (Equation 6):

$$2O_3 + H_2O_2 \xrightarrow{hv} 2OH\bullet + 3O_2 \qquad (6)$$

When the process is used for wastewater decontamination, and the products to be removed only weakly absorb UV irradiation, it is more cost effective to externally add hydrogen peroxide with a reduced flow of UV. In this way, this method allows a considerable reduction of the total organic carbon (TOC). Generally, the oxidation velocity in these three processes can be very high.

However, the cost of generating the necessary UV irradiation in each case is also very high, and requires the compounds to absorb in certain wavelength [84].

Ozone production is an energy intensive process, making it costly to implement. An ozone treatment system may increase the energy demand over a conventional wastewater treatment plant by 40-50 % [85].

### *3.2.4. Fenton oxidation*

Homogeneous oxidation with the Fenton reagent occurs in the presence of ferrous or ferric ions with hydrogen peroxide via a free radical chain reaction that produces hydroxyl radicals. It is considered to be a metal-catalyzed oxidation reaction, in which iron acts as the catalyst.

A mechanistic pathway based on hydroxyl radicals is commonly accepted for the description of the degradation of organic compounds by Fenton reaction. The main stages involved in the process are the following (Equations 7-10) [86]:

$$Fe^{2+} + H_2O_2 \rightarrow Fe^{3+} + OH^- + HO\bullet \quad (7)$$

$$Fe^{2+} + HO\bullet \rightarrow Fe^{3+} + OH^- \quad (8)$$

$$HO\bullet + RH \rightarrow H_2O + R\bullet \quad (9)$$

$$R\bullet + Fe^{3+} \rightarrow R^+ + Fe^{2+} \quad (10)$$

The photo Fenton process ($H_2O_2$/ $Fe^{2+}$/ UV) involves the HO• formation through photolysis of hydrogen peroxide ($H_2O_2$/ UV) and Fenton reaction ($H_2O_2$/ $Fe^{2+}$). In the presence of UV irradiation, the ferric ions ($Fe^{3+}$) produced in Equation 7 are photocatalytically converted to ferrous ions ($Fe^{2+}$), with formation of an additional equivalent of hydroxyl radical (Equation 11) [86].

$$Fe^{3+} + H_2O \rightarrow Fe^{2+} + H^+ + HO\bullet \quad (11)$$

Similarly to Equation 9, the hydroxyl radicals formed react with organic species, promoting their oxidation. Based on the fact that Fenton reaction is accelerated by light, photo Fenton reaction gives faster rates and higher degrees of mineralization comparing to conventional Fenton process. Due to the fact that this reaction can be driven by low energy photons, it can also be achieved using solar irradiation. This fact can significantly reduce the operational cost of the treatment. The major parameters affecting Fenton process are solution's pH, amount of ferrous ions, and concentration of $H_2O_2$, initial concentration of the pollutant and presence of other ions [86].

Process efficiency is closely related to the solution pH, whose optimal values are between 2 and 4 as well as the COD: $H_2O_2$: catalyst ratio in the feed. Moreover, the efficiency may be enhanced in the presence of UV due to the fact that the reaction can be driven by low energy photons irradiation and more hydroxyl radicals are produced in the so-called photo-Fenton reaction compared to dark Fenton [86]. The degradation of organic pollutants is significantly improved when UV–VIS light at wavelengths greater than 300 nm is added to the reaction. This process, which also employs UV light, reduces the formation of the sludge waste that is produced in the original Fenton process. It is then possible to reduce the size of the reactor because the velocity of reaction in this case is very high. However, it is necessary to carefully

control the pH of the medium. Generally, the pH range should be between 2.6 and 3 for the best performance of the system [53]. Optimization of the catalyst and oxidant concentrations relative to the effluent's pollution load renders the process suitable to treat strongly polluted hospital effluents or effluents from pharmaceuticals manufacturing. In most cases, Fenton oxidation is capable of mineralizing a substantial fraction of the pollution load yielding effluents that are less toxic and more readily agreeable to biological post-treatment [87]. Fenton systems are easy to handle and operate; adjusting working conditions accordingly, Fenton reactions may conveniently be employed to treat micropollution caused by residual pharmaceuticals in surface waters and also industrial effluents. It should be noticed that all previous studies regarding the application of Fenton and photo-Fenton processes for pharmaceuticals treatment deal with homogeneous reaction systems. Use of ferrous or ferric salts usually suffers two major drawbacks associated with (a) the narrow pH range of operation to avoid the formation and subsequent precipitation of iron oxyhydroxides and (b) the need to recover dissolved ions from the treated solution, thus requiring an additional treatment stage. In this respect, the immobilization of Fenton catalyst on a heterogeneous matrix would enable its use under non-controlled pH conditions as well as its easy recovery from the treated effluent. Fenton reactions operate at room temperature normal pressure and without the highly complicated apparatus; which should assume a smooth transition from laboratory scale to large scale [88].

### *3.2.5. Ultrasound irradiation (US)*

Ultrasound irradiation or sonolysis offers a new alternative against persistent water organic pollutants. Ultrasound (US) can degrade many pollutants [89]. Is a relatively new process in water treatment and, therefore, has received less attention than other AOPs. The formation of OH• radicals when ultrasounds are used is caused by high temperature and pressure conditions that are reached inside the bubbles generated by the ultrasounds. These conditions are so extreme that they are capable of breaking up the water molecules and produce radicals. Generally, in comparison with photolysis, this type of advanced oxidation process reduces costs since no irradiation is needed [89]. Sonochemical reactions are induced upon high-intensity acoustic irradiation of liquids at frequencies that produce cavitation (typically in the range 20–1000 kHz). Thus, cavitation serves as a means of concentrating the diffused energy of ultrasound into micro-reactors with the simultaneous release of reactive radicals with each reactor serving as a hot spot. Pyrolytic reactions inside or near the bubble and solution radical chemistry, are the two major pathways of sonochemical degradation [90]. Organics of low solubility and/ or high volatility are likely to undergo fast sonochemical degradation as they tend to accumulate inside or around the gas-liquid interface. In this respect, the process may be well suited to undertake pharmaceutical micro-pollutants [91].

Several factors may affect process efficiency in a complex way, *e.g.*, the frequency and intensity of ultrasound, reactor geometry, type and nature of contaminant, bulk temperature and the water matrix. The water matrix is also very important, *i.e.*, the presence of dissolved gases or solids usually improves performance as they serve as extra nucleation centres [91].

### *3.2.6. Sub-critical wet air oxidation (WAO)*

Sub-critical wet air oxidation (WAO) belongs to the family of AOPs and is a thermochemical process where hydroxyl radicals and other active oxygen species are formed at elevated temperatures (*i.e.*, 200-320 °C) and pressures (*i.e.,* 2-20 MPa) [92]. The process has great potential for the treatment of wastewaters with moderate to high organic content (*i.e.*, 10-100 $gL^{-1}$ COD) converting dissolved organic pollutants into highly oxidized intermediates and eventually to carbon dioxide and water.

At temperatures and pressures above the critical point of water (374 °C, 22 MPa), the process is referred to as super-critical water oxidation (SCWO) with its main feature being that gas and liquid phases form a homogeneous single phase. In this case, organics and oxygen become completely miscible, thus eliminating mass transfer limitations which, in conjunction with increased reaction temperatures, lead to very high reaction rates. In light of this, treatment of micro-pollutants by WAO is not an economically viable option as it would result in excessive specific energy consumption (*i.e.*, energy per unit mass of pollutant destroyed). Nonetheless, WAO may be well suited to treat partially or completely effluents from drug manufacturing or hospital wastes [93].

## 3.3. References

[1] C.G. Daughton, Water: Science and Issues, E. Julius Dasch (ed.), New York: Macmillan Reference USA 1 (2003) 158.
[2] S.A. Snyder, Mark J. Benotti, Water Sci. Technol. 61 1 (2010) 145.
[3] T. Ternes, C.G. Daughton, Environ. Health Persp. 107 6 (1999) 907.
[4] T. Heberer, Toxicol. Lett. 131 (2002) 5.
[5] B. Halling-Sorensen, S.N. Nielson, P.F. Lanzky, F. Ingerslev, H.C.H. Lutzhoft, S.E. Jorgensen, Chemosphere 36 (1998) 357.
[6] G. Boari, I.M. Mancini, E. Trulli, Options Mediterraneennes, Ser. A 37 (1997) 262.
[7] T. LaPara, C. Nakatsu, L. Pantea, J. Alleman, Water Res. 36 3 (2002) 638.
[8] D. Suman Raj, Y.Anjaneyulu, Process Biochem. 40 1 (2005) 165.
[9] J. Noble, Membrane Tech. 9 (2006) 7.
[10] C. Chang, J. Chang, S. Vigneswaran, J. Kandasamy, Desalination 234 1-3 (2008) 386.
[11] A. Enright, S. McHugh, G. Collins, V. O'Flaherty, Water Res. 39 19 (2005) 4587.
[12] F. El Gohary, S. Abou-Elea, Water Sci. Technol. 32 11 (1995) 13.
[13] N. Oz, O. Ince, B.Ince, J. Environ. Sci. Heal. A. 39 (2004) 2029.
[14] D. Sreekanth, D. Sivaramakrishna, V. Himabindu, Y. Anjaneyulu, Bioresource Technol. 100 9 (2009) 2534.
[15] T. LaPara, C. Nakatsu, L. Pantea, J. Alleman, Water Res. 35 18 (2001) 4417.
[16] T. LaPara, A. Konopka, C. Nakatsu, J. Alleman, J. Ind. Microbiol. Biot. 26 4 (2001) 203.
[17] K. Stamatelatou, V. Vavilin, G. Lyberatos, Bioresource Technol. 88 2 (2003) 131.
[18] C.P.L. Grady, G.T. Daigger, H.C. Lim, Biological Wastewater Treatment, 2nd ed., Marcel Dekker, New York, 1999.
[19] A. Joss, S. Zabczynski, A. Gobel, B. Hoffmann, D. Loffler, C.S. McArdell, T.A. Ternes, A. Thomsen, H. Siegrist, Water Res. 40 (2006) 1686.

[20] O.A.H. Jones, N. Voulvoulis, J.N. Lester, Water Res. 38 12 (2001) 1383.
[21] C. Bellona, J.E. Drewes, P. Xu, G. Amy, Water Res. 38 (2004) 2795.
[22] S. Snyder, S. Adham, A. Redding, F. Cannon, J. DeCarolis, J. Oppenheimer, E. Wert, Y. Yoon, Desalination, 202 1-3 (2007) 156.
[23] A. Watkinson, E. Murby, S. Costanzo, Water Res. 41 18 (2007) 4164.
[24] S.D. Kim, J. Cho, I.S. Kim, B.J. Vanderford, S.A. Snyder, Water Res. 41 5 (2007) 1013.
[25] Y. Yoon, P. Westerhoff, S.A. Snyder, E.C. Wert, J. Membrane Sci. 270 1-2 (2006) 88.
[26] J. Hrubec, C. Vankreijl, C. Orra, Sci. Total Environ. 27 1 (1983) 71.
[27] M. Annesini, F. Gironi, M. Ruzzi, C. Tomei, Water Res. 21 5 (1987) 567.
[28] P. Westerhoff, Y. Yoon, S. Snyder, E. Wert, Environ. Sci. Technol. 39 17 (2005) 6649.
[29] Y. Yoon, P. Westerhoff, S. Snyder, E. Wert, J. Membr. Sci. 270 1-2 (2006) 88.
[30] A. Alum, Y. Yoon, P. Westerhoff, M. Abbaszadegan, Environ.Toxicol. 19 3 (2004) 257.
[31] Z. Qiang, J.Macauley, M. Mormile, R. Surampalli, C. Adams, J. Agr. Food Chem. 54 21 (2006) 8144.
[32] S. Khetan, T. Collins, Chem. Rev. 107 6 (2007) 2319.
[33] B. Halling-Sorensen, S.N. Nielson, P.F. Lanzky, F. Ingerslev, H.C.H. Lutzhoft, S.E. Jorgensen, Chemosphere 36 (1998) 357.
[34] C. Adams, Y. Wang, K. Loftin, M. Meyer, J. Environ. Eng-ASCE 128 3 (2002) 253.
[35] P. Westerhoff, Y. Yoon, S. Snyder, E. Wert, Environ. Sci. Technol. 39 17 (2005) 6649.
[36] L. Abia, X.L. Armesto, L.M. Canle, M.V. Garcia, J.A. Santaballa, Tetrahedron 54 (1998) 521.
[37] X.L. Armesto, M.L. Canle, M.V. Garcia, J.A. Santaballa, Chem. Soc. Rev. 27 (1998) 453.
[38] M.C. Dodd, A.D. Shah, U. Von Gunten, C. Huang, Environ. Sci. Technol. 39 18 (2005) 7065.
[39] K. Pinkston, D. Sedlak, Environ. Sci. Technol. 38 14 (2004) 4019.
[40] C.G. Daughton, T.A. Ternes, Environ. Health Persp. Suppl. 107 (1999) 907.
[41] M. Stumpf, T.A. Ternes, R.D. Wilken, S.V. Rodrigues, W. Baumann, Sci. Total Environ. 225 1-2 (1999) 135.
[42] K. Kummerer, Chemosphere 45 (2001) 957.
[43] W. Giger, A.C. Alder, E.M. Golet, H.-P.E. Kohler, C.S. McArdell, E. Molnar, H. Siegrist, M.J.F. Suter, Chimia Int. J. Chem. 57 9 (2003) 485.
[44] A.M. Braun, L. Jacob, E. Oliveros, C.A.O. do Nascimento, Advances in Photochemistry, Wiley, New York 18 (1993) 235.
[45] R. Munter, P. Est. Acad. Sci. 50 2 (2001) 59.
[46] G.V. Buxton, C.L. Greenstock, W.P. Helman, A.B. Ross, J. Phys. Chem. 17 (1988) 513.
[47] M.A. Blesa, Red CYTED VIII-G (2001).
[48] F.E. Hancock, Today 53 (1999) 3.
[49] T.E Doll, F.H. Frimmel, Chemosphere 52 17 (2003) 57.
[50] V.J. Pereira, H.S. Weinberg, K.G. Linden, P.C. Singer, Environ. Sci. Technol. 41 16 (2007) 82.
[51] R.P. Schwarzenbach, P.M. Gschwend, D.M. Imboden, Environmental Organic Chemistry, Wiley-Interscience New York, 1993.

[52] K. Thoma, N. Kubler, E. Reimann, Pharmazie 52 (1997) 362.
[53] J.M. Poyatos, M.M. Munio, M.C. Almecija, J.C. Torres, E. Hontoria, F. Osorio, Water Air Soil Poll. 205 (2010) 187.
[54] I. Arslan-Alaton, S. Dogruel, J. Hazard. Mater. 112 (2004) 105.
[55] R. Andreozzi, V. Caprio, R. Marotta, A. Radovnikovic, J. Hazard. Mater. 103 (2003) 233.
[56] V.J. Pereira, K.G. Linden, H.S. Weinberg, Water Res. 41 (2007) 4413.
[57] F. Yuan, C. Hu, X. Hu, J. Qu, M. Yang, Water Res. 43 6 (2009) 1766.
[58] O. Legrini, E. Oliveros, A. Braun, Chem. Rev. 93 2 (1993) 671.
[59] T. Takashi, C. Shi-Cong, F. Mamoru, M. Tetsuro, Chem. Phys. Lett. 443 4-6 (2007) 313.
[60] R.R. Giri, H. Ozaki, S. Ota, R. Takanami, S. Taniguchi, Int. J. Environ. Sci. Te. 7 2 (2010) 251.
[61] D. Chatterjee, S. Dasgupta, J. Photoch. Photobio. C. 6 2-3 (2005) 186.
[62] O. Dalrymple, D. Yeh, M. Trotz, J. Chem. Technol. Biot. 82 2 (2007), 121.
[63] L.Colar, E.Ilinoiu, **S. Motoc**, F.Manea, R.Pode, G.Burtica, Chem. Bull. "Politehnica" Univ. (Timisoara) 55 69-1 (2010) 55.
[64] U. Gaya, A. Abdullah, J. Photoch. Photobio. C. 9 1 (2008) 1.
[65] J. Herrmann, Top. Catal. 34 1-4 (2005) 49.
[66] A. Chatzitakis, C. Berberidou, I. Paspaltsis, G. Kyriakou, T. Sklaviadis, I. Poulios, Water Res. 42 (2008) 386.
[67] L. Lhomme, S. Brosillon, D. Wolbert, Chemosphere 70 3 (2008) 381.
[68] T.E. Doll, F.H. Frimmel, Water Res. 39 (2005) 847.
[69] L.A. Perez-Estrada, S. Malato, W. Gernjak, A. Aguera, E.M. Thurman, I. Ferrer, A.R. Fernandez-Alba, Environ. Sci. Technol. 39 21 (2005) 8300.
[70] M. Addamo, V. Augugliaro, A. Paola, E. Garcia-Lopez, V. Loddo, G. Marci, L. Palmisano, J. Appl. Electrochem. 35 7-8 (2005) 765.
[71] J. Arana, J.H. Melian, J.D. Rodriguez, O.G. Diaz, A. Viera, J.P. Pena, P.M. Sosa, V.E. Jimenez, Catal. Today 76 2-4 (2002) 279.
[72] R.F. Dantas, M. Canterino, R. Marotta, C. Sans, S. Esplugas, R. Andreozzi, Water Res. 41 (2007) 2525.
[73] S. Irmak, O. Erbatur, A. Akgerman, J. Hazard. Mater. 126 (2005) 54.
[74] I.A. Balcioglu, M. Otker, Chemosphere 50 (2003) 85.
[75] M. Skoumal, P.L. Cabot, F. Centellas, C. Arias, R.M. Rodriguez, J.A. Garrido, E. Brillas, Appl. Catal. B-Environ. 66 (2006) 228.
[76] E. Cokgor, I. Alaton, O. Karahan, S. Dogruel, D. Orhon, J. Hazard. Mater. 116 1-2 (2004) 159.
[77] M. Huber, S. Canonica, G. Park, U. Von Gunten, Environ. Sci. Technol. 37 5 (2003) 1016.
[78] H. Nakada, A. Shinohara, K. Murata, S. Kiri, N. Managaki, N. Sato, H. Takada, Water Res. 41 19 (2007) 4372.
[79] R. Andreozzi, V. Caprio, R. Marotta, D. Vogna, Water Res. 37 5 (2003) 993.
[80] R. Andreozzi, M. Canterino, R. Marotta, N. Paxeus, J. Hazard. Mater. 122 3 (2005) 243.
[81] K. Ikehata, N. Naghashkar, M. El-Din, Ozone-Sci. Eng. 28 6 (2006) 353.
[82] E. Cokgor, O. Karahan, I. Arslan-Alaton, S. Meric, H. Saruhan, J. Environ. Sci. Heal. A 41 9 (2006) 1887.
[83] T. Ternes, J. Stuber, N. Herrmann, D. McDowell, A. Ried, M. Kampmann, B. Teiser, Water Res. 37 8 (2003) 1976.
[84] E. Rosenfeldt, K. Linden, Environ. Sci. Technol. 38 20 (2004) 5476.
[85] T. Larsen, J. Lienert, A. Joss, H. Siegrist, J. Biotechnol.113 1-3 (2004) 295.

[86] H. Shemer, Y. Kunukcu, K. Linden, Chemosphere 63 2 (2006) 269.
[87] N.S.S. Martinez, J.F. Fernandez, X.F. Segura, A.S. Ferrer, J. Hazard. Mater. 101 (2003) 315.
[88] V. Kavitha, K. Palanivelu, Chemosphere 55 9 (2004) 1235.
[89] S. Chitra, K. Paramasivan, P.K. Sinha, K.B. Lal, J. Clean. Prod. 12 (2004) 429.
[90] R.J. Emery, M. Papadaki, L.M. Freitas dos Santos, D. Mantzavinos, Environ. Int. 31 2005 207.
[91] L. Sanchez-Prado, R. Barro, C. Garcia-Jares, M. Llompart, M. Lores, C. Petrakis, N. Kalogerakis, D. Mantzavinos, E. Psillakis, Ultrason. Sonochem. 15 5 (2008) 689.
[92] J. Levec, A. Pintar, Catal. Today 124 (2007) 172.
[93] A.Z. Gotvajn, J. Zagorc-Koncan, T. Tisler, J. Environ. Eng-ASCE 133 (2007) 89.

# CHAPTER 4. ELECTROCHEMICAL DEGRADATION AND DETECTION METHODS USED FOR PHARMACEUTICAL FROM WASTEWATER

## 4.1. Electrodegradation methods used for pharmaceutical wastewater treatment

Water treatment by electricity was used for several years, but water or wastewater electrochemical treatment technologies did not find wide application by the limitation of relatively high capital investment and the expensive electricity supply. However, with the increasing standard of drinking water supply and the stringent environmental regulations regarding the wastewater discharge, electrochemical technologies have retained their importance worldwide during the past two decades. Nowadays, electrochemical technologies have reached such a state that they are not only comparable with other technologies in terms of cost but also, are more efficient and more compact. For some situations, electrochemical technologies may be the indispensable step in treating wastewaters containing refractory pollutants. In addition, electrochemical process is a clean process that does not generate by-product or other pollutants.

### *4.1.1. Electrocoagulation (EC)*

Electrocoagulation (EC) technology is a treatment process of applying electrical current to treat contaminants by *in-situ* generation of the coagulation agents [1]. This technique uses a current to dissolve Fe (or steel) or Al sacrificial anodes immersed in the polluted water, giving rise to the corresponding metal ions that yield different Fe(II) (and/ or Fe(III)) or Al(III) species with hydroxide ion depending on the medium pH. These species act as coagulants or destabilization agents that lead to the pharmaceuticals separation from the wastewater by sedimentation, producing some sludge. The coagulated particles can also be separated by electroflotation when they are attached to the bubbles of $H_2$ gas evolved at the cathode and transported to the top of the solution where they can be separated. The EC process is highly dependent on the physical–chemical characteristics of the effluent: nature, composition and concentration of the pollutants, solution conductivity, pH, electrolysis cell design (size/ area and electrodes distance), electrolysis time, current and electrodes material [2].

The main processes can take place during an EC treatment are:

– electrode reactions to produce metal ions from Fe or Al anodes and $H_2$ gas at the cathode;

– *in-situ* formation of coagulants in the water/ wastewater;

– removal of pharmaceuticals compounds with coagulants by sedimentation or by electroflotation with evolved $H_2$;

– other electrochemical and chemical reactions involving reduction of organic impurities and metal ions at the cathode and coagulation of colloidal particles;

Some advantages for applying EC are described below [3]:

– more effective and rapid organic matter separation than in coagulation;

– pH control is not necessary, except for extreme values;

– the amount of chemicals required is small;

– the amount of sludge produced is smaller when compared with coagulation;

– the operating costs are much lower than in most conventional technologies.

However, this method presents major disadvantages such [3]:

– anode passivation and sludge deposition on the electrodes that can inhibit the electrolytic process in continuous operation mode;

– high concentrations of iron and aluminium ions in the effluent that have to be removed.

*Fe or steel anode*

When an iron or steel anode is utilized in EC, $Fe^{2+}$ is dissolved in the wastewater from Fe oxidation at the anode (standard potential $E^0$ = -0.44 V vs. SHE) as follows [4, 5]:

$$E = E^{0'} + \frac{0.059}{n}\log_{10}\frac{[Ox]}{[\mathrm{Re}d]} \qquad Fe \rightarrow Fe^{2+} + 2e^- \qquad (1)$$

whereas hydroxide ion and $H_2$ gas are generated at the cathode from the reaction ($E^0$ = -0.83 V vs. SHE):

$$2H_2O + 2e^- \rightarrow 2OH^- + H_{2(g)} \qquad (2)$$

$OH^-$ production from reaction (2) causes an increase in pH during electrolysis and insoluble $Fe(OH)_2$ precipitates at pH > 5.5 and remains in equilibrium with $Fe^{2+}$ up to pH 9.5 or with monomeric species such as $Fe(OH)^+$, $Fe(OH)_2$ and $Fe(OH)_3^-$ at higher pH values. The formation of insoluble $Fe(OH)_2$ can be written as:

$$Fe^{2+} + 2OH^- \rightarrow Fe(OH)_{2(s)} \qquad (3)$$

and the overall reaction for the electrolytic process from the sequence of reactions 1-3 is:

$$Fe + 2H_2O \rightarrow Fe(OH)_{2(s)} + H_{2(g)} \qquad (4)$$

In the presence of $O_2$, dissolved $Fe^{2+}$ is oxidized to insoluble $Fe(OH)_3$, see equations (4) and (5):

$$4Fe^{2+} + 10H_2O + O_{2(g)} \rightarrow 4Fe(OH)_{3(s)} + 8H^+ \qquad (5)$$

and protons can be directly reduced to $H_2$ gas at the cathode:

$$8H^+ + 8e^- \rightarrow 4H_{2(g)} \quad (6)$$

The corresponding overall reaction obtained by combining reactions 1, 5 and 6 is:

$$4Fe + 10H_2O + O_{2(g)} \rightarrow 4Fe(OH)_{3(s)} + 4H_{2(g)} \quad (7)$$

In acidic media of pH < 5.0, a greater quantity of Fe anode than that expected from Faraday law following reaction (1) is dissolved owing to the chemical attack of protons [6].

The insoluble $Fe(OH)_2$ and/ or $Fe(OH)_3$ flocks retain colloids and ionic species and coagulate to form particles that are separated from the wastewater by sedimentation or electroflotation.

*Al anode*

In the case of EC with Al, the anodic reaction leads to soluble $Al^{3+}$ ($E^0$ = 1.66 V vs. SHE) [7]:

$$Al \rightarrow Al^{3+} + 3e^- \quad (8)$$

and the cathodic reaction produces hydroxide ion and $H_2$ gas:

$$3H_2O + 3e^- \rightarrow 3OH^- + (3/2)H_{2(g)} \quad (9)$$

Soluble monomeric and polymeric cations are also converted into insoluble $Al(OH)_3$ flocks by a complex precipitation kinetics. The overall reaction is:

$$Al + 3H_2O \rightarrow Al(OH)_{3(s)} + (3/2)H_{2(g)} \quad (10)$$

However, when an *Al* cathode is also used, it can be chemically attacked by $OH^-$ generated during $H_2$ evolution at high pH values as follows [8]:

$$Al + 3H_2O + OH^- \rightarrow Al(OH)_4^- + (3/2)H_{2(g)} \quad (11)$$

And treated wastewater contains higher amount of aluminium ions than those expected from reaction (8). The soluble species are converted into insoluble $Al(OH)_3$ flocs that adsorb ions and even soluble organic compounds and/ or trap colloidal particles, usually coagulating near neutral pH. Note that a Fe or steel anode is not attacked by $OH^-$ in alkaline medium, thus avoiding the formation of an excess of $Fe(OH)_4^-$ species.

The EC method has been successfully applied to the remediation of some synthetic and industrial pharmaceutical wastewaters. Some authors studied decontamination of wastewaters containing pharmaceuticals compounds, *e.g.,* synthetic salicylic acid, ranitidine, with good efficiencies using Al/ Al, mild steel/ mild steel or stainless steel/ stainless steel pairs electrodes [9-11].

Coupling electrocoagulation using iron electrodes (as cathode and anode) followed by photocatalysis in UV/$TiO_2$/$H_2O_2$ applied to treat effluents from a pharmaceutical and cosmetic factory was studied [12]. The results showed that the combination of electrocoagulation followed by catalyzed photo-oxidation improves the quality of the effluent with peptides residues, such as peptone fragments. The electrocoagulation removed the majority of the colloidal organic substances and suspended materials. However, refractory compounds still remained in this water effluent. In the sequence, by employing the heterogeneous photocatalysis, these refractory compounds were degraded up to mineralization. Such combined process of electrocoagulation and photocatalysis proved to be efficient.

### *4.1.2. Electro-Fenton (EF)*

This electrochemical technique seems more appealing than the common Fenton technique since it allows the continuous electrogenerate and/ or regenerate the reactants ($H_2O_2$ and $Fe^{2+}$) that increases the efficiency.

The electro-Fenton technology uses three- and two-electrodes, divided and undivided cells with cathode materials like graphite, carbon felt and gas diffusion electrodes (GDEs) and anode materials like graphite, Pt, metal oxides and boron-doped diamond (BDD). The efficiency of the oxidation process is a function of operation parameters such as temperature, solution pH, $O_2$ feeding, stirring rate or liquid flow rate, electrolyte composition, applied potential or current, catalyst and pollutant contents.

The mineralization of sulfanilic acid has been studied by electro-Fenton [13] using an undivided electrochemical cell with a boron-doped diamond (BDD) anode and an air diffusion cathode able to generate $H_2O_2$. Partial decontamination of 1.39 mM sulfanilic acid solutions was achieved by EF until 100 mA $cm^{-2}$ at optimum conditions of 0.4 mM $Fe^{2+}$ and pH 3.0. The increase in current density and substrate content led to an almost total mineralization. The kinetics for sulfanilic acid decay always followed a pseudo-first-order reaction. Hydroquinone and *p*-benzoquinone were detected as aromatic intermediates, whereas acetic, maleic, formic, oxalic, and oxamic acids were identified as generated carboxylic acids.

Electro-Fenton was applied for degradation/ mineralization of clofibric acid [14], salicylic acid [15], chloroxylenol [16], ibuprofen [17] and the antibiotic enrofloxacin [18], using undivided Pt/GDE and BDD/GDE cells. The best results obtained from TOC removal efficiency point of view were achieved using BDD electrode, *e.g.* for clorfibric acid 93 % TOC removal efficiency in comparison with 73 % obtained using Pt electrode, for ibuprofen 81 % TOC removal efficiency in comparison with 58 % obtained using Pt electrode. Almost total mineralization was found for clorfibric acid, which cannot be attained with Pt, confirming the interest of the BDD/GDE system as an alternative oxidation technology. In the case of salicylic acid, it formed stable Fe(III)-salicylate complexes that were slowly removed.

### *4.1.3. Photoelectrocatalysis (PEC)*

The electrochemical application of photocatalysis is the photoelectrocatalysis (PEC) method, which provides much higher efficiency for wastewater remediation. It consists in the application of a constant bias anodic potential ($E_{anod}$) usually to a $TiO_2$-based thin film anode subjected to UV illumination. The electrochemical cells used in PEC are tank or flow reactors that allow the passage of UV light through a quartz glass to reach the exposed surface of the anode. The photoinduced electrons

are then continuously extracted from the anode by an external electrical circuit to be injected into the cathode.

The superiority of photoelectrocatalysis over photocatalysis can be related to the suppression of the recombination process between the photogenerated electron/ hole pairs by the external electric field.

In the literature there are not many researching regarding the use of PEC technique applied for degradation of pharmaceutical compounds. The treatment of ibuprofen and naproxen using PEC method [19] was study with porous $Bi_2MoO_6$ film deposited onto BDD, with 11 $cm^2$ area exposed to a 150W Xe lamp to simulate visible light and immersed into 60 mL of solution in 0.12 $mgL^{-1}$ $Na_2SO_4$ filling a cylindrical quartz cell. For 10 $mgL^{-1}$ ibuprofen at $E_{anod}$= 2 V vs. SCE, 86 % drug decay and 72 % TOC removal were found for PEC, values much higher than the corresponding 64 % and 42 % obtained for electrochemical oxidation and 21 % and 8 % for photocatalysis. These results suggest the possible use of PEC for pharmaceutical wastewaters treatment with sunlight as irradiation source, although more research is needed to demonstrate its viability in practice.

### *4.1.4. Electrooxidation (EO)*

Electrochemical oxidation or electrooxidation (EO) is the most popular electrochemical procedure for removing organic pollutants from wastewaters [2, 20, 21]. This technique has been recently used for degradation of the pharmaceutical compounds from the aqueous solutions. It consists in the oxidation of pollutants in an electrolytic cell by:

– direct anodic oxidation (or direct electron transfer to the anode), which yields very poor decontamination;

– chemical reaction with electrogenerated species from water discharge at the anode such as physically adsorbed ''active oxygen'' (physisorbed hydroxyl radical (•OH)) or chemisorbed ''active oxygen'' (oxygen in the lattice of a metal oxide (MO) anode). The action of these oxidizing species leads to the total or the partial decontamination, respectively.

The existence of indirect or mediated oxidation with different heterogeneous species formed from water discharge has allowed the proposal of two main approaches for the pollution abatement in wastewaters by EO [2, 22].

– the electrochemical conversion method, in which refractory organics are selectively transformed into biodegradable compounds, usually carboxylic acids, with chemisorbed ''active oxygen'';

– the electrochemical combustion (or electrochemical incineration) method, where organics are completely mineralized, *i.e.*, oxidized to $CO_2$ and inorganic ions, with physisorbed •OH. This radical is the second strongest oxidant known after fluorine, with a high standard potential ($E^0$ = 2.80 V vs. SHE) that ensures its fast reaction with most organics giving dehydrogenated or hydroxylated derivatives up to conversion into $CO_2$.

In both cases high cell voltages are applied to the electrochemical cell for the simultaneous oxidation of pollutants and water, thus maintaining the anode activity. The use of low cell voltages avoiding $O_2$ evolution frequently causes the loss of anode activity because of some by-products formed from direct anodic oxidation can be adsorbed on its surface and hence, this procedure is not utilized for wastewater treatment in practice. It has been found that the nature of the anode material influences strongly both the selectivity and efficiency of the EO process.

#### 4.1.4.1. Direct anodic oxidation

Electrooxidation of pollutants can occur directly on anodes by generating physically adsorbed "active oxygen" (adsorbed hydroxyl radicals, •OH) or chemisorbed "active oxygen" (oxygen in the oxide lattice, $MO_{x+1}$) [22]. This process is usually called anodic oxidation or direct oxidation. The physically adsorbed "active oxygen" causes the complete combustion of organic compounds (R), and the chemisorbed "active oxygen" ($MO_{x+1}$) participates in the formation of selective oxidation products:

$$R + MO_x(\bullet OH)z = CO_2 + zH^+ + ze^- + MO_x \quad (12)$$

$$R + MO_{x+1} = RO + MO_x \quad (13)$$

In general, •OH is more effective for pollutant oxidation in comparison with O in $MO_{x+1}$. Because oxygen evolution can also take place at the anode, high overpotentials for $O_2$ evolution is required in order to the reactions (12) and (13) to proceed with high current efficiency. Otherwise, the most of the current supplied will be wasted to split water. The anodic oxidation does not need to add a large amount of chemicals to wastewater or to feed $O_2$ to cathodes, with no tendency of producing secondary pollution and fewer accessories required. These advantages make anodic oxidation more attractive than other electrooxidation processes. The important part of an anodic oxidation process is obviously the anode material. Anode materials used for pharmaceuticals degradation found in the literature include: glassy carbon [23], Ti/$RuO_2$, Ti/Pt–Ir [24], fiber carbon [25], $MnO_2$ [26], Pt–carbon black [27], porous carbon felt [28], stainless steel [29], reticulated vitreous carbon [30] and boron-doped diamonds [31-33] electrodes.

#### 4.1.4.2. Indirect electrooxidation processes

Electrooxidation of pollutants can be fulfilled through different ways. Use of the chlorine and hypochlorite generated anodically to destroy pollutants is well known. This technique can effectively oxidize many inorganic and organic pollutants at high chloride concentration, typically larger than 3 $gL^{-1}$ [25, 34-36].

One disadvantage is the possible formation of chlorinated organic compounds intermediates or final products that hinders the wide application of this technique [34]. Moreover, if the chloride content in the raw wastewater is low, a large amount of salt must be added to increase the process efficiency [36]. Pollutants can also be degraded by the electrochemically generated hydrogen peroxide [37-39]. The electrically generated ozone is also reported for the wastewater treatment [40].

Another kind of electrooxidation was proposed in 1992 [41], the mediated electrooxidation, in treating mixed and hazardous wastes. In this process, metal ions, usually called mediators, are oxidized on an anode from a stable, low valence state to a reactive, high valence state, which in turn attack organic pollutants directly, and may also produce hydroxyl free radicals that promote destruction of the organic pollutants. Subsequently, the mediators are regenerated on the anode, forming a closed cycle. The typical mediators include $Ag^{2+}$, $Co^{3+}$, $Fe^{3+}$, $Ce^{4+}$ and $Ni^{2+}$ [41-44].

Mediated electrooxidation usually needs to operate in highly acidic media. In addition, there is the secondary pollution from the heavy metals added. These disadvantages limit its application.

#### 4.1.4.3. The direct and indirect electrooxidation of synthetic solutions and real wastewaters

The recent researches have been shown that the boron-doped diamond (BDD) anode yields a much higher mineralization degree than other "non-active" anodes such as $PbO_2$ and $SnO_2$, as well as "active" anodes, such as Pt and $RuO_2$, regardless of the presence/ absence of chloride ion and the electrolytic system. Several researchers studied the influence of variables over the electrooxidation process with BDD electrode. Some authors [45, 46] studied the role of four operative parameters to optimize the treatment of single solutions of ketoprofen, naproxen and carbamazepine using BDD. Current density was always found the most influential parameter. Another study shown a degradation of clofibric acid solutions revealing a 98 % TOC decay using a BDD anode [47], with hydroxyl radicals (BDD(•OH)) formed at the anode surface showing a much higher oxidation power than Pt(•OH) on Pt. Despite the higher quantity of BDD(•OH) produced, the relative proportion of available oxidizing radicals decreases due to the higher rate of parasitic reactions that waste more charge without valuable oxidation events. This anode is very effective for any drug content since it can reduce 98 % TOC of a near saturation solution, with consumption of 30 $AhL^{-1}$ at 300 mA. These researchers indicate that the degradation process is controlled by the diffusion of organic molecules toward the anode surface. When the clofibric acid concentration decays, a more rapid pollutant removal was found using Pt than BDD. This unexpected behaviour was explained by the existence of stronger interactions between clorfibric acid and Pt favouring its reaction with Pt (•OH). For each anode, the same decay rate following a pseudo first-order kinetics was obtained at pH 3.0 and 12.0, as expected if the formation of Pt (•OH) or BDD (•OH) is pH–independent. While all aromatics are destroyed with both anodes, carboxylic acids persist using Pt and are efficiently removed using BDD. The high mineralization power of anodic oxidation (AO) with BDD is due to the destruction of the generated carboxylic acids. Another study [48, 49] obtained similar results for the degradation of paracetamol and diclofenac. More than 97 % TOC removal was achieved with a BDD anode for 1 $gL^{-1}$ paracetamol in comparation with Pt that yields a more reduced degradation, in the pH ranged from 2 to 12. Hydroquinone and 1,4-benzoquinone were detected as aromatic by-products, while oxalic and oxamic acids were identified as ultimate carboxylic acids that are completely removed with BDD, but remain stable using Pt. In contrast, the mineralization of diclofenac with BDD was only effective in neutral phosphate buffer of pH 6, the diclofenac degradation pathway products are: 2-hydroxyphenylacetic acid, 2,5-dihydroxyphenylacetic acid, 2,6-dichloroaniline, and 2,6-dichlorohydroquinone, which were transformed into carboxylic acids. A comparatively removal of paracetamol with "non-active" anodes like BDD and $Ti/SnO_2$ and the "active" $Ti/IrO_2$ anode using a divided plug-flow reactor was studied [50]. Oxidation of paracetamol at boron-doped diamond (BDD) and at $Ti/SnO_2$ anodes in a plug-flow divided electrochemical reactor led to electrochemical combustion, whereas at $Ti/IrO_2$ benzoquinone was the exclusive oxidation product, except at very long electrolysis times. The difference is explicable in terms of the different mechanisms of oxidation: direct oxidation at the anode for $Ti/IrO_2$ vs. indirect oxidation involving electrogenerated hydroxyl radicals at BDD and $Ti/SnO_2$.

At BDD, at which the efficiency of degradation of paracetamol was greatest, the rate of electrolysis at constant concentration was linearly dependent on the current, and at constant current linearly depended on the concentration. Current efficiencies for mineralization up to 26 % were achieved without optimization.

Other study [51] reported the decay kinetics of the sulfonamide antibiotic sulfamethoxazole at BDD in the anodic compartment of a plug-flow. A change from pseudo zero-order to pseudo first-order reaction was observed after 75 min of electrolysis of 50 mL of 1 mM drug in 0.025 M $Na_2SO_4$ at 20 mA and pH 6-7 under recirculation at 1 mL $min^{-1}$. The explication for this behaviour was that the kinetics varied from a pure current control (zero order) to a pure mass transport control (first order) as a result of the decrease in drug concentration, thus slowing down the process. The mineralization efficiency increased with increasing both current and sulfamethoxazole concentrations, which are the most significant variables for its destruction by AO.

In another study [52], a near 100 % mineralization efficiency was obtained for ibuprofen. Tests were performed with model solutions of ibuprofen, with concentrations ranging from 0.22 to 1.75 mM for the Ti/Pt/$PbO_2$ electrode and 1.75 mM for the BDD electrode, using 0.035 M $Na_2SO_4$ as the electrolyte, in a batch cell, at different current densities (10, 20 and 30 mA $cm^{-2}$). By comparing the results obtained on both electrodes it can be said that at the current density of 20 mA $cm^{-2}$, the combustion efficiency is much higher for the BDD anode, meaning that the rate of mineralization is higher for the BDD anode. However, at 30 mA $cm^{-2}$, identical values are obtained for both anodes, meaning that no metabolites are accumulated during the degradation process. For both electrodes, at 20 mA $cm^{-2}$, the mineralization efficiency have similar decay with the applied specific charge, with slightly higher values obtained for the BDD electrode, a fact that is responsible for the higher combustion efficiency. At 30 mA $cm^{-2}$ with the Ti/Pt/$PbO_2$ anode, the mineralization efficiency decays are similar to those presented at 20 mA $cm^{-2}$ but slightly lower, which can be explained by the fact that at both current densities the processes are controlled by diffusion and the current that is not used to degrade organic compounds increases with current density. For the same current density but with the BDD anode, the mineralization efficiency has similar decays but very different from those obtained for 20 mA $cm^{-2}$. The unexpected decay is probably due to the high oxygen evolution near the electrode surface that prevents the organic molecules from approaching the anode surface allowing, however, a combustion efficiency of 100 %, since a slow combustion in the presence of high concentration of oxidant species, like hydroxyl radicals, leads to complete mineralization.

It has been also studied the use of other anode materials for electrooxidation of pharmaceuticals. Tetracycline degradation was studied by electrooxidation on a Pt, Ti/$RuO_2$-$IrO_2$ anode [53, 54]. In the case of the first electrode a very slow decay of tetracycline, without practical mineralization, was obtained (the aromatic rings of tetracycline were broken, losing its biological activity). In case of the former electrode, the results obtained showed a large decay of this drug, it followed a pseudo first order reaction and its rate increased with increasing current density, but it was not affected by pH and drug content. Tetracycline was directly oxidized at the anode via electron transfer without $CO_2$ production. Another study [55] reported the effective removal of drug residues like aspirin, tetracycline, and gentamicine with "active" anodes of $MnO_2$-C and Pt, although greater biological availability was found with progressive oxidation of the drugs.

The degradative action of "active" anodes is strongly enhanced when chloride ion is present in the synthetic solution since generated active chlorine, alone or in combination with hydroxyl radicals, oxidizes the organic matter.

Paracetamol degradation in 0.1 M $NaClO_4$ at Ti/$RuO_2$ and BDD electrode was studied [56]. 80 % and 95 % paracetamol destruction after 300 min of electrooxidation at 80 mA was achieved. In 0.1 M NaCl, the rate of degradation was much faster (30 min) at both anodes. For the Ti/$RuO_2$ anode, no degradation took place in 0.1 M $NaClO_4$ and TOC was only reduced by 26 % in 0.1 M NaCl, whereas the BDD anode caused 84 % and 54 % mineralization in such media, respectively. This behaviour confirms the paracetamol oxidation by direct electron transfer to Ti/$RuO_2$ in perchlorate medium and the generation of active chlorine species ($Cl_2$, HClO, and/ or $ClO^-$) that rapidly destroy the drug and promote its partial mineralization in chloride medium. In contrast, the oxidation with BDD in perchlorate solution occurs via •OH that mineralizes the drug in large extent. The lower mineralization achieved under the latter conditions can be explained by the scavenging effect of $Cl^-$ ion and HClO on •OH, yielding chlorine radical, chlorine dioxide and chlorate ion. The formation of chloro-derivatives using electro-oxidation with active chlorine was demonstrated by Zhao et al. (2009) [57] for the mineralization of a diclofenac solution with a BDD anode. In the presence of 0.1 M NaCl at pH 6.7, dichlorodiclofenac was determined as the main intermediate and subsequent chlorinated by-products generated were slowly removed yielding 72 % TOC reduction.

The degradation of ofloxacin and lincomycin in 0.01 M $Na_2SO_4$ and 0.02 M NaCl at Pt, Ti/$IrO_2$-$Ta_2O_5$, graphite and 3D activated carbon pellets was studied [58] using a bench-scaled divided flow cell with electrodes of 200 $cm^2$ and applying up to 40 mA $cm^{-2}$. The oxidation process followed a pseudo first-order kinetics in sulphate medium, being accelerated in the presence of chloride by the formation of hypochlorite ion. The best anode was the 3D electrode, followed by Pt, in which 85 % of ofloxacin removal and 50 % COD decay were determined after 240 min of electrolysis at 20 mA $cm^{-2}$ in 0.01 M $Na_2SO_4$.

The study of real pharmaceutical wastewaters by electrochemical oxidation is more difficult than that of synthetic wastewaters because they are composed of a complex mixture of compounds including ions like $NH_4^+$, $Cl^-$, $NO_3^-$, and $SO_4^{2-}$. The indirect oxidation of organic and inorganic species with BDD(•OH) and active chlorine is expected using the powerful BDD anode.

The electrochemical destruction of reverse osmosis concentrates generated in tertiary Sludge Treatment Plant (STPs) was studied. The wastewater having a pH range of 7.4–8.1 containing 124-140 $mgL^{-1}$ COD and several pharmaceuticals with contents between 1.5 and 27 $\mu gL^{-1}$, as well as 630 $mgL^{-1}$ $Cl^-$ was subjected to the electrooxidation studied [59]. Volumes of 2 L of the effluent were electrolyzed in a flow plant with an undivided cell equipped with two circular 70 $cm^2$ BDD electrodes. Appling 5 and 20 mA $cm^{-2}$ caused the complete COD decay in 480 and 300 min, respectively. For the latter current density, $NH_4^+$ ion was completely oxidized to $NO_3^-$ ion and $Cl^-$ ion was partially transformed into active chlorine species including $ClO_3^-$ ion. Moreover, all drugs were completely destroyed at a similar rate for both current densities, verifying pseudo first-order kinetics because their diffusion toward the anode limited their reaction with generated oxidants. Because of the complexity of the electrochemical oxidation of real wastewaters with BDD due to generation of potentially toxic inorganic ions by-products, the parasitic processes can be diminished using less potent "active" anodes and applying the electrooxidation with active chlorine. Comparatively, Radjenovic et al. (2011) [60] studied the

electrochemical destruction of reverse osmosis concentrates generated by membrane treatment of secondary STW effluent containing 27 pharmaceuticals and pesticides with contents between 8.1 and 33.7 $\mu gL^{-1}$ using a divided flow reactor with a 24 $cm^2$ Ti/$RuIrO_2$ anode. TOC degradation reached 9 % for a current densities of 5 mA $cm^{-2}$, and 27 %, respectively, at 25 mA $cm^{-2}$. In this current density range, free and total chlorine were largely accumulated in the system. The active chlorine species generated for the current densities of 15 mA $cm^{-2}$ promoted the total destruction of most pharmaceuticals, except ibuprofen and iopromide.

### 4.1.4.4. Electrode materials used in electrooxidation

In case of implementing a new technology, electrode materials plays the most important role. In this section will be presented the most significant parameters used in direct and indirect electrooxidation.

*Overpotential of oxygen evolution*

The anodic activity depends on the value of overpotential of oxygen evolution. A comparison of most extensively investigated anode materials is presented in Table 4.1. The formation potentials of typical oxidants are presented in Table 4.2, to understand the performance of the anodes. It is clear that $IrO_2$, Pt, and graphite show much smaller values of overpotential of oxygen evolution. This indicates that effective oxidation of pollutants on these anodes occurs only at very low current densities or in the presence of high concentrations of chlorides or metallic mediators. When the current density is high, significant decrease of the current efficiency is expected from the production of oxygen.

**Table 4.1.** Potential of oxygen evolution of different anodes, V vs. NHE.

| Anode | Potential value, V | Conditions |
|---|---|---|
| Pt | 1.3 | 0.5 M $H_2SO_4$ |
| Pt | 1.6 | 0.5 M $H_2SO_4$ |
| $IrO_2$ | 1.6 | 0.5 M $H_2SO_4$ |
| Graphite | 1.7 | 0.5 M $H_2SO_4$ |
| $PbO_2$ | 1.9 | 1.0 M $HClO_4$ |
| $SnO_2$ | 1.9 | 0.5 M $H_2SO_4$ |
| Pb-Sn (93:7) | 2.5 | 0.5 M $H_2SO_4$ |
| $TiO_2$ | 2.2 | 1.0 M $H_2SO_4$ |
| Si/BDD | 2.3 | 0.5 M $H_2SO_4$ |
| Ti/BDD | 2.7 | 0.5 M $H_2SO_4$ |
| DiaChem | 2.8 | 0.5 M $H_2SO_4$ |

The boron-doped diamond (BDD) film on titanium substrate and DiaChem electrodes [61] gives the highest value of oxygen evolution overpotential. Thus, anodic oxidation can take place on its surface at significantly high current density with minimal amount of oxygen evolution side reaction. This leads to an effective and efficient process. It is indeed the most active anode for oxidation of various pollutants.

**Table 4.2.** Formation potential of typical chemical reactants [61].

| Oxidants | Formation potentials, V |
|---|---|
| $H_2O/•OH$ | 2.80 |
| $O_2/O_3$ | 2.07 |
| $SO_4^{2-}/S_2O_8$ | 2.01 |
| $MnO_2/MnO_4^{2-}$ | 1.77 |
| $H_2O/H_2O_2$ | 1.77 |
| $Cl^-/ClO_2^-$ | 1.57 |
| $Ag^+/Ag^{2+}$ | 1.50 |
| $Cl^-/Cl_2$ | 1.36 |
| $Cr^{3+}/Cr_2O_7^{2-}$ | 1.23 |
| $H_2O/O_2$ | 1.23 |

*"Active" and "non-active" electrodes*

The different behaviour of electrodes in EO considering two limiting cases: the so-called "active" and "non-active" anodes. Typical examples are Pt, $IrO_2$ and $RuO_2$ for the first and $PbO_2$, $SnO_2$ and BDD for the secondary. The proposed model assumes that the initial reaction in both kind of anodes (generically denoted as M) corresponds to the oxidation of water molecules leading to the formation of physisorbed hydroxyl radical (M(•OH)):

$$M + H_2O \rightarrow M\left(HO^{\bullet}\right) + H^+ + e^- \qquad (14)$$

Both the electrochemical and chemical reactivity of heterogeneous M(•OH) are dependent on the nature of the electrode material. The surface of active anodes interacts strongly with •OH and then, a so called higher oxide or superoxide (MO) may be formed following reaction (15). This may occur when higher oxidation states are available for a metal oxide anode, above the standard potential for oxygen evolution ($E^0$ = 1.23 V vs. SHE).

$$M\left(HO^{\bullet}\right) \rightarrow MO + H^+ + e^- \qquad (15)$$

The redox couple MO/M acts as a mediator in the oxidation of organics by reaction (16), which competes with the side reaction of oxygen evolution via chemical decomposition of the higher oxide species from reaction (17).

$$MO + R \rightarrow M + RO \qquad (16)$$

$$MO \rightarrow M + \frac{1}{2}O_2 \qquad (17)$$

In contrast, the surface of a non-active anode interacts so weakly with •OH that allows the direct reaction of organics with M(•OH) to give fully oxidized reaction products such as $CO_2$ as follows:

$$M\left(HO^{\bullet}\right) + R \rightarrow M + mCO_2 + nH_2O + H^+ + e^- \qquad (18)$$

where *R* is an organic compound with m carbon atoms and without any heteroatom, which needs a = (2m + n) oxygen atoms to be totally mineralized to $CO_2$. The oxidative reaction (16) with the surface redox couple MO/M is much more selective than the mineralization reaction (18) with physisorbed heterogeneous hydroxyl radical. The latter reaction also competes with the side reactions of M(•OH) such as direct oxidation to $O_2$ from reaction (19) or indirect consumption through dimerization to hydrogen peroxide by reaction (20):

$$M\left(HO^{\bullet}\right) \rightarrow M + \frac{1}{2}O_2 + H^+ + e^- \qquad (19)$$

$$2M\left(\bullet OH\right) \rightarrow 2M + H_2O_2 \qquad (20)$$

A non-active electrode does not participate in the direct anodic reaction of organics and does not provide any catalytic active site for their adsorption from the aqueous medium. It only acts as an inert substrate and as a sink for the removal of electrons. In principle, only outer-sphere reactions and water oxidation are possible with this kind of anode. Hydroxyl radical produced from water discharge by reaction (14) is subsequently involved in the oxidation process of organics.

The above model supposes that the electrochemical activity (related to the overvoltage for $O_2$ evolution) and chemical reactivity (related to the rate of organics oxidation) of physisorbed M(•OH) are strongly linked to the strength of the M-•OH interaction. As a general rule, the weaker the interaction, the lower the anode reactivity for organics oxidation with faster chemical reaction with M(•OH). The BDD anode is the best non-active electrode verifying this behaviour, then being proposed as the preferable anode for treating organics by EO [62].

### 4.1.4.5. Global parameters used in anodic oxidation

The use of the electrochemical oxidation of the organic species can be estimated using the so-called *Electrochemical Oxidability Index (EOI*) [63].

*Electrochemical Oxidability Index (EOI)* – expresses the average current efficiency and is a measure of the facility of the electrochemical oxidation of the organic pollutant at given experimental conditions:

$$EOI = \frac{\int_0^{\tau} ICE dt}{\tau} \qquad (21)$$

where *t* -time of electrolysis at which ICE is almost zero.

*Instantaneous Current Efficiency (ICE)*. For the determination of the current efficiency during the electrochemical oxidation of the organic pollutant two methods have been used: the oxygen flow rate method and the COD (Chemical Oxygen

Demand) method. By the oxygen flow rate method, for oxidation of the organic pollutant at given experimental conditions, EOI can be calculated using the relation:

$$ICE = \frac{v_0 - (v_t)_{org}}{v_0} \quad (22)$$

where $v_0$ - oxygen flow rate in absence of the organic pollutant in the electrolyte ($cm^3.min^{-1}$)

$(v_t)_{org}$ - oxygen flow rate at a given time t in the presence of organic pollutant ($cm^3\ min^{-1}$)

By the COD method, during electrolysis COD can be measured and ICE can be calculated using the relation:

$$ICE = \frac{\left[(COD)_t - (COD)_{t+\Delta t}\right]}{8I\Delta t} F \cdot V \quad (23)$$

where $(COD)_t$ - chemical oxygen demand at time t (g [O] $dm^{-3}$)

$(COD)_{t+\Delta t}$ - chemical oxygen demand at time t+$\Delta$t (g [O] $dm^{-3}$)

*I*- current (I)

*F*- Faraday constant (96 487 C)

*V*- volume of electrolyte ($dm^3$)

The choice of the method to measure ICE depends on the solubility of the electrolysis product. Thus, the COD method is used only if the electrolysis products are soluble in the electrolyte and the oxygen flow rate method where the electrolysis products may be soluble or insoluble. Measurements of ICE by both techniques give information about the formation of polymeric products at the anode during the treatment.

From the technological point of view the EOI value gives information about the specific energy consumption (kWh/ kg COD) for the electrochemical treatment.

$$E_{sp} = 3.35 \frac{V_c}{EOI} \quad (24)$$

Considering a linear relation between the cell potential ($V_c$) and the current density *(i*)

$$Vc = Vd + \rho.l.i \quad (25)$$

Equation (22) becomes:

$$E_{sp} = 3.35 \frac{(V_d + \rho li)}{EOI} \quad (26)$$

where $E_{sp}$- specific energy consumption (kWh/ kg COD)

$V_c$-applied potential (V)

$V_d$-decomposition potential (V)
$\rho$ -resistivity of the wastewater ($\Omega$cm)
$l$ -interelectrode distance (cm)
$I$ -current density (A/ $cm^2$)

*Electrochemical Oxygen Demand (EOD).* It expresses the amount of "electrochemically" formed oxygen used for oxidation of the organic pollutants. The EOD value can be calculated using the relation:

$$EOD = \frac{8EOI \times Q}{F} \quad [g\ O_2\ (g\ organic\ pollutant)^{-1}] \qquad (27)$$

where $Q$- specific electrical charge passed [Ah (g organic pollutant)$^{-1}$]

*Degree of oxidation (X)*. The degree of oxidation (X expresses the ratio between the amount of "electrochemically" formed oxygen used for oxidation of the organic pollutants (EOD), to the amount needed for complete oxidation (COD*).

$$X = \frac{EOD}{COD^*} \qquad (28)$$

where COD* is the initial COD value expressed in $gO_2$ / g organic pollutant $^{-1}$
$COD^* = COD^0\ [(g_{org}/L)^0\ ]^{-1}$
$COD^0$ and $[g_{org}/L]^0$ are the initial COD and the initial concentration of pollutant, respectively [60].
Using relation (27), $X$ becomes:

$$X = 8\frac{EOI}{COD^*} \cdot \frac{Q}{F} \qquad (29)$$

Values of $X$ close to 1 indicate complete oxidation and values of $X$ close to zero indicate that the organic pollutants present in the wastewater are not electrochemically oxidized. The electrochemical method for the treatment of wastewater containing pollutants is economically viable only if high EOD values can be achieved [64].

By an electrochemical treatment of wastewater either a partial (reduction of toxicity) or a complete decomposition of the pollutants can be achieved. Complete decomposition of organic material means the oxidation to carbon dioxide and as consequence, relatively high energy consumption for large organic molecules.

## 4.2. Electrochemical techniques in sensor applications

Electrochemical methods for sensing pollutants may be categorized into those bases on several approaches [65]:

- Potentiometric;
- Amperometric-coulometric;
- Voltammetric;
- Conductometric.

Figure 4.1 contains a schematic decision "tree" for the implementation of electroanalysis in environmental application. The performance criteria widely can vary. For example, the "end-pipe" monitoring of water quality require stringent performance from sensor at ppm and ppb levels [65].

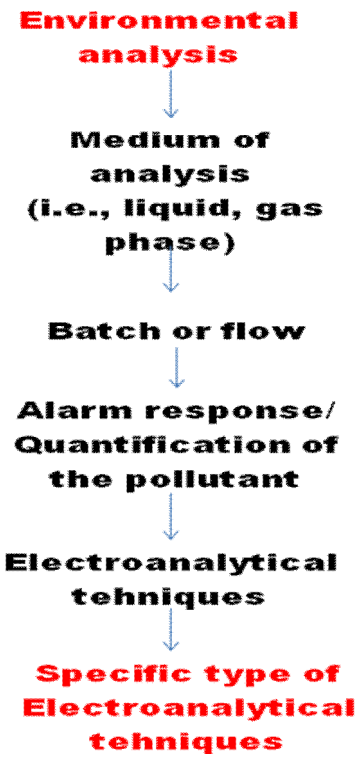


**Figure 4.1.** A schematic decision "tree" for the implementation of electroanalysis in environmental application.

The uses of voltammetric techniques in analytical chemistry are highly appealing to the analytical chemist owing to their high sensitivity, low cost, simplicity of instrumentation and ease of implementation. Furthermore, voltammetric techniques offer the possibility to determine the analyte concentration directly in the sample without pretreatment or chemical separation, as well as, to analyze colored materials and samples with dispersed solid particles [66-68]. Figure 4.2 present some examples of the potential excitation signals for some commonly used voltammetric techniques.

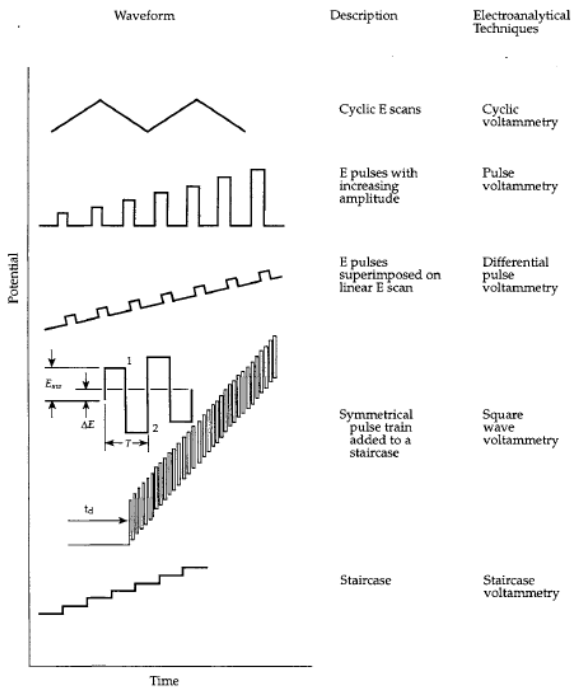


**Figure 4.2.** Examples of the potential excitation signals for some commonly used voltammetric techniques.

### *4.2.1. Cyclic voltammetry (CV)*

Cyclic voltammetry (CV) is often the first experiment performed in an electrochemical study of a compound, a biological material, or an electrode surface. It is effectively used in the fields of environmental electrochemistry, organic chemistry, inorganic chemistry, and biochemistry. The effectiveness of CV results from its capability for rapidly observing the redox behaviour over a wide potential range. The resulting voltammogram is analogous to a conventional spectrum in the sense that it conveys information as a function of an energy scan. Cyclic voltammetry has become a popular tool since the last 40 years for studying electrochemical reaction [69]. CV is perhaps the most versatile electroanalytical technique in pharmaceutical analysis [70, 71]. It is often the first experiment performed in an electrochemical study of drugs in raw material [72], pharmaceuticals [73], and biological material [74].

Cyclic voltammetry (CV) is a very versatile electrochemical technique. The effectiveness results from its capability for rapidly observing redox behaviour over a wide potential range. The characteristic shape of cyclic voltammograms current responses is governed by mass transport/ diffusion processes in the solution phase. In order to understand the origin of this shape, the observed current response at each potential as being "composed" of two "simpler" current responses based on:

– the conventional "transient" or potential step technique, in which the decay of the current at a given potential is monitored as a function of time, and;

– the conventional "steady-state" technique in which the current is independent of time.

This technique provides rapid information on the thermodynamic redox processes, on the kinetics of heterogeneous electron- transfer reactions, and on coupled chemical reactions or adsorption processes. This is accomplished with a three-electrode arrangement whereby the potential relative to some reference electrode is scanned at a working electrode, while the resulting current flowing through a counter (or auxiliary) electrode is monitored in a supporting electrolyte. The technique is ideally suited for a quick search of redox couples present in a system, and once located a couple may be characterized by more careful analysis of the cyclic voltammogram. More precisely, the controlling electronics is designed such that the potential between the reference and the working electrode can be adjusted, but the big impedance between these two electrodes effectively forces any resulting current to flow through the counter electrode. Usually the potential is scanned back and forth linearly with time between two extreme values using a triangular potential waveform (Figure 4.3). When the potential of the working electrode is more positive than that of a redox couple present in the solution, the corresponding species may be oxidized (*i.e.,* electrons going from the solution to the electrode) and produce an anodic current. Similarly, on the return scan, as the electrode potential of the working electrode is more positive than that of a redox couple, reduction (*i.e.,* electrons flowing away from the electrode) may occur to cause a cathodic current. By "International Union of Pure and Applied Chemistry" (IUPAC) convention, anodic currents are positive and cathodic currents negative [75].

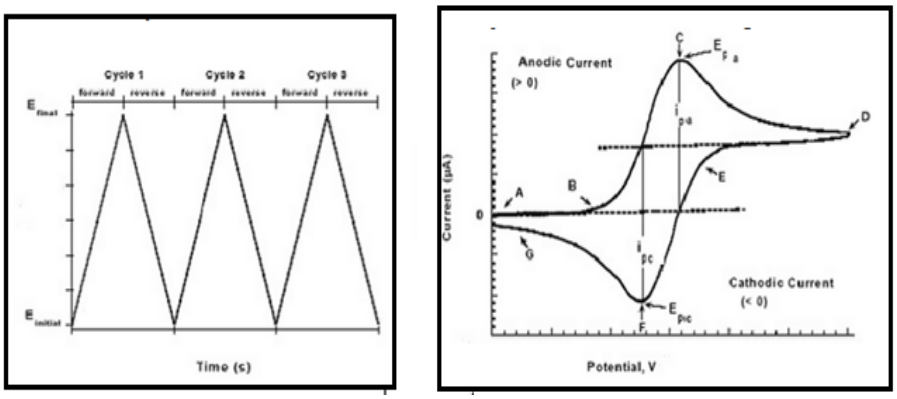


**Figure 4.3.** Cyclic voltammograms potential waveform with switching potentials (left) and the expected response of a reversible redox couple during a single-potential cycle (right) [69].

The magnitude of the observed faradaic current can provide information on the overall rates of the many processes occurring at the working electrode surface. As is the case for any multi–step process, the overall rate is determined by the slowest step.

For a redox reaction induced at a working electrode, the rate determining step may be any one of the following individual steps depending on the system:

– rate of mass transport of the electro-active species;

– rate of adsorption or de-sorption at the electrode surface;

– rate of the electron transfer between the electro-active species and the electrode, or rates of the individual chemical reactions which are part of the overall reaction scheme.

For the oxidation reaction involving n electrons:

$$Red \rightarrow Ox + ne^{-}$$

The Nernst Equation gives the relationship between the potential and the concentrations of the oxidized and reduced forms of the redox couple at equilibrium (at 298 K):

$$E = E^{0'} + \frac{0.059}{n}\log_{10}\frac{[Ox]}{[\mathrm{Re}d]} \qquad (30)$$

where $E$ is the applied potential, $E^{o'}$ is the formal reduction potential, [$O_X$] and [Red] are the surface concentrations at the electrode/ aqueous electrolyte interface, and n is the number of electrons involved in the redox reaction.

Note that the Nernst equation may or may not be valid depending on the system or on the experimental conditions.

A typical voltammogram is shown in Figure 4.2. The scan shown starts at a slightly negative potential, (A) up to some positive switching value, (D) at which the scan is reversed back to the starting potential. The current is first observed to peak at $E_{pa}$ (with value $i_{pa}$) indicating that an oxidation is taking place and then drops due to depletion of the reducing species from the diffusion layer. During the return scan the processes are reversed (reduction is now occurring) and a peak current is observed at $E_{pc}$ (corresponding value,).

#### 4.2.1.1. Reversible System

Providing that the charge–transfer reaction is reversible, that there is no surface interaction between the electrode and the reagents, and that the redox products are stable (at least in the time frame of the experiment), the ratio of the reverse and the forward current $i_{pr} / i_{pf} = 1.0$ (in Figure 2 $i_{pa} = i_{pf}$ and $i_{pc} = i_{pr}$). In addition, for such a system it can be shown that:

– the corresponding peak potentials $E_{pa}$ and $E_{pc}$ are independent of scan rate and concentration;

– the formal reduction potential for a reversible couple $E^{o'}$ is centred between anodic and cathodic peak potentials:

$$E^{o'} = \frac{E_{pa} + E_{pc}}{2} \qquad (31)$$

– the peak separation $\Delta E_p$ for a reversible couple is given by:

$$\Delta E_p = E_{pa} - E_{pc} = \frac{0.059}{n} \quad (32)$$

at all scan rates (however, the measured value for a reversible process is generally higher due to uncompensated solution resistance and non-linear diffusion. Larger values of $\Delta E_p$, which increase with increasing scan rate, are characteristic of slow electron transfer kinetics).

To distinguish between reversible (diffusion-controlled) and irreversible (charge-transfer controlled) kinetics of an electrode process potential scan-rate is used as diagnostic tool – the rate of reagent transport is proportional to the square root of the scan-rate. Thus, in one experimental set a shift in reversibility might be executed and analysis of $\Delta E_p$ vs. $v^{1/2}$ gives information on reversibility and applicability of further calculations.

In simple terms, the working electrode may be regarded as a "reagent" of adjustable oxidizing or reducing strength. However, this is a purely conceptual image. In fact, the electrochemical processes are occurring at the interface of two different phases, the electrode and the electro-active species in solution. In other words, the processes under studies are heterogeneous in nature.

For the electron transfer to occur, the molecules in solution have to approach the electrode. In a cyclic voltammetry experiment, the solution is kept unstirred and in this situation, mass transport can occur only by diffusion due to concentration gradients created around the electrode surface. Such concentration–distance profiles at different steps of a cyclic voltammogram scan are illustrated in Figure 4. 4. The magnitude of the observed signal will be very much a function of the diffusion properties of the system. Intuitively, the current intensity (*i.e.,* the flow of electrons) is expected to depend on the surface area of the working electrode and the concentration of the electro-active species. Also, one can expect the voltage scanning rate to affect the concentration profile around the electrode which itself directly affects the rate of charge transport, and for this matter the diffusion coefficient appears explicitly. The expression of the peak current (A) for the forward sweep in a reversible system at 298 K is given by the Randles–Sevcik equation [76]:

$$I_{pf} = (2.69 \times 10^5) n^{3/2} A D^{1/2} C^* v^{1/2} \quad (33)$$

where $n$ is the number of electrons involved in the redox process, A is the active area of the working electrode ($cm^2$), D is the diffusion coefficient ($cm^2\ s^{-1}$), C* is the bulk concentration of the electroactive species (mol $cm^{-3}$), and v is the potential scan rate ($Vs^{-1}$).

In the present experiment, the dependence of $i_{pf}$ on scan rate and concentration will be examined.

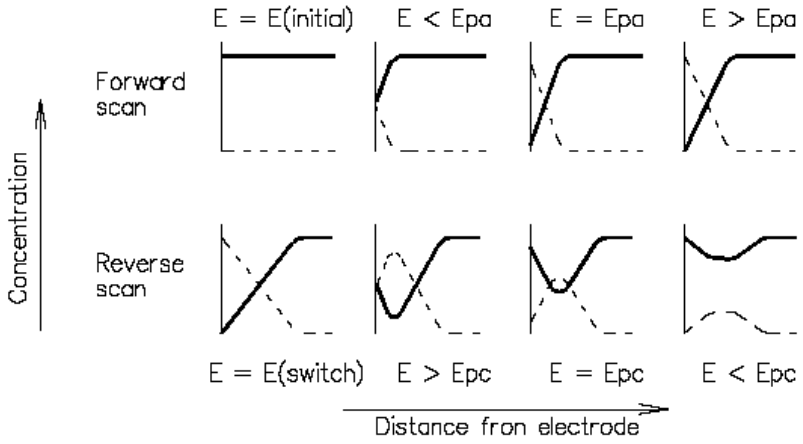


**Figure 4.4.** Qualitative diagrams showing concentration-distance profile at various stages of the cyclic voltammogram the solid lines correspond to the reducing species and the dotted lines to the oxidizing species [69].

A similar indicator of reversible electron transfer is called the current function, whose value is given by ($i_p/v^{1/2}$). The current function should be constant for all scan rates for which the electron transfer is fast enough to maintain the equilibrium ratio between the reduced and the oxidized forms of the redox couple predicted by the Nernst equation.

At this point, it is instructive to note that when describing electrochemical reversibility it is important to consider not only the value of $k^o$ (standard rate constant), but the scan rate for which Nernstian equilibrium cannot be maintained at the electrode surface. At these scan rates, the observed voltammetry will display characteristics of quasireversible or irreversible behaviour, such as the spreading out of voltammetric peaks over wider potential ranges, decreased peak currents, and increased values for $\Delta E_p^{\,2}$.

### 4.2.1.2. Irreversible and Quasi-reversible Systems

For irreversible processes (those with sluggish electron exchange), the individual peaks are reduced in size and widely separated. Totally irreversible systems are characterized by a shift of the peak potential with the scan rate:

$$E_p = E^{\circ} - \frac{RT}{\alpha n_a F}[0.78 - \ln\frac{k^{\circ}}{D^{1/2}} + \ln(\frac{\alpha n_a F \upsilon}{RT})^{1/2}] \qquad (34)$$

where $\alpha$ is the transfer coefficient, and $n_a$ is the number of electrons involved in the charge-transfer step. Thus, $E_p$ occurs at potentials higher than $E^o$, with the overpotential related to $k^o$ (standard rate constant) and $\alpha$, independent of the $k^o$ value, such peak displacement can be compensated by an appropriate change of the

scan rate. The peak potential and the half-peak potential (at 25 °C) will differ by $48/\alpha n$ mV. Hence, the voltammogram becomes more drawn-out as $\alpha n$ decreases.

The peak current, given by:

$$i_p = (2.99 * 10^5) n(\alpha n_a)^{1/2} AC^* D^{1/2} v^{/2} \qquad (35)$$

Is still proportional to the bulk concentration, but will be lower in height (depending upon the value of v). Assuming a value of 0.5, the ratio of the reversible-to-irreversible current peaks is 1.27 (*i.e.,* the peak current for the irreversible process is about 80 % of the peak for a reversible one). For quasi-reversible systems the current is controlled by both the charge transfer and mass transport. The shape of the cyclic voltammogram is a function of the ratio $k^0 / \left(\pi vnFD / RT\right)^{1/2}$. As the ratio increases, the process approaches the reversible case. For small values of it, the system exhibits an irreversible behaviour. Overall, the voltammograms of a quasi-reversible system are more spreader out and exhibit a larger separation in peak potentials compared to a reversible system.

### *4.2.2. Differential-Pulse Voltammetry (DPV)*

Differential-pulse voltammetry is an extremely useful technique for measuring trace levels of organic and inorganic and it is based on its superior elimination of the capacitive/ background current. This is achieved by sampling the current twice: once before pulse application and then at the end of the pulse. The current sampling is indicated by filled circles in Figure 4.5.

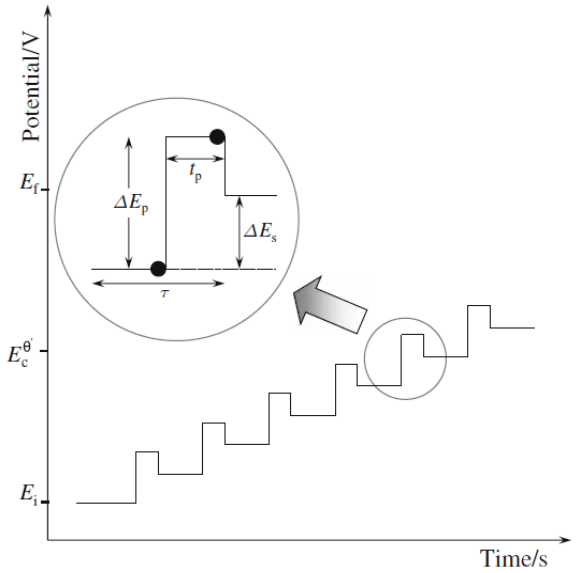


**Figure 4.5.** Potential diagram for DPV [69].

The system of this measurement is usually the same as that of standard voltammetry. The potential between the working electrode and the reference electrode is changed as a pulse from an initial potential to an inter-level potential and remains at the inter-level potential for about 5 to 100 milliseconds; then it changes to the final potential, which is different from the initial potential. The pulse is repeated, changing the final potential, and a constant difference is kept between the initial and the inter-level potential. The value of the current between the working electrode and auxiliary electrode before and after the pulse are sampled and their differences are plotted versus potential [69].

The DPV technique can be used to study the redox properties of extremely small amounts of chemicals because of the following features:

– the effect of the charging current can be minimized, so high sensitivity is achieved;

– background current is extracted, so electrode reactions can be analyzed more precisely.

The main characteristics of DPV are:

– reversible reactions show symmetrical peaks, and irreversible reactions show asymmetrical peaks;

– the detection limit is about $10^{-8}$ M.

### *4.2.3. Square-Wave Voltammetry (SWV)*

Square-wave voltammetric (SWV) technique is among the most sensitive means, for the direct evaluation of concentrations; it can be widely used for the trace analysis, especially on pharmaceutical compounds [77-80]. This method is the source of a fair amount of confusion. The problem arises from the number of waveforms employed, which are frequently described as simply square-wave voltammetry.

The advantage of SWV is that a response can be found at a high effective scan rate, thus reducing the scan time. For this reason SWV is employed more often than differential pulse voltammetry (DPV) techniques. SWV is one of the fastest pulse techniques that can be applied in both electrokinetic and analytic measurements and reduce the problems with blocking of the electrode surface. Also, in comparison to both linear sweep and cyclic voltammetry, it as a much broader dynamic range and lower limit of detection because of its efficient discrimination of capacitance current. Analytical determinations can be made at concentrations as low as 10 nM. SWV is 4 and 3 times higher than the DPV response, for reversible and irreversible systems, respectively. Therefore, typical SWV measurements take only 1-5 s whereas DPV requires much longer analysis times at about 2-4 min [81].

Frequencies of 1-100 cycles per second allow the use of extremely fast potential scan rates. This speed, coupled with computer control and signal averaging, allows for experiments to be performed repetitively and increases the signal-to-noise ratio. The net current has only very small charging current contributions, and in typical experiments the total faradaic charge is much less than equivalent to a monolayer of material. That is, the system is charged very little by the perturbation. The position and shape of the net current response are remarkably insensitive to size and shape of electrode [81]. A further advantage of the current difference output is that, when the signal lies in the oxygen reduction plateau, the response due to the reduction of oxygen is subtracted out.

In square-wave voltammetry, a square-wave is superimposed on the potential staircase sweep. Oxidation or reduction of species is registered as a peak or through in the current signal at the potential at which the species begins to be oxidized or reduced. In staircase voltammetry the potential sweep is a series of stair steps (Figure 4.6). The current is measured at the end of each potential change, right before the next, so that the contribution to the current signal from the capacitive charging current is minimized. The differential current is then plotted as a function of potential, and the reduction or oxidation of species is measured as a peak or through.

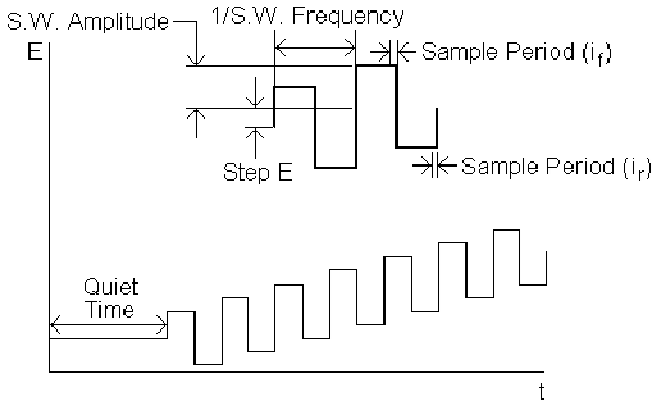


**Figure 4.6.** Square-wave form showing the amplitude of SWV [69].

### *4.2.4. Chronoamperometry (CA)*

Chronoamperometry (CA) is an electrochemical technique in which the potential of the working electrode is stepped and the resulting current from Faradaic processes occurring at the electrode (caused by the potential step) is monitored as a function of time. A stationary working electrode and unstirred solution are used. The resulting current-time dependence is monitored.

Chronoamperometry is often used for measuring the diffusion coefficient of electroactive species or the surface area of the working electrode. It can also be applied to study the mechanisms of the electrode processes.

#### 4.2.4.1. Pulsed amperometric detection (PAD)

Johnson and coworkers [82, 83] were the first to introduce pulsed amperometric detection as an electroanalytical technique (PAD) using platinum electrodes. They used it for the detection of alcohols, formic acid, and cyanide in flow-injection systems [84]. Later, Johnson and other researchers also developed PAD methods for amino acids, aldehydes, carbohydrates, sulphite, and sulphide [85-87]. Following the first reports [82, 83], a number of interesting and important articles appeared in the literature discussing different aspects and applications of the triple-pulse potential waveform or pulsed amperometric detection (PAD) [88-96].

Pulsed amperometric detection (PAD) is an excellent method for quantitative detection of numerous organic compounds that adsorb at noble metal electrodes but cannot be detected satisfactorily by conventional amperometry at constant applied (dc) potential. PAD relies on repeated applications of a multiple-pulse (mostly triple pulse) waveform consisting of regeneration/ detection, oxidation and reduction potentials. The last two of those three steps are designed for electrode cleaning. The first of the three steps usually combines regeneration of the electrode surface with a short period of signal acquisition by integration of currents resulting from the detection enabling electrode reaction. The second step should remove all reaction products and the third step restores the oxidation state of electrode surface for the detection enabling electrode reaction of analytes of interest. Many different waveforms have been reported for the detection with platinum electrodes.

Fig. 4.7 presents a schematic diagram of PAD waveform.

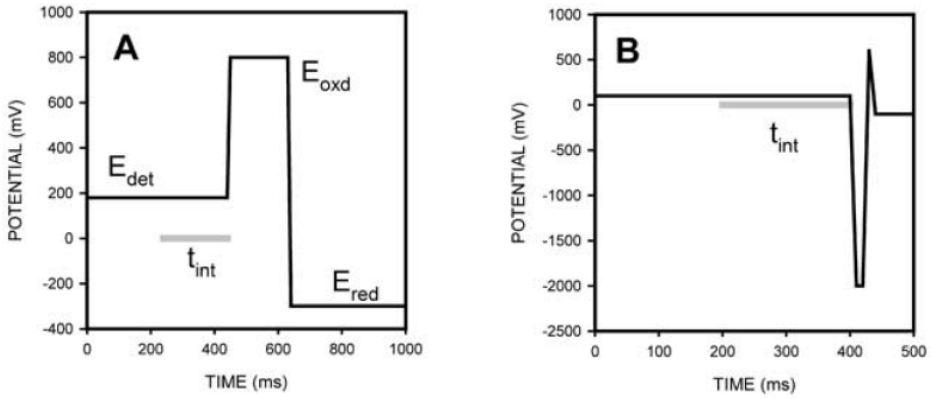


**Figure 4.7.** Schematic of the PAD waveform [69].

## 4.3. References

[1] E. Butler, H. Yung-Tse, Y.R. Yu-Li, M.S. Al Ahmad, Water 3 (2011) 495.
[2] E. Brillas, P.L. Cabot, J. Casado, M. Tarr, (Ed.) Marcel Dekker, New York, (2003) 235.
[3] G. Chen, Sep. Purif. Technol. 38 (2004) 11.
[4] N. Daneshvar, A. Oladegaragoze, N. Djafarzadeh, J. Hazard. Mater. 129 (2006) 116.
[5] N. Daneshvar, A.R. Khataee, A.R.A. Ghadim, M.H. Rasoulifard, J. Hazard. Mater. 148 (2007) 566.
[6] P. Canizares, C. Jimenez, F. Martinez, C. Saez, M.A. Rodrigo, Ind. Eng. Chem. Res. 46 (2007) 6189.
[7] J.A. Alinsafi, M. Khemis, M.N. Pons, J.P. Leclerc, A. Yaacoubi, A. Benhammou, A. Nejmeddine, Chem. Eng. Process. 44 (2005) 461.
[8] J. Gregory, J. Duan, Pure Appl. Chem. 73 (2001) 2017.
[9] W.L. Chou, C.T. Wang, K.Y. Huang, T.C. Liu, Desalination 271 (2011) 55.
[10] A. Deshpande, K.S. Lokesh, R.S. Bejankiwar, T.P.H. Gowda, J. Environ. Sci. Eng. 47 2005 21.

[11] A.M. Deshpande, S. Satyanarayan, S. Ramakant, J. Environ. Eng. 135 (2009) 716.
[12] M. Boroski, A.C. Rodrigues, J.C. Garcia, L.C. Sampaio, J. Nozaki, N. Hioka, J. Hazard. Mater. 162 (2009) 448.
[13] A. El-Ghenymy, J.A. Garrido, F. Centellas, C. Arias, P.L. Cabot, R.M. Rodríguez, E. Brillas, J. Phys. Chem. 116 13 (2012) 3404.
[14] I. Sires, C. Arias, P.L. Cabot, F. Centellas, J.A. Garrido, R.M. Rodriguez, E. Brillas, Fenton. Chemosphere 66 (2007) 1660.
[15] E.Guinea, C. Arias, P.L. Cabot, J.A. Garrido, R.M. Rodriguez, F. Centellas, E. Brillas, Water Res. 42 (2008) 499.
[16] M. Skoumal, C. Arias, P.L. Cabot, F. Centellas, J.A. Garrido, R.M. Rodriguez, E. Brillas, Chemosphere 71 (2008) 1718.
[17] M. Skoumal, R.M. Rodriguez, P.L. Cabot, F. Centellas, J.A. Garrido, C. Arias, E. Brillas, Electrochim. Acta 54 (2009) 2077.
[18] E. Guinea, J.A. Garrido, R.M. Rodriguez, P.L. Cabot, C. Arias, F. Centellas, E. Brillas, Electrochim. Acta 55 (2010) 2101.
[19] X. Zhao, J. Qu, H. Liu, Z. Qiang, R. Liu, C. Hu, Appl. Catal. B-Environ. 91 (2009) 539.
[20] C.A. Martinez-Huitle , E. Brillas, Appl. Catal. B-Environ. 87 (2009) 105.
[21] G. Chen, Separation and Purification Technology 38 (2004) 11.
[22] C. Comninellis, Electrochim. Acta 39 (1994) 1857.
[23] M. Gattrell, D.W. Kirk, Can. J. Chem. Eng. 68 (1990) 997.
[24] O.J. Murphy, G.D. Hitchens, L. Kaba, C.E. Verostko, Water Res. 26 (1992) 443.
[25] L. Szpyrkowicz, J. Naumczyk, F. Zilio-Grandi, Toxicol. Environ. Chem. 44 (1994) 189.
[26] N.N. Rao, K.M. Somasekhar, S.N. Kaul, L. Szpyrkowicz, J. Chem. Technol. Biotechnol. 76 (2001) 1124.
[27] J.L. Boudenne, O. Cerclier, Water Res. 33 (1999) 494.
[28] A.M. Polcaro, S. Palmas, Ind. Eng. Chem. Res. 36 (1997) 1791.
[29] N.S. Abuzaid, Z. Al-Hamouz, A.A. Bukhari, M.H. Essa, Water Air Soil Poll. 109 (1999) 429.
[30] C.S. Hofseth, T.W. Chapman, J. Electrochem. Soc. 146 (1999) 199.
[31] **S. Motoc**, F. Manea, A. Pop, A. Baciu, G. Burtica, R. Pode, Environ. Eng. Manag. J. (2012) in press.
[32] **S. Motoc**, F. Manea, A. Pop, A. Baciu, G. Burtică, R. Pode, WIT Transactions on Ecology and the Environment (2012) 323.
[33] **S. Motoc,** F. Manea, A. Pop, R. Pode, G. Burtica, The 17th Int. Symp. on Analytical and Environmental Problems (2011) 396.
[34] J. Naumczyk, L. Szpyrkowicz, M.D.D. Faveri, F. Zilio-Grandi, Process Saf. Environ. (1996) 59.
[35] A.G. Vlyssides, C.J. Israilides, M. Loizidou, G. Karvouni, V. Mourafeti, Water Sci. Technol. 36 2–3 (1997) 271.
[36] S.H. Lin, C.L. Wu, J. Environ. Sci. Health A 32 (1997) 2125.
[37] E. Brillas, R. Sauleda, J. Casado, J. Electrochem. Soc. 144 (1997) 2374.
[38] E. Brillas, R. Sauleda, J. Casado, J. Electrochem. Soc. 145 (1998) 759.
[39] E. Brillas, E. Mur, R. Sauleda, L. Sanchez, F. Peral, X. Domenech, J. Casado, Appl. Catal. B Environ. 16 (1998) 31.
[40] W. El-Shal, H. Khordagui, O. El-Sebaie, F. El-Sharkawi, G.H. Sedahmed, Desalination 99 (1991) 149.

[41] J.C. Farmer, F.T. Wang, R.A. Hawley-Fedder, P.R. Lewis, L.J. Summers, L. Foiles, J. Electrochem. Soc. 139 (1992) 654.
[42] R.G. Hickman, J.C. Farmer, F.T. Wang, Mediated, ACS Symposium Series 518, Emerging Technologies in Hazardous Waste Management III, Am. Chem. S. (1993) 430.
[43] F. Bringmann, K. Ebert, U. Galla, H. Schmieder, J. Appl. Electrochem. 25 (1995) 846.
[44] A. Paire, D. Espinoux, M. Masson, M. Lecomte, Radiochim. Acta 78 (1997) 137.
[45] J.R.Dominguez, T. Gonzalez, P. Palo, J. Sanchez-Martin, Chem. Eng. J. 162 (2010) 1012.
[46] T. Gonzalez, J.R. Dominguez, P. Palo, J. Sanchez-Martin, J. Chem. Technol. Biotechnol. 86 (2010) 121.
[47] I. Sires, P.L. Cabot, F. Centellas, J.A. Garrido, R.M. Rodriguez, C. Arias, E. Brillas, Electrochim. Acta 52 (2006) 75.
[48] E. Brillas, I. Sires, C. Arias, P.L. Cabot, F. Centellas, R.M. Rodriguez, J.A. Garrido, Chemosphere 58 (2005) 399.
[49] E. Brillas, S. Garcia-Segura, M. Skoumal, C. Arias, Chemosphere 79 (2010) 605.
[50] K. Waterston, J.W. Wang, D. Bejan, N.J. Bunce, J. Appl. Electrochem. 36 (2006) 227.
[51] S. Li, D. Bejan, M.S. McDowell, N.J. Bunce, J. Appl. Electrochem. 38 (2008) 151.
[52] L. Ciriaco, C. Anjo, J. Correia, M. Pacheco, A. Lopes, Electrochim. Acta 54 (2009) 1464.
[53] M.D. Vedenyapina, Y. Eremicheva, V.A. Pavlov, A.A. Vedenyapin, Russ. J. Appl. Chem. 81 (2008) 800.
[54] H. Zhang, F. Liu, X. Wu, J. Zhang, D. Zhang, Asia Pac. J. Chem. Eng. 4 (2009) 568.
[55] D. Weichgrebe, E. Danilova, K.H. Rosenwinkel, A.A. Vedenjapin, M. Baturova, Water Sci. Technol. 49 4 (2004) 201.
[56] J. Boudreau, D. Bejan, N.J. Bunce, Can. J. Chem. 88 (2010) 418.
[57] X. Zhao, Y. Hou, H. Liu, Z. Qiang, Electrochim. Acta 54 (2009) 4172.
[58] C. Jara, D. Fino, V. Specchia, G. Saracco, P. Spinelli, Appl. Catal. B Environ. 70 (2007) 479.
[59] G. Perez, A.R. Fernandez-Alba, A.M. Urtiaga, I. Ortiz, Water Res. 44 (2010) 2763.
[60] J. Radjenovic, A. Bagastyo, R.A. Rozendal, Y. Mu, J. Keller, K. Rabaey, Water Res. 45 (2011) 1579.
[61] I. Troster, L. Schafer, M. Fryda, New Diam. Front. C. Technol. 12 2 (2002) 89.
[62] B. Marselli, J. Garcia-Gomez, P.A. Michaud, M.A. Rodrigo, C. Comninellis, J. Electrochem. Soc. 150 (2003) D79.
[63] K. Rajeshwar, J.G.Ibanez, Environmental Electrochemistry, Academic Press, 1997.
[64] C.A.C. Sequeira, Environmental Oriented Electrochemistry, Elsevier, 1994.
[65] K. Rajeshwar, J.G. Ibanez, Environmental Electrochemistry: Fundamentals and Applications in Pollution Sensors and Abatement, Elsevier Science & Technology Books, 1997.
[66] L. Codognoto, S.A.S. Machado, L.A. Avaca, Diam. Relat. Mater. 11 (2002) 1670.

[67] V.A. Pedrosa, L. Codognoto, L.A. Avaca, Quim. Nova 26 (2003) 844.
[68] D. Souza, S.A.S. Machado, L.A. Avaca, Quim. Nova 26 (2003) 81.
[69] F. Scholz, Electroanalytical Methods-Guide to Experiments and Applications Second, Revised and Extended Edition, Springer Heidelberg Dordrecht London New York, 2010.
[70] W. Guo, H. Lin, L. Liu, J. Song, J. Pharm. Biomed. Anal. 34 (2004) 1137.
[71] J.A. Acuna, C. de la Fuente, M.D. Vazquez, M.L. Tascon, M.I. Gomez, F. Mata, P.S. Batanero, J. Pharm. Biomed. Anal. 29 (2002) 617.
[72] L. Huang, L. Bu, F. Zhao, B. Zeng, J. Solid State Electr. 8 (2004) 976.
[73] A. Baciu, F. Manea, A. Remes, **S. Motoc**, G. Burtica, R. Pode, Environ. Eng. Manag. J. 9 11 (2010) 1555.
[74] B. Dogan, S.A. Ozkan, B. Uslu, Anal. Lett. 38 (2005) 641.
[75] S. Bollo, L.J. Nunez-Vergara, J.A. Squella, J. Electroanal. Chem. 562 (2004) 9.
[76] J. Wang, Analytical Electrochemistry, Third Edition, Wiley-VCH, 2006.
[77] B. Uslu, B. Dogan-Topal, S.A. Ozkan, Talanta 74 (2008) 1191.
[78] B. Dogan-Topal, B. Uslu, S.A. Ozkan, P. Zuman, Anal. Chem. 80 (2008) 209.
[79] B. Dogan-Topal, S. Tuncel, B. Uslu, S.A. Ozkan, Diam. Relat. Mater. 16 (2007) 1695.
[80] B. Dogan-Topal, B. Uslu, S.A. Ozkan, Comb. Chem. High T. Scr. 10 (2007) 571.
[81] B. Dogan-Topal, S.A. Ozkan, B. Uslu, The Analytical Applications of Square Wave Voltammetry on Pharmaceutical Analysis, The Open Chemical and Biomedical Methods Journal 3 (2010) 56.
[82] S. Hughes, P.L. Meschi, D.C. Johnson, Anal. Chim. Acta 132 (1981) 1.
[83] S. Hughes, D.C. Johnson, Anal. Chim. Acta 132 (1981) 11.
[84] J.A. Polta, D.C. Johnson, Anal. Chem. 57 (1985) 1373.
[85] D.S. Austin, J.A. Polta, T.Z. Polta, A.P.-C. Tang, T.D. Cabelka, D.C. Johnson, J. Electroanal. Chem. 168 (1984) 227.
[86] D.C. Johnson, D. Dobberpuhl, R. Roberts, P. Vandeberg, J. Chromatogr. 640 (1993) 79.
[87] J. Cheng, P. Jandik, X. Liu, C. Pohl, J. Electroanal. Chem. 608 (2007) 117.
[88] S. Hughes, D.C. Johnson, J. Agric. Food Chem. 30 (1982) 712.
[89] S. Hughes, D.C. Johnson, Anal. Chim. Acta 149 (1983) 1.
[90] G.G. Neuburger, D.C. Johnson, Anal. Chem. 59 (1987) 150.
[91] W.R. LaCourse, W.R. Johnson, D.C. Carbohydr. Res. 215 (1991) 159.
[92] D.C. Johnson, W.R. LaCourse, Electroanalysis 4 (1992) 367.
[93] R.E. Roberts, D.C. Johnson, Electroanalysis 6 (1994) 269.
[94] R.D. Rocklin, T.R. Tullsen, M.G. Marucco, J. Chromatogr. A. 671 (1994) 109.
[95] R.E. Roberts, D.C. Johnson, Electroanalysis 7 (1995) 1015.
[96] J. Wen, R.M. Cassidy, A.S. Baranski, J. Chromatogr. A 811 (1998) 181.

# CHAPTER 5. CARBON BASED ELECTRODES

Procedures in electroanalysis strongly depend on electrode material aspects, such as: chemical and physical properties of electrode surfaces, the effects of applied potential, adsorption, and coatings applied to the electrode surface to enhance the detection. Carbon-based materials usually have a wider potential range than the solid metal electrodes. The principal requirements for a good electrode material suitable for the electroanalysis are long-term stability, low residual current and wide potential range.

Carbon is useful electrode material, particularly characterized by high current densities, wide potential range and long term stability were desired.

Carbon-based electrodes are generally low cost and they are available in a variety of forms. Carbon has a rich surface chemistry. The slow kinetics of carbon oxidation leads to a wide useful potential range, especially in the anodic direction [1]. This specification is an important advantage over metal electrodes. Carbon-based electrodes exhibit significantly lower background oxidation currents compared to the metal electrodes. Carbon-based electrodes are currently in widespread use in electroanalytical chemistry, because of their broad potential window, low cost, rich surface chemistry, low background current, chemical inertness, and suitable for a lot of difficult applications.

## 5.1. Carbon paste electrodes

Carbon paste electrodes are mixtures prepared from graphite powder and various water-immiscible organic liquids of nonelectrolytic character. This kind of carbon paste electrodes are classified as bare or unmodified carbon electrodes [2].

After thorough mixing, the paste is packed into a small inert holder with electrical contact at the back. In fact, a major reason for developing carbon paste electrodes was the ease of surface renewal and reproducibility.

Carbon paste electrodes have some special characteristics and benefits, such as [2]:

- very low background currents (favorable signal- to-noise ratio);
- individual polarizability (with variable potential window);
- specific reaction kinetics (affected by both carbon paste constituents);
- electrode activity at the carbon paste surface as well as in the carbon paste bulk;
- variability in using various interactions and their synergistic effects (electrolysis, catalysis, adsorption, extraction, ion-pairing, and their combination);
- various alternative procedures for pretreating, conditioning and regenerating the electrode surface and carbon paste itself.

Electrodes themselves do not possess selectivity, except the direction of the applied potential. However, by modifying the electrode in a different style and degrees of selectivity may be introduced into the electrode itself. The carbon paste electrode can very easily be modified. In general, the main reason to modify carbon paste electrode is to obtain a new sensor with desired, often predefined properties.

Because of these reasons, carbon pastes are one of the most convenient materials for the preparation of modified electrodes used for pharmaceutical compounds determination [3-7]. However, the disadvantage of carbon paste electrodes is the tendency of the organic binder to dissolve in solutions containing an appreciable fraction of organic solvent.

## 5.2. Glassy Carbon Electrode

Glassy carbon (also known as vitreous carbon) is a class of non-graphitizing carbon that is widely used as an electrode material in electrochemistry and for high temperature crucibles. Glassy carbon is used very commonly because of its excellent mechanical and electrical properties, wide potential range, chemically inert nature, and impermeability to gases (practically gas-tight), and exhibits an extremely low porosity, conducts electricity and contains trace amount of gaseous and other impurities. It is easily mounted, punishable and compatible with all common solvents [8].

It is also highly resistant to acidic corrosion. Glassy carbon possesses isotropic properties and does not require a particular orientation in the electrode device. The rates of oxidation of certain glassy carbon in oxygen, carbon dioxide or water vapour are lower than those of any other carbon [9].

Reticulated vitreous carbon is an unusual variant of glassy carbon but it is highly porous [10], and chemically similar to the conventional glassy carbon. It has low density, a low thermal expansion, a high corrosion resistance, and high thermal and electrical conductivities. It has a low resistance to fluid flow, high surface area combined with self supporting rigidity and resistance to very high temperatures in non-oxidizing environments. It has exceptional chemical inertness over a very wide temperature range. It is useful for experiments requiring high surface area, such as controlled potential electrolysis. Its oxidation resistance is unusual for the carbon. It is also highly resistant to intercalation by materials, which disintegrated graphite. Also, it is inert to a wide range of very active reagents, such as: acids, bases and organic solvents.

As shown in Figure 5.1 reticulated vitreous carbon is an open-pore (sponge-like) material, this network combine the electrochemical properties of glassy carbon with many structural and hydrodynamic advantages. Reticulated vitreous carbon is widely used as a very useful electrode material because of its high current density, low electrical/ fluid flow resistance, minimal cell volume loss to electrodes [8]. The low volumetric carbon content ensures a uniform potential and current distribution through the material [1, 8, 10]. It has continuously been used as a model electrode in the design and construction of new electrochemical cell designs, both in fundamental and applied electrochemistry. Reticulated vitreous carbon has been used as an electrode material for electrochemical cell design in flowing systems, rotating systems, disc electrodes, sensors, etc. Reticulated vitreous carbon materials can be modified by metal and conductive organic coatings and by impregnation of organic, inorganic, and biochemical species. For reactivation of theirs active surface, nearly all glassy carbon electrodes are usually polished with smaller alumina particles (~0.05 mm) on a smooth polishing cloth successively [11]. Glassy carbon electrodes are the most common carbon-based electrodes in current use. It offers many applications in many different areas, one of them is for pharmaceuticals determination [12-17].

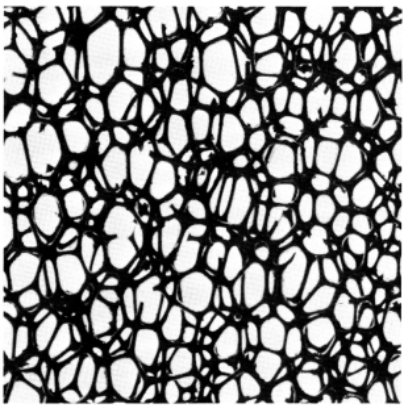

**Figure 5.1.** The open structure of reticulated vitreous carbon [8].

## 5.3. Graphite electrode

Graphite is a polymorph state of the carbon, and at surface temperatures and pressures it is the stable form of carbon. Graphite is one of the softest mineral known to man. Graphite can be produced from a wide variety of precursors, the most graphite bodies [11].

Carbon has an "amorphous" or non-ordered atomic structure, while graphite consists of parallel stacking of layers of carbon atoms in fused hexagonal rings. Graphite is soft and has a long range ordered structure in comparison to carbon. Highly ordered graphite such as pyrolytic graphite exhibits special properties. Pyrolytic graphite is very pure and exhibits anisotropic properties relative to its crystal orientation. The surface of the basal plane, in particular, is not very reactive. Its electrochemical behaviour and properties are quite similar to mercury, however, graphite has a high $H_2$ and $O_2$ over voltage with a wider potential range of stability compared to mercury [8].

Graphite composite electrodes are also members of the graphite electrodes. Graphite powder is mixed with suitable filler, and then bonded, either physically or chemically, to form a conductive solid composite, as *e.g.*, „Kel-graph" and wax-coated electrodes [11].

The application of the graphite electrode for voltammetry was improved by wax impregnation (ceresin or paraffin wax) of the electrode, by insulation and by surface renewal by lathing, and by pre-wetting of the electrode surface by a dilute solution of wetting agents. A common approach is impregnation with ceresin or paraffin wax, leading to the wax impregnated graphite electrode. Wax impregnated graphite electrode is similar to the carbon paste electrode in its composition, composite nature and its electroanalytical behaviour. However, wax impregnated graphite electrode is not as widely used as carbon paste, glassy carbon. Wax impregnated graphite electrode has a relatively high surface activity towards oxygen yielding at the edge of the aromatic plane due to several functional groups, such as hydroxyl, carbonyl, carboxyl or quinonic structures. Some of these end groups may allow the chemical binding of some modifiers (enzyme, antibody, drugs, etc.) onto the electrode surface. Others, such as the quinine structure may mediate electron transfer at the electrode surface [8]. The amount and nature of end groups present in the graphite structure depend on the degree of oxidation of the graphite material.

Some researchers explored the application of graphite for pharmaceuticals determination [18-21].

## 5.4. Screen printed electrode

Screen printed electrodes are easy to use and portable with simple and inexpensive fabrication techniques. Screen printed electrode is capable of producing a wide range of geometries and can be used to print whole electrode systems, reference, working and counter electrode, each with their own tailored characteristics. Most importantly, these can be made cheaply and with a high degree of precision. Conductive carbon (graphite powder based) "inks" has been used for many years in a variety of biosensor applications [22].

This technique consists of depositing inks of different electrochemical properties on an inert substrate in a film of controlled pattern and thickness. The most attractive characteristic of screen printing technology is its versatility in being able to print large number of inks on different substrates and the possibility of mixing modifiers to the base ink. The surface of a screen printed electrode is not nearly as pristine as more traditional electrodes produced from glassy carbon or pyrolytic graphite [22].

Screen printed carbon surfaces are rough, the proprietary binder compounds found in the carbon ink may introduce stray features in voltammograms and the heterogeneous kinetics at these electrode surfaces are a bit slow. Single use screen printed electrodes have several advantages such as avoidance of contamination, elimination of problems of loss of response due to fouling of the electrode and of enzyme denaturation. Gold, chelating agents, ferrocenes or enzymes such as glucose oxidase, ascorbic acid oxidase can be incorporated into the carbon ink. The procedure has the advantage of miniaturization, versatility and cheapness and in particular lends itself to the mass production of disposable electrodes. These electrodes are used in electrochemical measurements using potentiometry, amperometry, voltammetry, and stripping methods. The main benefit of screen printed carbon electrodes over conventional carbon-based electrodes are that the problems of carry over and surface fouling are alleviated, as they are used only once and then discarded [22, 23].

The new version of screen printed carbon electrodes is called groove electrodes. Groove electrodes can be classified as hybrid electrodes with a design originating from screen printed carbon electrodes, but with electrochemical properties typical for carbon pastes governed by the presence of liquid binder in the mixture [24]. Screen printed carbon electrodes have been applied in the pharmaceuticals determination [25-30].

## 5.5. Boron doped diamond electrode

As presented in Chapter 4, the main electrochemical oxidation process could occur on the BDD electrode.

a) *Direct electrochemical oxidation,* where the organic compound degradation occurs directly over the anode trough the adsorbed •OH, or chemisorbed active oxygen in the anode surface (often called "anodic oxidation, direct oxidation or electrochemical incineration"), by means of the following general equation [31, 32].

$$M + H_2O \rightarrow M(\bullet OH) + H^+ + e^- \quad (1)$$

where the pollutants are first adsorbed on the anode surface (M) and then destroyed by the anodic electron transfer reaction.

b) *Indirect electrochemical oxidation,* where the organic compounds are treated in the bulk solution by means of species generated in the electrode, such as •OH (by means of the Fenton reaction), $Cl_2$, hypochlorite, peroxodisulfate and ozone, as the most common electrochemically generated oxidants [33, 34].

### *5.5.1. BDD anodes for wastewater treatment applications*

Synthetic boron-doped diamond, with its high anodic stability and wide potential window for water discharge has undoubtedly proved to be an excellent material for the complete combustion of organics in wastewater treatment and water disinfection. Depending on the applied potential, the oxidation of organics at BDD electrodes can follow two mechanisms: direct electron transfer in the potential region before oxygen evolution (water stability), and indirect oxidation via electrogenerated hydroxyl radicals, in the potential region of oxygen evolution (water decomposition).

In the former case, an example is the decomposition behaviour of carboxylic acid [35]. The BDD electrode does not provide an active site for the adsorption of reactants, has no electrocatalytic activity for the direct oxidation of carboxylic acids In fact, the cyclic voltammograms recorded in the presence of these organics display no significant differences from the voltammogram of the supporting electrolyte (1M $H_2SO_4$). However, another study [36] reported that a shoulder, overlapping oxygen evolution, could be observed at about 2.3V versus SCE in the voltammograms of different carboxylic acids, which suggests the possible existence of a direct electron transfer with indirect oxidation via electrogenerated hydroxyl radicals. Both studies also demonstrated that, at a fixed potential in the region of oxygen evolution, the current density increases with carboxylic acid concentration, indicating that the pathway for the oxidation of these compounds involves intermediates that are formed during oxygen evolution (indirect mechanism).

The behaviour of BDD electrodes is quite different during the oxidation of aromatic and heterocyclic compounds. Many authors have demonstrated that, in the potential region of water stability, these compounds are oxidized at the BDD anode by direct electron transfer. However, the oxidation results in the deactivation of the electrode due to the deposition of a surface film as a consequence of the polymerisation of radical products that are generated anodically. On the contrary, during electrolysis at high anodic potential, close to oxygen evolution, there is no evidence of any electrode deactivation and, moreover, the polymeric film formed in the region before oxygen evolution, is destroyed (probably it involves the production of active intermediaries, like hydroxyl radicals) and electrode activity is restored.

Similar behaviour has also been obtained during the oxidation of 2-naphthol [37], benzoic acid [32], 4-chlorophenol [38], 3-methylpyridine [39], nitrophenol [40, 41] and polyhydroxybenzene [40].

On the basis of these results, it has been proposed a mechanism for the oxidation of organics with concomitant oxygen evolution, which assumes that both organic oxidation and oxygen evolution take place on a BDD via intermediation of hydroxyl radicals, generated from the discharge of water. Considerable •OH amounts may be electrogenerated on BDD anodes. These radicals, due to their weak

interaction with the BDD film, present high reactivity towards organics (reactions 2-4), these processes have been efficiently used in wastewater treatment [31, 42].

$$BDD + H_2O \rightarrow BDD(\bullet OH) + H^+ + e^- \quad (2)$$

$$BDD(\bullet OH) + R \rightarrow BDD + mCO_2 + nH_2O \quad (3)$$

According to the literature, reaction (3) is in competition with the side reaction of free •OH discharge to $O_2$ without any participation of BDD surface, following the next reaction:

$$BDD(\bullet OH) \rightarrow BDD + ½O_2 + H^+ + e^- \quad (4)$$

However, many authors have reported that during incineration process of BDD anodes at high potentials, a great number of organic pollutants are completely mineralized by the reaction with electrogenerated free •OH species [43].

So far, many papers have reported that during electrolysis at BDD electrodes at high potentials, a large number of organic pollutants including pharmaceutical compounds [44] are completely mineralized by the reaction with electrogenerated OH• radicals. It has been shown that the oxidation is controlled by the diffusion of the pollutants towards the electrode surface, where the hydroxyl radicals are produced, and the current efficiency is favoured by a high mass-transport coefficient, high organic concentration and low current density. Performing electrolysis in optimized conditions, without diffusion limitation, the current efficiency approaches 100 % [35].

The investigation of the behaviour of Si/BDD anodes has been reported for the oxidation of a wide range of pollutants [31, 32, 37-41, 45, 46], and complete mineralization was obtained with all the experimental conditions studied, and the current efficiency was influenced by the initial concentration and applied current. In particular, for high organic concentrations and low current densities, the COD decreased linearly and the Instantaneous Current Efficiency (ICE) remained about 100 %, indicating a kinetically controlled process, while for low organic concentrations or high current densities, the COD decreased exponentially and the ICE began to fall due to the mass-transport limitation and the side reactions of oxygen evolution. In order to describe these results, the authors developed a comprehensive kinetic model that allowed them to predict the trend of the COD and current efficiency for the electrochemical combustion of the organic with BDD electrodes and estimate the energy consumption during the process [35]. The formulation of the model was based on the estimation of the limiting current density from the value of the COD using the relationship:

$$i_{lim}(t) = 4Fk_mCOD(t) \quad (5)$$

where $i_{lim}$ is the limiting current density ($Am^{-2}$) at a given time $t$, 4 the number of exchanged electrons per mol of $O_2$, $F$=Faraday's constant ($C\ mol^{-1}$), $k_m$ the average mass transport coefficient in the electrochemical cell ($ms^{-1}$) and COD the chemical oxygen demand ($molO_2\ m^{-3}$) at a given time $t$.

Depending on the applied current density, and the limiting current density two different operating regimes were identified:

- $i_{appl} < i_{lim}$, the concentration of the organic was sufficiently high and the electrolysis was under current-limit control, the current efficiency was 100 % and the COD decreased linearly over time.

- $i_{appl} > i_{lim}$, the electrolysis was under mass-transport control, secondary reactions (such as oxygen evolution) commenced, resulting in a decrease in the current efficiency. In this regime the COD removal followed an exponential trend due to the mass-transport limitation.

### *5.5.2. BDD electrodes use in electroanalytical applications*

In electroanalytical applications, both bare and modified diamond electrodes can be used depending on the specific analytic task. A lot of work has been done in the last years concerning electroanalytical applications of diamond electrodes [47-53].

The special properties of doped diamond electrodes that make them especially well suited for electroanalytical applications:

— An extremely wide potential window in aqueous and nonaqueous electrolytes: in the case of high-quality diamond;

— Hydrogen evolution commences at about −1.25V versus SHE and oxygen evolution at +2.3V versus SHE, then the potential window may exceed 3V;

— The width of the window decreases with the quality of the film and the incorporation of non-diamond $sp^2$ carbon impurities, and its response resembles that obtained from glassy carbon and highly oriented pyrolytic graphite [54, 55];

— Corrosion stability in very aggressive media: the morphology of diamond electrodes is stable during long-term cycling from hydrogen to oxygen evolution even in acidic fluoride media [56, 57];

— An inert surface with low adsorption properties and a strong tendency to resist deactivation: the voltammetric response towards ferri/ ferrocyanide is remarkably stable for up to 2 weeks of continuous potential cycling [58];

— Very low double-layer capacitance and background current: the diamond-electrolyte interface is ideally polarisable and the current between −1000 and +1000 mV versus SCE is <50 $Acm^{-2}$. The double-layer capacitance is up to one order of magnitude lower than that of glassy carbon [59].

Even if contains low levels of nitrogen, boron, and other elements as dopants, natural diamond is essentially electrically insulating. Synthetic high purity diamond is one of the best insulator materials known with a break down voltage of up to 109 $Vm^{-1}$. However, boron-doping allows diamond to be turned into a good electrical conductor. A low temperature metal-to-insulator transition occurs at a boron-doping level of 3.92 x $10^{21}$ $cm^{-3}$. However, room temperature conductor and semi-conductor properties are observed already at much lower doping levels. Good conductivity and electrochemical properties are possible with a boron-doping level of typically $10^{20}$ $cm^{-3}$, which corresponds to about one boron atom per 1000 carbon atoms. The mobility of charge carriers in diamond is high enough to allow current to flow [60].

Several electroanalytical methods for the quantitative determination of the pharmaceuticals have been reported *e.g.*, paracetamol [61, 62], caffeine [61], cysteine [63], captopril [64], lidocaine [65], hormone [66], acetylsalicylic acid [67], acetaminophen [68], ascorbic acid [68].

## 5.6. Carbon nanofiber electrode

Carbon nanofibers (CNF) are produced from the catalytic decomposition of hydrocarbon gases or carbon monoxide over selected metal particles that include iron, cobalt, nickel, and some of their alloys at high temperatures. They are hollow cylinders with diameters around one hundred nanometers and lengths of a few tens of microns arranged as stacked cones, cups, or plates [69]. The mechanical strength and electronic properties of CNFs are similar to CNTs. The advantages of carbon nanofibers over carbon nanotubes are due to a dramatic cost difference and the fact that carbon nanofibers have grapheme edge planes, which are ledges of carbon that protrude from the surface of the nanofibers at regular intervals leading to easier physical bonding with other materials. This property is very useful when creating integrated composites of polymers and carbon fibers. They have a 2 to 100 time larger diameter compared to MWCNT or SWCNT and are less crystalline (with a kind of cup-stacked or stacked coin structure) [70]. Based on its high surface area, this electrode is suitable for various applications, *e.g*. for energy storage [71], in electroanalysis [72], or as support for catalysts [73].

Their use in electrochemical sensors is based on the fact that these materials can play dual roles. They can be used as immobilization matrix for special molecules and at the same time they are used as a transducer to produce the electrochemical signal [69].

In 2001, carbon nanofibers with diameters in the range of 10–500 nm were introduced as novel electrode materials for electrochemical applications for the first time [74].

Carbon nanofibers can be classified in nanoporos and nonporous nanocomposite electrode. The nonporous electrode was applied successfully in the cathodic deposition and anodic stripping of Pb metal. This study showed that carbon nanofiber materials have potential use in electroanalytical applications. At the nanoporous type, electrode surface behaved more like an assembly of microelectrodes than a planar electrode. This electrode was successfully applied for detection of zinc in 1.0 M HCl and the best signal to noise ratio was achieved for the scan rate of 40 $Vs^{-1}$. In the recent years, carbon nanofibers have been applied for pharmaceuticals determination [75-79].

## 5.7. Carbon nanotube electrode

Carbon nanotubes are cylindrical fullerenes. Carbon nanotubes are excellent electrode materials due to their good electrical conductivity, mechanical strength and a wide operational potential window. These tubes of carbon are usually only a few nanometers wide, but they can range from less than μm to several mm in length. The carbon nanotubes have closed topology and tubular structure that are typically a few nm in diameter and many μm in length [80].

Their unique molecular structure results in unique macroscopic properties, including high tensile strength, high electrical conductivity, high resistance to heat, and chemical inactivity. Based on the extraordinary properties presented above, carbon nanotubes have been used in a range of applications [81, 82], such as high sensitivity microbalances [83], gas detectors [84, 85], catalyst supports [86], electron sources in field emission-mode displays [87], tiny tweezers for nanoscale manipulation [88], and probe tips for scanning probe microscopy [89].

It can be divided into single-walled carbon nanotubes and multi-walled carbon nanotubes. Single-walled carbon nanotubes are composed of a single

graphite sheet rolled seamlessly with 1-2 nm diameter tube. Multiwalled carbon nanotubes are made of coaxial tubules each formed with a rolled graphite sheet, with diameters varying between 2-50 nm. Both types of carbon nanotubes have cylindrical shapes [8, 90-93]. A comparison between SWCNT and MWCNT is presented in Table 5.1. CNTs behave as either metals or semiconductors, depending on the diameter and the degree of helicity [94]. They are suitable for the modification of various electrodes due to their high electronic conductivity for the electron transfer reactions and better electrochemical and chemical stabilities in both aqueous and non-aqueous solutions [95]. Furthermore, construction of efficient electrochemical sensors using the CNTs-modified electrodes is very promising in that they promote electron-transfer reactions in several small biologically important molecules and large biomolecules [96, 97].

**Table 5.1.** Comparison between SWCNT and MWCNT [98].

| SWNT | MWNT |
|---|---|
| Single layer of grapheme | Multiple layer of grapheme |
| Catalyst is required for synthesis | Can be produced without catalyst |
| Bulk synthesis is difficult as it requires proper control over growth and atmospheric condition | Bulk synthesis is easy |
| Purity is poor | Purity is high |
| A chance of defect is more during functionalization | A chance of defect is less but once occurred it's difficult to improve |
| Less accumulation in body | More accumulation in body |
| Characterization and evaluation is easy<br>It can be easily twisted and are more pliable | It has very complex structure |

Carbon nanotubes have some advantages for the applications, *e.g.*, small size with larger surface, high sensitivity, fast response, and enhanced electron transfer when used as electrodes in electrochemical reactions [99, 100]. Usually, modified carbon nanotubes exhibit good electroanalytical results. Modifications on the carbon nanotube electrodes can be divided into two sections, electrochemical and chemical [99, 100].

Their unique surface area, stiffness, strength and resilience have led to much excitement in the field of pharmacy compound determination [101-107].

Much effort has been made in the development of a highly sensitive and selective method for the detection of dopamine (DA), which is one of the important catecholamine neurotransmitters in the mammalian central nervous system. Conventional electrodes are not suitable for the determination of DA due to the interference from ascorbic acid (AA) and uric acid (UA), which are co-existed in a real sample at 100 times higher concentration than DA. These compounds can be easily oxidized at the similar potential of DA and thus always interfere with DA detection. A CNT-polymer composite-modified electrode, with poly (styrenesulfonic acid) sodium salt and SWCNTs, were used for selective detection of DA [105].

The negatively charged poly (styrene sulfonic acid) sodium salt attracted positively charged DA in pH 7 PBS and selectively detected it from the interference of AA.

The merits of CNT-based sensors will bring dramatic changes to future sensor industry because of the continuous growing research interest in this field.

## 5.8. Zeolite modified electrodes

The term ''zeolite'' was initially used to designate a family of natural minerals that presented as particular properties the exchange of cations and the reversible desorption of water. This latter property gave origin to the generic name of zeolite [108].

Zeolites can be natural and synthetic minerals with common structural characteristics. The natural ones are formed in a variety of geological sites and from precursors, such as volcanic ash, clay, biogenic silica and different forms of quartz [109]. Zeolites are hydrated aluminosilicates belonging to the family of the tectosilicates, where the $SiO_4$ tetrahedra form three-dimensional supercages [109]. The negative sites are balanced by counterions, usually alkaline and alkalineearth cations, which can be substituted by other cations, thus, providing zeolites with the property of ion exchange.

The natural zeolites have been used for environmental remediation (organic compounds and heavy-metal ions. Also, natural zeolites have been found to be helpful in the control of malodours (*e.g.*, hydrogen sulphide and ammonia) emanating from confined livestock-rearing areas, kennels, pet shops, zoos and pet-litter trays. Their high surface area, and therefore their high adsorption capacity, as well as their ion-exchange properties make them very useful in these fields [110-114].

Another important inherent property of aluminosilicate zeolites is their catalytic action due to their strongly acidic nature (for example their technological importance in the petroleum industry) [115]. Some of the principal advantages of zeolites are their low cost of extraction, their availability in great volumes, and their excellent stability in chemical and thermal processes. They can also be submitted to diverse treatments in order to give them desired physical and chemical properties. These properties make zeolites an important material in electrochemistry.

The hydrophilic character of zeolites makes them materials well suited to the co-immobilization of enzymes and mediators in the preparation of biosensors [116].

Metal ion-doped zeolites allow exploitation of the ion exchange capacity of zeolites for the development of electrochemical sensors. Ion doped zeolite-modified electrodes have been developed for the determination of various compounds, *e.g.,* urea [117], phenol [118], nitrite/ nitrate [119], glycerol [120].

Carbon based composite electrodes (nanotubes, nanofibers or expanded graphite) electrodes modified with silver-doped zeolites are likely candidates for sensing pharmaceutical compounds [121-124].

## 5.9. References

[1] P.T. Kissinger, W.R. Heineman, (1996) Laboratory Techniques in Electroanalytical Chemistry, 2nd ed.; Marcel Dekker: New York.
[2] I. Svancara, K. VytRas, J. Barek, J. Zima, Critical Reviews in Anal. Chem. 31 4 (2010) 311.
[3] M. Behpour, E. Honarmand, S.M. Ghoreishi, Bull. Korean Chem. Soc. 31 4 (2010) 845.
[4] M. Behpour, S.M. Ghoreishi, E. Honarmand, Int. J. Electrochem. Sc. 5 (2010) 1922.
[5] D. Boyd, J.R.B. Rodriguez, P.T. Blanco, M.R. Smyth, J. Pharmaceut. Biomed. 12 9 (1994) 1069.

[6] M.T. Fernandez-Abedul, M.S. Velázquez-Rodriguez, J.R. Barreira-Rodriguez, A. Costa-Garcia, Anal. Lett. 30 8 (1997) 1491.
[7] A.R. Fiorucci, T.G. Cavalheiro, J. Pharmaceut. Biomed. 28 (2002) 909.
[8] J. Wang., Analytical Electrochemistry, 2nd ed. Wiley-VCH New York (2000).
[9] A.T. Markas, G. Hart, J.P. Hart, Analyst 120 1995.
[10] J.M. Friedrich, C. Ponce-de-Leon, G.W. Reade, F.C. Walsh, J. Electroanal. Chem. 561 (2004) 203.
[11] B. Uslua, S.A. Ozkana, Anal. Lett. 40 5 (2007) 817.
[12] F.F. Gaal, V.J. Guzsvany, L.J. Bjelica, J. Serb. Chem. Soc. 72 12 (2007) 1465.
[13] A.Liu, S. Zhang, L. Huang, Y. Cao, H. Yao, W. Chen, X. Lin, Chem. Pharm. Bull. 56 6 (2008) 745.
[14] S.S. Kalanur, J. Seetharamappa, P.G. Mamatha, M.D. Hadagali, P.B. Kandagal, Int. J. Electrochem. Sc. 3 (2008) 756.
[15] H. Yin, Y. Zhou, L. Cui, T. Liu, P. Ju, L. Zhu, S. Ai, Microchim. Acta 173 (2011) 337.
[16] G. Gopu, P. Manisankar, B. Muralidharan, C. Vedhi, Int. J. Electrochem. Sc. ID 269452 (2011) 11.
[17] X. Meng, Z. Xu, M. Wang, H. Yin, S. Ai, Anal. Methods (Anal. Method. Instrum.) 4 (2012) 1736.
[18] F. Wantz, C.E. Banks, R.G. Compton, Electroanal. 17 (2005) 1529.
[19] A.O. Santini, J.E. De Oliveira, H.R. Pezza, L. Pezza, J. Brazilian Chem. Soc. 17 (2006) 785.
[20] S. Komorsky-Lovric, B. Nigovic, J. Pharmaceut. Biomed. 36 (2004) 81.
[21] W. Gao, J. Song, N. Wu, J. Electroanal. Chem. 576 (2005) 1.
[22] J.P. Hart, A. Crew, E. Crouch, K.C. Honeychurch, R.M. Pemberton, Anal. Lett. 37 (2004) 789.
[23] K.C. Honeychurch, J.P. Hart, Anal. Chem. 22 (2003) 456.
[24] I. Svancara, P. Kotzian, M. Bartos, K. Vytras, Electrochem. Commun. 7 (2005) 657.
[25] M. Vasjari, A. Merkoci, J.P. Hart, S. Alegret, Microchim. Acta 150 (2005) 233.
[26] J.P. Hart, A. Crew, E. Crouch, K.C. Honeychurch, R.M. Pemberton, Anal. Lett. 37 5 (2005) 789.
[27] Y. Shih, J.-M. Zen, H.-H. Yang, J. Pharmaceut. Biomed. 29 5 (2002) 827.
[28] M.F. Bergamini, A.L. Santos, N.R. Stradiotto, M.V.B. Zanoni, J. Pharmaceut. Biomed. 43 (2007) 315.
[29] P.F. Bolado, P.J. Lamas-Ardisana, D.H. Santos, A.C. Garcia, Anal. Chim. Acta 638 (2009) 133.
[30] N.A Alarfaj, R.A. Ammar, M.F. El-Tohamy, Chem. Cent. J. 24 (2012) 6.
[31] C. Comninellis, Electrochim. Acta 39 11-12 (1994) 1857.
[32] F. Montilla, P.A. Michaud, E. Morallon, J.L. Vazquez, C. Comninellis, Electrochim. Acta 47 21 (2002) 3509.
[33] J.M. Peralta-Hernandez, C.A. Martinez-Huitle, J.L. Guzman-Mar, A. Hernandez-Ramirez, J. Environ. Manage. 19 5 (2009) 257.
[34] S. Songa, L. Zhana, Z. Hea, L. Lina, J. Tua, Z. Zhanga,J. Chena, L. Xu, J. Hazard. Mater. 175 1-3 (2010) 614.
[35] A. Fujishima, D.A. Tryk, T.N. Rao, Water Res. 39 (2005) 2687.
[36] P. Canizares, J. Lobato, R. Paz, M.A. Rodrigo, C. Saez, Water Res. 39 (2005) 2687.

[37] M. Panizza, P.A. Michaud, G. Cerisola, C. Comninellis, J. Electroanal. Chem. 507 (2001) 206.
[38] M.A. Rodrigo, P.A. Michaud, I. Duo, M. Panizza, G. Cerisola, C. Comninellis, J. Electrochem. Soc. 148 (2001) D60.
[39] J. Iniesta, P.A. Michaud, M. Panizza, C. Comninellis, Electrochem. Commun. 3 (2001) 346.
[40] P. Canizares, C. Saez, J. Lobato, M.A. Rodrigo, Ind. Eng. Chem. Res. 43 (2004) 1944.
[41] P. Canizares, C. Saez, J. Lobato, M.A. Rodrigo, Electrochim. Acta 49 (2004) 4641.
[42] O. Simond, V. Schaller, C. Comninellis, Electrochim. Acta 42 13-14 (1997) 2009.
[43] M. Panizza, G. Cerisola, Electrochim. Acta 51 2 (2005) 191.
[44] J.A. Garrido, E. Brillas, P.L. Cabot, F. Centellas, C. Arias, R.M. Rodriguez, Electrochim. Acta 25 (2007) 19.
[45] D. Gandini, C. Comninellis, A. Perret, W. Haenni, ICHEME Symp. Ser. 145 (1999) 181.
[46] L. Ouattara, I. Duo, T. Diaco, A. Ivandini, K. Honda, T.N. Rao, A. Fujishima, C. Comninellis, New Diam. Front. C. Tec. 13 (2003) 97.
[47] R.G. Compton, J.S. Foord, F. Marken, Electroanal. 15 (2003) 1349.
[48] O. Chailapakul, W. Siangproh, D.A. Tryk, Sens. Lett. 4 (2006) 99. 215.
[49] A. Fujishima, C. Terashima, K. Honda, B.V. Sarada, T.N. Rao, New Diam. Front. C. Tec. 12 (2002) 73. 216.
[50] L. Codognoto, S.A.S. Machado, L.A. Avaca, Diam. Relat. Mater. 11 (2002) 1670. 217.
[51] T.N. Rao, B.H. Loo, B.V. Sarada, C. Terashima, A. Fujishima, Anal. Chem. 74 (2002) 1578. 245.
[52] N.S. Lawrence, M. Pagels, A. Meredith, T.G.J. Jones, C.E. Hall, C.S.J. Pickles, H.P. Godfried, C.E. Banks, R.G. Compton, L. Jiang, Talanta 69 (2006) 829.
[53] J.M. Halpern, S. Xie, G.P. Sutton, B.T. Higashikubo, C.A. Chestek, H. Lu, H.J. Chiel, H.B. Martin, Diam. Relat. Mater. 15 (2006) 183.
[54] G.M. Swain, A.B. Anderson, J.C. Angus, MRS Bull. 23 (1998) 56.
[55] H.B. Martin, A. Argoitia, U. Landau, A.B. Anderson, J.C. Angus, J. Electrochem. Soc. 143 (1996) 133.
[56] G.M. Swain, J. Electrochem. Soc. 141 (1994) 33.
[57] R. Ramesham, M.F. Rose, Diam. Relat. Mater. 6 (1997) 17.
[58] G.M. Swain, Adv. Mater. 5 (1994) 388.
[59] G.M. Swain, R. Ramesham, Anal. Chem. 65 (1993) 345.
[60] R.G. Compton, J.S. Foord, F. Marken, Electroanal. 15 17 (2003)
[61] B.C. Lourencao, R.A. Medeiros, R.C. Rocha-Filho, L.H. Mazo, O. Fatibello-Filho, Talanta 78 3 (2009) 748.
[62] C. Radovan, C. Cofan, F. Manea, D. Dascalu, V. Chiriac, The 13th Symposium on Analytical and Environmental Problems, Szeged, 25 September 2006.
[63] N. Spataru , B.V. Sarada , E. Popa , D.A. Tryk, A. Fujishima, Anal. Chem. 73 3 (2001) 514.
[64] W. Siangproh, P. Ngamukot, O. Chailapakul, Sensors Actuat. B-Chem. 91 1–3 (2003) 60.
[65] R.T.S. Oliveira, G.R. Salazar-Banda, V.S. Ferreira, S.C. Oliveira, L.A. Avaca, Electroanal. 19 11 (2007) 1189.
[66] K.D. Santos, O.C. Braga, I.C. Vieira, A. Spinelli, Talanta. 80 5 (2010) 1999.

[67] C. Cofan, C. Radovan, Ind. Eng. Chem. ID 451830 (2011) 9.
[68] C. Radovan, C. Cofan, D. Cinghita, Electroanal. 20 12 (2008) 1346.
[69] A. Arvinte, F. Valentini, A. Radoi, R. Arduini, E. Tamburri, L. Rotariu, G. Palleschi, C. Bala, Electroanal. 19 (2007) 1455.
[70] R.L. Price, M.C. Waid, K.M. Haberstroh, T.J. Webster, Biomaterials 24 (2003) 1877.
[71] E.S. Steigerwalt, G.A. Deluga, C.M. Lukehart, J. Phys. Chem. B 106 (2002) 760.
[72] M. Musameh, J. Wang, A. Merkoci, Y. Lin, Electrochem. Commun. 4 (2002) 743.
[73] R. Vieira, C. Pham-Huu, N. Keller, M.J. Ledoux, Quim. Nova 26 (2003) 665.
[74] F. Marken, M.L. Gerrard, I.M. Mellor, R.J. Mortimer, C.E. Madden, S. Fletcher, K. Holt, J.S. Foord, R.H. Dahm, Electrochem. Commun. 3 (2001) 177.
[75] X. Tang, Y. Liu, H. Hou, T. You, Talanta 83 (2011) 1410.
[76] L.W.X. Zhang, H. Ju, Biosens. Bioelectron. 23 (2007) 479.
[77] B. Perez, M. del Valle, S. Alegret, A. Merkoci, Talanta 74 (2007) 398.
[78] Y. Liu, J. Huang, H. Hou, T. You, Electrochem. Commun. 10 (2008) 1431.
[79] J. Huang, Y. Liu, H. Hou, T. You, Biosens. Bioelectron. 24 (2008) 632.
[80] J. Wang, Electroanal. 17 (2005) 7.
[81] J. Kong, N.R. Franklin, C.W. Zhou, M.G. Chapline, S. Peng, K. Cho, H.J. Dai, Science 287 (2000) 622.
[82] T. Nishino, T. Ito, Y. Umezawa, Anal. Chem. 74 (2002) 4275.
[83] P. Poncharal, Z.L. Wang, D. Ugarte, W.A. de Heer, Science 283 (1999) 1513.
[84] G. Ovejero, J.L. Sotelo, A. Rodriguez, C. Diaz, R. Sanz, J. Garcia, Ind. Eng. Chem. Res. 46 (2007) 6449.
[85] P.G. Collins, K. Bradley, M. Ishigami, A. Zettl, Science 287 (2000) 1801.
[86] R. Vieira, C. Pham-Huu, N. Keller, M.J. Ledoux, Chem. Commun. (2002) 954.
[87] S. Fan, M.G. Chapline, N.R. Franklin, T.W. Tombler, A.M. Cassell, H. Dai, Science 283 (1999) 512.
[88] P. Kim, C.M. Lieber, Science 286 (1999) 2148.
[89] H. Dai, J.H. Hafner, A.G. Rinzler, D.T. Colbert, R.E. Smalley, Nature 384 (1996) 147.
[90] P.J.F. Harris, Crit. Rev. Solid State Mater. Sci. 30 (2005) 235.
[91] N.Q. Li, J.X. Wang, M.X. Li, Rev. Anal. Chem. 22 (2003) 19.
[92] B.S. Sherigara, W. Kutner, F. D'Souza, Electroanal. 15 (2003) 753.
[93] Q. Zhao, Z. Gan, Q. Zhuang, Electroanal. 14 (2002) 1609.
[94] L. Zhu, R. Yang, J. Zhai, C. Tian, Biosens. Bioelectron. 23 (2007) 528.
[95] P. Santhosh, K.M. Manesh, A. Gopalan, K.P. Lee, Sensors Actuat. B-Chem. 125 (2007) 92.
[96] P. Du, S. Liu, P. Wu, C. Cai, Electrochim. Acta 52 (2007) 6534.
[97] N. Sato, H. Okuma, Sens. Actuat. B-Chem. 129 (2008) 188.
[98] R. Hirlekar, M. Yamagar, H. Garse, M. Vij, V. Kadam, Asian Journal of Pharmaceutical and Clinical Research.
[99] P. He, Y. Xu, Y. Fang, Microchim. Acta 152 (2006) 175.
[100] G. Wildgoose, C.E. Banks, H.C. Leventis, R.G. Compton, Microchim. Acta 152 (2006) 187.
[101] R.H. Patil, R.N. Hegde, S.T. Nandibewoor, Colloid. Surface. B. 83 (2011) 133–138.

[102] H. Heli, S. Majdi, A. Jabbari, N. Sattarahmady, A.A. Moosavi-Movahedi, J. Solid State Electr. 14 (2010) 1515.
[103] L. Tzu-Lung, T. Yu-Chen, Sensors Actuat. B-Chem. 153 2 (2011) 439.
[104] R.N. Goyal, A. Tyagi, N. Bachheti, S. Bishnoi, Acta 53 (2008) 2802.
[105] Y. Zhang, Y. Cai, S. Su, Anal. Biochem. 350 (2006) 285.
[106] A.A. Ensafi, H. Karimi-Maleh, J. Electroanal. Chem. 640 (2010) 75–83.
[107] H. Beitollahi, I. Sheikhshoaie, Electrochim. Acta 56 (2011) 10259.
[108] A. Wulcarius, Electroanal. 8 (1996) 11
[109] S.M. Auerbach, K.A. Carrado, P.K. Dutta, M. Dekker, INC, New York-Basel, 2003.
[110] S. Bailey, T. Olin, M. Bricka, D. Adrian, Water Res. 33 (1999) 2469.
[111] M. Elizalde-Gonzalez, J. Mattusch, W. Einicke, R. Wennrich, Chem. Eng. J. 81 (2001) 187.
[112] M. Rozic, S. Cerjan-Stefanovic, S. Kurajica, V. Vancina, E. Hodzic, Water Res. 34 (2000) 3675.
[113] R.S. Bowman, Micropor. Mesopor. Mat. 61 (2003) 43.
[114] M. Ackley, S. Rege, H. Saxena, Micropor. Mesopor. Mat. 61 (2003) 25.
[115] A. Corma, J. Catal. 216 (2003) 298.
[116] B. Liu, F. Yan, J. Kong, J. Deng, Anal. Chim. Acta 386 (1999) 31.
[117] F.Manea, A. Pop, C. Radovan, P. Malchev, A. Bebeselea, G. Burtica, S. Picken, J. Schoonman, Sensors 8 (2008) 5806.
[118] A. Pop, F.Manea C. Radovan, P. Malchev. A. Bebeselea, C.Proca, G. Burtica, S. Picken, J. Schoonman, Electroanal. 20 22 (2008) 2460.
[119] F. Manea, A. Remes, C. Radovan, R. Pode, S. Picken, J. Schoonman, Talanta 83 (2010) 66.
[120] A. Pop, F. Manea, A. Remes, A. Baciu, C. Orha, N. Vaszilcsin, S. Picken, J. Schoonman, Sensors, IEEE (2011) 581.
[121] F. Manea, M. Ihos, A. Remes, G. Burtica, J. Schoonman, Electroanal. 22 17-18 (2010) 2058.
[122] F. Manea, **S. Motoc**, A. Pop, A. Remes, J. Schoonman, Nanoscale Res. Lett. (2012) 7331.
[123] A. Pop, F. Manea, C. Orha, **S. Motoc**, E. Ilinoiu, N. Vaszilcsin, J. Schoonman, Nanoscale Res. Lett. (2012) 7 266.
[124] **S. Motoc,** M. Ardelean, A. Pop, F. Manea, R. Pode, J. Schoonman, C. Savii, Proceedings of The 18th International Symposium on Analytical and Environmental Problems, (2012). 186.

# CHAPTER 6. MOTIVATION AND THESIS OBJECTIVES

Given the importance of clean water for mankind, numerous organizations are considering the potential application of nanoscience and environmental nanotechnologies to solve technical challenges associated with the removal and monitoring of water contaminants. Technology developers and others claim that these nanomaterials and nanotechnologies offer more effective, efficient, durable, and affordable approaches for removing specific types of pollutants from water, and represent also, the basis of smart sensors for the detection of water contaminants.

In the recent years, there has been increasing concern about the presence of pharmaceuticals in water. These compounds are included in what are currently known as emerging pollutants. Their presence can be explained in terms of both their use in medicine and the inefficiency of water purifying systems in their removal.

Moreover, the electrochemical methods possess the dual character in relation with both pollutants detection and destruction. These methods use the electron as the main reagent, but also require the presence of supporting electrolytes. In general, the supporting electrolytes exist in the wastewaters to be treated, but not always in sufficient concentrations. These processes can operate at ambient temperature without a need of temperature control. The applications of electrochemical technologies for wastewater treatment are benefiting taking into account their advantages, *e.g.*, versatility, environmental compatibility and potential cost effectiveness among others. However, the electrode material is the most important parameter in the electrochemical process and represents the key of process performance.

The aim of this study is to explore the dual character of the electrochemical techniques and electrode materials for the application in pharmaceuticals-containing water treatment and control. It is noteworthy that electrode materials for water quality monitoring are conceptually very similar to those used in the degradation of pollutants from water, so the development of suitable electrode materials and electrochemical techniques involves actually relatively easy adaptation from a field to another, taking into account the application peculiarities (*e.g.,* electrode geometry, design and operating conditions for degradation application).

Carbon based electrodes are widely used as electrode material due to their wide potential window suitable for the investigation of an electrochemical oxidation process, chemical inertness, low-cost. The low rate of electron transfer at some carbon based electrodes and electrodes fouling limit their practical applications and the questions to solve these aspects arise. Two main pathways to enhance the electrochemical oxidation on the carbon-based electrodes can be explored. The surface modification of carbon-based electrodes and pretreatment methods play an important role on the oxidation performances of the electrode.

Based on the above-presented considerations the specific objectives of this research are the following:

– Elaboration and manufacturing of some carbon-based composite electrode materials with useful properties for the electrooxidation of pharmaceuticals from water;

– Elaboration and manufacturing of silver-modified carbon based composites to improve the electrocatalytic activity of the electrode material for pharmaceuticals oxidation;

– Morphological, electrical and electrochemical characterization of the electrode materials;

– The evaluation of the electrode materials behaviour in different supporting electrolytes and in the presence of the target organics, which allows to establish the relationship between obtained electrode material and oxidation reaction type of organics (direct, indirect, electrochemical-mediated oxidation);

– Setting-up the optimal conditions for the degradation and mineralization of pharmaceuticals from water;

– Individual detection experiments performance, which provides specific informations, *i.e.*, amperometric detection type, detection potential value, concentration ranges, electrode sensitivity, stability, reproducibility and lifetime, detection limits, calibration, to elaborate the detection protocol;

– Simultaneous detection experiments performance to elaborate specific simultaneous detection protocol;

– Testing dual character of the selected electrode material and electrochemical technique for application in pharmaceuticals degradation and detection.

Our research was directed to the study of anodic response of ibuprofen (IBP), considered as the third most popular drug in the world, non-prescription, non-steroidal drug used as an anti-inflammatory analgesic and antipyretic in the human treatment of fever, migraine, muscle aches, rheumatoid arthritis, tooth aches, and osteoarthritis, which is found in waters/ industrial wastewaters. Several carbon based composite electrode, *i.e.,* carbon nanotubes-epoxy composite referred to as CNT, silver-doped zeolite-carbon nanotubes-epoxy composite referred to as AgZCNT, silver-doped zeolite-carbon nanofiber-epoxy composite referred to as AgZCNF, silver-decorated carbon-nanofiber-epoxy composite referred to as AgCNF, and AgZEG in comparison with commercial conventional glassy carbon (GC) and new boron-doped diamond (BDD) electrodes were studied for advanced oxidation of ibuprofen from aqueous solution. For the ibuprofen detection approach, the electrodes tested were: AgZCNT, AgZCNF, AgCNF and AgZEG. Also, sodium diclofenac (DCF) was selected to study the electrode performance for the simultaneous detection of pharmaceuticals from water.

Due to the great complexity of the objective proposed for the study, this study was conceived as a prerequisite stage that to precede the development of a new nano-enhanced electrochemical green technology for advanced integrated pharmaceuticals-containing water treatment and quality control.

# CHAPTER 7. CARBON-BASED COMPOSITE, MORPHO-STRUCTURAL, ELECTRICAL AND ELECTROCHEMICAL CHARACTERIZATION

## 7.1. Obtaining of the carbon-based composite electrodes

In this study, several unmodified/ modified electrodes were prepared in order to oxidize pharmaceuticals from aqueous solutions:

- Carbon nanotubes-epoxy composite, referred to as CNT;
- Silver-doped zeolite-carbon nanotubes-epoxy composite, referred to as AgZCNT;
- Silver-doped zeolite-carbon nanofiber-epoxy composite, referred to as AgZCNF;
- Silver-decorated carbon-nanofiber-epoxy composite, referred to as AgCNF;
- Silver-doped zeolite-expanded-graphite-epoxy composite, referred to as AgZEG.

### *7.1.1. Materials*

The epoxy resin used in the study was Araldite®LY5052/Aradur®5052 purchased from Huntsman Advanced Materials, Switzerland.

Silver-modified zeolite (AgZ) was prepared by ion-exchange using natural zeolite (NZ) from Mirsid, Romania, with 68 % wt. clinoptilolite.

Carbon nanotubes (CNT) synthesized by catalytic carbon vapour deposition were obtained from NanocylTM, Belgium. Their main characteristics, given by the manufacturer, consist of CNT content of 90 %, carbon purity of 90 %, average diameter of 9.5 nm, average length of 1.5 μm, and surface area of 250-300 $m^2/g$.

Carbon nanofibers (CNFs) with average diameter of 60–150 nm and average length of 30–100 μm were purchased from Applied Sciences Inc., Cedarville, Ohio (Pyrograf III -PR24 AGLD).

Expanded-graphite (EG) used in this study was conductive expanded graphite fillers powder purchased from Conductograph, SGL Carbon, Germany.

### *7.1.2. Methods*

#### 7.1.2.1. Preparation of carbon-based composite electrodes

*Carbon nanotubes (CNT) and silver-doped zeolite carbon nanotubes (AgZCNT) composite electrodes*

The dispersion of carbon nanotubes (CNT) in tetrahydrofuran, 99.9 % (THF, Sigma Aldrich) was achieved by ultrasonication using a Cole-Parmer® 750-Watt Ultrasonic Processor for about 10 min prior to mixing with the polymer resin. After the sonication process, the solution of CNT/ THF was sonicated again with epoxy

resin to obtain a more homogeneous mixture. An effective method based on the two-roll mill (TRM) of achieving high levels of dispersion and distribution was used to prepare the both electrodes. The ratio between the components was chosen to reach 20 % wt. content of CNT and, 20 % wt. content of silver-modified zeolite (AgZ), respectively. During processing the temperature was kept constant at 70 °C, the mixing speed was maintained at 10 and 20 rpm for about 40 min, after then the curing agent (weight ratio of epoxy resin: curing agent was 100:38) was added to the CNT- resin mixture and mixing was continued for an additional 20 min to ensure a uniform dispersion within the sample. The same procedure was applied for the AgZCNT electrode. The mixture was then poured into PVC tubes and cured in a vacuum oven at 80 °C for 24 h, after which it was left to cool down to room temperature, and the composite electrode with disc surface area of 0.196 $cm^2$ was obtained. The electrical contacts of the electrodes were assured using copper wire. Figure 7.1 shows the schematic presentation of the CNT and AgZCNT electrode preparation protocol.

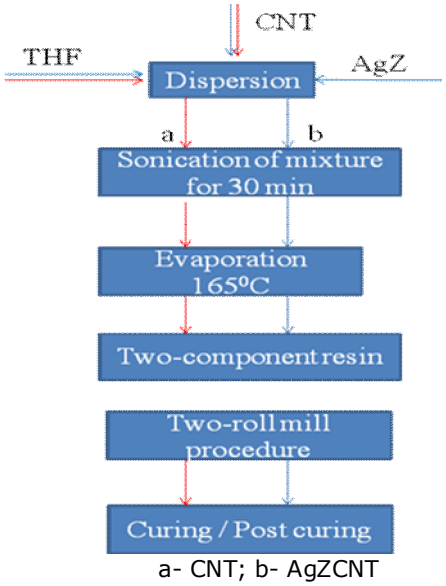


**Figure 7.1.** A schematic presentation of the CNT and AgZCNT based electrodes preparation protocol.

*Silver-decorated carbon nanofiber (AgCNF) and silver-doped zeolite carbon nanofiber (AgZCNF) composite electrodes*

Carbon nanofibers (CNF) with diameters of 60 to 150 nm and lengths of 30 to 100 μm were purchased from Applied Sciences Inc., Cedarville, Ohio (Pyrograf III - PR24 AGLD). Silver-modified zeolite was prepared by ion-exchange using natural zeolite (NZ) from Mirsid, Romania (68 % wt.). Araldite®LY5052/ Aradur®5052 two-component epoxy resin used in the study was purchased from Huntsman Advanced Materials, Basel, Switzerland.

The decoration of the CNF with silver nanoparticles was carried out by reducing silver ions in the presence of N, N-dimethylformamide (DMF). 1.1-g CNF

was added to 550 mL of DMF and the mixture was subjected to ultrasonication (Cole-Parmer 8900, Vernon Hills, Chicago, IL, USA) for 1 h; 40 mL of an $AgNO_3$ solution (0.02 M) was added to the mixture with a temperature of 60 °C to 62 °C during the stirring. After 1 h heating, the solution was kept without stirring at room temperature for 48 h for Ag deposition, and after filtration and subsequently washing with water, ethanol, and acetone, silver-decorated CNF was obtained. The composite electrodes were prepared by dispersion of CNFs in DMF, 99.9 % (DMF, Sigma-Aldrich, Corporation, St. Louis, USA) and epoxy resin (Araldite®LY5052) by ultrasonication, followed by the homogenization of the resulting paste with the zeolite particles and also with the hardener using a two-roll mill. The mixture was then poured into PVC tubes and cured at 60 °C for 24 h obtaining disc electrodes with a surface area of 0.196 $cm^2$. The ratios were chosen to obtain 20 % wt. CNFs for the AgCNF electrode and also 20 % wt. Ag-modified zeolite for the AgZCNF electrode. Figure 7.2 shows the schematic presentation of the electrodes preparation protocol.

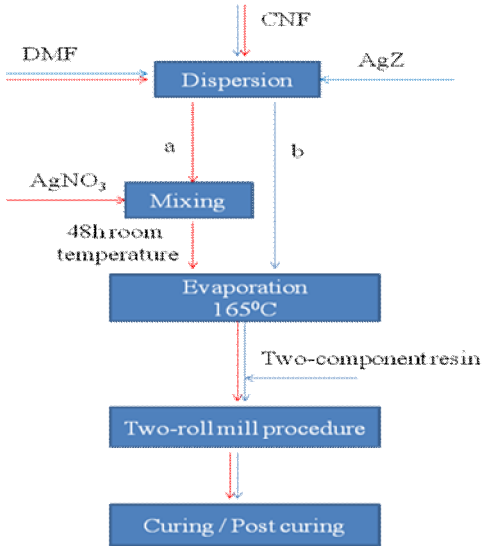


**Figure 7.2.** Composite electrode preparation scheme: a– AgCNF; b- AgZCNF.

*Silver-doped expanded graphite composite electrode (AgZEG)*

The composite electrode was obtained from two-component epoxy resin (LY5052, Araldite) mixed with conductive expanded graphite (EG) fillers powder (Conductograph, SGL Carbon) and silver-doped zeolite (clinoptilolite). Expanded graphite is special low density graphite, prepared by thermal expansion of randomly oriented natural graphite. The ratio between the components was chosen to reach 20 % wt. content of exfoliated graphite, 30 % wt. content of silver-doped zeolite. It was not possible to add the full amount of EG and AgZ to the matrix resin directly, due to the high surface area of the graphite flakes. Therefore, the mixing was performed in a roll-mill at room temperature. The two parts of the epoxy were mixed together and the full amount of EG was added in steps forming a thick paste. Then the epoxy was treated in a hot press at 50 $^0$C for 60 minutes. Simultaneously,

the material was shaped in a plate of 1 mm thickness. The plate was cooled down for about 12 h to room temperature. Figure 7.3 shows the schematic presentation of the electrodes preparation protocol.

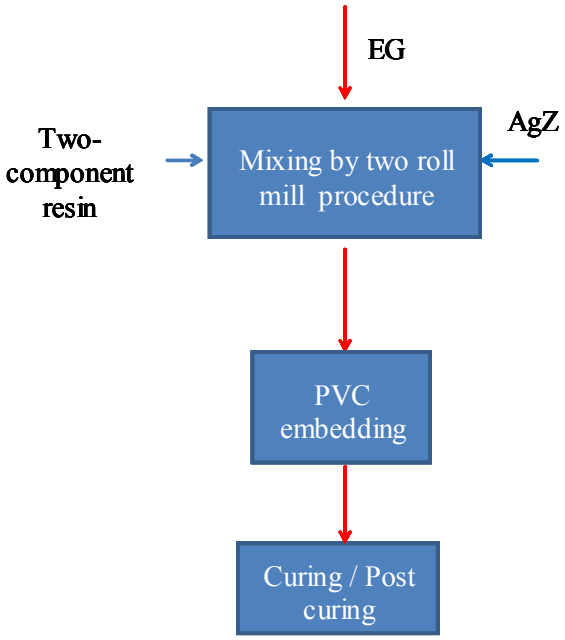


**Figure 7.3.** A schematic presentation of the AgZEG based electrodes preparation protocol.

### *7.1.3. Morpho-structural and electrical characterization of carbon-based composite electrodes*

#### 7.1.3.1. Scanning electron microscopy (SEM)

Scanning electron microscopy (SEM) images of fractured surfaces of the carbon-based composite electrodes were taken to study the bulk distribution and the structure of the conductive carbon filler within the epoxy matrix (Figures 7.4–7.6). Scanning electron microscopy (SEM) was performed using an Inspect S PANalytical instrument (PANalytical Spectris Australia Pty Ltd., Sydney, New South Wales, Australia).

Figure 7.4a and b shows the comparative scanning electron microscopy (SEM) images of the CNT and AgZCNT composites with 20 % wt. of CNTs and 20 % wt. of AgZ, respectively, proving a uniform distribution of both components within the epoxy matrix. A more porous structure is noticed for the AgZCNT composite, which was expected because of the presence of zeolite.

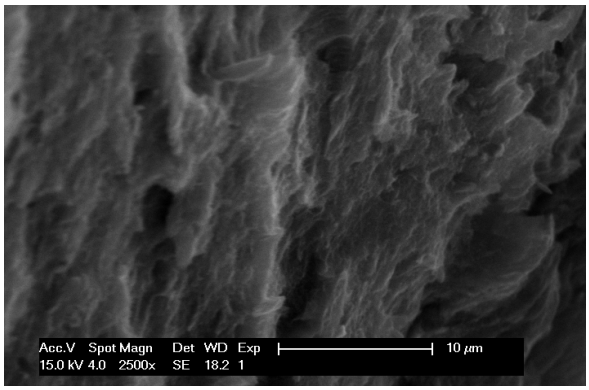


(a)

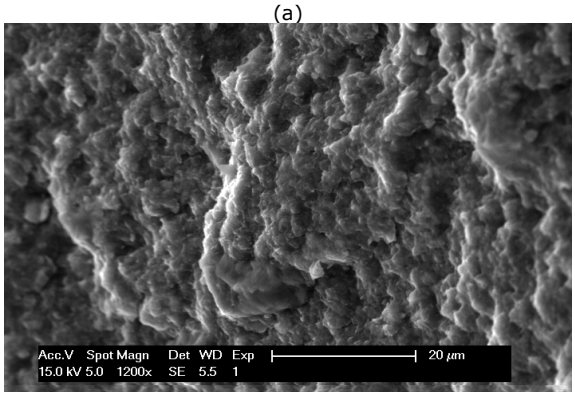


(b)

**Figure 7.4.** SEM imaging of the cross-section of electrode surface: a) CNT; b) AgZCNT.

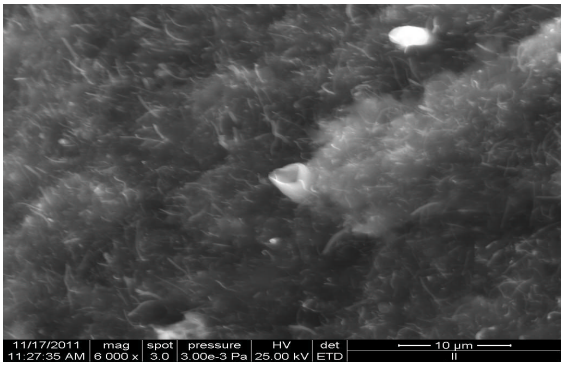


(a)

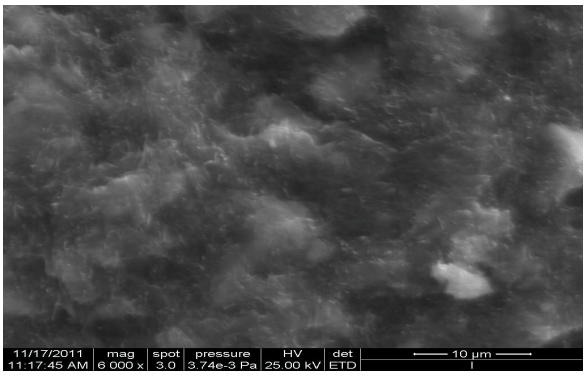


(b)

**Figure 7.5.** SEM imaging of the cross-section of electrode surface: a) AgCNF; b) AgZCNF.

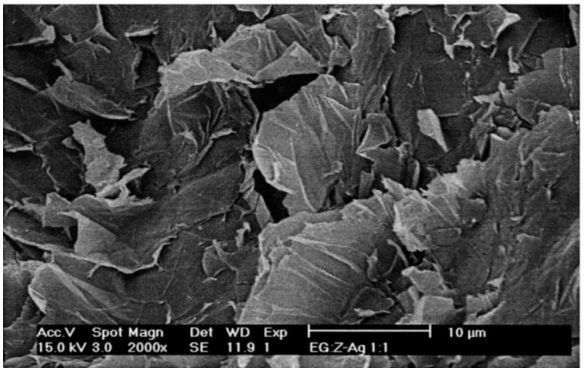


**Figure 7.6.** SEM imaging of the cross-section of AgZEG electrode surface.

Figure 7.5a and b presents the SEM image of both electrodes, *i.e.*, AgCNF and AgZCNF composite electrodes, and a homogeneous distribution of CNF within the epoxy matrix is observed. Higher content of Ag particles was found for silver-modified natural zeolite CNF-epoxy in comparison with silver-decorated CNF-epoxy composite material.

Figure 7.6 presents the SEM image of the AgZEG composite electrode and exhibits a closely spaced expanded graphite zones with random distribution and orientation due to the irregular shapes of both the expanded graphite particles and Ag-zeolite particles in the epoxy matrix. The AgZ particles are invisible on the composite surface because they are completely embedded into the epoxy resin, and are rarely exposed at the electrode surface.

### 7.1.3.2. Electrical conductivity

The electrical conductivity of a composite is strongly depended on the filler loading and there is often a percolation threshold concentration beyond which the electrical conductivity does not vary significantly. At low filler concentrations, the conductivity remains very close to the conductivity of the pure, electrically insulating polymer matrix since the fillers are dispersed individually or are present as small clusters in the matrix. Above the percolation threshold concentration, independent fillers tend to link together to form conductive networks. This leads to a significant increase in the electrical conductivity of the composite.

Several parameters, such as the choice of polymer, the aspect ratio of the filler [1, 2], the matrix/ filler and the filler/ filler interaction as well as, the degree of orientation of the filler [4, 5] affect the percolation threshold. In addition, the processing technique, mixing stresses applied during preparation, as well as the shaping procedure play very important roles.

The electrical conductivity of each electrode was determined by four-point resistance measurement. The results obtained by four-point probe resistance measurements (FPP) for electrical characterization of the carbon-based composite electrodes are presented in Table 7.1. It can be seen that the Ag-modified zeolite slightly affected the electrical conductivity of the composite, the value of about 1.177 $Scm^{-1}$ was determined for AgZCNT composite, which is much higher than the CNT composite electrical conductivity 0.247 $Scm^{-1}$. Even if the zeolite is an insulating material, the enhancement of the electrical conductivity in its presence should be attributed to the silver content within silver-modified zeolite. Due to a much higher content of silver within silver-modified zeolite in comparison with silver-decorated carbon nanofiber, the electrical conductivity was improved by ten times (0.409 $Scm^{-1}$ for AgZCNF vs. 0.040 $Scm^{-1}$ for AgCNF). In the case of the composite materials modified with silver doped zeolite, modified zeolite acts as a solid electrolyte and its conductivity depends on the mobility of the cations. The larger their mobility, the larger is the conductivity of the composite material. The higher electrical conductivity was recorded for the AgZEG composite electrode, probably due to the layering of the graphite flakes, which are parallel to the surfaces of the plate due to the pressing of the plate in the hot press providing better conditions for conduction of the electrical current across the thickness of the electrode.

**Table 7.1.** Electrical conductivity of the carbon-based composite electrode.

| Electrode type | Electrical conductivity, σ (S/cm) |
|---|---|
| CNT | 0.247 |
| AgZCNT | 1.177 |
| AgZCNF | 0.409 |
| AgCNF | 0.040 |
| AgZEG | 1.750 |

#### 7.1.3.3. Electrochemical measurements

Prior to use, the working electrodes were gradually cleaned, first polished with abrasive paper and then on a felt-polishing pad by using 0.3 μm alumina powder (Metrohm, Switzerland) in distilled water for 5 minutes and rinsing with distilled water.

All measurements were carried out using an Autolab potentiostat/ galvanostat PGSTAT 302 (Eco Chemie, The Netherlands) controlled with GPES 4.9 software and a three-electrode cell, with a saturated calomel electrode as reference electrode, a platinum counter electrode, and the working electrodes (see Figure 7.7).

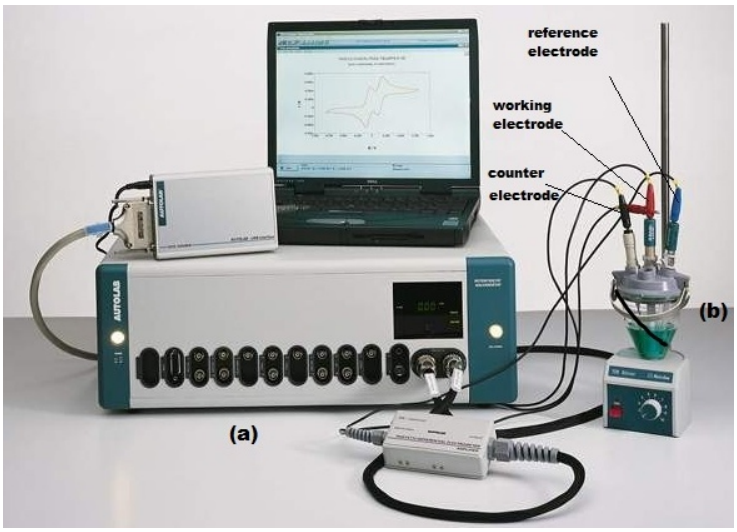


**Figure 7.7.** (a) Image of a potentiostat/ galvanostat type PGSTAT 302 (EcoChemie), (b) three electrodes cell (Metrohm).

## 7.2. Electrochemical characterization of carbon-based composite electrodes

Cyclic voltammetry (CV), being the most frequently used electroanalytical technique, is an outstanding tool for a preliminary determination of the redox properties of a given species, for understanding reaction intermediates, and for obtaining information about the stability of reaction products, and above all the most important advantage is its ability to characterize an electrode [7].

Thus, by using cyclic voltammetry recorded at different scan rates in the presence of 4 mM $K_3Fe(CN)_6$ the electrochemical behaviour of ferrocyanide was studied, which offers the opportunity to determine the characteristics of a cyclic voltammetric response originating from a reversible process. The reversibility of the system was estimated by the peak-to-peak separation (the separation between the anodic peak potential and the cathodic peak potential, $\Delta Ep = Ea - Ec$). For a reversible couple the $\Delta Ep$ is equal to 0.059/ n V (n, being the number of electrons exchanged in the redox reaction and in the present case is equal with 1), and is

independent of the scan rate, but under quasi- and irreversible conditions, the ΔEp depends on the voltage scan rate. Another important parameter that is related to the electrochemical reversibility of an electrode reaction is the peak current, and more specific, the ratio between the current of the anodic peak and that of the cathodic peak (ia/ ic), whose value is unity for a simple reversible couple. Beyond all parameters determination, which can predict if the study process is reversible or irreversible, the aim of the study of the electrochemical behaviour of the classical ferri/ ferrocyanide system is to determine the electroactive surface of used carbon-based electrodes [7]. Thus, Figure 7.8a-e shows the cyclic voltammograms of the all carbon-based composite electrodes used in this study recorded at different scan rates (0.025, 0.05, 0.1, 0.2 and 0.3 $Vs^{-1}$) in 1M $KNO_3$ supporting electrolyte and in the presence of 4 mM $K_3Fe(CN)_6$.

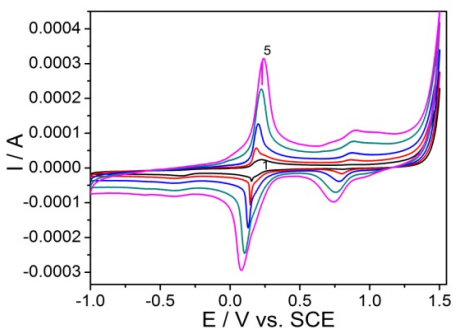


(a)

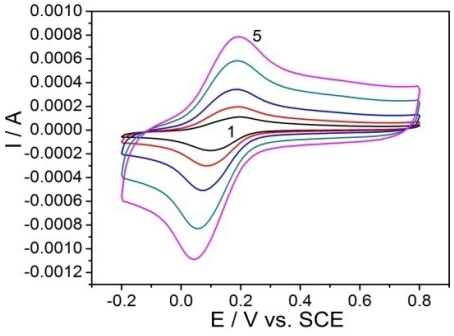


(b)

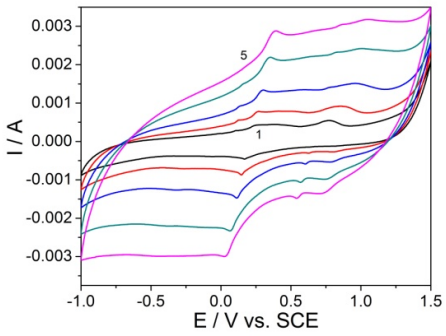


(c)

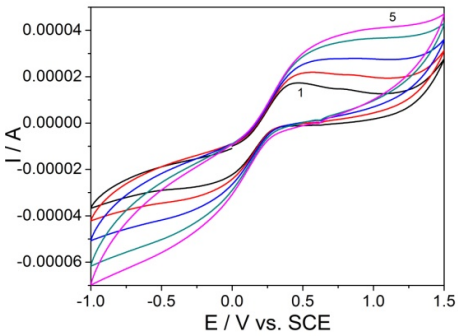


(d)

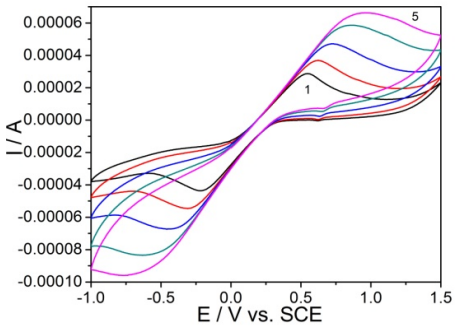


(e)

**Figure 7.8.** Cyclic voltammograms of carbon-based composite electrodes in 1M $KNO_3$ supporting electrolyte and in the presence of 4mM $K_3Fe(CN)_6$; at different potential scan rates 1- 0.025, 2- 0.05, 3- 0.1, 4- 0.2, 5- 0.3 $Vs^{-1}$; potential range: -1V→+1.5V, recorded using the electrodes: a) GC; b) CNT; c) AgZCNT; d) AgZCNF; e) AgCNF.

The relationship between the peak potential and the logarithm of scan rates is illustrated in Figure 7.9a-e, recorded at different scan rates (0.025, 0.05, 0.1, 0.2, 0.3, $Vs^{-1}$) with cyclic voltammetry of carbon-based electrodes.

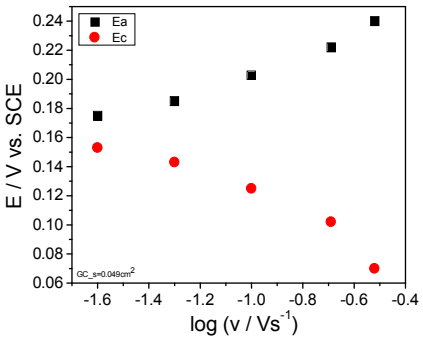


(a)

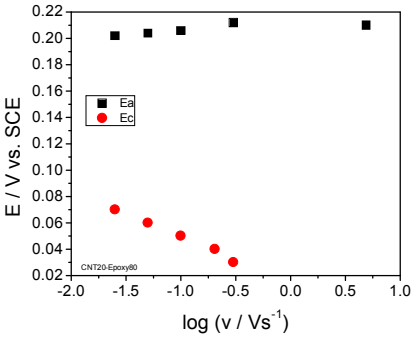


(b)

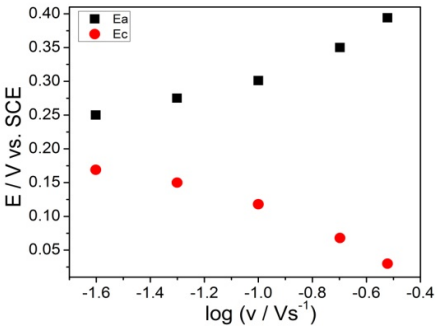


(c)

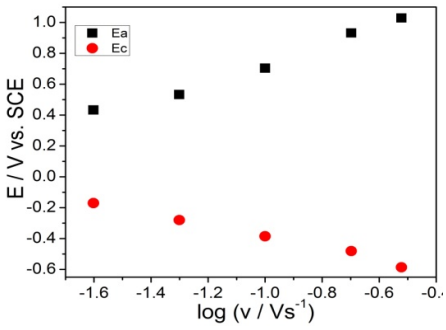


(d)

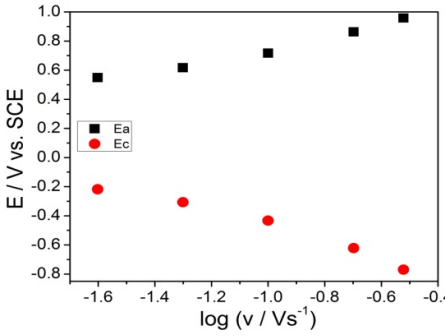


(e)

**Figure 7.9.** Plots of the anodic and cathodic peak potentials versus the logarithm of the scan rate: 0.025, 0.05, 0.1, 0.2, 0.3, Vs$^{-1}$, recorded by CV using the electrodes: a) GC; b) CNT; c) AgZCNT; d) AgZCNF; e) AgCNF.

The plots of the anodic and cathodic peak currents depending on the square root of the scan rate, also give information about the overall mechanistic aspects of the redox couple process that occurs on studied carbon-based electrodes. This dependence of the peak currents on square root of the scan rate is presented in the next figure (Figure 7.10a-e).

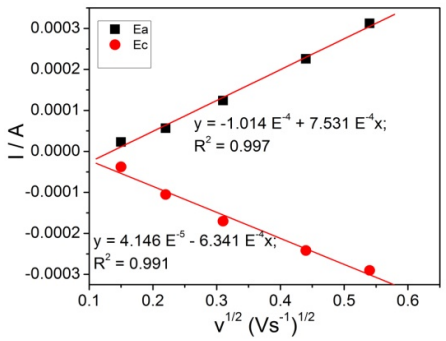


(a)

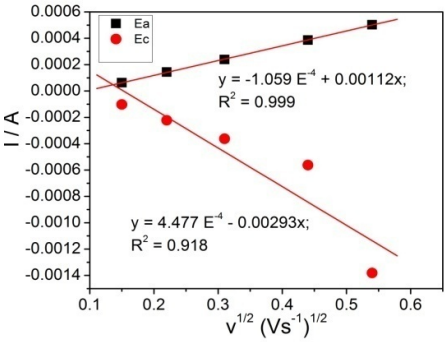


(b)

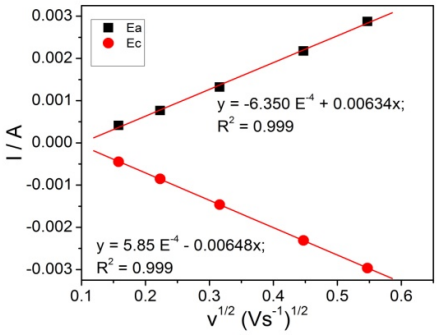


(c)

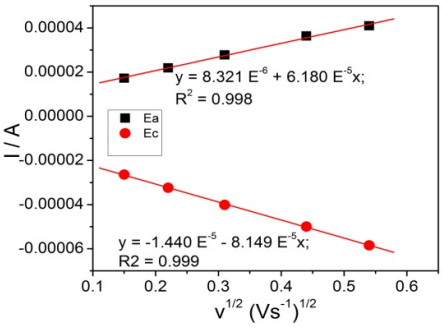


(d)

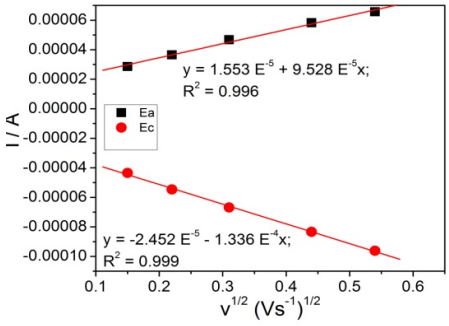


(e)

**Figure 7.10.** Calibrations plots of the anodic and cathodic peak currents versus the logarithm of the scan rate: 0.025, 0.05, 0.1, 0.2, 0.3, $Vs^{-1}$, recorded by CV using the electrodes: a) GC; b) CNT; c) AgZCNT; d) AgZCNF; e) AgCNF.

The parameters that characterized the electrochemical behaviour of the classical ferri/ ferrocyanide redox system, which is very well-known as reversible redox system, on the tested electrodes are gathered in Table 7.2.

**Table 7.2.** The electrochemical parameters of the redox system (ferri/ ferocyanide) determined from the anodic and cathodic branches of CVs.

| GC | | | | | |
|---|---|---|---|---|---|
| Anodic | | | | | |
| Scan rate / $Vs^{-1}$ | E/V | I/A | ΔIa/A | ΔE = Ea - Ec, V | ia / ic |
| 0.025 | 0.240 | $2.292 \cdot 10^{-5}$ | $1.856 \cdot 10^{-5}$ | | |
| 0.050 | 0.185 | $5.644 \cdot 10^{-5}$ | $4.968 \cdot 10^{-5}$ | | |
| 0.100 | 0.203 | $1.239 \cdot 10^{-4}$ | $1.018 \cdot 10^{-4}$ | 0.100 | 0.860 |
| 0.200 | 0.222 | $2.256 \cdot 10^{-4}$ | $2.035 \cdot 10^{-4}$ | | |
| 0.300 | 0.240 | $3.124 \cdot 10^{-4}$ | $2.809 \cdot 10^{-4}$ | | |
| Cathodic | | | | | |
| Scan rate / $Vs^{-1}$ | E/V | I/A | ΔIc/A | ΔE = Ea - Ec, V | ia / ic |
| 0.025 | 0.153 | $-3.767 \cdot 10^{-5}$ | $3.278 \cdot 10^{-5}$ | | |
| 0.050 | 0.143 | $-1.053 \cdot 10^{-4}$ | $9.572 \cdot 10^{-5}$ | | |
| 0.100 | 0.125 | $-1.703 \cdot 10^{-4}$ | $1.545 \cdot 10^{-4}$ | 0.100 | 0.860 |
| 0.200 | 0.102 | $-2.418 \cdot 10^{-4}$ | $2.167 \cdot 10^{-4}$ | | |
| 0.300 | 0.070 | $-2.903 \cdot 10^{-4}$ | $2.532 \cdot 10^{-4}$ | | |
| CNT | | | | | |
| Anodic | | | | | |
| Scan rate / $Vs^{-1}$ | E/V | I/A | ΔIa/A | ΔE = Ea - Ec, V | ia / ic |
| 0.025 | 0.202 | $1.084 \cdot 10^{-4}$ | $0.628 \cdot 10^{-4}$ | | |
| 0.050 | 0.204 | $1.932 \cdot 10^{-4}$ | $1.436 \cdot 10^{-4}$ | 0.156 | 1.050 |
| 0.100 | 0.206 | $3.364 \cdot 10^{-4}$ | $2.389 \cdot 10^{-4}$ | | |
| 0.200 | 0.210 | $5.750 \cdot 10^{-4}$ | $3.861 \cdot 10^{-4}$ | | |

| | | | | | |
|---|---|---|---|---|---|
| 0.300 | 0.212 | $7.724 \cdot 10^{-4}$ | $5.027 \cdot 10^{-4}$ | | |
| | | | Cathodic | | |
| Scan rate / $Vs^{-1}$ | E/V | I/A | ΔIc/A | ΔE = Ea - Ec, V | ia / ic |
| 0.025 | 0.070 | $-1.660 \cdot 10^{-4}$ | $-1.025 \cdot 10^{-4}$ | | |
| 0.050 | 0.060 | $-2.926 \cdot 10^{-4}$ | $-2.223 \cdot 10^{-4}$ | | |
| 0.100 | 0.050 | $-5.000 \cdot 10^{-4}$ | $-3.627 \cdot 10^{-4}$ | 0.156 | 1.050 |
| 0.200 | 0.040 | $-8.229 \cdot 10^{-4}$ | $-5.625 \cdot 10^{-4}$ | | |
| 0.300 | 0.030 | $1.000 \cdot 10^{-4}$ | $-13.814 \cdot 10^{-4}$ | | |
| | | | AgZCNT | | |
| | | | Anodic | | |
| Scan rate / $Vs^{-1}$ | E/V | I/A | ΔIa/A | ΔE = Ea - Ec, V | ia / ic |
| 0.025 | 0.250 | $4.130 \cdot 10^{-4}$ | $1.168 \cdot 10^{-4}$ | | |
| 0.050 | 0.275 | $7.666 \cdot 10^{-4}$ | $2.089 \cdot 10^{-4}$ | | |
| 0.100 | 0.301 | $1.320 \cdot 10^{-3}$ | $4.066 \cdot 10^{-4}$ | 0.207 | 0.790 |
| 0.200 | 0.350 | $2.170 \cdot 10^{-3}$ | $6.030 \cdot 10^{-4}$ | | |
| 0.300 | 0.394 | $2.870 \cdot 10^{-3}$ | $8.080 \cdot 10^{-4}$ | | |
| | | | Cathodic | | |
| Scan rate / $Vs^{-1}$ | E/V | I/A | ΔIc/A | ΔE = Ea - Ec, V | ia / ic |
| 0.025 | -0.0307 | $-4.471 \cdot 10^{-4}$ | $-1.946 \cdot 10^{-4}$ | | |
| 0.050 | -0.118 | $-8.534 \cdot 10^{-4}$ | $-3.490 \cdot 10^{-4}$ | | |
| 0.100 | -0.136 | $-1.460 \cdot 10^{-3}$ | $-5.386 \cdot 10^{-4}$ | 0.207 | 0.790 |
| 0.200 | -0.223 | $-2.310 \cdot 10^{-3}$ | $-7.390 \cdot 10^{-4}$ | | |
| 0.300 | -0.182 | $-2.960 \cdot 10^{-3}$ | $-8.720 \cdot 10^{-4}$ | | |
| | | | AgZCNF | | |
| | | | Anodic | | |
| Scan rate / $Vs^{-1}$ | E/V | I/A | ΔIa/A | ΔE = Ea - Ec, V | ia / ic |
| 0.025 | 0.433 | $1.723 \cdot 10^{-5}$ | $1.371 \cdot 10^{-5}$ | | |
| 0.050 | 0.533 | $2.188 \cdot 10^{-5}$ | $1.613 \cdot 10^{-5}$ | | |
| 0.100 | 0.704 | $2.778 \cdot 10^{-5}$ | $1.788 \cdot 10^{-5}$ | 1.106 | 0.695 |
| 0.200 | 0.932 | $3.636 \cdot 10^{-5}$ | $1.908 \cdot 10^{-5}$ | | |
| 0.300 | 1.029 | $4.095 \cdot 10^{-5}$ | $1.852 \cdot 10^{-5}$ | | |
| | | | Cathodic | | |
| Scan rate / $Vs^{-1}$ | E/V | I/A | ΔIc/A | ΔE = Ea - Ec, V | ia / ic |
| 0.025 | -0.170 | $-2.641 \cdot 10^{-5}$ | $-2.337 \cdot 10^{-5}$ | | |
| 0.050 | -0.280 | $-3.238 \cdot 10^{-5}$ | $-2.659 \cdot 10^{-5}$ | 1.106 | 0.695 |
| 0.100 | -0.385 | $-4.011 \cdot 10^{-5}$ | $-2.969 \cdot 10^{-5}$ | | |
| 0.200 | -0.481 | $-4.994 \cdot 10^{-5}$ | $-3.262 \cdot 10^{-5}$ | | |

| | | | | | |
|---|---|---|---|---|---|
| 0.300 | -0.182 | $-2.960 \cdot 10^{-3}$ | $-8.720 \cdot 10^{-4}$ | | |
| AgCNF | | | | | |
| Anodic | | | | | |
| Scan rate / $Vs^{-1}$ | E/V | I/A | ΔIa/A | ΔE = Ea - Ec, V | ia / ic |
| 0.025 | 0.549 | $2.859 \cdot 10^{-5}$ | $2.613 \cdot 10^{-5}$ | | |
| 0.050 | 0.617 | $3.652 \cdot 10^{-5}$ | $3.220 \cdot 10^{-5}$ | | |
| 0.100 | 0.717 | $4.677 \cdot 10^{-5}$ | $3.945 \cdot 10^{-5}$ | 1.210 | 0.684 |
| 0.200 | 0.863 | $5.828 \cdot 10^{-5}$ | $4.506 \cdot 10^{-5}$ | | |
| 0.300 | 0.958 | $6.567 \cdot 10^{-5}$ | $4.825 \cdot 10^{-5}$ | | |
| Cathodic | | | | | |
| Scan rate / $Vs^{-1}$ | E/V | I/A | ΔIc/A | ΔE = Ea - Ec, V | ia / ic |
| 0.025 | -0.218 | $-4.345 \cdot 10^{-5}$ | $-4.043 \cdot 10^{-5}$ | | |
| 0.050 | -0.307 | $-5.466 \cdot 10^{-5}$ | $-4.901 \cdot 10^{-5}$ | | |
| 0.100 | -0.433 | $-6.684 \cdot 10^{-5}$ | $-5.665 \cdot 10^{-5}$ | 1.210 | 0.684 |
| 0.200 | -0.622 | $-8.337 \cdot 10^{-5}$ | $-6.389 \cdot 10^{-5}$ | | |
| 0.300 | -0.770 | $-9.619 \cdot 10^{-5}$ | $-6.869 \cdot 10^{-5}$ | | |

Analyzing the results presented in Figures 7.8-7.10 and Table 7.2 and taking into account that the current ratio between the anodic and the cathodic peaks is the parameter which allows judging the chemical reversibility of an electrode reaction. An electrode process is defined as electrochemically reversible if the rate of the electron transfer is higher than the rate of the mass transport.

The best results were reached for CNT-based composite electrodes, for which ia/ ic ~ 1.05 in comparison with CNF-based composite electrodes characterized by ia/ ic ~ 0.684 – 0.695. The difference from the ideal behaviour can be mostly attributed to the non-compensated resistance of the supporting electrolyte, but can suggest the electrochemical reversibility of the electron transfer on the cyclic voltammetric time scale [8]. The dependence of the Ip value on the square root of the scan rate in solutions of $KNO_3$ must be linear and to pass the origin of the coordinates. Also, the intercepts of the ordinate depend principally on the nature and the concentration of the supporting electrolyte. This behaviour can be explained by the fact that the ion pairs of the ferricyanide and the cation of the supporting electrolyte influence the shapes of these dependences and, therefore, the rate of the electrode processes is controlled both by the diffusion and adsorption of these components [9]. However, all tested electrodes exhibited a peak potential separation higher than 0.05V, suggesting that the electron transfer rate is slow, and thus the cyclic voltammetric curves are quasi-reversible [10]. This may be explained by the fact that the thickness of the diffusion layer surrounding the electrode increases during the voltammogram is swept from the Ea to Ec. At slow scan rate, the diffusion layer is thicker and hence at faster scan rate the diffusion layer is thinner. While the thickness of the diffusion layer controls the rate of mass transport to the electrode, it follows that at faster scan rate the process can be called quasi-reversible, and at slower scan rate the larger the peak-to-peak separation is, and consequently the competition between the redox kinetics of the ferri/ ferrocyanide

system at the electrode and the mass transport results if the overall process is reversible or irreversible [11].

Thus, after the evaluation of the reversibility of the electrode processes, based on the Randles-Sevcik equation [12], the apparent diffusion coefficient and the electroactive surface area of the carbon-based composite electrodes from this study were determined (see Table 7.3). For all composite electrodes electroactive surface areas larger than the geometrical ones for each electrode were obtained.

$$I_p = 2.69 \times 10^5 A D^{1/2} n^{3/2} v^{1/2} C \qquad (1)$$

where $A$ represents the area of the electrode ($cm^2$), $n$ is the number of electrons participating in the reaction and is equal to 1, $D$ is the apparent diffusion coefficient of the molecule in solution, and $C$ is the concentration of the probe molecule in the solution and is 4 mM, and $v$ is the scan rate ($Vs^{-1}$).

The values of the apparent diffusions coefficients along with the electroactive surface areas are presented in Table 7.3. For comparison, the geometric areas are included.

**Table 7.3.** Apparent diffusion coefficients and the electroactive surface areas of carbon-based composite electrodes.

| Scan rate / $Vs^{-1}$ | Apparent diffusion coefficient, ($cm^2$ $s^{-1}$) | Electroactive area, $cm^2$ | Total apparent diffusion coefficient, ($cm^2$ $s^{-1}$) | Total Electroactive area, $cm^2$ | Geometric area, $cm^2$ |
|---|---|---|---|---|---|
| | | | GC | | |
| 0.025 | $5.960 \cdot 10^{-7}$ | 0.058 | | | |
| 0.050 | $2.376 \cdot 10^{-6}$ | 0.117 | | | |
| 0.100 | $3.691 \cdot 10^{-6}$ | 0.145 | $3.394 \cdot 10^{-6}$ | 0.132 | 0.049 |
| 0.200 | $4.965 \cdot 10^{-6}$ | 0.169 | | | |
| 0.300 | $5.345 \cdot 10^{-6}$ | 0.175 | | | |
| | | | CNT | | |
| 0.025 | $6.153 \cdot 10^{-6}$ | 0.187 | | | |
| 0.050 | $1.507 \cdot 10^{-5}$ | 0.294 | | | |
| 0.100 | $2.037 \cdot 10^{-5}$ | 0.341 | $2.668 \cdot 10^{-5}$ | 0.473 | 0.196 |
| 0.200 | $2.530 \cdot 10^{-5}$ | 0.380 | | | |
| 0.300 | $6.652 \cdot 10^{-5}$ | 0.617 | | | |
| | | | AgZCNT | | |
| 0.025 | $2.184 \cdot 10^{-5}$ | 0.151 | | | |
| 0.050 | $3.498 \cdot 10^{-5}$ | 0.192 | | | |
| 0.100 | $5.021 \cdot 10^{-5}$ | 0.230 | $4.300 \cdot 10^{-5}$ | 0.411 | 0.196 |
| 0.200 | $5.511 \cdot 10^{-5}$ | 0.241 | | | |
| 0.300 | $5.288 \cdot 10^{-5}$ | 0.236 | | | |
| | | | AgZCNF | | |

| | | | | | |
|---|---|---|---|---|---|
| 0.025 | $0.309 \cdot 10^{-6}$ | 0.075 | | | |
| 0.050 | $0.205 \cdot 10^{-6}$ | 0.065 | | | |
| 0.100 | $0.127 \cdot 10^{-6}$ | 0.054 | $0.153 \cdot 10^{-6}$ | 0.313 | 0.196 |
| 0.200 | $0.075 \cdot 10^{-6}$ | 0.043 | | | |
| 0.300 | $0.052 \cdot 10^{-6}$ | 0.038 | | | |
| | | | AgCNF | | |
| 0.025 | $0.996 \cdot 10^{-6}$ | 0.075 | | | |
| 0.050 | $0.741 \cdot 10^{-6}$ | 0.065 | | | |
| 0.100 | $0.519 \cdot 10^{-6}$ | 0.054 | $0.569 \cdot 10^{-6}$ | 0.346 | 0.196 |
| 0.200 | $0.333 \cdot 10^{-6}$ | 0.043 | | | |
| 0.300 | $0.256 \cdot 10^{-6}$ | 0.038 | | | |

Based on the above presented results, it can be concluded that all carbon-based composite electrodes were successfully obtained by the two-roll mill procedure.

The morphological, structural, and electrical characterization results of the above presented compositions of the carbon-based composite electrode reveal:

– the conductive fillers, *i.e.*, expanded graphite, carbon nanotubes, and carbon nanofibres are well-distributed and dispersed within the epoxy matrix taking into account the specific preparation method involving dispersion within a suitable solvent by sonication;

– silver presence in the form of silver-modified natural zeolite dispersed within the carbon composition was evidenced by SEM images.

Based on the results of the electrical conductivity measurements, it can be noticed that for the same content of the conductive filler (20 %, wt.) the electrical conductivity decreased as: AgZEG>AgZCNT>AgZCNF>CNT>AgCNF. This should be in direct relation with electrical properties of the conductive filler and also, with the dispersion and homogeneous degree of the conductive filler within the epoxy matrix. The presence of silver-modified natural zeolite within the composite composition improved the electrical properties due to the silver presence. All prepared carbon-based composite electrodes are characterized by the electrical conductivities so as to be suitable for the electrochemical applications.

The electrochemical behaviour of the well-known ferri/ ferrocyanide standard redox system allowed determining the electroactive surface area of these electrodes. Based on the ratio between the electroactive and geometrical surface area, it can be concluded that CNT-based composite electrodes exhibited the best electroactive properties. Also, the good electroactive properties were found for CNF-based composite electrodes. In addition, some aspects related to the diffusion-control and adsorption processes on the electrode surface were discussed.

## 7.3. References

[1] J.Y. Yi, G.M. Choi, J. Electroceram. 3 (1999) 361.
[2] D. Hecht, L. Hu, G. Gruner, Appl. Phys. Lett. 89 (2006) 133112.
[3] K. Miyasaka, K. Watanabe, E. Jojima, H. Aida, M. Sumita, K.J. Ishikawa, Mater. Sci. 17 (1982) 1610.
[4] S.H. Munson- McGee, Phys. Rev. B. 43 (1991) 3331.
[5] F. Du, J.E. Fischer, K.I. Winey, Phys. Rev. B. 72 (2005) 121404(R).
[6] F.C. Dalmas, C. Gauthier, L. Chazeau, R. Dendievel, Comp. Sci. Technol. 67 (2007) 829.
[7] J.E. O'Reilly, Biochim. Biophys. Acta 292 (1973) 209.
[8] P. Zanello, Inorganic Electrochemistry Theory, Practice and Application, Ed. The Royal Society of Chemistry, 2003.
[9] V.N. Kiryushov, L.I. Skvortsova, T.P. Aleksandrova, J. Anal. Chem. 66 5 (2011) 510.
[10] J.M. Nugent, K.S.V. Santhanam, A. Rubio, P.M. Ajayan, Nano Lett. 1 2 (2001) 87.
[11] R.G. Compton, C.E. Banks, Imperial College Press (2011) 107.
[12] A. Baciu, A. Remes, E. Ilinoiu, F. Manea, S.J. Picken, J. Schoonman, Environ. Eng. Manag. J. 11 2 (2012) 1968.

# CHAPTER 8. ELECTROCHEMICAL DEGRADATION OF PHARMACEUTICALS USING CARBON-BASED ELECTRODES

## 8.1. Introduction

Over the past century, the evolution in the sciences has led to major breakthroughs that have expanded and vastly improved human life in the area of exploration and development of pharmaceuticals. Pharmaceuticals and endocrine disrupting compounds (EDCs) represent a structurally diverse class of emerging contaminants that have been detected throughout the environment, especially in wastewater that impacted surface water, groundwater, estuarine water, and drinking water. The widely used non-steroidal anti-inflammatory drugs: ibuprofen, naproxen, diclofenac and some of their metabolites are very often detected in sewage, surface and ground water, drinking water, tap water, ocean water, sediments and soil. Although, the amount of these pharmaceuticals in the aquatic environment is low, its continuous input may constitute in the long term a potential risk for aquatic and terrestrial organisms. Therefore, over the past few years they are considered to be an emerging environmental problem [1-7].

Ibuprofen (IBP) is the most consumed medicines all over the world, having an estimated annual production of several kilotons, *e.g.*, 345 t in Germany in 2001 [1]. Industrial pollution occurs because of the release of untreated effluents from the pharmaceutical companies (IBP is a non-prescription, non-steroidal drug, widely used as an anti-inflammatory and antipyretic drug especially prescribed for the treatment of fever, migraine, muscle aches, arthritis and tooth aches), whereas, the domestic contamination is due to the use of IBP as a medicinal drug by human beings and animals.

Various treatment processes for ibuprofen removal from wastewater have been reported, *e.g.*, active carbon [8], ultrafiltration [9], biological [10], photo-Fenton [11], supramolecular solid-phase extraction [12], photolytic [13], gamma irradiation [14]. The selection of the treatment methods have to take into account the process performance in relation with process efficiency and economic aspects.

Electrochemical methods represent a very promising way to achieve the total degradation of wastewaters containing persistent pollutants. Recent studies have been conducted on the electrodegradation of pharmaceutical pollutants [15-17]. These are based on direct electrolysis, where pollutants are removed by direct electron transfer at the electrode or indirect electrolysis, where pollutants are destroyed in the bulk solution by active species generated at the electrode.

In general, the electrochemical methods exhibit several advantages, *e.g.*, environmental compatibility, since the used reagent is the electron, versatility, because pollutants can be treated using different reactors and electrode materials of distinct forms and configurations. In addition, processes can be easily scaled from laboratory to industrial plant, security, due to the mild operative conditions employed and the small amounts of generally innocuous chemicals used, and energy efficiency, since electrochemical processes are operated at low pressure and

temperature (environmental conditions), using low cost equipment and simple operations.

The key of the electrochemical performance is given by the electrode material. Carbon, in many respects, represents an ideal electrode. Its attractive features include access to a wide anodic potential range, low electrical resistance and residual currents and a reproducible surface structure.

A large variety of carbon forms suitable for the degradation of pharmaceuticals by electrochemical degradation have been reported, *e.g.,* glassy carbon (GC) [18-22], carbon pastes (CP) [23], boron-doped diamond (BDD) [3, 16, 24-28], and carbon nanotubes [29-32].

Recently, the use of carbon-nanotubes (CNTs) as a catalyst has recently attracted growing attention for environmental applications, including the oxidation of organic compounds present in polluted waters by catalytic wet oxidation or electrooxidation.

The aim of this chapter study is to characterize the electrochemical behaviours of several types of carbon-based electrodes, *i.e.,* boron-doped diamond (BDD), glassy carbon (GC), carbon nanotubes-epoxy composite (CNT), silver-doped zeolite-carbon nanotubes-epoxy composite (AgZCNT) and silver-doped zeolite-expanded-graphite-epoxy composite (AgZEG) electrodes in the presence of ibuprofen (IBP), which was chosen as a model of the pharmaceutical pollutant from water. The electrochemical characterization and applications of the electrode for IBP degradation and mineralization were performed using cyclic voltammetry (CV), chronoamperometry (CA) and multiple-pulsed amperometry (MPA) techniques. The electrochemical performances of the electrodes were assessed in terms of degradation and mineralization process efficiency and electrochemical efficiency. Also, the effect of chlorine/ hypochlorite oxidation agent generated *in-situ* was investigated to improve the electrochemical performance of CNT electrode.

## 8.2. Experimental

*Reagents*

Standard solution of 1 $gL^{-1}$ ibuprofen was prepared from analytical reagent from BASF SE, (Ludwigshafen, Germany) using distilled water and 0.1 M NaOH solution. In Figure 8.1 is shown the molecular structure of ibuprofen.

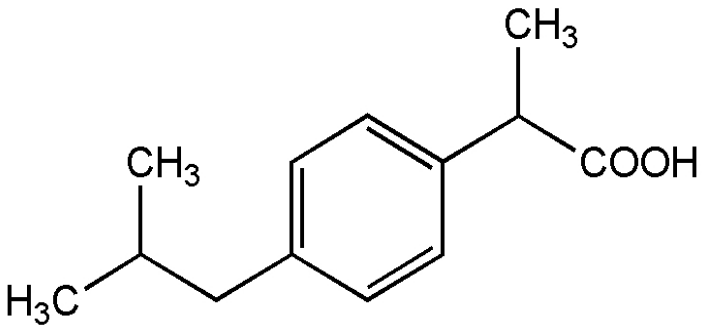


**Figure 8.1.** Molecular structure of ibuprofen.

0.1 M $Na_2SO_4$, and mixture of 0.075 M $Na_2SO_4$ and 0.025 M NaCl solutions as supporting electrolytes for the characterization and application of electrodes materials were freshly prepared from $Na_2SO_4$ and NaCl of analytical purity (Merck) with distilled water.

*Working electrodes*

The carbon-based composite working electrodes used for the detection of IBP are gathered in Table 8.1.

**Table 8.1.** Carbon-based composite working electrode tested for the electrochemical detection of IBP.

| Carbon-based composite electrode | Geometrical area/ $cm^2$ | Electroactive surface area/ $cm^2$ |
|---|---|---|
| CNT | 0.196 | 0.473 |
| AgZCNT | 0.196 | 0.411 |
| AgZEG | 0.196 | 0.320 |

The commercial glassy carbon electrode (GC) was supplied by Metrohm, Switzerland and boron-doped diamond electrode (BDD) was supplied by Windsor Scientific Ltd., UK.

*Electrochemical characterization of the electrodes*

The electrochemical behaviour of the BDD, GC, CNT, AgZCNT, and AgZEG electrodes in the presence of ibuprofen (IBP) were studied by cyclic voltammetry (CV) in 0.1 M $Na_2SO_4$ supporting electrolyte. The effect of chloride presence was studied for CNT electrode using 0.075 M $Na_2SO_4$ and 0.025 M NaCl supporting electrolyte. Subsequently, an electrochemical pretreatment by three repetitive cycling between -0.5 V to +1.5 V vs. Ag/ AgCl in the same supporting electrolyte was performed. Prior to use, the working electrodes were gradually cleaned, first polished with abrasive paper and then on a felt-polishing pad by using 0.5 μm alumina powder (Metrohm, Switzerland) in distilled water for 5 minutes and rinsing with distilled water.

The electrochemical behaviour of the electrodes were performed using an Autolab potentiostat/ galvanostat PGSTAT 302 (Eco Chemie, The Netherlands) controlled with GPES 4.9 software and a three-electrode cell, with a Ag/ AgCl reference electrode, a platinum counter electrode and carbon-based working electrode.

*Electrolysis experiments under potentiostatic conditions*

The electrochemical performance of the electrodes were determined also, using an Autolab potentiostat/ galvanostat PGSTAT 302 (Eco Chemie, The Netherlands) controlled with GPES 4.9 software and a three-electrode cell, with a Ag/ AgCl reference electrode, a platinum counter electrode and carbon-based working electrode by application of chronoamperometry (CA) and multiple-pulsed amperometry (MPA) techniques under the working conditions gathered in Table 8.2.

**Table 8.2.** Electrochemical working conditions for each type of electrode.

| Electrode material | Technique | Working conditions | Supporting electrolyte |
|---|---|---|---|
| BDD | CA | $E_{ox}$= +1. 5 V | 0.1 M $Na_2SO_4$ |
| | | $E_{ox}$= +2 V | 0.1 M $Na_2SO_4$ |
| GC | CA | $E_{ox}$= +1. 5 V | 0.1 M $Na_2SO_4$ |
| | | $E_{ox}$= +2 V | 0.1 M $Na_2SO_4$ |
| CNT | CA | $E_{ox}$= +1.25 V | 0.1 M $Na_2SO_4$ |
| | | $E_{ox}$= +1. 5 V | 0.1 M $Na_2SO_4$ |
| | | $E_{ox}$= +1.75 V | 0.1 M $Na_2SO_4$ |
| | | $E_{ox}$= +1. 5 V | 0.075 M $Na_2SO_4$ and 0.025 M NaCl |
| | MPA | $E_{oxidation}$= +1.5 V; $E_{reactivation}$= +1.75 V; $E_{conditioning}$= -0.5 V | 0.1 M $Na_2SO_4$ |
| | | $E_{oxidation}$= +1.5 V; $E_{reactivation}$= +1.75 V | 0.1 M $Na_2SO_4$ |
| | | $E_{oxidation}$= +1.5 V; $E_{reactivation}$= +1.75 V | 0.075 M $Na_2SO_4$ and 0.025 M NaCl |
| AgZCNT | CA | $E_{ox}$= +1.25 V | 0.1 M $Na_2SO_4$ |
| | | $E_{ox}$= +1. 5 V | 0.1 M $Na_2SO_4$ |
| | | $E_{ox}$= +1.75 V | 0.1 M $Na_2SO_4$ |
| AgZEG | CA | $E_{ox}$= +1.25 V | 0.1 M $Na_2SO_4$ |
| | | $E_{ox}$= +1. 5 V | 0.1 M $Na_2SO_4$ |
| | | $E_{ox}$= +1.75 V | 0.1 M $Na_2SO_4$ |

*Bulk electrolysis experiments*

The electrochemical experiments were carried out at room temperature (22-25 °C) by batch process using an undivided cell of 0.7 $dm^3$ volume, in 0.1 M $Na_2SO_4$ supporting electrolyte. The BDD/Nb electrodes (100 mm x 50 mm x 1 mm) with 280 $cm^3$ geometric area provided by CONDIAS, Germany were used as anodes, and stainless steel plates (100 mm x 50 mm x 1 mm) were employed as cathodes under vertical arrangement. A regulated DC power supply (HY3003, MASTECH) was used under galvanostatic regime at current densities of 5 and 10 mA $cm^{-2}$.

*Analytical procedures*

After a certain time of electrolysis, samples were drawn from the cell and IBP degradation was followed by UV-VIS spectroscopy using a Varian Cary UV-VIS spectrophotometer. IBP mineralization was checked by TOC and COD parameters, which were analyzed using a Shimadzu TOC analyzer and respective, standard method. An Inolab WTW pH meter was used to measure the solution pH. General parameters for the assessment of the performance of the applied processes were used.

Thus, the IBP degradation was calculated based on IBP concentration determined by absorbance recorded at 220 nm wavelength (see Figure 8.2). The process degradation efficiency ($\eta$) was determined using the Equation (1) [33]:

$$\eta = \frac{(IBP_0 - IBP)}{IBP_0} \times 100 \quad (\%) \qquad (1)$$

The *electrochemical efficiency* for IBP oxidation was determined based on equation (2) [33]:

$$E_{IBP} = \frac{(IBP_0 - IBP)}{Q * S} \times V \ (\text{mg / C}\cdot\text{cm}^2) \qquad (2)$$

where $IBP_0$-IBP represent the change in the IBP concentration determined spectrophotometrically during experiments for a charge consumption of Q corresponding to various electrolysis time, V is the sample volume (30 $cm^3$) and S is the area of the electrode surface ($cm^2$).

The *mineralization degree* was assessed also based on equation (1) using COD and TOC parameters instead of IBP concentration determined spectrophotometrically. The electrochemical efficiency for IBP mineralization defined as an overall efficiency for complete oxidation to $CO_2$ was determined based on Equation (2) modified as (2' and 2") taking into consideration the change in TOC and COD measurements during experiments, determining $TOC_0$ – TOC and $COD_0$-COD, respectively:

$$E_{TOC} = \frac{(TOC_0 - TOC)}{Q * S} \times V \ (\text{mg/ C}\cdot\text{cm}^2) \qquad (2')$$

$$E_{COD} = \frac{(COD_0 - COD)}{Q * S} \times V \ (\text{mg/ C}\cdot\text{cm}^2) \qquad (2'')$$

The *mineralization current efficiency* (MCE, %), defined also as current output for direct faradayc complete oxidation, for each electrolyzed solution was calculated based on Equation (3) [33]:

$$MCE = \frac{nFV_s\Delta(TOC)_{\text{exp}}}{4.32 \times 10^7 mIt} \times 100 \ (\%) \qquad (3)$$

where *n* is the number of electrons consumed in the mineralization process of IBP, F is the Faraday constant (= 96 487 C $mol^{-1}$ ), Vs is the solution volume ($dm^3$), $\Delta(TOC)_{exp}$ is the experimental TOC decay (mg $dm^{-3}$), 4.32 x $10^7$ is a conversion factor for units homogenization (= 3 600 s $h^{-1}$ x 12 000 mg of carbon $mol^{-1}$), m is the number of carbon atoms in IBP dye, I is the applied current (A), and t is time (h). The number of electrons consumed is determined based on the overall mineralization reaction of IBP to $CO_2$ ($C_{13}H_{17}O_2 + 24H_2O = 13CO_2 + 65H^+ + 65e^-$).

The *specific energy consumption*, $W_{sp}$, was calculated with the Equation (4) [33]:

$$W_{sp} = \frac{\left(Q * V^{-1}\right)U}{1000} \text{ (kWh dm}^{-3}\text{)} \qquad (4)$$

where *Q* represents the specific charge consumption, *U* is the cell voltage (V), *V* is the solution volume ($dm^3$).

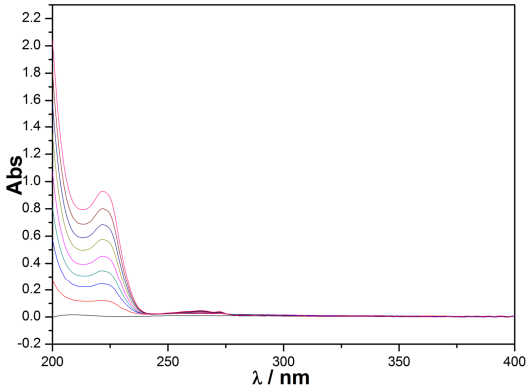


(a)

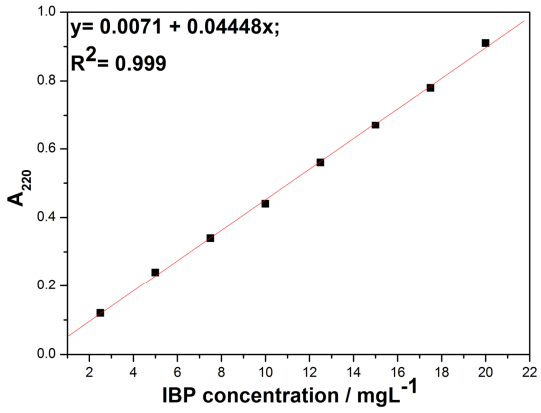


(b)

**Figure 8.2.** (a) UV-VIS spectra recorded at different IBP concentration between 2.5- 20 $mgL^{-1}$; (b) Calibration plots of IBP concentrations recorded at 220 nm.

## 8.3. Results and discussion

### *8.3.1. Commercial glassy carbon (GC) and boron-doped diamond (BDD) electrodes*

#### 8.3.1.1. Electrochemical behaviour of IBP on GC and BDD electrodes

Figure 8.3 shows the cyclic voltammograms (CVs) recorded at scan rate of 0.05 $Vs^{-1}$ in 0.1 M $Na_2SO_4$ supporting electrolyte and in the presence of 10 and 30 $mgL^{-1}$ IBP on GC and respective, BDD electrodes in order to clarify the relationship between experimental variables and the electrode response. Cyclic voltammograms recorded at GC electrode in the presence of the IBP (Figure 8.3a) show that IBP oxidation starts from the potential value of about 0.65 V vs. Ag/ AgCl, while for the BDD electrode the oxidation process starts much later (about 1 V vs. Ag/ AgCl) (Figure 8.3b). However, it must be mentioned the difference between the potential windows of GC and BDD electrode, the last one exhibited larger potential windows. The voltammetric parameters determined based on CV shape in the presence/ absence of IBP are gathered in Table 8.3.

**Table 8.3.** Voltammetric parameters determined by cyclic voltammetry recorded in 0.1 M $Na^2SO^4$ supporting electrolyte and in the presence of IBP; potential scan rate of 0.05 $Vs^{-1}$; potential range: -0.5 to +1.5 V /Ag/ AgCl.

| IBP conc./ $mgL^{-1}$ | Electrode material | $E_{oxidation}$ starting/ V | $E_{oxygen}$ evolution/ V | Useful signal/ µA |
|---|---|---|---|---|
| 10 | GC | 0.65 | 1.00 | 5.76 |
| | BDD | 1.00 | 1.50 | 2.92 |
| 30 | GC | 0.65 | 1.00 | 12.74 |
| | BDD | 1.00 | 1.50 | 2.20 |

It can be noticed for each electrode that even if the anodic current increased in the presence of IBP at the potential value prior to oxygen evolution, no limiting current characteristics to the diffusion process occurred. However, the effect of IBP increasing on CV shapes showed a different behaviour of the electrode. A linear dependence was noticed for GC between anodic current recorded at the potential value +1.38 V and IBP concentration over IBP concentrations ranged from 10 to 50 $mgL^{-1}$ (Figure 8.4a). Decreasing the anodic current was noticed for BDD electrode with IBP increasing beyond 10 $mgL^{-1}$, which informed about the electrode fouling under this concentrations range (Figure 8.4b).

It is obvious that increasing initial concentration decreased the rate of IBP oxidation due to faster electrode fouling. On the other hand, it is known that increasing the bulk solution concentration should increase the rate of IBP oxidation if the process is mass transfer-controlled [34]. Based on all above-presented voltammetric results, the direct oxidation of IBP on GC electrode should be mass transfer-controlled. The significant electrode fouling occurred at BDD electrode for the oxidation of IBP under water stabilization. In general, the electrode fouling owes the complex mechanism of aromatic compounds oxidation on carbon-based electrode, which involves both the adsorption of reactant/ intermediate or final oxidation products and the formation of passive, nonconductive layer of oligomer products of oxidation process on its surface [34-37].

The lack of the cathodic current corresponding to anodic one informed about the irreversibility of the IBP anodic oxidation on BDD electrode. These results confirmed that IBP can be oxidized by the direct electron transfer process at the electrode surface under water stability potential. However, during the repetitive cyclic voltammetry scanning the anodic peak current decreased because of the electrode fouling occurred during the oxidation process (the results are not shown here). The loss of the electrode activity could inform about the direct oxidation of the IBP on the electrode surface by the electron transfer and no direct generation of the hydroxyl radicals. Based on these results, the potential/ current density belongs to the potential range corresponding to the water decomposition to generate sufficient amount of the hydroxyl radicals to operate the further electrolysis under potentiostatic/ galvanostatic regime.

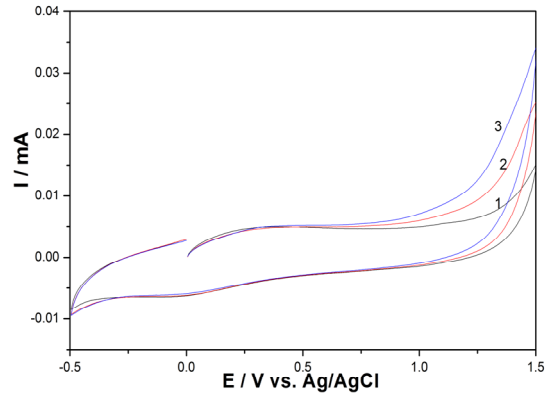


(a)

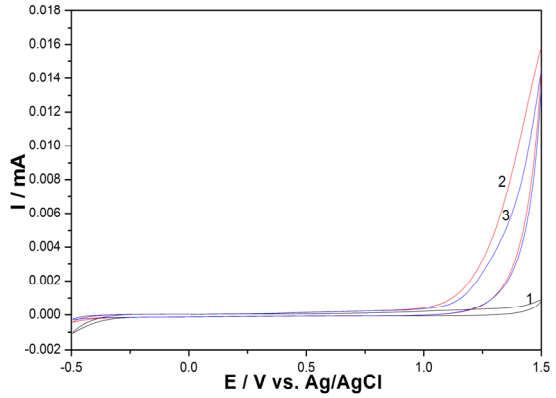


(b)

**Figure 8.3.** Cyclic voltammograms recorded in 0.1 M $Na_2SO_4$ supporting electrolyte (curve 1) and in the presence of various IBP concentrations: 10 $mgL^{-1}$ IBP (curve 2) and 30 $mgL^{-1}$ IBP (curve 3) using: GC electrode (a) BDD electrode (b); potential scan rate: 0.05 $Vs^{-1}$; potential range: -0.5 to +1.5 V /Ag/ AgCl.

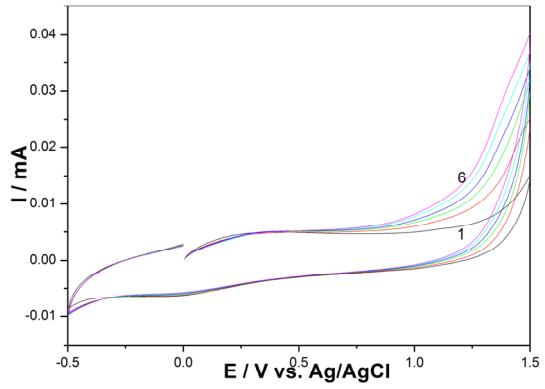


(a)

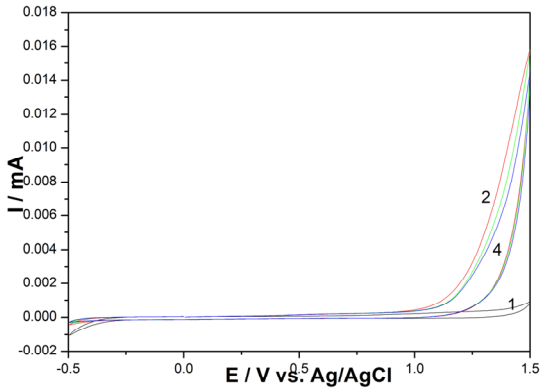


(b)

**Figure 8.4.** Cyclic voltammogram recorded in 0.1 M $Na_2SO_4$ supporting electrolyte (curve 1) and in the presence of various IBP concentrations: curves 2- 6: 10- 50 $mgL^{-1}$ IBP using: GC electrode (a) and BDD electrode (b); potential scan rate: 0.05 $Vs^{-1}$; potential range: -0.5 to +1.5 V /Ag/ AgCl.

### 8.3.1.2. Electrochemical application of GC and BDD electrodes in IBP oxidation process under potentiostatic regime by chronoamperometry

Due to chronoamperometry technique should be regarded as very suitable to simulate the practical operation of the electrolysis process under potentiostatic conditions, it was applied to assess the electrode performance for IBP degradation and mineralization. Taking into account that the direct anodic oxidation of IBP should occurred on the electrode surface at the potential value belongs to the potential windows, but the electrode fouling is expected, the oxidation process was

carried out at the potential values belongs to water decomposition (see Table 8.3). To obtain information about electrode fouling and the electrochemical activity of GC and BDD electrodes used for IBP oxidation at the anodic potential values of +1.5 V and respective, +2 V vs. Ag/ AgCl, chronoamperometric measurements were performed. Chronoamperometry is very useful to simulate the electrooxidation application under potentiostatic conditions to determine the optimum operating electrolysis conditions. Figure 8.5a and b presents the chronoamperograms recorded at BDD and GC electrodes in 0.1 M $Na_2SO_4$ supporting electrolyte for the time duration of 2 h, and each electrode exhibited a different behaviour in relation with the applied potential value.

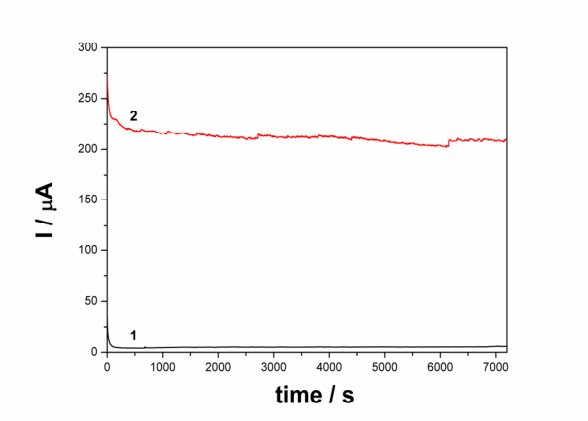


(a)

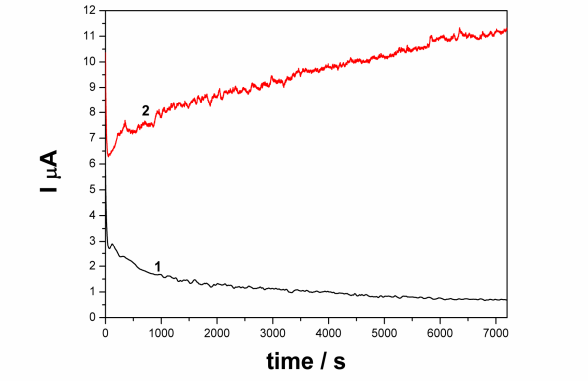


(b)

**Figure 8.5.** Chronoamperograms (CAs) recorded at E= +1.5 V vs. Ag/ AgCl (curve 1) and E= +2 V vs. Ag/ AgCl in 0.1 M $Na_2SO_4$ supporting electrolyte and in the presence of 10 $mgL^{-1}$ IBP concentration using a) GC electrode and b) BDD electrode.

At the applied potentials, the electrolysis is under mass transport-control and the secondary reactions of oxygen evolution are involved with a decreasing

current efficiency [38]. Thus, during the chronoamperograms running at the potential value of +1.5 V vs. Ag/ AgCl the recorded current decreased because of the electrode fouling due to the oxidation products adsorption on the electrode surface. At this potential value, this effect is more pronounced for BDD electrode because the oxygen evolution had just started, while for GC electrode the oxygen evolution occurred. In contrast, at the applied potential value of +2 V vs. Ag/ AgCl, BDD electrode exhibited the activated electrode surface for the IBP electrooxidation and the current increased. This effect was not noticed for GC, for which a slight current decreasing was recorded.

The determination of IBP concentrations after chronoamperometry running under the potentiostatic conditions were performed by spectrophotometric, classical COD and TOC methods to assess the process degradation efficiency ($\eta$) and the electrochemical efficiency (E). The example of the evolution of UV-VIS spectra profile of 10 $mgL^{-1}$ IBP before/ after CA applying under potential value of +1.5 V vs. Ag/ AgCl at BDD electrode for two hours of the electrolysis time is presented in Figure 8.6.

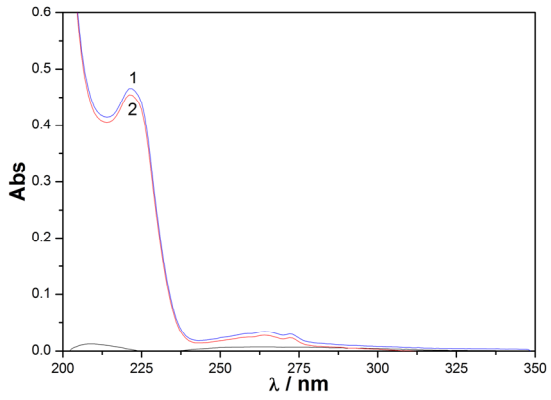


**Figure 8.6.** Evolution of UV-VIS spectra of 10 $mgL^{-1}$ IBP before (curve 1) /after (curve 2) CA applying at BDD electrode at potential value of +1.5 V vs. Ag/ AgCl.

The results regarding the electrode performance for the electrooxidation of IBP are gathered in Table 8.4.

**Table 8.4.** The electrode performance for the electrooxidation of IBP using chronoamperometry.

| Electrode material | Working conditions | $\eta_{conc}$/% | $E_{conc}$/g C $cm^{-2}$ | $\eta_{COD-Cr}$/ % | $E_{COD-Cr}$/ g C $cm^{-2}$ | $\eta_{TOC}$/% | $E_{TOC}$/g C $cm_{-2}$ |
|---|---|---|---|---|---|---|---|
| GC | $E_{ox}$= +1.5 V | 15 | 6.050 | 8 | 12.100 | -* | -* |
| | $E_{ox}$= +2 V | 45 | 0.440 | 32 | 1.320 | 6 | 0.065 |
| BDD | $E_{ox}$= +1.5 V | 12 | 39.620 | 10 | 127.200 | 1 | 3.430 |
| | $E_{ox}$= +2 V | 50 | 9.550 | 44 | 33.810 | 7 | 1.390 |

*not determined

Based on these above-presented results, it can be seen that BDD electrode exhibited superiority in relation with its performance for IBP degradation and mineralization. The optimum working conditions for applied potential will be selected in relation with the specific requirements linked to the technical-economical ratio. Further studies were carried out under galvanostatic conditions using BDD electrode.

### 8.3.1.3. Bulk electrolysis of IBP on BDD electrode

The anodic oxidation of IBP on BDD/ Nb electrodes in 0.1 M $Na_2SO_4$ supporting electrolyte has been performed under galvanostatic regime and bulk electrolysis conditions, at two different current densities. The current densities of 5 and 10 mA $cm^{-2}$ were selected taking into account the CV results in relation to the conditions suitable for the formation of hydroxyl radicals at the BDD surface.

Solutions of 10 $mgL^{-1}$ IBP in 0.1 M $Na_2SO_4$ supporting electrolyte at pH 5 were degraded by applying two current densities of 5 and 10 mA $cm^{-2}$. In each series, the IBP degradation efficiency was monitored in terms of $A_{220}$ and TOC parameters. Under all current density conditions applied for the electrooxidation process, the degradation of IBP occurred under the action of hydroxyl radical generated, physisorbed or remained near the BDD surface. Also, in sulphate media, besides hydroxyl radicals other weaker oxidants can be generated, *e.g.*, $S_2O_8^{2}$, $H_2O_2$ and $O_3$ [39].

The results regarding the electrode performance for the electrooxidation of IBP are gathered in Tables 8.5 and 8.6.

**Table 8.5.** The electrode performance for the electrooxidation of IBP, current density of 5 mA $cm^{-2}$, pH 5.

| Time | I/A | U/V | Q/Ah | $QV^{-1}$ /Ah $dm^{-3}$ | Wsp/ KWh $dm^{-3}$ | V/ $dm^3$ | pH | $\eta_{220}$ | $\eta_{TOC}$ | $E_{220}$/ µg C $cm^{-2}$ | $E_{TOC}$/ µg C $cm^{-2}$ | MCE |
|---|---|---|---|---|---|---|---|---|---|---|---|---|
| 0 | 1.40 | 0 | 0 | 0 | - | 0.70 | 10.42 | - | - | - | - | - |
| 15 | 1.40 | 4.50 | 0.35 | 0.50 | 2.25 | 0.70 | 10.55 | 17.39 | 5 | 0.35 | 1.10 | 1.27 |
| 30 | 1.40 | 4.50 | 0.70 | 1.00 | 4.50 | 0.70 | 10.47 | 34.78 | 15 | 0.36 | 1.70 | 1.90 |
| 60 | 1.40 | 4.50 | 1.40 | 2.00 | 9.00 | 0.70 | 10.74 | 47.83 | 25 | 2.40 | 1.40 | 1.57 |
| 90 | 1.40 | 4.50 | 2.10 | 3.00 | 13.50 | 0.70 | 10.18 | 49.00 | 27 | 1.70 | 1.00 | 1.13 |
| 120 | 1.40 | 4.50 | 2.80 | 4.00 | 18.00 | 0.70 | 10.53 | 50.00 | 31 | 1.30 | 0.87 | 0.98 |
| 150 | 1.40 | 4.60 | 3.50 | 5.00 | 23.00 | 0.70 | 9.97 | 58.00 | 35 | 1.20 | 0.78 | 0.88 |

**Table 8.6.** The electrode performance for the electrooxidation of IBP, current density of 10 mA $cm^{-2}$, pH 5.

| Time | I/A | U/V | Q/Ah | $QV^{-1}$ /Ah $dm^{-3}$ | Wsp/ KWh $dm^{-3}$ | V/ $dm^3$ | pH | $\eta_{220}$ | $\eta_{TOC}$ | $E_{220}$/ µg C $cm^{-2}$ | $E_{TOC}$/ µg C $cm^{-2}$ | MCE |
|---|---|---|---|---|---|---|---|---|---|---|---|---|
| 0 | 2.80 | 0 | 0 | 0 | - | 0.70 | 10.57 | - | - | - | - | - |
| 15 | 2.80 | 5.20 | 0.70 | 1.00 | 5.20 | 0.70 | 10.85 | 25 | 7 | 2.60 | 0.78 | 0.88 |
| 30 | 2.80 | 5.10 | 1.40 | 2.00 | 10.20 | 0.70 | 10.95 | 39 | 21 | 2.00 | 1.18 | 1.33 |
| 60 | 2.80 | 5.10 | 2.80 | 4.00 | 20.40 | 0.70 | 10.47 | 56 | 29 | 1.40 | 0.81 | 0.91 |
| 90 | 2.80 | 5.10 | 4.20 | 6.00 | 30.60 | 0.70 | 11.00 | 62 | 38 | 1.10 | 0.71 | 0.80 |
| 120 | 2.80 | 5.20 | 5.60 | 8.00 | 41.60 | 0.70 | 11.03 | 72 | 49 | 0.92 | 0.69 | 0.77 |
| 150 | 2.80 | 5.20 | 7.00 | 10.00 | 52.00 | 0.70 | 10.91 | 80 | 56 | 0.82 | 0.63 | 0.70 |

The IBP removal efficiency expressed in terms of $A_{220}$, which represents the aromatic ring cleavage degree, was influenced by the current density. 80 % removal efficiency for current density of 10 mA $cm^{-2}$ was achieved after 150 min, and for current density of 5 mA $cm^{-2}$ the removal efficiency reached only 58 %. From Figure 8.7 it can be seen that after 150 minutes of the electrolysis time the IBP mineralization degree reached 35 % for the current density of 5 mA $cm^{-2}$ and 56 % for current efficiency at 10 mA $cm^{-2}$.

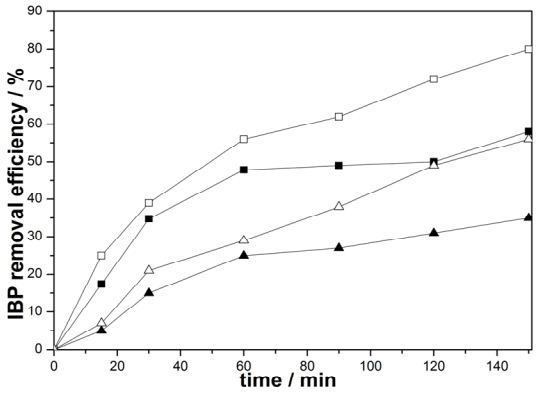


**Figure 8.7.** Effect of the current density on the evolution of IBP removal efficiency versus electrolysis time; operating conditions: 10 $mgL^{-1}$ IBP, 0.1 M $Na_2SO_4$ supporting electrolyte, pH 5. Removal efficiency: aromatic ring cleavage (■) j= 5 mA $cm^{-2}$, (□) j= 10 mA $cm^{-2}$; TOC removal (▲) j=5 mA $cm^{-2}$, (Δ) j= 10 mA $cm^{-2}$.

A different behaviour regarding the assessment of the electrooxidation performance for IBP aromatic ring cleavage and mineralization was found based on the electrochemical efficiency determination, which takes into account the charge consumed during the electrooxidation process (Figure 8.8). In addition, the relationship between mineralization current efficiency, specific energy consumption and electrolysis time for each current density is shown in Figure 8.9. For the same electrolysis time, at higher current density the charge consumed and implicit, specific energy consumption increased. For all process parameters that characterize the electrochemical performance for IBP aromatic ring cleavage and mineralization, applying the current density of 5 mA $cm^{-2}$ allowed to reach the best results from technical-economical point of view at the electrolysis time of 150 minutes. This aspect is supported by the mineralization current efficiencies in relation with the specific electrical energy consumption, shown in Figure 8.9.

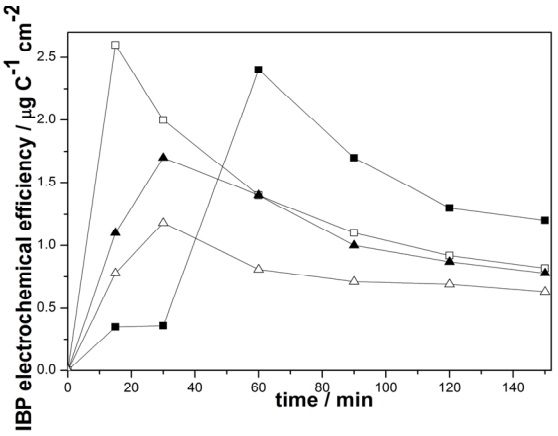


**Figure 8.8.** Evolution of electrochemical efficiency for IBP removal versus electrolysis time; operating conditions: 10 $mgL^{-1}$ IBP, 0.1 M $Na_2SO_4$ supporting electrolyte, pH 5. Electrochemical efficiency: aromatic ring cleavage (■) j= 5 mA $cm^{-2}$, (□) j= 10 mA $cm^{-2}$; TOC removal (▲) j= 5 mA $cm^{-2}$, (Δ) j= 10 mA $cm^{-2}$.

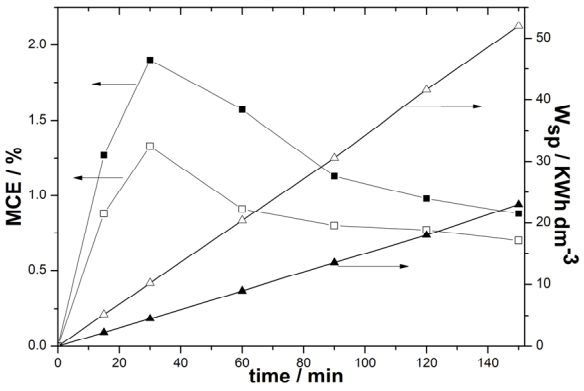


**Figure 8.9.** Correlation between mineralization current efficiency, specific energy consumption and electrolysis time; operating conditions: 10 $mgL^{-1}$ IBP, 0.1 M $Na_2SO_4$ supporting electrolyte, pH 5. Mineralization current efficiency: (■) j= 5 mA $cm^{-2}$, (□) j= 10 mA $cm^{-2}$; specific energy consumption: (▲) j= 5 mA $cm^{-2}$, (Δ) j= 10 mA $cm^{-2}$.

For the electrooxidation processes the pseudo first-order equations were chosen to determine the apparent rate constants ($k_{app}$ and $k'_{app}$), calculated based on the relations of $\ln(C_0/C_t)=k_{app}(t)$, and respective, $\ln(C_0/C_t)=k'_{app}(Q)$, in which Q represents the electrical charge passed during electrooxidation of IBP. Kinetics results determined for all parameters, $A_{220}$ and TOC are presented in Table 8.7. For

this short time of electrolysis, based on the apparent rate constant, the complete degradation of IBP followed two stages: the first of aromatic ring cleavage and the last one represented by the mineralization that is the slowest one.

The rate of the IBP degradation process was influenced by the current density, when the rate of the degradation process was assessed based on the electrolysis time, at higher current density the IBP degradation occurred faster. However, the assessment of IBP degradation rate based on the charge consumed showed that at the current density of 10 mA $cm^{-2}$ the aromatic ring degradation and mineralization occurred faster with applying the current density of 10 mA $cm^{-2}$. These kinetics results correlated with electrochemical efficiencies recommended the optimum current density of 10 mA $cm^{-2}$. As example of the evolution of UV-VIS spectra profile of 10 $mgL^{-1}$ IBP before/ after electrooxidation applying under the current density of 5 mA $cm^{-2}$, pH 5 is presented in Figure 8.10.

**Table 8.7.** Current density influence on the apparent rate constants versus time and electrical charge consumed; initial conditions: 10 $mgL^{-1}$ IBP, pH 5.

| j/mA $cm^{-2}$ | $k_{app220}$/ $min^{-1}$ | $R^2$ | $k_{app'220}$ /$C^{-1}$ | $R^2$ | $k_{appTOC}$ /$min^{-1}$ | $R^2$ | $k_{app'TOC}$ /$C^{-1}$ | $R^2$ |
|---|---|---|---|---|---|---|---|---|
| 5 | 0.005 | 0.900 | 0.224 | 0.900 | 0.003 | 0.955 | 0.120 | 0.955 |
| 10 | 0.010 | 0.980 | 0.443 | 0.988 | 0.005 | 0.994 | 0.230 | 0.994 |

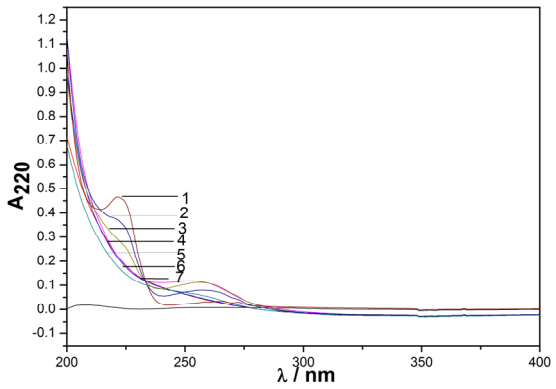


**Figure 8.10.** The evolution of UV-VIS spectra profile of 10 $mgL^{-1}$ IBP before/ after electrooxidation applying under the current density of 5 mA $cm^{-2}$, initial concentration (curve 1), after 15 min of electrolysis (curve 2), after 30min of electrolysis (curve 3), after 60 min of electrolysis (curve 4), after 90 min of electrolysis (curve 5), after 120 min of electrolysis (curve 6), after 150 min of electrolysis (curve 7); pH 5.

### *8.3.2. Carbon nanotubes-epoxy (CNT) composite electrode*

#### 8.3.2.1. Electrochemical behaviour of IBP on CNT electrode

Figure 8.11 shows the comparative cyclic voltammograms (CVs) recorded at scan rate of 0.05 $Vs^{-1}$ in 0.1 M $Na_2SO_4$ and respective, 0.075 M $Na_2SO_4$ and 0.025 M NaCl supporting electrolytes and in the presence of 50 $mgL^{-1}$ IBP on CNT electrode. In the absence of chloride, no oxidation peak appeared, even if the anodic current increased in the presence of IBP starting from the potential value of 0 V vs. Ag/ AgCl (behaviour almost similar to GC electrode). However, it must be noticed the occurrence of the oxidation and the reduction processes at the potential value of about +0.315 V /Ag/ AgCl and respective, +0.065 V /Ag/ AgCl of multi-walled carbon nanotubes in 0.1 M $Na_2SO_4$ supporting electrolyte. These processes are enhanced in the presence of IBP (curves 1 and 3 from Figure 8.11).

The chloride was introduced into the supporting electrolyte composition to generate *in-situ* hypochlorite by chloride oxidation on CNT surface. The CV shape is modified in the presence of $Cl^-$, an oxidation peak occurred at the potential value of about + 1 V /Ag/ AgCl that could be attributed to the chloride oxidation. Also, a very clear oxidation peak of IBP is evidenced in the presence of chloride, and the IBP oxidation signal is strongly improved (235 μA in comparison with 37 μA in absence of chloride, for 50 $mgL^{-1}$ IBP). In according with the literature [40], the products of IBP oxidation could be 2-(4-isobutylphenyl)-2-hydroxypropionic acid and 1-(1-hydroxyethyl)-4-isobuylbenzene. During the reverse scanning no cathodic peaks appeared that informed about the irreversibility of the IBP oxidation process. CVs recorded in the presence of various IBP concentrations informed that the anodic peak current recorded at about +1.2 V vs. Ag/ AgCl increases direct proportionally with increasing IBP concentrations in solution, which could inform about diffusion controlled IBP oxidation process. In the absence of chloride, despite the anodic peak did not appear, the anodic current increased with IBP concentration increasing (see Figure 8.12a and b).

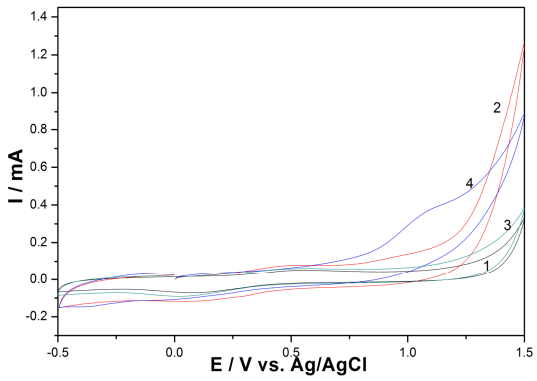


**Figure 8.11.** Cyclic voltammograms recorded at CNT electrode in: 0.1 M $Na_2SO_4$ supporting electrolyte (curve 1); 0.075 M $Na_2SO_4$ and 0.025 M NaCl supporting electrolyte (curve 2); 50 $mgL^{-1}$ IBP in 0.1 M $Na_2SO_4$ supporting electrolyte (curve 3); 50

$mgL^{-1}$ IBP in 0.075 M $Na_2SO_4$ and 0.025M NaCl supporting electrolyte (curve 4); potential scan rate: 0.05 $Vs^{-1}$; potential range: -0.5 to +1.5 V /Ag/ AgCl.

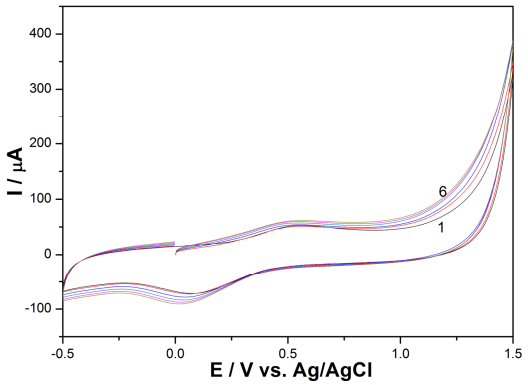


(a)

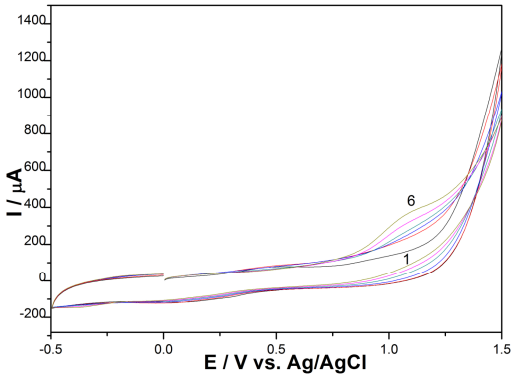


(b)

**Figure 8.12.** Cyclic voltammogram recorded on CNT electrode in: (a) 0.1 M $Na_2SO_4$ supporting electrolyte (curve 1) and (b) 0.075 M $Na_2SO_4$ and 0.025 M NaCl (curve 1) and in the presence of various IBP concentrations: curves 2-6: 10- 50 $mgL^{-1}$ IBP; potential scan rate: 0.05 $Vs^{-1}$; potential range: -0.5 to +1.5 V /Ag/ AgCl.

### 8.3.2.2. Electrochemical application of CNT electrode in IBP oxidation process under potentiostatic regime by chronoamperometry (CA) and multiple-pulsed amperometry (MPA)

Figure 8.13 a presents the chronoamperograms recorded at CNT electrode in 0.1 M $Na_2SO_4$ and mixture of 0.075 M $Na_2SO_4$ and 0.025 M NaCl supporting electrolyte for the time duration of 2 h, under various applied potentials (see Table 8.8), which belongs also to the water decomposition potential range. As we expected, the results show that the higher applied potential the higher current was recorded, which will decrease the current efficiency. Also, the presence of chloride led to higher current recording, which means higher charge consuming due to the secondary process of hypochlorite or chlorine evolution. The results regarding the electrode performance for the electrooxidation of IBP are presented in Table 8.8.

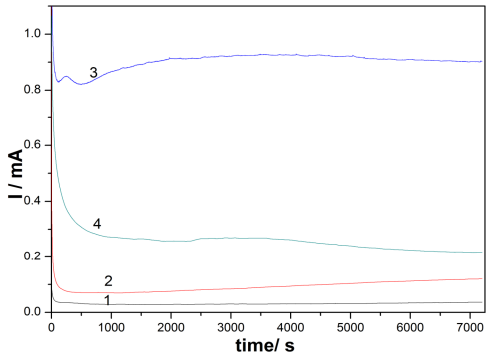


**Figure 8.13.** Chronoamperograms (CAs) of CNT electrode at: +1.25 V vs. Ag/ AgCl in 0.1 M $Na_2SO_4$ supporting electrolyte (curve 1); +1.5 V vs. Ag/ AgCl in 0.1 M $Na_2SO_4$ supporting electrolyte (curve 2); +1.75 V vs. Ag/ AgCl in 0.1 M $Na_2SO_4$ supporting electrolyte (curve 3); +1.5 V vs. Ag/ AgCl in 0.075 M $Na_2SO_4$ and 0.025 M NaCl supporting electrolyte (curve 4); in the presence of 10 $mgL^{-1}$ IBP concentration.

**Table 8.8.** CNT electrode performance for the electrooxidation of IBP using chronoamperometry and multiple-pulsed amperometry.

| Technique | Working conditions | Supporting electrolyte | $\eta_{conc}$/ % | $E_{conc}$/g C $cm^{-2}$ | $\eta_{COD-Cr}$/ % | $E_{COD-Cr}$/g C $cm^{-2}$ | $\eta_{TOC}$/ % | $E_{TOC}$/g C $cm^{-2}$ |
|---|---|---|---|---|---|---|---|---|
| CA | $E_{ox}$= +1.25 V | 0.1 M $Na_2SO_4$ | 50 | 0.93 | 43.00 | 3.09 | 32.49 | 2.09 |
| | $E_{ox}$= +1. 5 V | 0.1 M $Na_2SO_4$ | 72 | 1.43 | 66.70 | 4.80 | 35.50 | 0.74 |
| | $E_{ox}$= +1.75 V | 0.1 M $Na_2SO_4$ | 72 | 1.35 | 67.00 | 4.82 | 37.21 | 0.08 |
| | $E_{ox}$= +1. 5 V | 0.075 M $Na_2SO_4$ and 0.025M NaCl | 75 | 0.81 | 69.00 | 2.71 | 27.50 | 0.27 |
| MPA | $E_{oxidation}$= +1.5V; $E_{reactivation}$=+1.75V; $E_{conditioning}$= -0.5V | 0.1 M $Na_2SO_4$ | 77 | 0.45 | 72.69 | 1.92 | 9.76 | 0.06 |
| | $E_{oxidation}$= +1.5V; $E_{reactivation}$= +1.75V | 0.1 M $Na_2SO_4$ | 74 | 0.44 | 69.00 | 1.82 | 9.45 | 0.06 |
| | $E_{oxidation}$= +1.5V; $E_{reactivation}$= +1.75V | 0.075M $Na_2SO_4$ and 0.025M NaCl | 78 | 0.21 | 75.00 | 0.73 | 30.54 | 0.07 |

In comparison with GC and BDD electrodes, it can be seen that CNT electrode exhibited the best performance regarding the process degradation efficiency (75 % vs. 50 % for BDD and respective, 45 % for GC). Even if this electrode was operated only at +1.5 V vs. Ag/ AgCl, higher charge consumption was recorded and thus, the electrochemical degradation efficiency decreased. The similar situation was noticed for the removal of organic load expressed as COD parameter and corresponding to IBP presence. The best performance in relation with the process efficiency was reached for CNT electrode but for the electrochemical efficiency point of view the BDD electrode allowed to achieve the best results. Also, using CNT electrode the best mineralization degree was reached but with higher charge consumption in comparison with BDD electrode. Moreover, the presence of chloride in the supporting electrolyte improved the process efficiency in terms of IBP degradation and especial of mineralization. This could be explained by the chlorine/ hypochlorite attack over IBP and by-products in addition of the direct oxidation on the electrode surface.

It is known that a simple method for *in-situ* renewing the electrode surface is based on the anodic treatment. This relies on selecting the working electrode potential high enough to oxidize the insulating film and making it water soluble without damaging the electrode. Multiple-pulsed amperometry (MPA) has proved to be extremely sensitive for *in-situ* cleaning and reactivating the electrode surface during the electroanalytical oxidation [38]. Two different schemes for MPA applying for IBP electrodegradation were tested based on the CV shape in the presence of IBP. The first scheme consisted of three potential levels for IBP oxidation (E= +1.5 V /Ag/ AgCl for time duration of 50 ms), the electrode reactivation by advanced oxidation (E= +1.75 V /Ag/ AgCl for time duration of 50 ms) and electrode conditioning (E= -0.5 V /Ag/ AgCl for time duration of 50 ms) and the second one

consisted of two potential levels, for IBP oxidation (E= +1.5 V /Ag/ AgCl for time duration of 50 ms) and for electrode reactivation by the advanced oxidation (E= +1.75 V /Ag/ AgCl for time duration of 50 ms). This last scheme was tested also in the presence of chloride in the supporting electrolyte. The multiple-pulsed amperograms recorded for each scheme are presented in Figure 8.14a and 8.14b, and no electrode fouling was noticed for MPA applying under all proposed scheme.

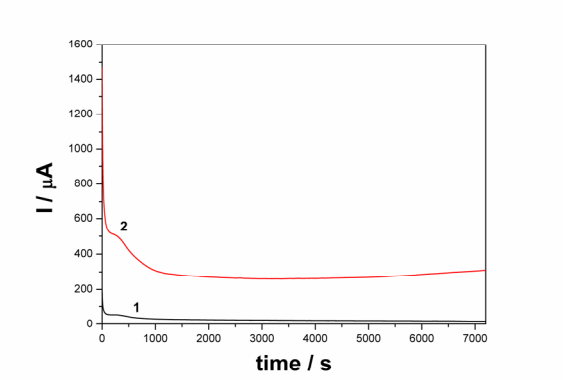


(a)

**Figure 8.14.** (a) Multiple-pulsed amperograms (MPAs) recorded using CNT electrode in 0.1 M $Na_2SO_4$ supporting electrolyte and in the presence of 10 $mgL^{-1}$ IBP concentration, at $E_{oxidation}$ = +1.5 V, $E_{reactivation}$= +1.75 V, $E_{conditioning}$= -0.5 V vs. Ag/ AgCl (curve 1); $E_{oxidation}$ = +1.5 V, $E_{reactivation}$= +1.75 V vs. Ag/ AgCl (curve 2).

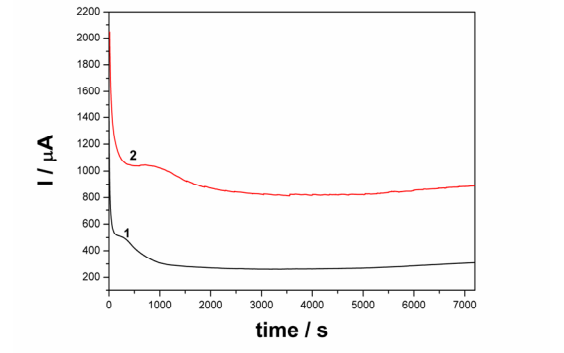


(b)

**Figure 8.14.**(b) Multiple-pulsed amperograms (MPAs) recorded using CNT electrode recorded in the presence of 10 $mgL^{-1}$ IBP concentration, at $E_{oxidation}$ = +1.5 V vs. Ag/ AgCl, $E_{reactivation}$= +1.75 V vs. Ag/ AgCl in: 0.1 M $Na_2SO_4$ supporting electrolyte (curve 1) and 0.075 M $Na_2SO_4$ and 0.025 M NaCl supporting electrolyte (curve 2).

The results regarding the electrode performance for the electrooxidation of IBP in relation with the process degradation efficiency (η) and the electrochemical efficiency (E) are gathered in Table 8.8.

It can be noticed that in comparison with CA, a slight improvement of the electrode performance for IBP electrodegradation and mineralization was achieved by MPA applying. Also, the best results in relation with both the process degradation efficiency ($\eta$) and the electrochemical efficiency (E) were reached by applying the two levels of potential pulses. The presence of chloride in the supporting electrolyte enhanced also the electrode performance especial in relation with the mineralization degree. By comparison CA and MPA applying under the studied operating conditions linked to the economic criteria, the best results were reached by applying CA at the potential value of +1.5 V vs. Ag/ AgCl in the presence of chloride.

### *8.3.3. Silver-doped zeolite carbon nanotube-epoxy composite (AgZCNT) and silver-doped zeolite expanded-graphite-epoxy composite (AgZEG) electrodes*

To improve the electrocatalytic activity towards IBP oxidation, silver-doped zeolite (AgZ) was introduced within composite composition to reach 20 %, wt. AgZ and 20 %, wt. CNT. For comparison, CNT was replaced with expanded graphite resulting AgZ-expanded graphite composite (AgZEG) electrode.

#### 8.3.3.1. Electrochemical behaviour of IBP on AgZCNT and AgZEG electrodes

Figure 8.15a shows the cyclic voltammograms (CVs) recorded at scan rate of 0.05 $Vs^{-1}$ in 0.1 M $Na_2SO_4$ supporting electrolyte at AgZCNT in comparison with CNT electrode to characterize comparatively their electrochemical behaviour in the supporting electrolyte. The difference between CNT and expanded graphite (EG) as the electrochemical behaviour is given in Figure 8.15b that presents CVs recorded comparatively at AgZCNT and AgZEG composite electrodes in 0.1 M $Na_2SO_4$ supporting electrolyte.

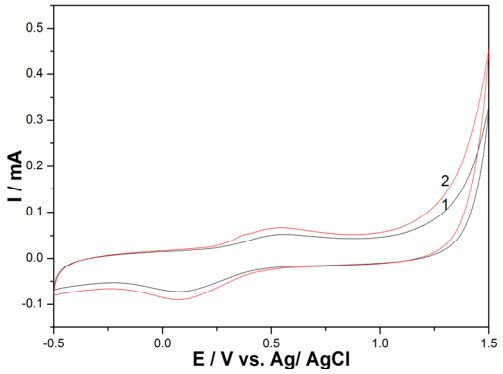


(a)

**Figure 8.15.** (a) Cyclic voltammograms recorded in 0.1 M $Na_2SO_4$ supporting electrolyte using: 1- CNT electrode and 2- AgZCNT electrode; potential scan rate: 0.05 $Vs^{-1}$; potential range: -0.5 to +1.5 V /Ag/ AgCl.

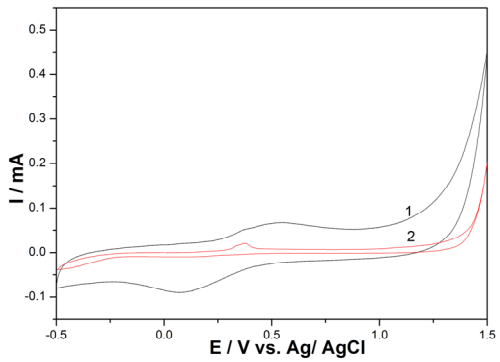


(b)

**Figure 8.15.** (b) Cyclic voltammograms recorded in 0.1 M $Na_2SO_4$ supporting electrolyte using: 1- AgZCNT electrode and 2- AgZEG electrode; potential scan rate: 0.05 $Vs^{-1}$; potential range: -0.5 to +1.5 V /Ag/ AgCl.

The presence of AgZ within the composite composition led to higher background current corresponding to the capacitive component and slight shifting of the oxygen evolution potential to less positive value, which are characteristics to the electrocatalytic property of the electrode material [41]. Also, by comparison of the CNT and EG, it can be seen that CNT exhibited enhanced electrocatalytic effect linked to capacitive current and the oxygen evolution potential.

Figures 8.16 and 8.17 show CVs recorded at AgZCNT and AgZEG composite electrodes at the scan rate of 0.05 $Vs^{-1}$ in 0.1 M $Na_2SO_4$ supporting electrolyte and in the presence of various IBP concentrations to elucidate the relationship between experimental variables and the electrode response. A different electrochemical behaviour of the studied electrodes was found. CVs recorded at AgZCNT seems to be similarly with ones recorded at CNT, no peak corresponding to the silver presence was noticed. However, the useful signal corresponding to IBP is about 20 times higher than recorded on CNT electrode. This behaviour could be explained by the enhanced electrocatalytic properties of both composite components, *i.e.*, AgZ and CNT, which should be overlapped. CVs recorded at AgZEG electrode suggested the redox processes of silver species in the oxidation process of IBP, which starts at the potential value of about +0.3 V vs. Ag/ AgCl corresponding also to Ag/ Ag(I) couple and follow the several steps. The interest step is given by the oxidation process recorded at the potential value of about +1.2 V vs. Ag/ AgCl, where a very clear oxidation peak appeared only in the presence of IBP, which increased linearly with IBP concentration increasing (see Fig. 8.17b). Comparing the useful signal corresponding to the oxidation of various IBP concentrations (Figures 8.16b and 8.17b), it can be noticed that even if the peak is more evidenced for AgZEG, the electrode response is enhanced for AgZCNT (about two times).

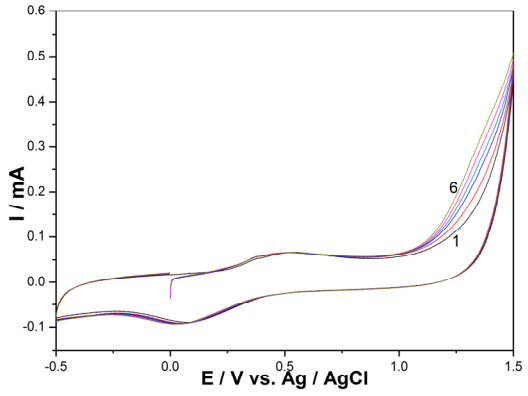


(a)

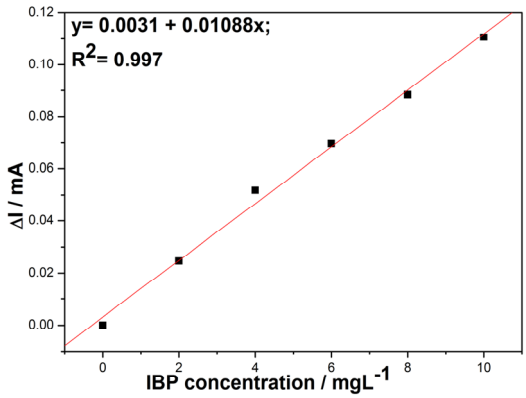


(b)

**Figure 8.16.** (a) Cyclic voltammograms recorded using AgZCNT electrode in 0.1 M $Na_2SO_4$ supporting electrolyte (1) and in the presence of various IBP concentrations: curves 2-6: 2-10 $mgL^{-1}$ IBP; potential scan rate: 0.05 $Vs^{-1}$; potential range: -0.5 to +1.5 V /Ag/ AgCl; (b) The calibration plots of the current recorded at E= +1.2 V vs. Ag/ AgCl vs. IBP concentration.

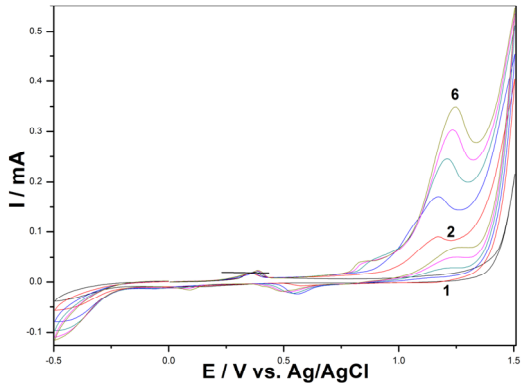


(a)

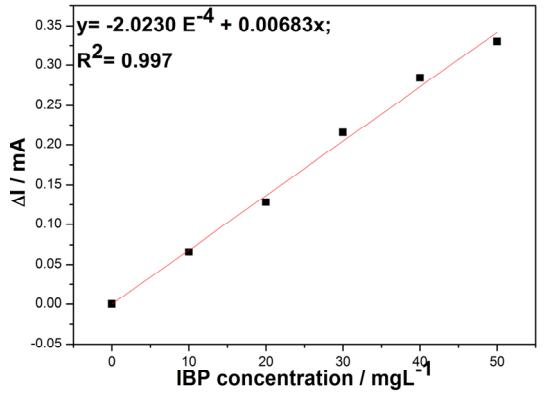


(b)

**Figure 8.17.** (a) Cyclic voltammograms recorded using AgZEG electrode in 0.1 M $Na_2SO_4$ supporting electrolyte (1) and in the presence of various IBP concentrations: curves 2- 6: 10-50 $mgL^{-1}$ IBP; potential scan rate: 0.05 $Vs^{-1}$; potential range: -0.5 to +1.5 V/Ag/ AgCl; (b) The calibration plots of the current recorded at E= +1.2 V vs. Ag/ AgCl vs. IBP concentration.

In Figures 8.18 and 8.19 are presented the effect of the scan rate on the first CV of both AgZCNT and AgZEG composite electrodes, in 0.1 M $Na_2SO_4$ + 10 $mgL^{-1}$ IBP. No electrode cleaning during CV running at different scan rates was performed. The anodic peaks are proportional to the square root of the scan rate (Figure 8.18a and 8.19a), which indicates control by mass transport for both electrodes. No intercept of 0 suggested that the adsorption steps and specific surface reaction cannot be neglected, being more significant for AgZEG versus AgZCNT electrode. The lack of the cathodic peak corresponding to the anodic one

for the oxidation of IBP indicates the irreversibility of this process, confirmed also by oxidation potential value shifting to more positive potentials (Figure 8.18b and 8.19b).

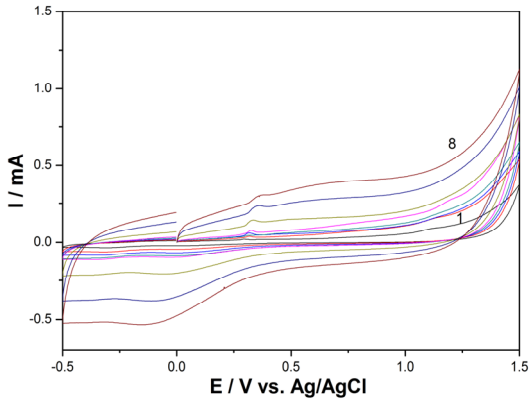


(a)

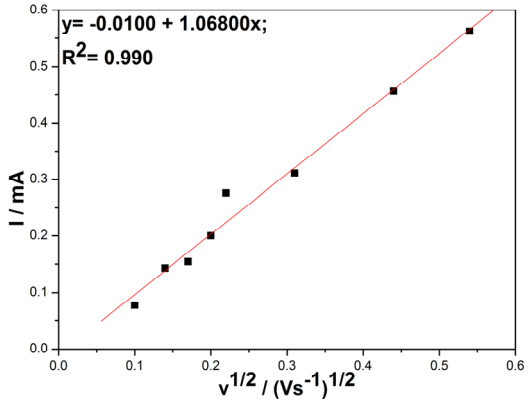


(b)

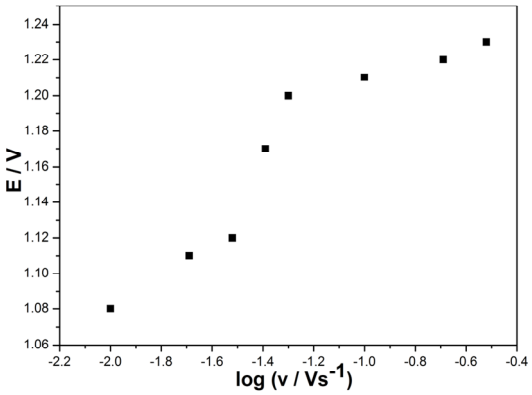


(c)

**Figure 8.18.** (a) Cyclic voltammogram recorded using AgZCNT electrode in 10 $mgL^{-1}$ IBP and 0.1 M $Na_2SO_4$ supporting electrolyte with different scan rates 0.01, 0.02, 0.03, 0.04, 0.05, 0.1, 0.2, 0.3 $Vs^{-1}$ (curves 1- 8); (b) The anodic peak current vs. square root of scan rate; (c) The peak potential E vs. log (v).

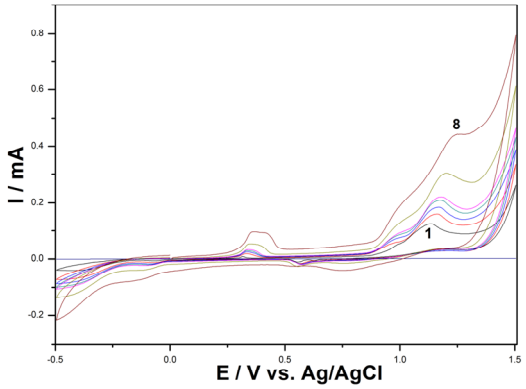


(a)

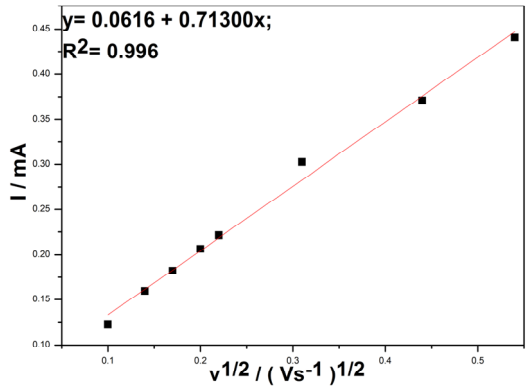


(b)

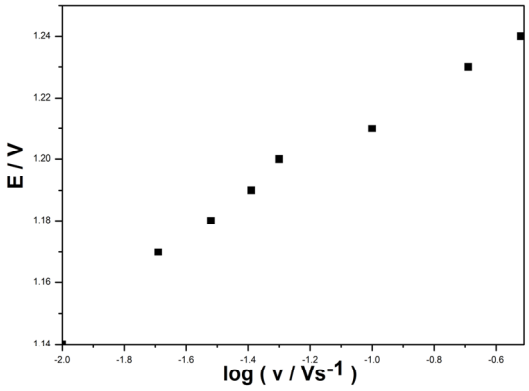


(c)

**Figure 8.19.** (a) Cyclic voltammogram recorded using AgZEG electrode in 10 $mgL^{-1}$ IBP and 0.1 M $Na_2SO_4$ supporting electrolyte with different scan rates 0.01, 0.02, 0.03, 0.04, 0.05, 0.1, 0.2, 0.3 $Vs^{-1}$ (curves 1- 8); (b) The anodic peak current vs. square root of scan rate; (c) The peak potential E vs. log (v).

AgZCNT and AgZEG composite electrodes exhibited very good performance for the effective mineralization in comparison with CNT, BDD and GC electrodes, for which effective mineralization were not achieved.

The AgZEG electrode features in relation with the diffusion-controlled electrooxidation of IBP was exploited for IBP detection, suggesting a dual exploitation of this electrode both in IBP degradation and its control by IBP monitoring using cyclic voltammetric technique.

### 8.3.3.2. Electrochemical application of AgZCNT and AgZEG composite electrodes in IBP oxidation under potentiostatic regime by chronoamperometry (CA)

Based on the results achieved for CNT electrode for IBP degradation and mineralization, the same working conditions of CA were applied. In Figure 8.20 are shown as example the chronoamperograms recorded at the potential value of +1.25 V/ Ag/ AgCl for both electrodes. For all potential values applied no electrode fouling was noticed for both electrodes. The electrode performance for IBP degradation and mineralization and expressed in terms of process efficiency for $A_{220}$, COD and TOC reduction are shown in Table 8.9, and it can be noticed that very good efficiencies were reached for both electrodes. The process efficiency was slight improved for AgZCNT but in terms of the electrochemical efficiency that take into consideration the charge consumed the AgZEG exhibited better performance in relation with $A_{220}$ and COD removal. However, the best mineralization degree was achieved using AgZCNT electrode.

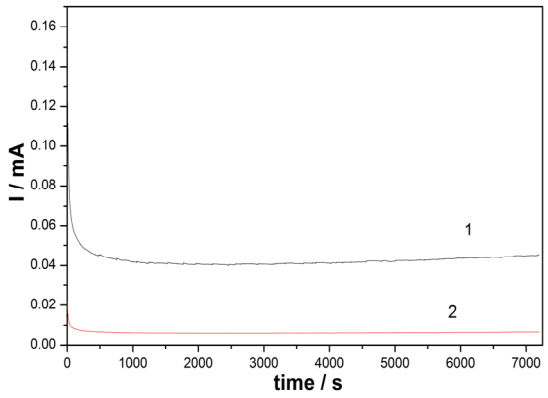


**Figure 8.20.** Chronoamperograms (CAs) recorded at +1.25 V vs. Ag/ AgCl in 0.1 M $Na_2SO_4$ supporting electrolyte for: 1-AgZCNT and 2- AgZEG.

**Table 8.9.** The electrode performance in the electrooxidation of IBP using chronoamperometry.

| Electrode material | Working conditions | $\eta_{conc}$/ % | $E_{conc}$/ g C $cm^{-2}$ | $\eta_{COD-Cr}$/ % | $E_{COD-Cr}$/ g C $cm^{-2}$ | $\eta_{TOC}$/ % | $E_{TOC}$/ g C $cm^{-2}$ |
|---|---|---|---|---|---|---|---|
| AgZCNT | $E_{ox}$= +1.25 V | 69 | 1.72 | 65 | 4.67 | 60.84 | 2.58 |
| | $E_{ox}$= +1. 5 V | 78 | 1.97 | 67 | 4.82 | 63.25 | 3.57 |
| | $E_{ox}$= +1.75 V | 82 | 2.05 | 69 | 4.96 | 67.24 | 3.80 |
| AgZEG | $E_{ox}$= +1.25 V | 49 | 2.35 | 45 | 6.16 | 35.00 | 1.02 |
| | $E_{ox}$= +1. 5 V | 70 | 3.36 | 50 | 6.85 | 45.00 | 1.30 |
| | $E_{ox}$= +1.75 V | 75 | 3.60 | 55 | 7.45 | 53.00 | 1.53 |

### 8.3.3.3. Dual exploitation of AgZEG electrode in electrochemical oxidation of IBP regarding its degradation and process control

Based on the above-presented electrochemical behaviour of AgZEG electrode in the presence of various concentrations of IBP, which demonstrated a linear dependence of the peak current versus IBP concentrations, characteristics to the mass transport control process, much desired aspect for the voltammetric/ amperometric detection, this electrode was tested to assess IBP monitoring before and after electrolysis applying. The assessments of IBP concentrations after chronoamperometry under potentiostatic conditions were performed by using the cyclic voltammetric detection with the similar electrode. In Figure 8.21 are shown as example, CVs recorded in 0.1 M $Na_2SO_4$ supporting electrolyte (curve 1), in the presence of initial concentration of IBP before CA applying (curve 4) and the presence of residual IBP concentration after CA applying at the potential value of +1.75 V vs. Ag/ AgCl using AgZCNT electrode (curve 2) and AgZEG electrode (curve 3).

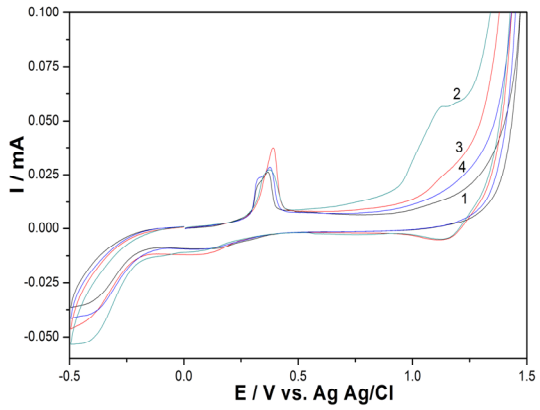


**Figure 8.21.** CVs recorded using AgZEG electrode in 0.1 M $Na_2SO_4$ supporting electrolyte (curve 1) in the presence of 10 $mgL^{-1}$ IBP: before CA applying (curve 2) and after CA applying at +1.75 V vs. Ag/ AgCl using AgZCNT electrode (curve 3) and AgZEG electrode (curve 4).

A comparison between UV-VIS and cyclic voltammetric assessment of IBP to determine process efficiency for AgZCNT and AgZEG electrodes is presented in Table 8.10.

**Table 8.10.** The reduction degree of IBP concentration assessed spectrophotometrically and voltammetrically by applying the chronoamperometry.

| Electrode material | Working conditions | $\eta_{conc/}$ % | Voltammetric signal reduction/ % |
|---|---|---|---|
| AgZCNT | $E_{ox}$= +1.25 V | 69 | 68.00 |
| | $E_{ox}$= +1. 5 V | 78 | 82.00 |
| | $E_{ox}$= +1.75 V | 82 | 85.00 |
| AgZEG | $E_{ox}$= +1.25 V | 49 | 45.00 |
| | $E_{ox}$= +1. 5 V | 70 | 68.50 |
| | $E_{ox}$= +1.75 V | 75 | 72.90 |

Similar values for IBP reduction degree were determined using both assessment methods, which denote the practical utility of AgZEG electrode for IBP concentration monitoring during its electrodegradation process.

The performance of all tested electrodes for IBP electrodegradation and mineralization under the working conditions are summarized in Table 8.11.

**Table 8.11.** The electrode performance in the electrooxidation of IBP.

| Electrode material | Applied technique | Working conditions | Supporting electrolyte | $\eta_{conc}$ /% | $E_{conc}$/g C $cm^{-2}$ | $\eta_{COD-Cr}$/% | $E_{COD-Cr}$/ g C $cm^{-2}$ | $\eta_{TOC}$/ % | $E_{TOC}$ /g C $cm^{-2}$ |
|---|---|---|---|---|---|---|---|---|---|
| GC | CA | $E_{ox}$= +1.5 V | 0.1 M $Na_2SO_4$ | 15 | 6.05 | 8.00 | 12.10 | -* | -* |
| | | $E_{ox}$= +2 V | 0.1 M $Na_2SO_4$ | 45 | 0.44 | 32.00 | 1.32 | 6.00 | 0.06 |
| BDD | CA | $E_{ox}$= +1.5 V | 0.1 M $Na_2SO_4$ | 12 | 39.62 | 10.00 | 127.20 | 1.00 | 3.43 |
| | | $E_{ox}$= +2 V | 0.1 M $Na_2SO_4$ | 50 | 9.55 | 44.00 | 33.81 | 7.00 | 1.39 |
| CNT | CA | $E_{ox}$= +1.25 V | 0.1 M $Na_2SO_4$ | 50 | 0.93 | 43.00 | 3.09 | 32.49 | 2.09 |
| | | $E_{ox}$= +1.5 V | 0.1 M $Na_2SO_4$ | 72 | 1.43 | 66.70 | 4.80 | 35.5 | 0.74 |
| | | $E_{ox}$= +1.75 V | 0.1 M $Na_2SO_4$ | 72 | 1.35 | 67.00 | 4.82 | 37.21 | 0.08 |
| | | $E_{ox}$= +1. 5 V | 0.075 M $Na_2SO_4$ and 0.025M NaCl | 75 | 0.81 | 69.00 | 2.71 | 27.5 | 0.27 |
| | MPA | $E_{ox}$= +1.5 V $E_{reactiv}$= +1.75 V $E_{cond}$= -0.5 V | 0.1 M $Na_2SO_4$ | 77 | 0.45 | 72.69 | 1.92 | 9.76 | 0.06 |
| | | $E_{ox}$= +1.5 V; $E_{reactiv}$= +1.75 V | 0.1 M $Na_2SO_4$ | 74 | 0.44 | 69.00 | 1.82 | 9.45 | 0.06 |
| | | $E_{ox}$= +1.5 V; $E_{reactiv}$= +1.75 V | 0.075M $Na_2SO_4$ and 0.025M NaCl | 78 | 0.21 | 75.00 | 0.73 | 30.54 | 0.07 |
| AgZCNT | CA | $E_{ox}$= +1.25 V | 0.1 M $Na_2SO_4$ | 69 | 1.72 | 65.00 | 4.67 | 60.84 | 2.58 |
| | | $E_{ox}$= +1.5 V | 0.1 M $Na_2SO_4$ | 78 | 1.97 | 67.00 | 4.82 | 63.25 | 3.57 |

| | | | | | | | | | |
|---|---|---|---|---|---|---|---|---|---|
| | | $E_{ox}$= +1.75 V | 0.1 M $Na_2SO_4$ | 82 | 2.05 | 69.00 | 4.96 | 67.24 | 3.80 |
| AgZEG | CA | $E_{ox}$= +1.25 V | 0.1 M $Na_2SO_4$ | 49 | 2.35 | 45.00 | 6.16 | 35.00 | 1.02 |
| | | $E_{ox}$= +1.5 V | 0.1 M $Na_2SO_4$ | 70 | 3.36 | 50.00 | 6.85 | 45.00 | 1.30 |
| | | $E_{ox}$= +1.75 V | 0.1 M $Na_2SO_4$ | 75 | 3.60 | 55.00 | 7.45 | 53.00 | 1.53 |

*no determined

The effective mineralization assessment was performed based on the ratio between TOC and $A_{220}$ reducing efficiency ($\eta_{TOC}$/ $\eta_{Abs}$) for all tested electrodes and the results are gathered in Table 8.12. Based on the effective mineralization assessment as ratio between TOC and $A_{220}$ reducing efficiency ($\eta_{TOC}$/ $\eta_{Abs}$), which must be near to 1 (see Table 8.11) correlated with electrochemical efficiency for TOC reduction, it can be concluded that AgZCNT electrode exhibited the best performance. Also, the use of AgZEG led to almost effective mineralization. These results informed about the necessity of electrocatalyst presence to reach mineralization (silver or carbon nanotubes).

**Table 8.12.** The electrode performance for the effective mineralization of IBP.

| Electrode material | Applied technique | Working conditions | Supporting electrolyte | ($\eta_{TOC}$/ ($\eta_{Abs}$) |
|---|---|---|---|---|
| GC | CA | $E_{ox}$= +1.5 V | 0.1 M $Na_2SO_4$ | 0 |
| | | $E_{ox}$= +2 V | 0.1 M $Na_2SO_4$ | 0.13 |
| BDD | CA | $E_{ox}$= +1.5 V | 0.1 M $Na_2SO_4$ | 0.08 |
| | | $E_{ox}$= +2 V | 0.1 M $Na_2SO_4$ | 0.14 |
| CNT | CA | $E_{ox}$= +1.25 V | 0.1 M $Na_2SO_4$ | 0.65 |
| | | $E_{ox}$= +1. 5 V | 0.1 M $Na_2SO_4$ | 0.49 |
| | | $E_{ox}$= +1.75 V | 0.1 M $Na_2SO_4$ | 0.52 |
| | | $E_{ox}$= +1. 5 V | 0.075 M $Na_2SO_4$ and 0.025M NaCl | 0.37 |
| | MPA | $E_{oxidation}$= +1.5 V; $E_{reactivation}$= +1.75 V; $E_{conditioning}$= -0.5 V | 0.1 M $Na_2SO_4$ | 0.13 |
| | | $E_{oxidation}$= 1.5 V; $E_{reactivation}$= 1.75 V | 0.1 M $Na_2SO_4$ | 0.13 |
| | | $E_{oxidation}$= +1.5 V; $E_{reactivation}$= +1.75 V | 0.075M $Na_2SO_4$ and 0.025M NaCl | 0.39 |
| AgZCNT | CA | $E_{ox}$= +1.25 V | 0.1 M $Na_2SO_4$ | 0.88 |
| | | $E_{ox}$= +1. 5 V | 0.1 M $Na_2SO_4$ | 0.81 |
| | | $E_{ox}$= +1.75 V | 0.1 M $Na_2SO_4$ | 0.82 |
| AgZEG | CA | $E_{ox}$= +1.25 V | 0.1 M $Na_2SO_4$ | 0.71 |
| | | $E_{ox}$= +1. 5 V | 0.1 M $Na_2SO_4$ | 0.64 |
| | | $E_{ox}$= +1.75 V | 0.1 M $Na_2SO_4$ | 0.71 |

Based on the presented results, it may be concluded:

The comparative study regarding the electrochemical behaviour of ibuprofen (IBP) on the carbon-based composite electrode tested in this study, *i.e.*, carbon nanotubes-epoxy composite (CNT), silver-doped zeolite-carbon nanotubes-epoxy composite (AgZCNT) and silver-doped zeolite-expanded-graphite-epoxy composite (AgZEG) electrodes allowed to select the operating conditions for its electrochemical degradation/ mineralization from the aqueous solution. In addition, IBP electrochemical behaviour of IBP on the carbon-based composite electrodes was compared with the commercial glassy carbon (GC) and boron-doped diamond (BDD) electrode.

Cyclic voltammetry (CV) results showed that the anodic current increased in the presence of IBP without the presence of the corresponding oxidation peak at the commercial GC and BDD electrodes, and also, for CNT composite electrode. Also, some information related to the direct electrochemical activity towards IBP electrooxidation was found, the best one being determined for CNT electrode. BDD electrode exhibited the electrode fouling under the IBP concentrations ranged from 10 to 50 $mgL^{-1}$. Silver presence within the electrode composition led to a different behaviour of IBP using CV and the anodic peak corresponding to IBP oxidation was found for both AgZCNT and AgZEG composite electrodes, which should inform about a possible diffusion-controlled oxidation process. The most evidenced oxidation peak was found for AgZEG, but the best electrochemical sensitivity for IBP oxidation was determined for AgZCNT composite electrode.

Chronoamperometry (CA) and multiple-pulsed amperometry (MPA) techniques were used to simulate the potentiostatic electrolysis envisaging also, the possibility of *in-situ* electrode reactivation by MPA. The selection of the operating conditions for CA and MPA based on CV results as reference. No direct electrochemical oxidation of IBP on the tested electrode was performed due to the electrode fouling the implicit, the electrode activity loss. All electrolysis experiments were performed under water decomposition potential range, where the radical hydroxyl are generated leading to an advanced electrooxidation process but with high energy consumption due to the secondary oxygen evolution occurring.

The assessment of the electrode performance in terms of absorbance, organic load and TOC reduction degrees and in terms of the electrochemical efficiencies, which takes into account the charge passed during the electrochemical process showed that BDD electrode exhibited the better performance for IBP degradation/ mineralization in comparison with GC electrode. The practical utility of BDD electrode for IBP degradation/ mineralization was proved by bulk electrolysis under optimum galvanostatic operating conditions of 10 mA $cm^{-2}$ current density.

The influence of chloride presence in order to generate *in-situ* the oxidation agent (hypochlorite/ chlorine) did not improve significantly the process efficiency and moreover, the electrochemical efficiency was negatively influenced due to an excess of charge consumed for oxidant generation.

MPA applying on CNT composite electrode improved slightly the process efficiency, but the electrochemical efficiency decreased. Under these working conditions, based on the technical-economical criteria MPA applying is not suitable for IBP in comparison with CA applying.

Dual character of AgZEG electrode was tested for both IBP electrodegradation/ electromineralization and process control by IBP electrochemical detection and very good results were achieved. IBP electrochemical detection results were compared with IBP spectrophotometric determination ones, and similar results were obtained, which denoted the accuracy of the electrochemical detection

method. AgZEG electrode exhibited specific features, which makes it suitable for dual applications, IBP electrodegradation and electrochemical detection.

## 8.4. References

[1] K. Fent, A.A. Weston, D. Caminada, Aquati. Toxicol. 76 (2006) 122.
[2] M.D. Hernando, A.R. Fernandez-Albab, R. Taulera, D. Barcelo, Talanta 65 (2005) 358.
[3] M. Klavarioti, D. Mantzavinos, D. Kassinos, Environ. Int. 35 (2009) 402.
[4] A. Kumar, I. Xagoraraki, Reg. Toxicol. Pharm. 57 (2010) 146.
[5] C. Miege, J.M. Choubert, L. Ribeiro, M. Eusebe, M. Coquery, Environ. Pollut. 157 (2009) 1721.
[6] A. Nikolaou, S. Meric, D. Fatta, Anal. Bioanal. Chemi. 387 (2007) 1225.
[7] T.L. ter Laak, M. Van der A, C.J. Houtman, P.G. Stoks, A.P. van Wezel, Environ. Int. 36 (2010) 403.
[8] A.S. Mestre, J. Pires, J.M.F. Nogueira, J.B. Parra, A.P. Carvalho, C.O. Ania, Bioresource Technol. 100 (2009) 1720.
[9] D. Jermanna, W. Pronka, M. Bollera, A.I. Schafer, J. Membrane Sci. 329 (2009) 75.
[10] U. Marco-Urrea, M. Perez-Trujillo, T. Vicent, G. Caminal, Chemosphere 74 (2009) 765.
[11] F. Mendez-Arriaga, S. Esplugas, J. Gimenez, Water Res. 44 (2010) 589.
[12] J.V. Castell, M.J. Gomez, M.A. Miranda, I.M. Morera, Photochemistry and Photobiology 46 (2008) 991.
[13] E.M. Costi, I. Goryacheva, M.D. Sicilia, S. Rubio, D. Perez-Bendito, J. Chromatogr. A 1210 (2008) 1.
[14] J.V. Castell, M.J. Gomez, M.A. Miranda, I.M. Morera, Photochem. Photobiol. 46 (2008) 991.
[15] B.G. Zheng, Z. Zheng, J.B. Zhang, X.Z. Luo, J.Q. Wang, Q. Liu, L.H. Wang, Desalination 276 (2011) 379.
[16] L. Ciriaco, C. Anjo, J. Correia, M.J. Pacheco, A. Lopes, Electrochim. Acta 54 (2009) 1464.
[17] J.A. Garrido, E. Brillas, P.L. Cabot, F. Centellas, C. Arias, R.M. Rodriguez, Electrochim. Acta 25 (2007) 19.
[18] E. Isarin-Chavez, R.M. Rodriquez, P.L. Cabot, F. Centellas, C. Arias, J.A. Garrido, E. Brillas, Water Res. 45 (2011) 4119.
[19] R.N. Hegde, N.P. Shetti, S.T. Nandibewoor Talanta 79 (2009) 361.
[20] S.A. Ozkan, B. Uslu, P. Zuman, Anal. Chim. Acta 501 (2004) 227.
[21] R.H. Patil, R.N. Hegde, S.T. Nandibewoor, Colloid. Surface. B. 83 (2011) 133.
[22] M. Shamsipur, M. Najafi, M.R.M. Hosseini, Bioelectrochemistry 77 (2010) 120.
[23] M. Tabeshnia, H. Heli, A. Jabbari, A.A. Moosavi-Movahedi, Turkish J. Chem. 34 (2010) 35.
[24] S. Shahrokhian, A. Souri, H. Khajehsharifi, J. Electroanal. Chem. 565 (2004) 95.
[25] E. Brillas, S. Garcia-Segura, M. Skoumal, C. Arias, Chemosphere 79 (2010) 605.
[26] J.R. Dominguez, T. Gonzalez, P. Palo, J. Sanchez-Martin, Chem. Eng. J. 162 (2010) 1012.

[27] M. Murugananthan, S. Yoshihara, T. Rakuma, T. Shirakashi, J. Hazard. Mater. 154 (2008) 213.
[28] I. Sires, P.L. Cabot, F. Centellas, J.A. Garrido, R.M. Rodriguez, C. Arias, E. Brillas, Electrochim. Acta 52 (2006) 75.
[29] X. Zhao, Y. Hou, H. Liu, Z. Qiang, J. Qu, Electrochim. Acta 54 (2009) 4172.
[30] H. Heli, S. Majdi, A. Jabbari, N. Sattarahmady, J. Solid State Electr. 14 (2010) 1515.
[31] L. Li, Y. Xing, Energies 2 (2009) 789.
[32] H. Tang, J. Chen, L. Nie, S. Yao, Y. Kuang, Electrochim. Acta 51 (2006) 3046.
[33] S. Yang, X. Zhang, H. Mi, X. Ye, J. Power Sources 175 (2008) 26.
[34] **S. Motoc**, F. Manea, A. Pop, R. Pode, C. Teodosiu, Environ. Eng. Manag. J. 11 3 (2012) 627.
[35] M.S. Ureta-Zanaru, P. Bustos, C. Berrios, M.C. Diez, M.L. Mora, C. Gutierrez, Electrochim. Acta 47 (2002) 2399.
[36] L. Gherardini, P.A. Michaud, M. Panizza, Ch. Comninellis, N. Vatistas, J. Electrochem. Soc. 148 (2001) 78.
[37] J.M. Skowronski, P. Krawczyk, J. Solid State Electr.11 (2007) 223.
[38] F. Manea, G. Burtica, A. Bebeselea, A. Pop, I. Corb, J. Schoonman, Environmental Science and Technology, Vol. 1.
[39] A. Bebeselea, C. Proca, F. Manea, C. Radovan, G. Burtica, J. Schoonman, Environ. Eng. Manag. J.8 (2009) 817.
[40] M.S. Canals, Advanced oxidation processes applied to mineralize paracetamol, chloroxylenol, ibuprofen and diclofenac in aqueous medium, PhD Thesis, (2009), Universitat de Barcelona, Departament de Quimica Fisica, Barcelona, Spain.
[41] **S. Motoc**, A. Remes, A. Pop, F. Manea, J. Schoonman, Environ. Eng. Manag. J. (2012) in press.

# CHAPTER 9. ELECTROCHEMICAL DETECTION OF PHARMACEUTICALS USING CARBON-BASED ELECTRODES

## 9.1. Electrochemical detection of ibuprofen using carbon-based composite electrodes

Ibuprofen (IBP) is the third most popular drug in the world, non-prescription, non-steroidal drug used as an anti-inflammatory analgesic and antipyretic in the human treatment of fever, migraine, muscle aches, rheumatoid arthritis, tooth aches, and osteoarthritis [1-7].

IBP and its first biotic products (hydroxy and carboxy-ibuprofen) have been frequently detected, among other pharmaceutical residues, in sewage waters and effluents and also in surface waters [1, 8, 9]. According to the literature, several kilotons of this compound are produced worldwide each year, part of which is rejected to the effluents [1]. The industrial pollution occurs due to the release of these untreated effluents. Therefore, IBP and its metabolized products enter into environmental water via sewage treatment plants, and sometimes, the metabolites formed are more harmful than the parent organic compounds [2].

According to Directive 2001/83/EC which was subsequently amended by Directive 2004/27/EC, an environmental assessment is required only if the estimated environmental concentration of the pharmaceutical at the point of the entry is above $0.01 \mu g L^{-1}$ [10]. As example of the presence of pharmaceuticals in Romanian rivers, according to Caliman F.A and Gavrilescu M., 2009, along the river Somes between the cities Cluj-Napoca and Dej, the concentration of the pharmaceuticals detected were between 10-9700 $ngL^{-1}$ (*e.g.,* caffeine: 230-9700 $ngL^{-1}$, carbamazepine: 30-70 $ngL^{-1}$, galaxolide: 10-310 $ngL^{-1}$, and ibuprofen: 30-120 $ngL^{-1}$) [11].

Taking into account the above-presented considerations, drugs analysis of water plays an important role in water quality control, and the development of sensitive, rapid, simple, and reliable methods for their determination is very important. Few analytical methods were reported in the literature for determination of IBP [12]. These include gas chromatography-mass spectrometry (GC-MS) [13], high performance liquid chromatography (HPLC), evaporative light scattering detection (ELSD) [14], spectrofluorometry [15], capillary zone electrophoresis [16], and chemometric-assisted spectrophotometric methods [17]. Most of these methods are costly and require expertise in addition to the time-consuming pretreatment steps [12].

The use of the electroanalytical methods for the determination of a variety of organic and inorganic substances exhibited a major interest based on the continuous improvements in techniques and instrumentation allowing reaching the lowest limit of detection (LOD) compatible with environmental regulations. The electrode material represents the key to achieve very good electroanalytical performance in the electrochemical detection. In our previous works, an silver-doped zeolite-expanded-graphite-epoxy composite (AgZEG) was reported for the

electrochemical detection of 4-chlorophenol and urea from aqueous solution [18, 19].

This study aims to characterize the electrochemical behaviour of ibuprofen on silver-modified carbon-based composite electrodes by cyclic voltammetry in order to detect this substance in water. To establish the optimum conditions for detection of ibuprofen, the electroanalytical performances of the electrode were determined using cyclic voltammetry (CV), differential-pulsed voltammetry (DPV), square-wave voltammetry (SWV), chronoamperometry (CA), and multiple-pulsed amperometry (MPA) techniques.

## *Experimental*

### *Reagents*

A standard solution of 1 $gL^{-1}$ ibuprofen was prepared using the analytical reagent from BASF SE, (Ludwigshafen, Germany) using distilled water and 0.1 M NaOH solution. Supporting electrolyte for the characterization and application of the electrode material in the detection process was 0.1 M $Na_2SO_4$ solution, which was freshly prepared from analytical grade $Na_2SO_4$ of analytical purity (Merck) with distillated water.

### *Working electrodes*

The carbon-based composite working electrodes used for the detection of IBP are gathered in Table 9.1. The experimental results presented in Chapter 8 showed that no anodic peak corresponding to IBP oxidation was found on carbon-based electrode without catalyst presence. Based on these findings, several silver-based electrodes were tested in order to detect IBP from the aqueous solution, *e.g.*, silver-doped zeolite-expanded-graphite-epoxy composite (AgZEG), silver-doped zeolite-carbon nanotubes-epoxy composite (AgZCNT), 146silver-doped zeolite-carbon nanofiber composite (AgZCNF), and silver-decorated carbon nanofiber-epoxy composite (AgCNF) electrodes.

**Table 9.1.** Carbon-based composite working electrodes tested for the electrochemical detection of IBP.

| Carbon-based composite electrode | Geometrical area/ $cm^2$ | Electroactive surface area/ $cm^2$ |
|---|---|---|
| AgZCNT | 0.196 | 0.411 |
| AgZCNF | 0.196 | 0.313 |
| AgCNF | 0.196 | 0.346 |
| AgZEG | 0.196 | 0.320 |

### *Apparatus and procedures*

The electrochemical performances of the carbon-based composite electrodes were studied by cyclic voltammetry (CV), differential-pulsed voltammetry (DPV), square-wave voltammetry (SWV), chronoamperometry (CA) and multiple-pulsed amperometry (MPA).

Electrochemical measurements were performed in unstirred solutions using a computer controlled Autolab potentiostat/ galvanostat PGSTAT 302 (EcoChemie,

The Netherlands), with a standard three-electrode configuration. The three-electrode system consisted of a carbon-based composite working electrode, a platinum wire as counter electrode, and a silver/ silver chloride reference electrode (Ag/ AgCl). Before each voltammogram, each composite electrode was carefully polished with abrasive paper and then on a felt-polishing pad by using 0.3 μm alumina powder (Metrohm, Switzerland). All experiments were carried out with a typical cell of 50 mL at room temperature (25 °C).

***Results and discussion***

### *9.1.1. AgZEG composite electrode*

The electrochemical behaviour of IBP on the AgZEG composite electrode was described in the previous chapter, and the diffusion-controlled oxidation process for the direct oxidation of IBP on the electrode surface was found, which is indeed desired for the electroanalysis application. Based on the linear dependence between the anodic peak currents and IBP concentrations a sensitivity of 6.83 μA $mgL^{-1}$ was determined with a good correlation factor (0.997). Moreover, this electrode was tested as dual application both in IBP electrodegradation and determination and very promising results were achieved. In this context, the present study will be focused on the elaboration of the IBP detection scheme at the AgZEG composite electrode.

The detection measurements were performed using cyclic voltammetry (CV), linear-scan voltammetry (LSV), differential-pulsed voltammetry (DPV), square-wave voltammetry (SWV), and chronoamperometry (CA).

CV results were presented in the previous section and the electroanalytical parameters determined using this technique are gathered in Table 9.2.

***Linear-scan voltammetry results***

Figure 9.1 shows linear-scan voltammograms recorded with the AgZEG composite electrode in the presence of different IBP concentrations and a linear dependence of the anodic oxidation current densities recorded at the potential values of +1.4 V vs. Ag/ AgCl can be observed. A slightly more positive shift of the oxidation potential was noticed based on the LSV peculiarities, but the direct anodic oxidation at least two stages is confirmed also by LSV. According with the literature [20], the products of IBP oxidation could be 2-(4-isobutylphenyl)-2-hydroxypropionic acid and 1-(1-hydroxyethyl)-4-isobuylbenzene. Applying LSV led to similar detection performance for IBP in comparison with CV, which informed that reverse scanning did not assure the electrode surface reactivation. The electroanalytical parameters are presented in Table 9.2.

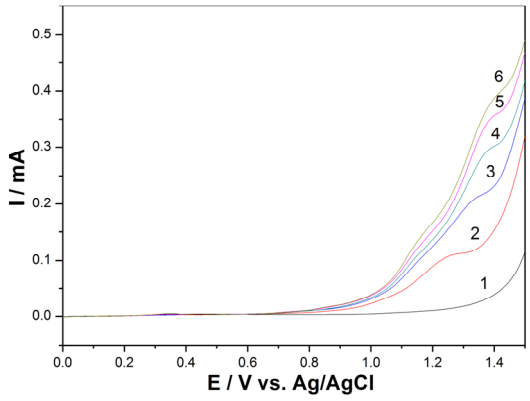


(a)

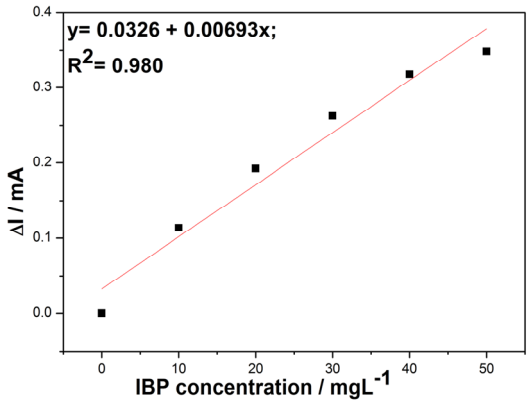


(b)

**Figure 9.1.** (a) Linear-scan voltammograms recorded with a AgZEG electrode in 0.1 M $Na_2SO_4$ supporting electrolyte (1) and in the presence of various IBP concentrations: 2- 10 $mgL^{-1}$, 3- 20 $mgL^{-1}$, 4- 30 $mgL^{-1}$, 5- 40 $mgL^{-1}$, 6- 50 $mgL^{-1}$; potential scan rate: 0.05 $Vs^{-1}$; potential range: 0 to +1.5V /Ag/ AgCl. (b) Calibration plots of anodic peak current recorded at +1.4 V vs. Ag/ AgCl vs. IBP concentrations.

***Differential-pulsed voltammetry results***

In order to achieve better electroanalytical performance, has been tested differential- pulsed voltammetry, a technique that achieves a minimization of the effects of background noise, in particular of the brought the capacitive current, allowing the improvement of the useful signal. Using this specific technique requires to establish the optimum operating conditions for the step potential, which

represents the potential increment between two subsequent current measurements and modulation amplitude [21].

The operating conditions for the DPV technique are presented in Table 9.2, and the corresponding DPV results are shown in Figures 9.2a-9.5a. Also, the calibration plots are presented in Figures 9.2b-9.5b. It can be noticed that the DPV variables influenced the oxidation process of IBP. Too high step potential value in comparison with the modulation amplitude did not allow evidencing the two stages of the oxidation process. The best sensitivity was achieved for the step potential of 0.05 V and the modulation amplitude of 0.1 V vs. Ag/ AgCl, which should be considered as the optimum variables for DPV operation.

**Table 9.2.** The operating parameters for DPV testing in relation with the sensitivity for IBP detection.

| Step potential/ mV | Modulation amplitude/ mV | Peak potential/ V vs. Ag/ AgCl | Sensitivity/ $\mu A/ mgL^{-1}$ |
|---|---|---|---|
| 0.01 | 0.05 | +1.17 | 4.70 |
| | | +1.35 | 6.59 |
| 0.05 | 0.02 | +1.20 | 2.02 |
| 0.05 | 0.05 | +1.20 | 4.57 |
| 0.05 | 0.10 | +0.86 | 2.91 |
| | | +1.17 | 14.70 |

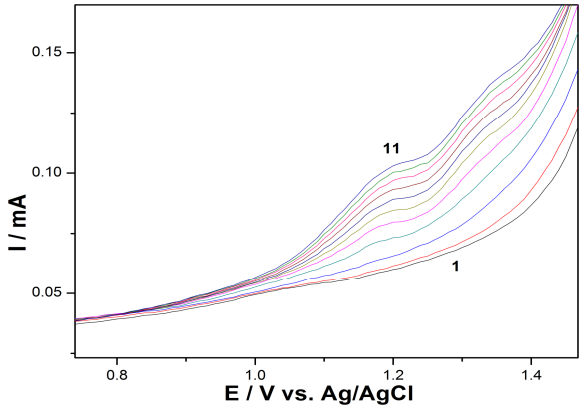


(a)

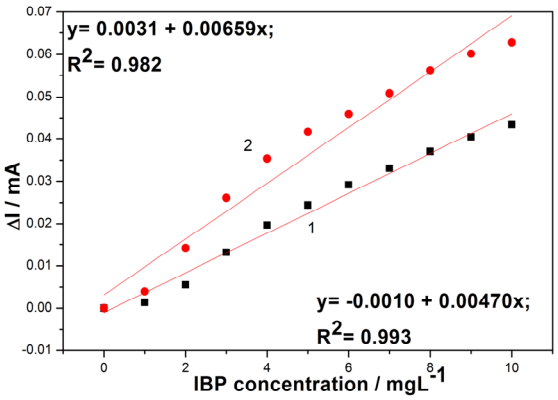


(b)

**Figure 9.2.** (a) Differential-pulsed voltammograms recorded with a AgZEG electrode with a modulation amplitude of 0.05 V, a step potential of 0.01 V and scan rate of 0.05 $Vs^{-1}$ between 0 and +1.5 V vs. Ag/ AgCl in 0.1 M $Na_2SO_4$ supporting electrolyte (1) and in the presence of different IBP concentrations: curves 2-11: 1-10 $mgL^{-1}$. (b) Calibration plots of the currents recorded at E= +1.17 (1) and E= +1.35 V (2) vs. Ag/ AgCl versus IBP concentrations.

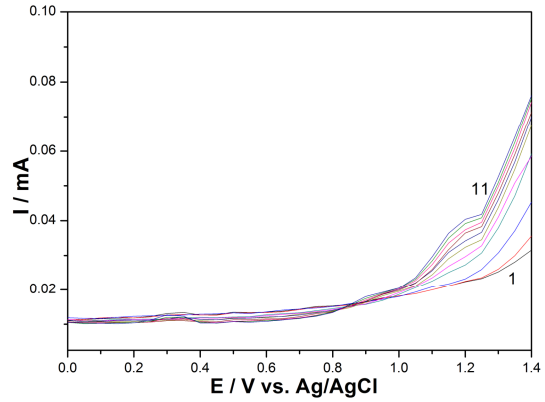


(a)

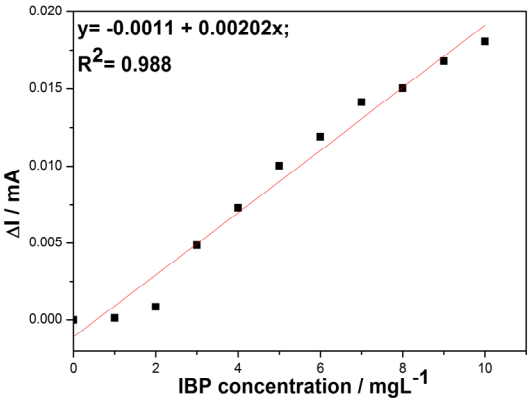


(b)

**Figure 9.3.** (a) Differential-pulsed voltammograms recorded with a AgZEG electrode with a modulation amplitude of 0.02 V, a step potential of 0.05 V and scan rate of 0.1 $Vs^{-1}$ between 0 and +1.5 V vs. Ag/ AgCl in 0.1 M $Na_2SO_4$ supporting electrolyte (1) and in the presence of different IBP concentrations: curves 2-11: 1-10 $mgL^{-1}$. (b) Calibration plots of the currents recorded at E= +1.2 V vs. Ag/ AgCl versus IBP concentrations.

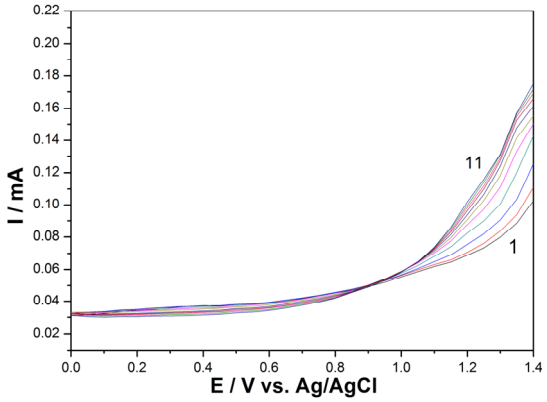


(a)

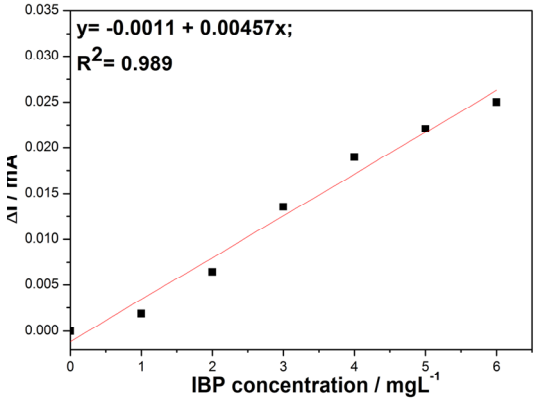


(b)

**Figure 9.4.** (a) Differential-pulsed voltammograms recorded with a AgZEG electrode with a modulation amplitude of 0.05 V, a step potential of 0.05 V and scan rate of 0.1 $Vs^{-1}$ between 0 and +1.5 V vs. Ag/ AgCl in 0.1 M $Na_2SO_4$ supporting electrolyte (1) and in the presence of different IBP concentrations: curves 2-11: 1-10 $mgL^{-1}$. (b) Calibration plots of the currents recorded at E= +1.2 V vs. Ag/ AgCl versus IBP concentrations.

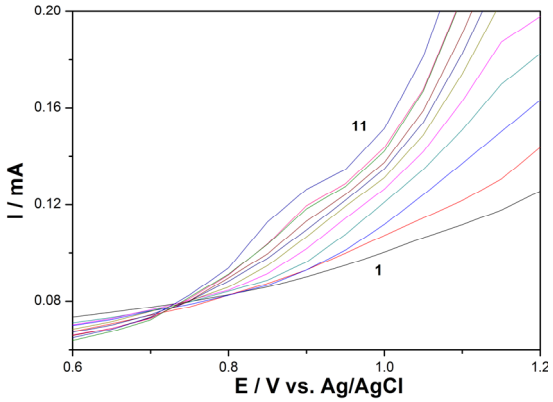


(a)

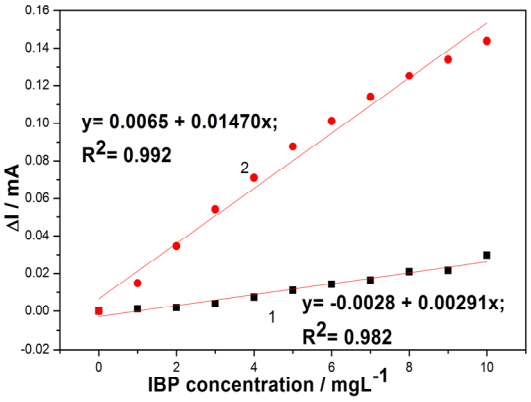


(b)

**Figure 9.5.** (a) Differential-pulsed voltammograms recorded with a AgZEG electrode with a modulation amplitude of 0.1 V, a step potential of 0.05 V and scan rate of 0.1 $Vs^{-1}$ between 0 and +1.5 V vs. Ag/ AgCl in 0.1 M $Na_2SO_4$ supporting electrolyte (1) and in the presence of different IBP concentrations: curves 2-11: 1-10 $mgL^{-1}$. (b) Calibration plots of the currents recorded at E= +0.86 V (1) and E= +1.17 V (2) vs. Ag/ AgCl versus IBP concentrations.

*Square-wave voltammetry*

To provide data that could be compared with the DPV results, a square-wave voltammetric study of IBP electrochemical oxidation was performed. To achieve a more sensitive peak current, the optimum conditions in relation with the step potential, the modulation amplitude, and the frequency were studied, and are being presented in Table 9.3.

**Table 9.3.** The operating parameters for SWV testing in relation with the sensitivity for IBP detection.

| Step potential/ mV | Modulation amplitude/ mV | Frequency/ Hz | Peak potential/ V vs. Ag/AgCl | Sensitivity/ μA $mgL^{-1}$ |
|---|---|---|---|---|
| 0.05 | 0.05 | 25 | +0.90 | 8.14 |
| | | | +1.20 | 23.70 |
| 0.05 | 0.10 | 25 | +1.20 | 46.20 |
| 0.10 | 0.10 | 25 | +0.86 | 32.90 |
| | | | +1.10 | 57.70 |
| 0.20 | 0.10 | 25 | +1.20 | 52.80 |
| 0.05 | 0.10 | 10 | +0.95 | 47.50 |

Four combinations of the step potentials, *i.e.*, 0.05, 0.1, and 0.2 V were applied for the modulation amplitudes of 0.05 and 0.1 V and the frequency of 25 Hz. The SWVs recorded with the corresponding calibration plots are presented in Figures 9.6-9.9. Under these operating conditions the anodic peak currents increased linearly with IBP concentrations and the best results were achieved for the step potential of 0.1 V and the modulation amplitude of 0.1, which were selected as optimum values.

The frequency of 10 Hz was applied for comparison with 25 Hz and the results are similar (See Figure 9.10). The best sensitivity and the lowest limit of detection were recorded under operating conditions of 0.1 V pulse amplitude, 0.1 step potential, and 25 Hz frequency, which were selected as optimum operating conditions using SWV voltammetry with the AgZEG composite electrode.

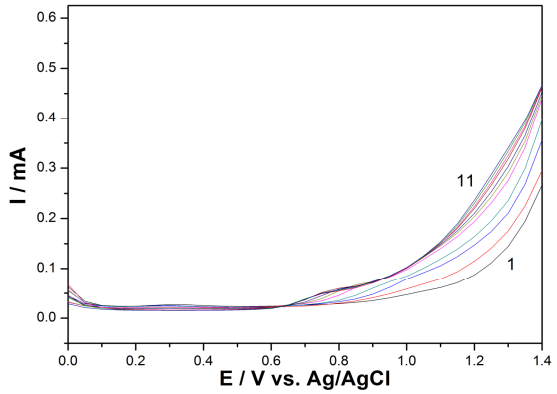


(a)

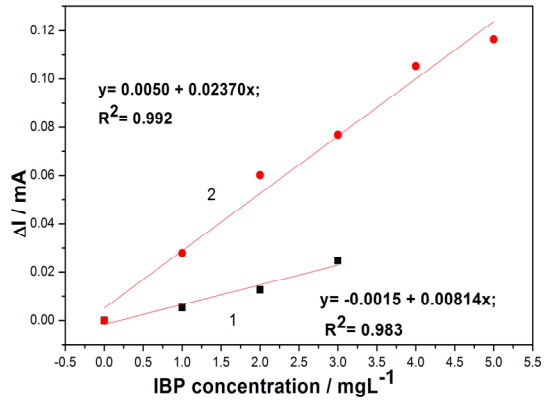


(b)

**Figure 9.6.** (a) Square-wave voltammograms recorded with a AgZEG electrode with a modulation amplitude of 0.05 V, a step potential of 0.05 V, the frequency of 25 Hz and the scan rate of 0.1 $Vs^{-1}$ between 0 and +1.5 V vs. Ag/ AgCl in 0.1 M $Na_2SO_4$ supporting electrolyte (1) and in the presence of different IBP concentrations: curves 2-11: 1-10 $mgL^{-1}$. (b) Calibration plots of the currents recorded at E= +0.9 V (1) and E= +1.2 V (2) vs. Ag/ AgCl versus IBP concentrations.

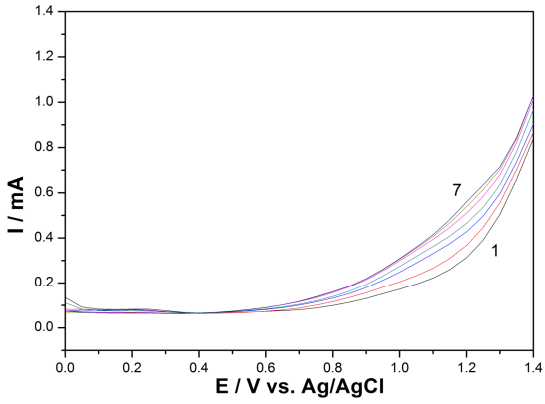


(a)

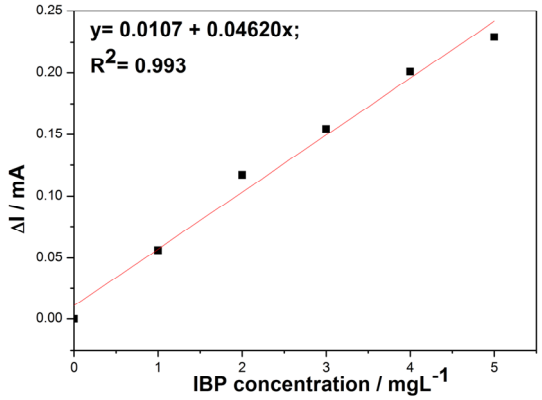


(b)

**Figure 9.7.** (a) Square-wave voltammograms recorded with a AgZEG electrode with a modulation amplitude of 0.1 V, a step potential of 0.05 V, the frequency of 25 Hz and the scan rate of 0.1 $Vs^{-1}$ between 0 and +1.5 V vs. Ag/ AgCl in 0.1 M $Na_2SO_4$ supporting electrolyte (1) and in the presence of different IBP concentrations: curves 2-11: 1-10 $mgL^{-1}$. (b) Calibration plots of the currents recorded at E= +1.2 V vs. Ag/ AgCl versus IBP concentrations.

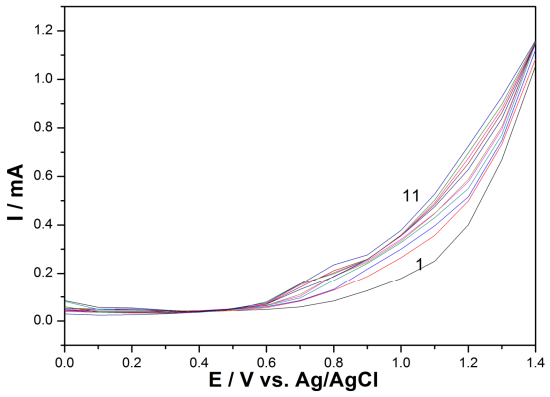


(a)

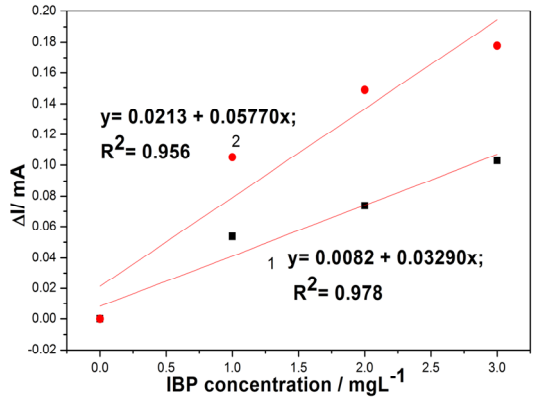


(b)

**Figure 9.8.** (a) Square-wave voltammograms recorded with a AgZEG electrode with a modulation amplitude of 0.1 V, a step potential of 0.1 V, the frequency of 25 Hz and the scan rate of 0.1 $Vs^{-1}$ between 0 and +1.5 V vs. Ag/ AgCl in 0.1 M $Na_2SO_4$ supporting electrolyte (1) and in the presence of different IBP concentrations: curves 2-11: 1-10 $mgL^{-1}$. (b) Calibration plots of the currents recorded at E= +0.86 V (1) and E= +1.2 V (2) vs. Ag/ AgCl versus IBP concentrations.

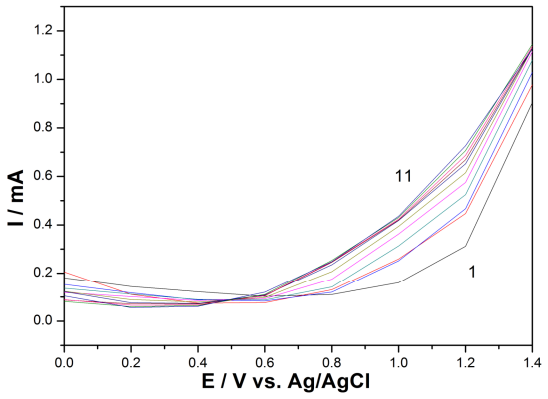


(a)

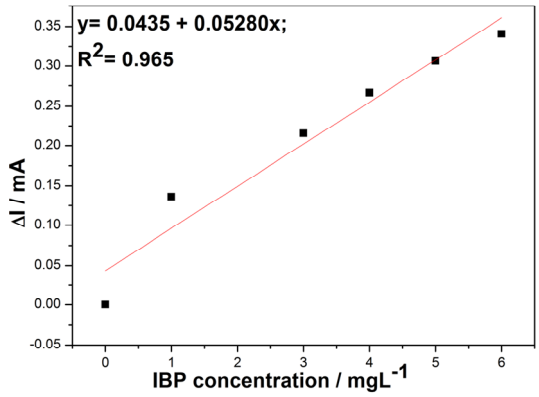


(b)

**Figure 9.9.** (a) Square-wave voltammograms recorded with a AgZEG electrode with a modulation amplitude of 0.1 V, a step potential of 0.2 V, the frequency of 25 Hz and the scan rate of 0.1 $Vs^{-1}$ between 0 and +1.5 V vs. Ag/ AgCl in 0.1 M $Na_2SO_4$ supporting electrolyte (1) and in the presence of different IBP concentrations: curves 2-11: 1-10 $mgL^{-1}$. (b) Calibration plots of the currents recorded at E= +1.2 V vs. Ag/ AgCl vs. IBP concentrations.

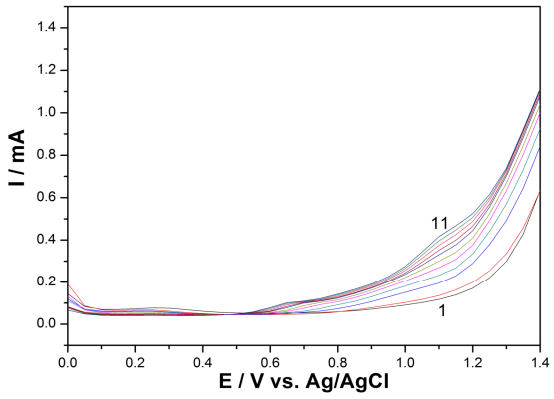


(a)

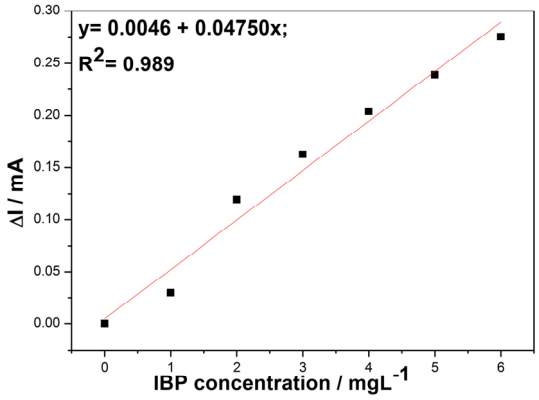


(b)

**Figure 9.10.** (a) Square-wave voltammograms recorded with a AgZEG electrode with a modulation amplitude of 0.1 V, a step potential of 0.05 V, the frequency of 10 Hz and the scan rate of 0.1 $Vs^{-1}$ between 0 and +1.5 V vs. Ag/ AgCl in 0.1 M $Na_2SO_4$ supporting electrolyte (1) and in the presence of different IBP concentrations: curves 2-11: 1-10 $mgL^{-1}$. (b) Calibration plots of the currents recorded at E= +0.95 V vs. Ag/ AgCl vs. IBP concentrations.

In comparison with CV, LSV, and DPV, the SWV technique operated under the optimum conditions allowed to achieve better electroanalytical performance regarding the sensitivity, the relative standard deviation, the lowest limit of detection, and the limit of quantification of IBP using a AgZEG composite electrode (Table 9.4).

***Chronoamperometric results***

The chronoamperometry technique is considered as the easiest detection method envisaging practical application. Based on the cyclic voltammetry results as the reference for operating parameters, the chronoamperometry was tested at the potential value of +1.25 V vs. Ag/ AgCl. Figure 9.11a shows chronoamperometric measurements of IBP with the AgZEG electrode. This figure presents the current-time profiles obtained by setting the working electrode at +1.25 V vs. Ag/ AgCl for various concentrations of ibuprofen. The useful net current signals recorded at 50 seconds are linearly dependent on IBP concentration in the explored concentration range between 10 and 70 $mgL^{-1}$ IBP (Figure 9.11b).

The amperometric response of the AgZEG electrode obtained for successive and continuous addition of 10 $mgL^{-1}$ IBP to 0.1 M $Na_2SO_4$ solution (batch system analysis -BSA) at an applied potential of +1.25 V vs. Ag/ AgCl is shown in Figure 9.12a. The response of the electrode is practically linear in the concentration range from 10 $mgL^{-1}$ to 50 $mgL^{-1}$ (Figure 9.12b).

The sensitivities achieved by both chronoamperometric techniques were similarly and about half of the one reached by cyclic voltammetry, probably due to a slight electrode fouling occurred. However, based on the electroanalytical

parameters reached using this technique, it could be affirmed that the CA detection method exhibits the potential for practical application.

The lowest limit of detection (LOD) and the lowest limit of quantification (LQ) were evaluated based on 3SB/ b, and respective 10SB/ b, where SB is the standard deviation of the mean value of three voltammograms/ amperograms of the blank and b is the slope of the straight line in the analytical curve obtained by each voltammetric/ amperometric technique [22].

The electroanalytical parameters determined for all electrochemical techniques using the AgZEG composite electrode are gathered in Table 9.4. The reproducibility of the electrode using the above-mentioned techniques was evaluated for three replicate measurements of IBP detection as relative standard deviation (RSD) and it is concluded that the IBP detection at the AgZEG composite electrode is reproducible. Also, it can be noticed that the best electroanalytical parameters were reached by square-wave voltammetry operated at the step potential of 0.05 V, the modulation amplitude of 0.1 V and the frequency of 25 Hz.

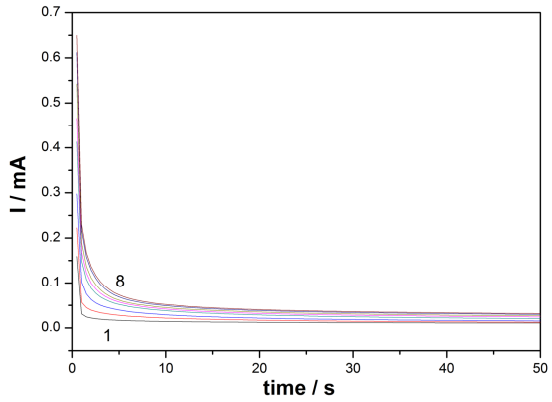


(a)

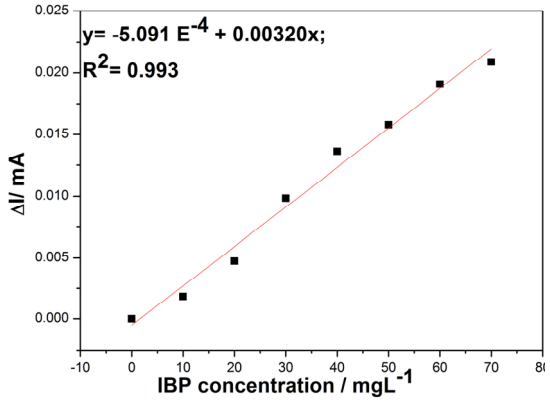


(b)

**Figure 9.11.** (a) Chronoamperograms recorded with a AgZEG electrode in the absence (curve 1) and the presence of (curve 2) 10 $mgL^{-1}$, (curve 3) 20 $mgL^{-1}$, (curve 4) 30 $mgL^{-1}$, (curve 5) 40 $mgL^{-1}$, (curve 6) 50 $mgL^{-1}$, (curve 7) 60 $mgL^{-1}$, (curve 8) 70 $mgL^{-1}$; 0.1 M $Na_2SO_4$ supporting electrolyte; electrode potential of +1.25 V vs. Ag/ AgCl; (b) The calibration plots of current, read at 50 seconds, vs. IBP concentration.

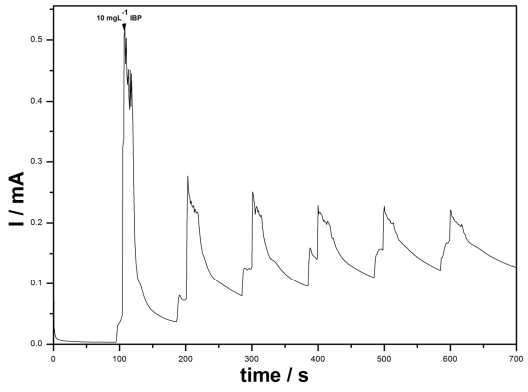


(a)

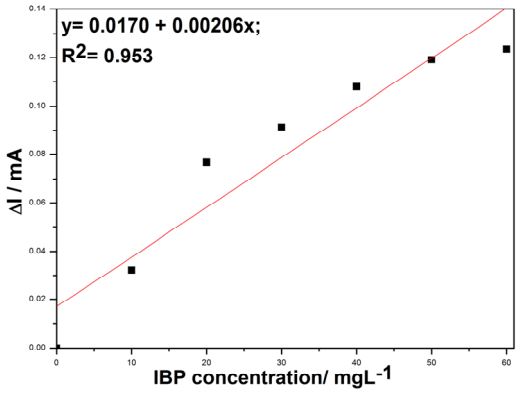


(b)

**Figure 9.12.** (a) Amperometric response (BSA) of the AgZEG electrode for the successive and continuous addition of 10 $mgL^{-1}$ IBP. Applied potential: +1.25 V vs. Ag/ AgCl. (b) The calibration plots of useful signal vs. IBP concentration.

**Table 9.4.** The electroanalytical parameters of voltammetric/ amperometric detection of IBP with a AgZEG composite electrode using electrochemical techniques.

| Technique | Potential value V/ Ag / AgCl | Sensitivity μA/ $mgL^{-1}$ | Correlation coefficient, $R^2$ | Relative standard deviation, RSD, % | The lowest limit of detection, LOD, $mgL^{-1}$ | Limit of quantification, LQ, $mgL^{-1}$ | Concentration range, $mgL^{-1}$ |
|---|---|---|---|---|---|---|---|
| CV | +1.20 | 6.83 | 0.997 | 4.82 | 0.09 | 0.29 | 10-50 |
| LSV | +1.40 | 6.93 | 0.980 | 4.92 | 1.27 | 4.25 | 10-50 |
| DPV | +0.86 | 2.91 | 0.982 | 0.34 | 0.31 | 1.03 | 1-10 |
| | +1.17 | 14.70 | 0.992 | 1.27 | 0.03 | 0.09 | |
| SWV | +0.86 | 32.90 | 0.978 | 0.01 | 0.11 | 0.36 | 1-10 |
| | +1.10 | 57.70 | 0.956 | 0.01 | 0.01 | 0.03 | |
| CA | +1.40 | 3.20 | 0.993 | 4.82 | 0.52 | 1.74 | 10-70 |
| CA-BSA | +1.25 | 2.06 | 0.953 | 3.50 | 0.80 | 2.66 | 10-60 |

### *9.1.2. AgZCNT composite electrode*

Based on the extraordinary properties of CNTs in relation with the mechanical resistance, electrical, and electrocatalytic features, the EG filler was

replaced with CNT in order to enhance the electrode performance. The electrochemical behaviour of IBP using the CNT composite electrode was described in the previous chapter envisaging its application for the electrodegradation. The study of the scan-rate effect on the CV shape informed about the diffusion-controlled oxidation process for the direct oxidation of IBP on the electrode surface, which is really desired for the electroanalysis application. Based on the linear dependence between the anodic peak current recorded at the potential value of +1.2 V vs. Ag/ AgCl and the IBP concentrations, a sensitivity of 10.9 μA $mgL^{-1}$ was determined with a good correlation factor (0.997), which is more promising in comparison with the AgZEG electrode.

The electroanalytical procedures to characterize for this electrode involve cyclic voltammetry (CV), differential-pulsed voltammetry (DPV), square-wave voltammetry (SWV), and chronoamperometry (CA).

***Differential-pulsed voltammetry***

Differential-pulsed voltammetry (DPV) has been employed as a very sensitive and fast electrochemical method for the evaluation of the performance of the AgZCNT electrode for the IBP assessment. The effects of DPV working parameters on the response of the AgZCNT electrode have been studied using different modulation amplitudes (MA), step potentials (SP) and corresponding scan rates, while scanning the potential from +0.5 to +1.2 V vs. Ag/ AgCl (Figure 9.13) in order to achieve the best performance of the electrode.

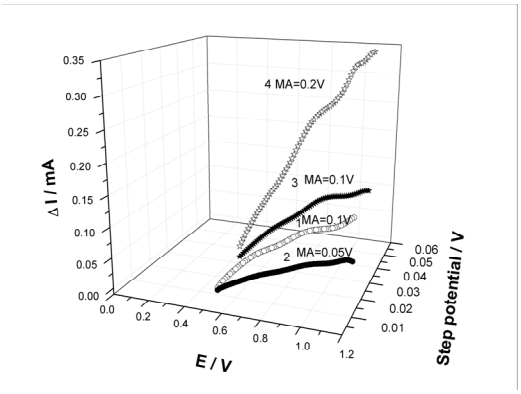


**Figure 9.13.** Differential-pulsed voltammograms recorded in 0.1 M $Na_2SO_4$ supporting electrolyte and in the presence of 10 $mgL^{-1}$ IBP concentration under different conditions of: 1-MA= 0.05 V, SP= 0.01 V; 2-MA= 0.1 V, SP= 0.01 V; 3- MA= 0.1 V, SP= 0.025 V; 4- MA= 0.2 V, SP= 0.025 V, on AgZCNT electrode.

As example, two series of DPVs recorded under the step potential of 0.05 V and the modulation amplitude of 0.1 and 0.2 V, respectively, are presented in Figures 9.14-9.15.

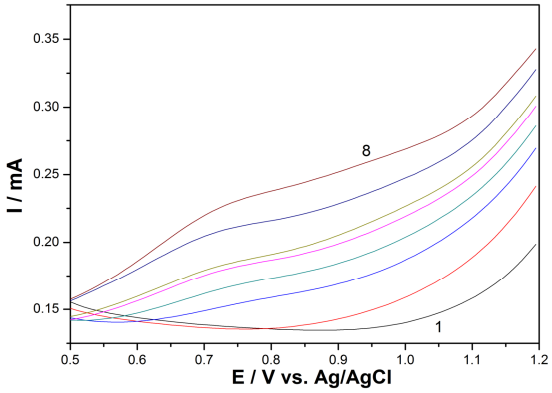


(a)

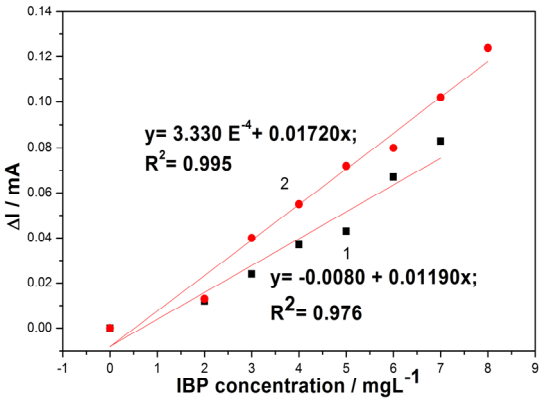


(b)

**Figure 9.14.** (a) Differential- pulsed voltammograms recorded with a AgZCNT electrode with a modulation amplitude of 0.1 V, a step potential of 0.025 V and scan rate of 0.1 $Vs^{-1}$ between 0 and +1.5 V vs. Ag/ AgCl in 0.1 M $Na_2SO_4$ supporting electrolyte (1) and in the presence of different IBP concentrations: curves 2-8: 1-7 $mgL^{-1}$. (b) Calibration plots of the currents recorded at E= +0.7 V (1) and E= +0.95 V (2) vs. Ag/ AgCl versus IBP concentrations.

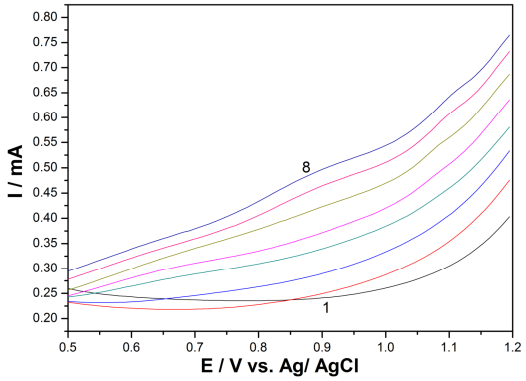


(a)

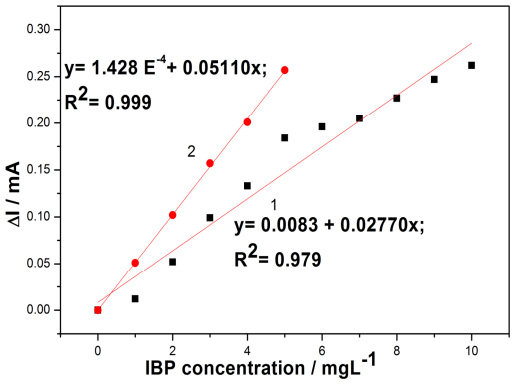


(b)

**Figure 9.15.** (a) Differential- pulsed voltammograms recorded with a AgZCNT electrode with a modulation amplitude of 0.2 V, a step potential of 0.025 V and scan rate of 0.1 $Vs^{-1}$ between 0 and +1.5 V vs. Ag/ AgCl in 0.1 M $Na_2SO_4$ supporting electrolyte (1) and in the presence of different IBP concentrations: curves 2-8: 1-7 $mgL^{-1}$. (b) Calibration plots of the currents recorded at E= +0.9 V (1) and E= +1.1 V (2) vs. Ag/ AgCl versus IBP concentrations.

The linear dependences of the peak currents recorded at +0.9 and +1.1 V vs. Ag/ AgCl versus IBP concentrations were achieved for the IBP concentrations ranging from 1 to 10 $mgL^{-1}$. The best electrode sensitivity for IBP determination using the optimum DPV condition (51.1 μA $mgL^{-1}$) was obtained for a modulation amplitude of 0.2 V with an effective scan rate of 0.025 $Vs^{-1}$ and step potential of 0.025 V for the potential value of +1.1 V vs. Ag/ AgCl. The sensitivities, the lowest limit of detection, the limit of quantification and the relative standard deviation determined using the DPV technique for three replicates are presented in Table 9.5.

***Square-wave voltammetry***

Square-wave voltammetry was also applied in order to improve the electroanalytical parameters for IBP detection. Based on the optimum conditions determined for DPV in relation with the modulation amplitude and the scan rate, the effect of the frequency (f) was studied (see Figure 9.16) and 25 Hz was found to be the best frequency used for IBP detection. A series of SWV recorded under the optimized conditions is presented in Figure 9.17. The anodic peak current observed at +1.1 V vs. Ag/ AgCl increased linearly with the IBP concentration in the range of 1-10 $mgL^{-1}$ (Figure 9.17b). The sensitivity for IBP detection under these working conditions was 44.8 μA $mgL^{-1}$ with a correlation coefficient better than 0.998 (Figure 9.17b). All electroanalytical parameters obtained using SWV are shown in Table 9.5.

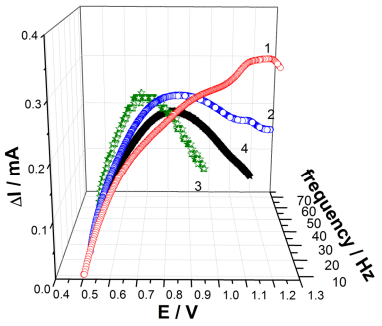


(a)

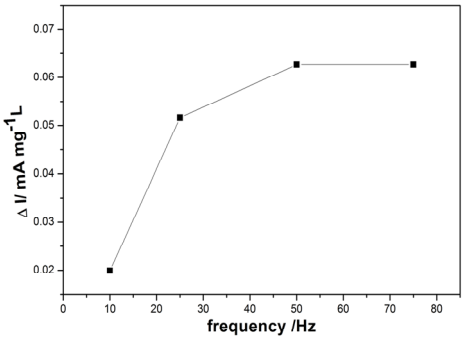


(b)

**Figure 9.16.** (a) SWVs recorded under different conditions: f= 10Hz (1); f= 25 Hz (2); f= 50 Hz (3); f= 75 Hz (4); with a AgZCNT electrode in 0.1 M $Na_2SO_4$ supporting electrolyte and in the presence of various IBP concentrations: 1-10 $mgL^{-1}$; scan rate= 0.025 $Vs^{-1}$, amplitude= 0.2 V. (b) Correlation between sensitivities achieved at different frequencies applied.

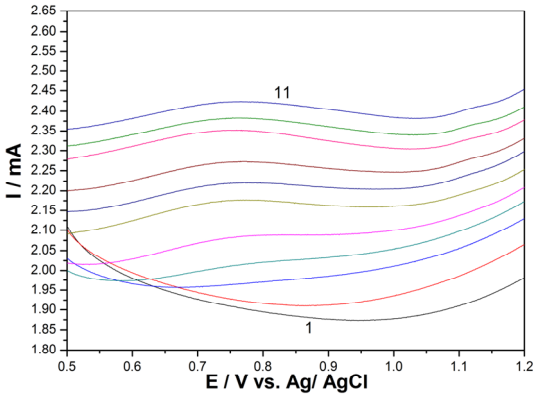


(a)

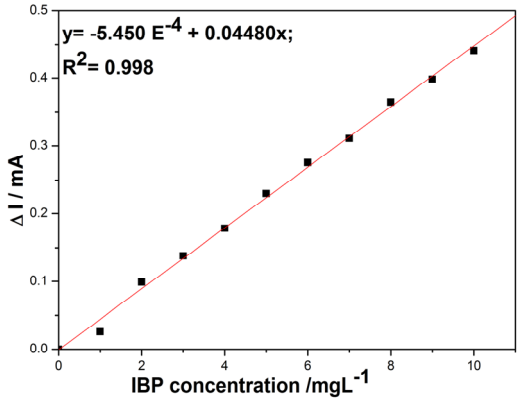


(b)

**Figure 9.17.** (a) Square-wave voltammograms recorded with a AgZCNT electrode with a modulation amplitude of 0.2 V, a step potential of 0.025 V, frequency of 10 Hz and scan rate of 0.1 $Vs^{-1}$ between 0 and +1.5 V vs. Ag/ AgCl in 0.1 M $Na_2SO_4$ supporting electrolyte (1) and in the presence of different IBP concentrations: curves 2-11: 1-10 $mgL^{-1}$. (b) Calibration plots of the currents recorded at E= +1.1 V vs. Ag/ AgCl versus IBP concentrations.

***Chronoamperometry***

Based on the voltammetric results, chronoamperometry was applied as the easiest electrochemical technique used for IBP detection at the detection potential value of +1.2 V vs. Ag/ AgCl, which was applied continuously using the standard addition method and the IBP concentration step of 2 $mgL^{-1}$ (Figure 9.18a). The detection potential value was chosen based on the consideration to be in line with

the cyclic voltammetry, but slightly more positive to avoid electrode fouling. It must be noticed that the sensitivity was lower in comparison with voltammetric techniques (2.5 vs. 11.2 μA $mgL^{-1}$ for CV) (Figure 9.18b) probably due to the fact that electrode fouling occurred.

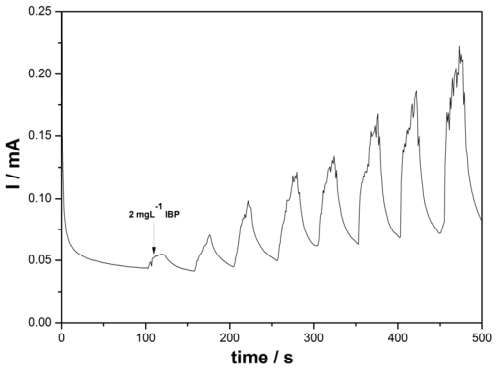


(a)

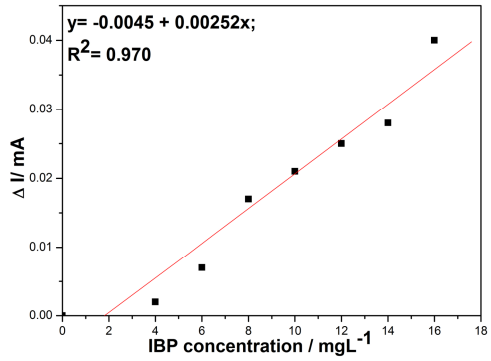


(b)

**Figure 9.18.** (a) Amperometric response (BSA) of the AgZCNT electrode for the successive and continuous addition of 2 $mgL^{-1}$ IBP. Applied potential: +1.25 V vs. Ag/ AgCl. (b) The calibration plots of the useful signal vs. IBP concentration.

The reproducibility of the electrode using the above-mentioned techniques was evaluated for three replicate measurements of IBP detection for each technique. The relative standard deviation (RSD) of maximum 3.29 % revealed the good reproducibility of the electrode.

**Table 9.5.** Electroanalytical performance of the AgZCNT electrode for the detection of IBP.

| Used technique | Peak potential (V) | Electrode sensitivity (μA $mgL^{-1}$) | Correlation coefficient ($R^2$) | Relative standard deviation, RSD, % | The lowest limit of detection, LOD, $mgL^{-1}$ | Limit of quantification, LQ, $mgL^{-1}$ |
|---|---|---|---|---|---|---|
| CV | +1.20 | 10.9 | 0.997 | 1.76 | 0.55 | 1.84 |
| DPV | +0.90 | 27.7 | 0.979 | 2.89 | 0.76 | 2.53 |
| | +1.10 | 51.1 | 0.999 | 2.51 | 0.08 | 0.28 |
| SWV | +1.10 | 44.8 | 0.998 | 0.14 | 0.19 | 0.62 |
| CA | +1.25 | 2.52 | 0.970 | 1.64 | 0.84 | 2.80 |

The best electroanalytical parameters for IBP determination were achieved for the differential-pulsed voltammetry and square-wave voltammetry techniques under optimized conditions of modulation amplitude of 0.2 V, step potential of 0.025 V with an effective scan rate of 0.025 $Vs^{-1}$, and the frequency of 25 Hz. DPV was the electrochemical method selected for the validation.

A recovery test was also performed by analyzing three parallel tap water samples, which contain 2 $mgL^{-1}$ IBP. This test was run in 0.1 M $Na_2SO_4$ supporting electrolyte and a recovery of 98.5 % was found with a RSD of 2.5 % using DPV under optimized conditions. Finally, the results obtained by this method were compared with those obtained by means of a UV-VIS spectrophotometric method, and it can be concluded that the results obtained by the two methods are very close and the accuracy of the proposed voltammetric method is excellent.

### *9.1.3. AgZCNF and AgCNF composite electrodes*

Besides carbon nanotubes (CNTs), carbon nanofibers (CNFs) are one of the most promising reinforcing materials for epoxy-based composites for the carbon-based electrode for the application in electroanalysis due to its excellent mechanical, electrical, and electrocatalytical properties. In comparison with CNTs, CNFs are advantageous from an economical point of view, being less expensive. In this study, CNFs were incorporated to replace CNTs to compare the electroanalytical parameters for IBP detection. In addition, two types of silver incorporation into the electrode composition were applied: by chemical deposition and via natural zeolite that was prior modified with silver ions by ion-exchange. Thus, the two types of the electrodes named silver-doped zeolite-carbon nanofiber-epoxy (AgZCNF) and silver-decorated carbon nanofiber-epoxy (AgCNF) were tested for the electrochemical detection of IBP.

***Electrochemical behaviour of IBP on AgZCNF and AgCNF composite electrodes***

Figure 9.19 and 9.20 show the cyclic voltammograms (CVs) recorded using the AgZCNF and AgCNF electrode with the scan rate of 0.05 $Vs^{-1}$ in 0.1 M $Na_2SO_4$ supporting electrolyte and in the presence of various IBP concentrations ranging from 1 $mgL^{-1}$ to 8 $mgL^{-1}$. Similar shapes of the voltammograms can be noticed for both electrodes and the oxidation peak corresponding to the Ag/ $Ag^+$ couple appeared at the potential value of +0.3 V vs. Ag/ AgCl, which is more evidenced for

AgZCNF in direct relation with the silver content. The current corresponding to the IBP oxidation peak recorded at about +1.3 V vs. Ag/ AgCl increased progressively with its concentration (see Figure 9.19b and 9.20b). On the following reverse scan from +1.5 to-0.5 V vs. Ag/ AgCl, no corresponding reduction peak is observed, revealing the electrode process at both electrodes to be totally irreversible.

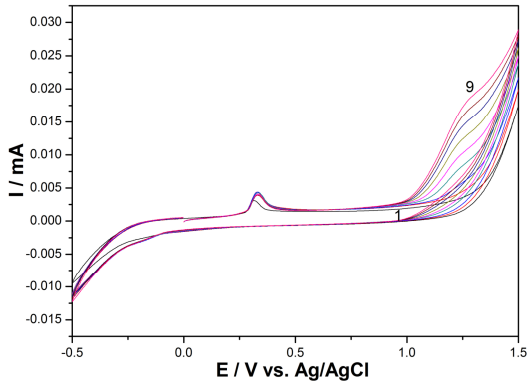


(a)

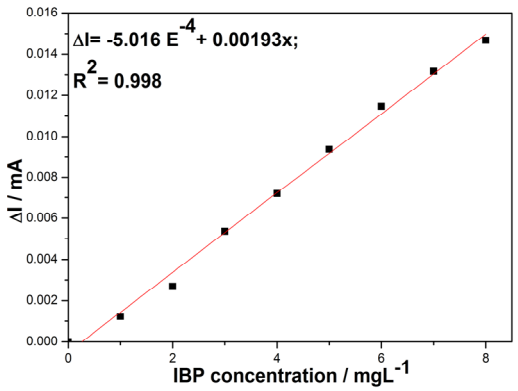


(b)

**Figure 9.19.** (a) CVs recorded using AgZCNF electrodes in 0.1M $Na_2SO_4$ supporting electrolyte (curve 1) and in the presence of various IBP concentrations: 1-8 $mgL^{-1}$ (curves 2-9); potential scan rate of 0.05 $Vs^{-1}$. (b) Calibration plots of anodic peak current recorded at +1.29 V vs. Ag/ AgCl vs. IBP concentrations.

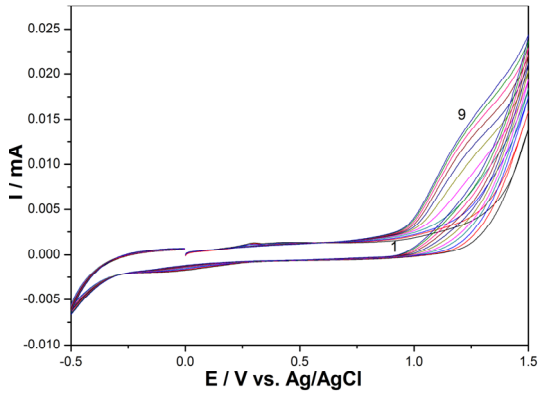


(a)

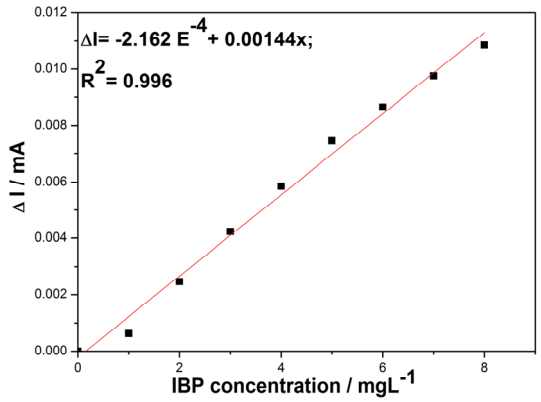


(b)

**Figure 9.20.** (a) CVs recorded using AgCNF electrodes in 0.1M $Na_2SO_4$ supporting electrolyte (curve 1) and in the presence of various IBP concentrations: 1-8 $mgL^{-1}$ (curves 2-9); potential scan rate of 0.05 $Vs^{-1}$; (b)Calibration plots of anodic peak current recorded at **+**1.3 V vs. Ag/ AgCl vs. IBP concentrations.

In order to elucidate some mechanistic aspects of the overall oxidation process of IBP on both composite electrodes linked to the influence of various scan rates (0.01-0.2 $Vs^{-1}$) on the CVs recorded on each composite electrode in the presence of 10 $mgL^{-1}$ was studied (Figure 9.21 and 9.22). The linear dependence of peak currents corresponding to IBP anodic oxidation with the square root of scan rates suggested a mass-transfer controlled process, and no zero intercept indicated that adsorption and surface interaction processes can be not neglected. Based on the value of the slope determined for each composite electrode, it can be seen that the diffusion process is slightly favoured for AgCNF in comparison with AgZCNF

electrode. For both composite electrodes, the peak potential shifted towards positive potential when increasing *v*, indicating that the electrooxidation process of IBP is irreversible.

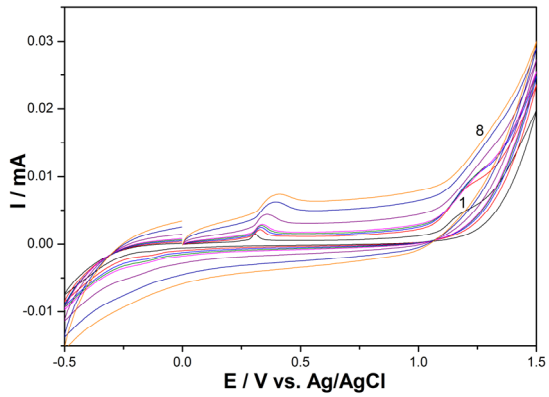


(a)

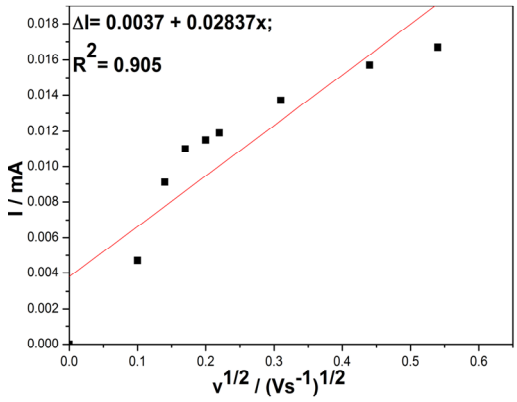


(b)

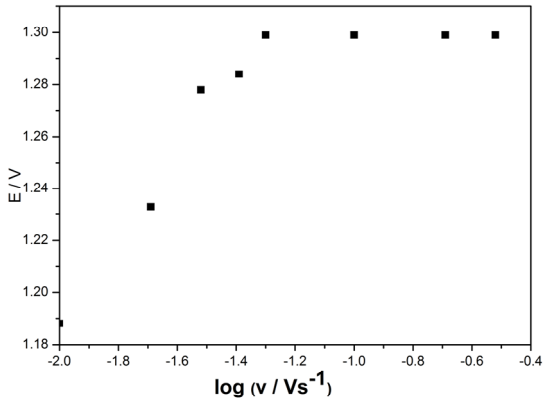


(c)

**Figure 9.21.** (a) Cyclic voltammograms recorded using a AgZCNF electrode with 10 $mgL^{-1}$ IBP in a 0.1 M $Na_2SO_4$ supporting electrolyte with different scan rates 10, 20, 30, 40, 50, 100, 200, 300 $mVs^{-1}$; (b) The anodic peak current vs. the square root of the scan rate; (c) The dependence of the potential value vs. the logarithm of the scan rate.

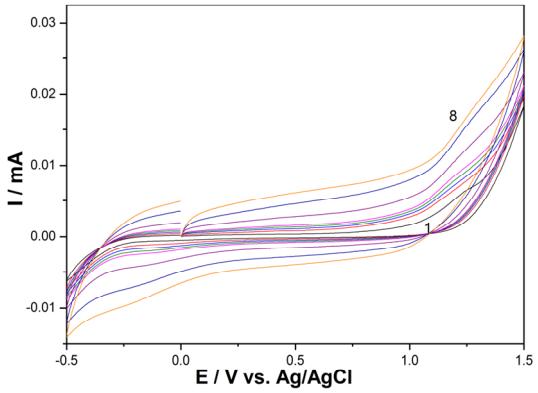


(a)

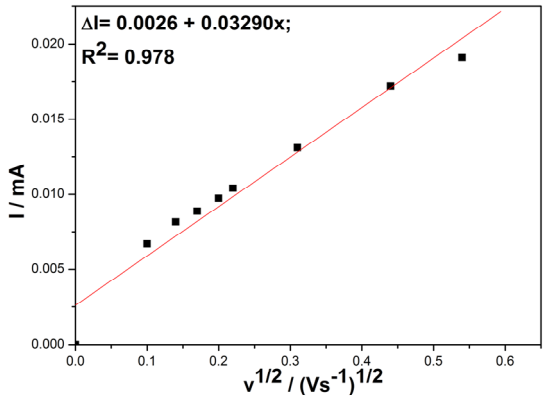


(b)

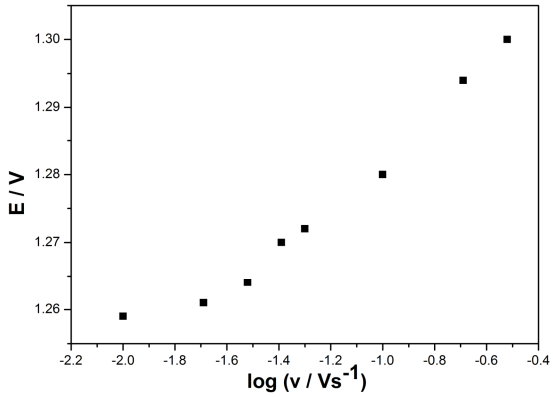


(c)

**Figure 9.22.** (a) Cyclic voltammograms recorded using a AgCNF electrode with 10 $mgL^{-1}$ IBP in a 0.1 M $Na_2SO_4$ supporting electrolyte with different scan rates 10, 20, 30, 40, 50, 100, 200, 300 $mVs^{-1}$; (b) The anodic peak current vs. the square root of the scan rate; (c) The dependence of the potential value vs. the logarithm of the scan rate.

***Detection measurements***

Taking into consideration the detection results achieved for AgZCNT regarding the optimum operating conditions for DPV and SWV techniques, the same detection scheme was applied for AgZCNF and AgCNF for the comparative assessment.

The differential-pulsed voltammetry (DPV) technique was applied under optimized parameters. Figures 9.23 and 9.24 present DPVs recorded at both electrodes, including the linear dependences of the anodic currents versus IBP

concentrations. The operating conditions of the DPV technique for these electrodes are the optimum established for AgZCNT, *i.e.*, the step potential of 0.025 V and the modulation amplitude of 0.2 V. The best sensitivity was reached for the AgZCNF composite electrode, which can be explained by the higher value of the background current for AgZCNF in comparison with AgCNF. This behaviour informed about a smaller amount of silver particles in AgCNF, which is in accordance with SEM results.

The electroanalytical parameters, *e.g.*, the sensitivity, the lowest limit of detection, the limit of quantification and relative standard deviation achieved using this technique are presented in Table 9.6.

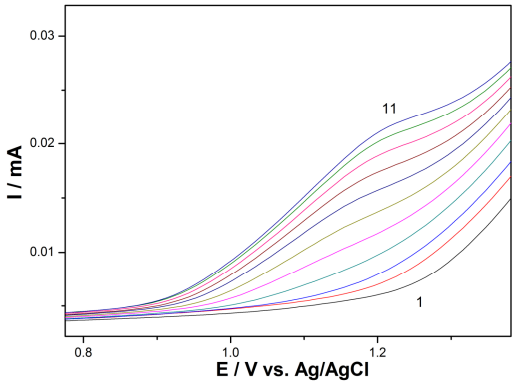


(a)

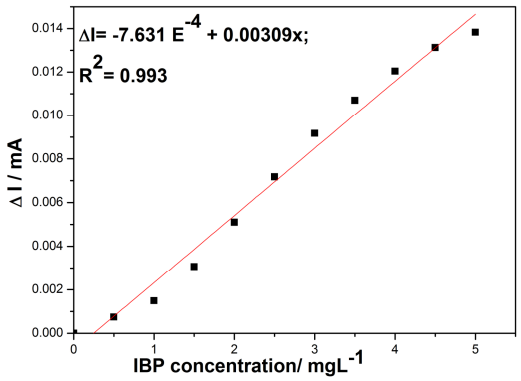


(b)

**Figure 9.23.** (a) DPVs recorded using a AgZCNF electrode in 0.1 M $Na_2SO_4$ supporting electrolyte (curve 1) and in the presence of various IBP concentrations: 0.5-5 $mg \cdot L^{-1}$ (curves 2-11); (b) Calibration plots of the current densities versus the IBP concentrations of the DPVs recorded at E= +1.17 V vs. Ag/ AgCl.

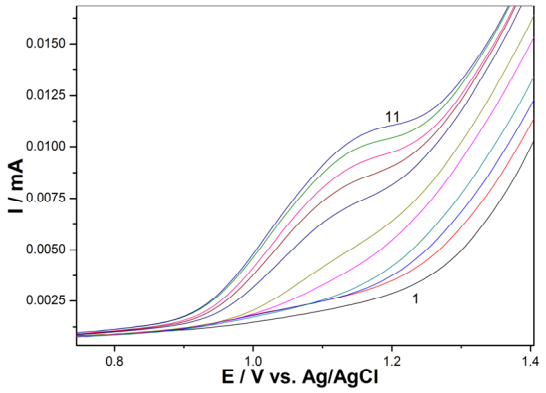


(a)

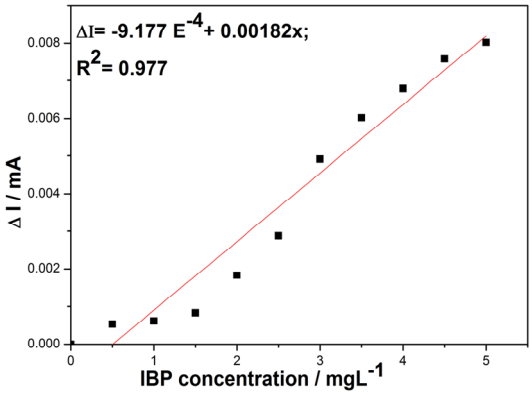


(b)

**Figure 9.24.** (a) DPVs recorded using a AgCNF electrode in 0.1 M $Na_2SO_4$ supporting electrolyte (curve 1) and in the presence of various IBP concentrations: 0.5-5 $mgL^{-1}$ (curves 2-11); (b) Calibration plots of the current densities versus the IBP concentrations of the DPVs recorded at E= +1.15 V vs. Ag/ AgCl.

To explore the sorption capacity of both electrodes towards IBP, a pre-concentration-voltammetric detection scheme was tested after the optimum accumulation time setting based on the results of the effect of accumulation time on the currents of the differential-pulsed anodic peak recorded at +1.15 V vs. Ag/ AgCl corresponding to IBP oxidation. The accumulation time is considered to be the time maintaining at open-circuit potential before running the differential-pulsed voltammetry. The enhancement factor was determined as the ratio of the peak current recorded at different accumulation times to that recorded without a pre-concentration scheme and the maximum value of about 4 was reached for AgCNF

and about 2 for AgZCNF at the accumulation time of 20 minutes, respectively (Figure 9.25). For longer accumulation times, no higher current response was obtained (the results are not shown here). Applying the pre-concentration-voltammetric detection scheme using the AgCNF electrode the sensitivity for IBP detection was improved, a value of 4.15 μA $mgL^{-1}$ was achieved in comparison with 1.81 μA $mgL^{-1}$ without pre-concentration.

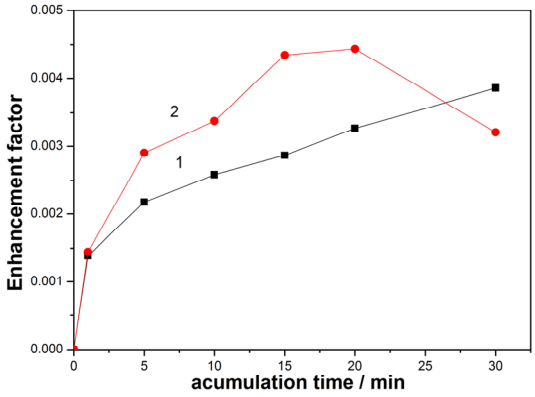


**Figure 9.25.** Enhancement factor for the oxidation of 1 $mgL^{-1}$ IBP as function of the accumulation time, with background current subtraction: 1- AgZCNF electrode and 2-AgCNF electrode. Detection was performed in 0.1 M $Na_2SO_4$ supporting electrolyte by DPVs recorded at +1 V vs. Ag/ AgCl, potential scan rate 0.05 $Vs^{-1}$.

Also, SWV under optimized operating parameters was applied for both composite electrodes and the results are presented in Figure 9.26 and 9.27. The detection results obtained by this technique were similarly with those reached by DPV. All electroanalytical parameters are gathered in Table 9.6.

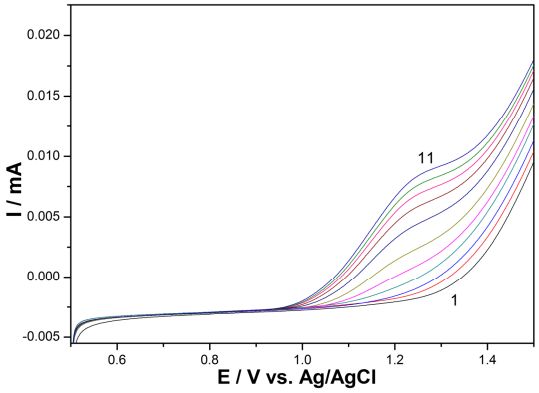


(a)

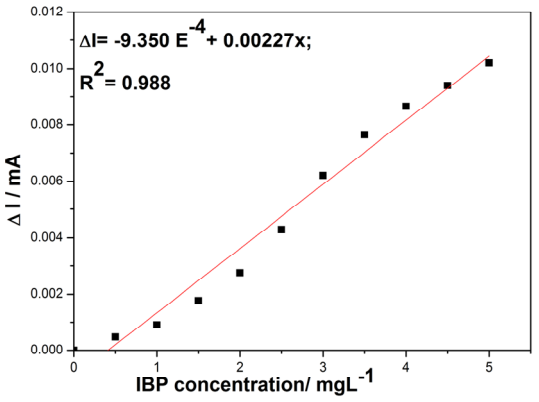


(b)

**Figure 9.26.** (a) Square-wave voltammograms recorded using a AgZCNF electrode with a modulation amplitude of 0.2 V, a step potential of 0.025 V, frequency of 25 Hz and scan rate of 0.1 $Vs^{-1}$ between 0 and +1.5 V vs. Ag/ AgCl in 0.1 M $Na_2SO_4$ supporting electrolyte (1) and in the presence of different IBP concentrations: curves 2-11: 1-10 $mgL^{-1}$. (b) Calibration plots of the currents recorded at E= +1.25 V vs. Ag/ AgCl versus IBP concentrations.

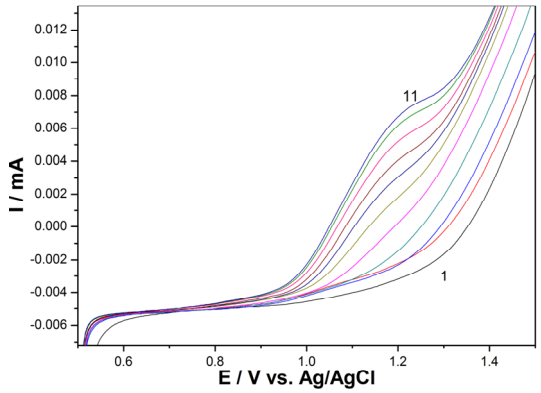


(a)

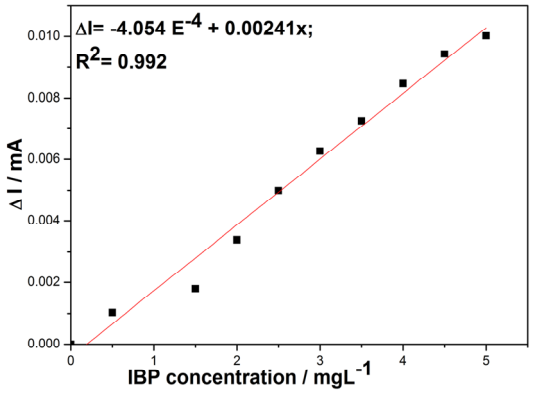


(b)

**Figure 9.27.** (a) Square-wave voltammograms recorded on AgCNF electrode with a modulation amplitude of 0.2 V, a step potential of 0.025 V, frequency of 25 Hz and scan rate of 0.1 $Vs^{-1}$ between 0 and +1.5 V vs. Ag/ AgCl in 0.1 M $Na_2SO_4$ supporting electrolyte (1) and in the presence of different IBP concentrations: curves 2-11: 1-10 $mgL^{-1}$. (b) Calibration plots of the currents recorded at E= +1.2 V vs. Ag/ AgCl versus IBP concentrations.

The simplest electroanalytical procedure should involve the recording of the chronoamperogram, based on the reference provided by the cyclic voltammograms. Thus, for the AgCNF electrode the continuous chronoamperograms were recorded at the potential value of + 1.3 V vs. Ag/ AgCl within the IBP concentration range between 0.5 and 5 $mgL^{-1}$ (Figure 9.28). The sensitivity was compared to CV for AgCNF, and it has been noticed that no electrode fouling occurred, the sensitivity achieved by CA being slightly better than the one reached using CV (see Table 6).

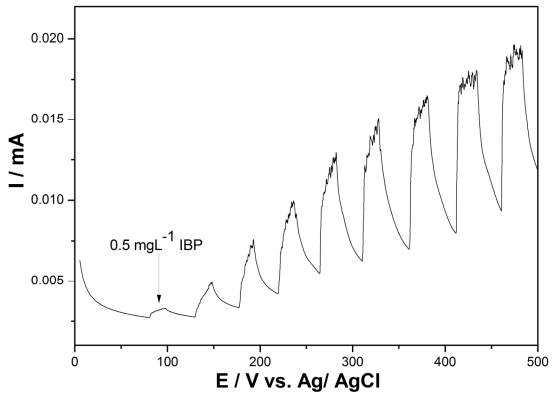


(a)

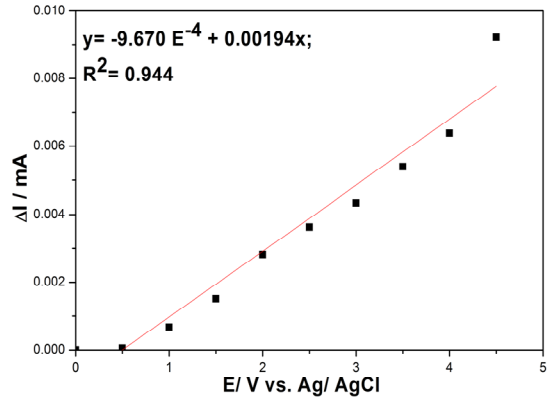


(b)

**Figure 9.28.** (a) Amperometric response (BSA) of the AgCNF electrode for the successive and continuous addition of 0.5 $mgL^{-1}$ IBP. Applied potential: +1.25 V vs. Ag/ AgCl. (b) The calibration plots of useful signal vs. IBP concentration.

All electroanalytical parameters obtained by applying AgZCNF and AgCNF composite electrodes using CV, DPV, SWV, and CA are gathered in Table 9.6, and the best electroanalytical performance was achieved using the detection scheme based on preconcentration-differential pulsed voltammetry.

**Table 9.6.** Electroanalytical performance of the AgZCNF and AgCNF composite electrodes for the detection of ibuprofen.

| Electrode material | Used technique | Peak potential (V) | Electrode sensitivity (μA $mgL^{-1}$) | Correlation coefficient ($R^2$) | Relative standard deviation RSD, % | The lowest limit of detection LOD, $mgL^{-1}$ | Limit of quantification LQ, $mgL^{-1}$ |
|---|---|---|---|---|---|---|---|
| AgZCNF | CV | +1.29 | 1.930 | 0.998 | 3.500 | 0.030 | 0.099 |
| | DPV | +1.17 | 3.090 | 0.993 | 3.750 | 0.008 | 0.026 |
| | SWV | +1.25 | 2.270 | 0.988 | 1.400 | 0.075 | 0.247 |
| AgCNF | CV | +1.30 | 1.440 | 0.996 | 3.200 | 0.020 | 0.066 |
| | DPV | +1.15 | 1.820 | 0.977 | 3.900 | 0.010 | 0.033 |
| | Preconcentration/ DPV | +1.00 | 4.150 | 0.998 | 4.250 | 0.001 | 0.003 |
| | SWV | +1.2 | 2.410 | 0.992 | 3.800 | 0.008 | 0.026 |
| | CA | +1.3 | 1.940 | 0.944 | 1.250 | 0.020 | 0.066 |

The most representative comparative results regarding IBP detection at carbon-based composite electrode using the electrochemical technique regarding the best results in relation with the lowest detection potential value, the sensitivity, the lowest limit of detection, and the lowest limit of quantification are presented in Table 9.7.

**Table 9.7.** The comparative electroanalytical parameters of amperometric detection of IBP at carbon-based composite electrode using electrochemical techniques.

| Electrode material | Used technique | Peak potential (V) | Electrode sensitivity (μA $mgL^{-1}$) | Correlation coefficient ($R^2$) | Relative standard deviation RSD, % | The lowest limit of detection LOD, $mgL^{-1}$ | Limit of quantification LQ, $mgL^{-1}$ |
|---|---|---|---|---|---|---|---|
| AgZCNT | CV | +1.20 | 10.900 | 0.997 | 1.760 | 0.550 | 1.840 |
| | DPV | +0.90 | 27.700 | 0.979 | 2.890 | 0.760 | 2.530 |
| | | +1.10 | 51.100 | 0.999 | 2.510 | 0.082 | 0.280 |
| | SWV | +1.10 | 44.800 | 0.998 | 0.140 | 0.190 | 0.620 |
| | CA | +1.25 | 2.520 | 0.970 | 1.640 | 0.840 | 2.800 |
| AgZCNF | CV | +1.29 | 1.930 | 0.998 | 3.500 | 0.030 | 0.099 |
| | DPV | +1.17 | 3.090 | 0.993 | 3.750 | 0.008 | 0.026 |
| | SWV | +1.25 | 2.270 | 0.988 | 1.400 | 0.075 | 0.247 |
| AgCNF | CV | +1.30 | 1.440 | 0.996 | 3.200 | 0.020 | 0.066 |
| | DPV | +1.15 | 1.820 | 0.977 | 3.900 | 0.010 | 0.033 |
| | Preconce | +1.00 | 4.150 | 0.998 | 4.250 | 0.001 | 0.003 |

| | | | | | | | |
|---|---|---|---|---|---|---|---|
| | tration/ DPV | | | | | | |
| | SWV | +1.20 | 2.410 | 0.992 | 3.800 | 0.008 | 0.026 |
| | CA | +1.30 | 1.940 | 0.944 | 1.250 | 0.020 | 0.066 |
| AgZEG | CV | +1.20 | 6.830 | 0.997 | 4.820 | 0.090 | 0.290 |
| | LSV | +1.40 | 6.930 | 0.980 | 4.920 | 1.270 | 4.250 |
| | DPV | +0.86 | 2.910 | 0.982 | 0.340 | 0.310 | 1.030 |
| | | +1.17 | 14.700 | 0.992 | 1.270 | 0.030 | 0.090 |
| | SWV | +0.86 | 32.900 | 0.978 | 0.010 | 0.110 | 0.360 |
| | | +1.10 | 57.700 | 0.956 | 0.010 | 0.010 | 0.030 |
| | CA | +1.40 | 3.200 | 0.993 | 4.820 | 0.520 | 1.740 |
| | CA-BSA | +1.25 | 2.060 | 0.953 | 3.500 | 0.80 | 2.660 |

Based on the presented results, it may be concluded:

– All tested electrodes, *i.e.*, AgZCNT, AgZCNF, AgCNF, and AgZEG composite electrodes exhibited the availability for the direct anodic oxidation of ibuprofen (IBP), giving them a real potential for the amperometric/ voltammetric detection of IBP.

– Even if several characteristics regarding the direct electrooxidation of IBP are common for all silver-based composite electrodes, specific peculiarities linked to carbon structure gave them slightly differences related to the electrode performances for IBP detection. Also, silver content and form influenced the electrode performance for IBP detection.

– The electrode performance for IBP detection in relation with the sensitivities increased as: AgZCNT>AgZEG>AgZCNF>AgCNF. Also, the best limit of detection and quantification were achieved for the AgZCNT electrode. However, better reproducibility of AgZEG linked to the economic criteria makes this electrode to exhibit the great potential for practical application;

– The exploitation of pulsed voltammetric/ amperometric techniques allowed enhancing the electroanalytical parameters for IBP detection;

– The selection of the electrode type, the electrochemical technique, and the operating conditions will be made taking into account the specific requirements imposed by the practical utility.

– The IBP detection procedure involving a pre-concentration step was developed:

Step 1- pre-concentration- electrode maintaining at the potential value corresponding to the open circuit potential for 20 minutes.

Step 2- detection step- running the pulsed voltammetry under optimized operating variables (optimizations of the operating variables are specific to each electrode type).

## 9.2. References

[1] L. Ciriaco, C. Anjo, J. Correia, M.J. Pacheco, A. Lopes, Electrochim. Acta 54 (2009) 1464.

[2] J. Madhavan, F. Grieser, M. Ashokkumar, J. Hazard. Mater. 178 (2010) 202.

[3] I. Ali, P. Singh, H.Y. Aboul-EneinY, B. Sharma, Anal. Lett. 42 12 (2009) 1747.

[4] R. Uddin, N. Saffoon, N.H. HudaH, Y.M. Jhanker, J. Pharm. Sci. 3 1 (2010) 63.
[5] J. Manrique, F. Martinez, Lat. Am. J. Pharm. 26 3 (2007) 344.
[6] M.R. Khoshayand, H. Abdollahi, M. Shariatpanahi, A. Saadatfard, A. Mohammadia, Spectrochim. Acta A 70 (2008) 491.
[7] S.S. Mitic, G.Z. Miletic, A.N. Pavlovic, B.B. Arsic, V.V. Zivanovic, J. Serb. Chem. Soc. 73 8–9 (2008) 879.
[8] X. Zhao, J. Qu, H. Liu, Z. Qiang, R. Liu, C. Hu, Appl. Catal. B Environ. 91 (2009) 539.
[9] S. Weigel, U. Berger, E. Jensen, R. Kallenborn, H. Thoresen, H. Huhnerfuss, Chemosphere 56 (2004) 583.
[10] EMEA, Guideline on the Environmental Risk Assessment of Medicinal Products for Human Use, The European Agency for the Evaluation of Medicinal Products: Committee for Medicinal Products for Human Use, EMEA/CHMP/SWP/4447/00, 2006.
[11] F.A. Caliman, M. Gavrilescu, Clean 37 4-5 (2009) 277.
[12] E.M. Ghoneim, H.S. El-Desoky, Bioelectrochemistry 79 (2010) 241.
[13] J.L.P. Pavon, A.M.C. Ferreira, M.E.F. Laespada, B.M Cordero J. Chromatogr. A 1216 (2009) 6728.
[14] M.R. Whelan, J.L. Ford, M.W. Powell, J. Pharmaceut. Biomed. 30 (2002) 1355.
[15] P. Valderrama, R.J. Poppi, Chemometrics and Intelligent Laboratory Systems, (2010), in press.
[16] R. Hamoudova, M. Pospisilova, J. Pharmaceut. Biomed. 41 (2006)1463.
[17] W.S. Hassan, Am. J. Appl. Sci. 5 8 (2008) 1005.
[18] A. Pop, F. Manea, C. Radovan, P. Malchev, A. Bebeselea, C. Proca, G. Burtica, S. Picken, J. Schoonman, Electroanal. 20 (2008) 2460.
[19] F. Manea, A. Pop, C. Radovan, P. Malchev, A. Bebeselea, G. Burtica, S. Picken, J. Schoonman, Sensors 8 (2008) 5806.
[20] M.S. Canals, Advanced oxidation processes applied to mineralize paracetamol, chloroxylenol, ibuprofen and diclofenac in aqueous medium [Doctoral Dissertation]. Universitat de Barcelona, Departament de Quimica Fisica (2009).
[21] **S. Motoc**, F. Manea, A. Pop, R. Pode, G. Burtica, Adv. Sci, Eng. and Med. 3 1-2 (2011) 7.
[22] L. Codognoto, V.G. Zuin, D. de Souza, J.H. Yariwake, S.A.S. Machado, A. Avaca, Microchem. J. 77 (2004) 177.

# CHAPTER 10. SIMULTANEOUS ELECTROCHEMICAL DETECTION OF PHARMACEUTICALS USING CARBON BASED COMPOSITE ELECTRODES

## 10.1. Electrochemical detection of diclofenac using carbon-based composite electrodes

Sodium diclofenac (DCF), sodium[o-(2,6-dichloroanilino) phenyl] acetate, a widely used anti-inflammatory drug, can be found in many wastewater treatment plants effluents [1-3]. Also, based on water cycle and taking into account that sometimes, the wastewater treatment plants are not effective in diclofenac removal and mineralization, the rivers, lakes and ground water may be contaminated. DCF belongs to a new very important water pollutant class by type of pharmaceuticals because of their potential impact on human health and environment [2].

These aspects require the development of a simple, sensitive and reliable determination method of DCF in aqueous solution. Several methods for the quantitative determination of diclofenac have been reported, *e.g.*, spectrophotometric, fluorometric, chromatographic and electrochemical methods [4-11].

In the last years, the electrochemical methods have attracted interest as electroanalysis, because of the fast response, large sensitivities, simple operation, and the possibilities of miniaturization. Because the electrooxidation of sodium diclofenac proceeds very slowly and almost no current response was observed at the usual electrode, a few studies reported the voltammetric/ amperometric detection of diclofenac at conventional electrodes. The voltammetric/ amperometric methods at modified electrodes [7-9] and potentiometric techniques [10-11] have been reported for the determination of diclofenac.

Many research studies [1, 12-16] have been reported about the extraordinary properties of boron-doped diamond (BDD) electrode, *e.g.*, wider potential window for water stability, chemical and mechanical stability, low background currents, resistance to fouling. These properties make this electrode very promising for electroanalysis.

This study aimed to investigate the electrochemical behaviour of DCF on carbon based electrodes, carbon nanotubes-epoxy composite (CNT), silver-doped zeolite-carbon nanotubes-epoxy composite (AgZCNT) and silver-doped zeolite-expanded-graphite-epoxy composite (AgZEG) in comparison cu commercial boron-doped diamond (BDD) and glassy carbon (GC) electrode and to test the suitability of these electrodes for voltammetric/ amperometric detection of DCF. The electrochemical oxidation of DCF on CNT and BDD electrode, the kinetics aspects and the parameters suitable for detection were studied by cyclic voltammetry (CV) technique. The electroanalytical parameters for voltammetric/ amperometric detection of DCF on BDD electrode will be established by using chronoamperomtry (CA), square-wave voltammetry (SWV) and differential-pulsed voltammetry (DPV). The optimized detection procedure was tested on DCF spiked tap water sample.

### *10.1.1. Experimental*

Electrochemical measurements were carried out in a Metrohm three electrode cell equipped with a BDD electrode (commercial product), a 3 mm diameter stationary disc embedded in a teflon rod as the working electrode, a platinum foil counter electrode and a saturated calomel (SCE) reference electrode. The BDD electrode supplied by Windsor Scientific Ltd. for electroanalytical use was a mirror polished doped polycrystalline industrial diamond (microcrystalline; doping degree about 0.1% boron). The voltammograms and chronoamperograms were obtained by using an Autolab PGStat 304 EcoChemie system controlled by a PC running GPES Software version 4.9. Prior to the electrochemical measurements, the working electrode was carefully cleaned, degreased and treated by polishing with alumina powder (0.1 mm), and finally washed with double distilled water. The interface of the working electrode with the aqueous medium was stabilized by repeated cycling in a supporting electrolyte solution within an extended potential range between -0.5 V and +1.5 V vs. SCE. $Na_2SO_4$ was analytical reagent grade from Merck, and DCF was used as received from Amoli Organics Ltd.

All solutions were prepared with doubly distilled and deionised water.

### *10.1.2. Results and discussion*

Some aspects regarding diclofenac (DCF) oxidation and determination at CNT, AgZCNT, AgZEG, BDD and GC electrodes were studied by CV. Cyclic voltammograms obtained at each electrode in the presence of various DCF concentrations ranges in 0.1 M $Na_2SO_4$ are shown in Figures 10.1-10.5.

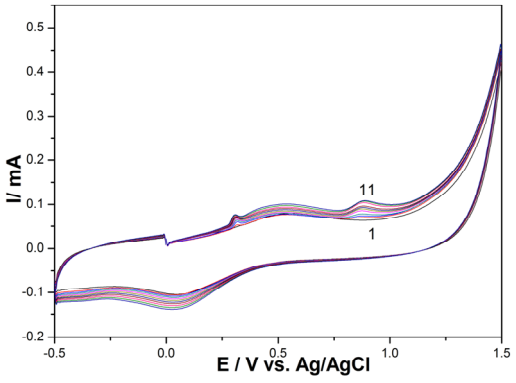


(a)

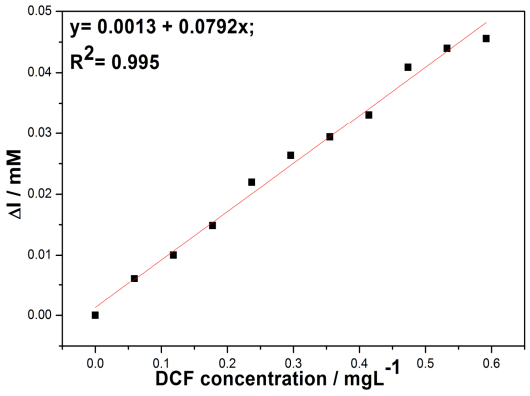


(b)

**Figure 10.1.** (a) Cyclic voltammograms recorded using CNT in 0.1 M $Na_2SO_4$ supporting electrolyte (curve 1) and in the presence of various DCF concentrations: curves 2-11: 0.0592-0.592 $mgL^{-1}$ DCF; potential scan rate of 0.05 $Vs^{-1}$; potential range -0.5 to +1.5 V vs. Ag/ AgCl. (b) Calibration plots of the peak current vs. DCF concentration.

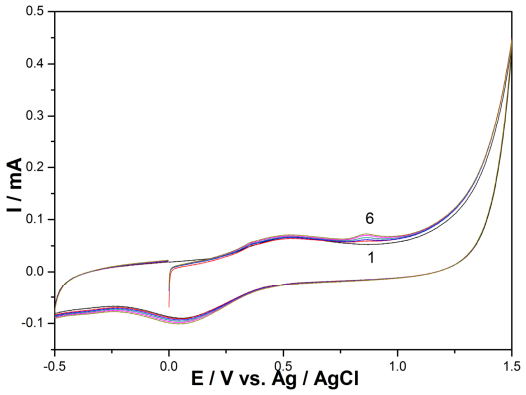


(a)

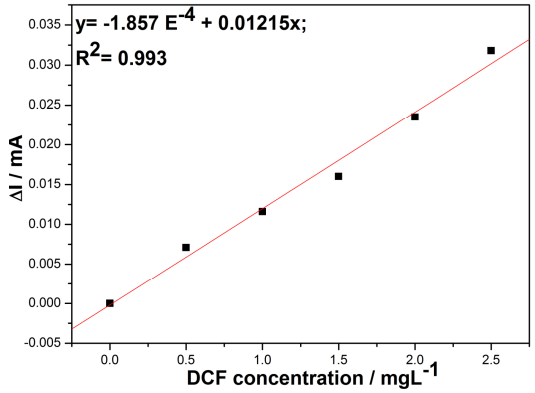


(b)

**Figure 10.2.** (a) Cyclic voltammograms recorded using AgZCNT in 0.1 M $Na_2SO_4$ supporting electrolyte (curve 1) and in the presence of various DCF concentrations: curves 2-6: 0.5- 2.5 $mgL^{-1}$ DCF; potential scan rate of 0.05 $Vs^{-1}$; potential range -0.5 to +1.5 V vs. Ag/ AgCl. (b) Calibration plots of the peak current vs. DCF concentration.

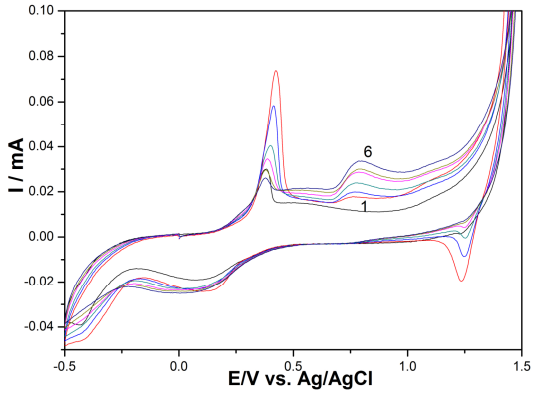


(a)

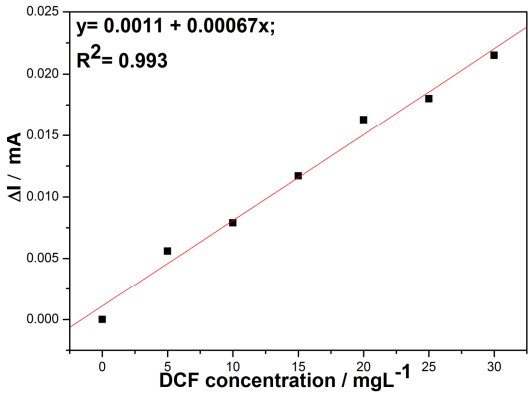


(b)

**Figure 10.3.** (a) Cyclic voltammograms recorded using AgZEG in 0.1 M $Na_2SO_4$ supporting electrolyte (curve 1) and in the presence of various DCF concentrations: curves 2-6: 5-30 $mgL^{-1}$; potential scan rate of 0.05 $Vs^{-1}$; potential range -0.5 to +1.5 V vs. Ag/ AgCl. (b) Calibration plots of the peak current vs. DCF concentration.

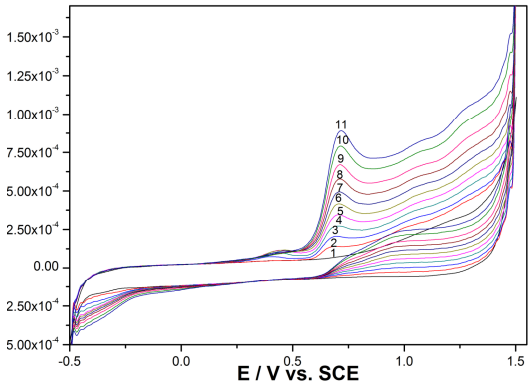


(a)

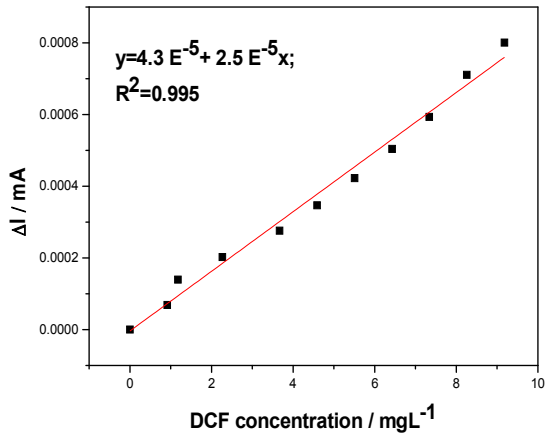


(b)

**Figure 10.4.** (a) Cyclic voltammograms recorded using BDD electrode in 0.1 M $Na_2SO_4$ supporting electrolyte (1) and in the presence of different DCF concentrations: 0.918- 9.18 $mgL^{-1}$ (curves 2-11); potential scan rate 0.05 $Vs^{-1}$; potential range: -0.5 V to +1.5 V/ SCE; (b) Calibration plot of the currents recorded at E= +0.70 V/ SCE vs. DCF concentration.

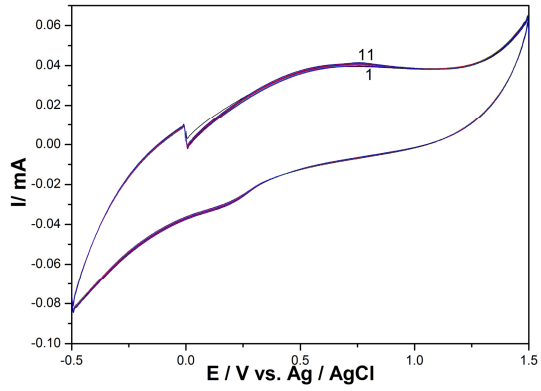


**Figure 10.5.** Cyclic voltammograms recorded using GC electrode in 0.1 M $Na_2SO_4$ supporting electrolyte (1) and in the presence of different DCF concentrations: 5-30 $mgL^{-1}$ (curves 2-11); potential scan rate 0.05 $Vs^{-1}$; potential range: -0.5 V to +1.5 V vs. Ag/ AgCl;

The sensitivity achieved for each electrode using CV is gathered in Table 10.1.

**Table 10.1.** Sensitivity of the electrochemical detection of DCF using CV.

| Electrode Material | Sensitivity/ μA $mgL^{-1}$ |
|---|---|
| CNT | 79.20 |
| AgZCNT | 12.10 |
| AgZEG | 0.69 |
| BDD | 0.25 |
| GC | -* |

*no signal was found

CV shapes recorded at CNT and AgZCNT are similarly, the peak corresponding to DCF oxidation appeared at the same potential value of about +0.75 V vs. Ag/ AgCl and the sensitivity is better for CNT in comparison with AgZCNT. This behaviour could be explained by DCF oxidation directly on the carbon surface and not via Ag-electro-catalysis. The better sensitivity reached for CNT is directly linked to CNT content within the composite composition. Also, the worse sensitivity found for AgZEG is related to the less electrocatalytic properties of the expanded-graphite versus carbon-nanotubes.

In comparison with the data reported in the literature regarding DCF oxidation on BDD electrode [17], the different shape of voltammograms was obtained. Two peaks and two waves starting with the potential value of about +0.4 V vs. SCE were noticed, which correspond to direct oxidation of DCF that occurred in several steps. Because the first peak did not increase linearly with DCF concentration, the next peak recorded at low potential value of about +0.7 V/ SCE is interesting for the detection applications. The current recorded at the potential value of +0.7 V vs. SCE increased linearly with DCF concentrations under the studied concentration range, with the good correlation coefficient (0.995).

Based on these preliminary studies, it can be concluded that except GC electrode, all carbon based electrodes tested in this study, CNT, AgZCNT, AgZEG and BDD exhibited useful peculiarities for the voltammetric detection of DCF in the aqueous solution. The electrooxidation of DCF occurred directly on the carbon surface, the silver catalyst presence did not enhance the electrode performance for DCF detection.

Taking into account the above-presented results obtained for IBP detection using carbon-based electrodes, which requires silver electrocatalyst within carbon-based composition in relation to direct electrodetection of DCF on carbon-based electrodes, two electrodes, *i.e.*, AgZEG and AgZCNT were selected for the further studies regarding the possibility to detect simultaneously IBP and DCF.

## 10.2. Simultaneous electrochemical detection of ibuprofen and diclofenac using silver-doped zeolite-carbon nanotubes-epoxy composite (AgZCNT) composite and silver-doped zeolite-expanded-graphite-epoxy composite (AgZEG) electrodes

### *10.2.1. Introduction*

In general, the simultaneous detection of ibuprofen (IBP) and diclofenac (DCF) is required in biological samples for clinical and toxicological screening, pharmacokinetic studies, as well as in therapeutic monitoring. Also, their presence in wastewater effluents and in consequence in water media, should impose the fast, simple and precise methods for their simultaneous detection in the aquatic environments. A few methods have been reported in the literature for their simultaneous detection using HPLC [18, 19], solid-phase extraction [20, 21].

The aim of this study is to determined comparatively electroanalytical parameters for the simultaneous detection of IBP and DCF on AgZEG and AgZCNT electrodes using voltammetric/ amperometric techniques.

### *10.2.2. Experimental*

The experimental conditions are the same with the above-presented in Subsection 10.1.

### *10.2.3. Results and discussion*

CV, DPV, SWV and CA electrochemical techniques were tested to detect simultaneously IBP and DCF

*AgZEG composite electrode*

Figures 10.6-10.7 shows CVs recorded at AgZEG electrode in 0.1 M $Na_2SO_4$ and in the presence of 5 $mgL^{-1}$ DCF (curve 2), followed by continuously adding 5 $mgL^{-1}$ IBP resulting mixture of 5 $mgL^{-1}$ DCF and 5 $mgL^{-1}$ IBP (curve 3) and followed by a new adding 5 $mgL^{-1}$ DCF resulting the mixture of 10 $mgL^{-1}$ DCF and 5 $mgL^{-1}$ IBP (curve 4). The two peaks corresponding to the oxidation of each pharmaceutical, DCF and IBP appeared at the potential value of +0.75V vs. Ag/ AgCl and respective, +1.25 V vs. Ag/ AgCl, being very clear distinguished. The peak separation of almost 500 mV is considered to be more than sufficient to allow the simultaneous detection of these analytes.

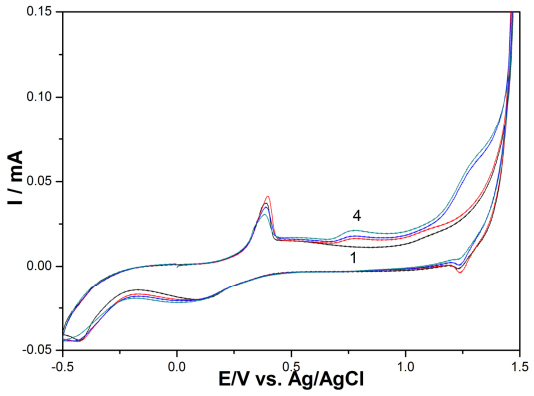


**Figure 10.6.** Cyclic voltammograms recorded using the AgZEG electrode in 0.1 M $Na_2SO_4$ supporting electrolyte (curve 1) and in the presence of: 5 $mgL^{-1}$ DCF (curve 2), 5 $mgL^{-1}$ DCF + 5 $mgL^{-1}$ IBP (curve 3), 10 $mgL^{-1}$ DCF + 5 $mgL^{-1}$ IBP (curve 4); potential scan rate of 0.05$Vs^{-1}$; potential range -0.5 to +1.5 V vs. Ag/ AgCl.

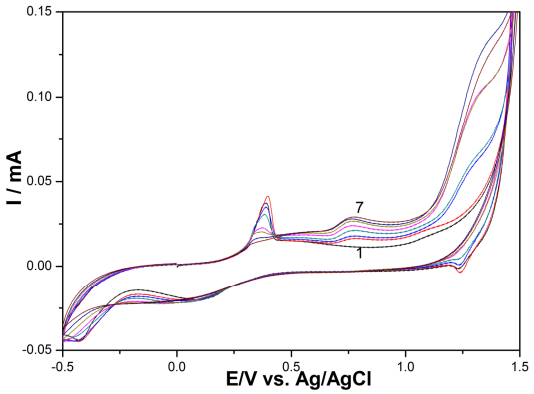


(a)

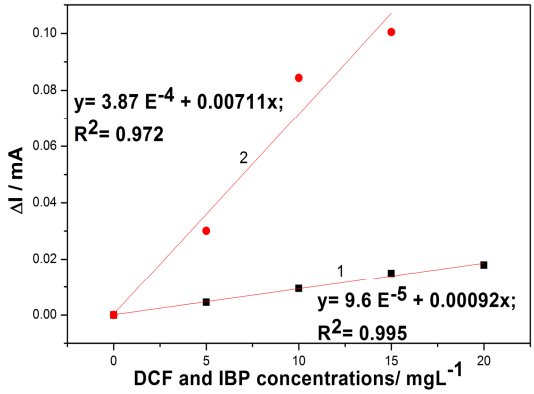


(b)

**Figure 10.7.** (a) Cyclic voltammograms recorded using the AgZEG electrode in 0.1 M $Na_2SO_4$ supporting electrolyte (curve 1) and in the presence of: 5 $mgL^{-1}$ DCF (curve 2), 5 $mgL^{-1}$ DCF + 5 $mgL^{-1}$ IBP (curve 3), 10 $mgL^{-1}$ DCF + 5 $mgL^{-1}$ IBP (curve 4), 10 $mgL^{-1}$ DCF + 10 $mgL^{-1}$ IBP (curve 5), 15 $mgL^{-1}$ DCF + 10 $mgL^{-1}$ IBP (curve 6), 15 $mgL^{-1}$ DCF + 15 $mgL^{-1}$ IBP (curve 7); potential scan rate of 0.05$Vs^{-1}$; potential range -0.5 to +1.5 V vs. Ag/ AgCl. (b) Calibration plots of the peak current vs. pharmaceutical concentration: DCF (curve 1) and IBP (curve 2).

DPV technique was also tested for the simultaneous detection of IBP and DCF, being carried out in the potential range of -0.5 to +1.5 V vs. Ag/ AgCl. Each component was added consecutively and continuously without electrode cleaning between DPV running. Two well-defined peaks at about +0.7 and +1.2 V vs. Ag/ AgCl were observed, corresponding to the differential pulse voltammograms of DCF and IBP, respectively. In comparison with CV, enhanced signals corresponding to the oxidation of both pharmaceuticals were found. Figure 10.8 presents the comparative DPV results obtained for the simultaneous of DCF and IBP. Electroanalytical parameters determined for this technique for both analytes are presented in Table 10.2 in comparison with individual detection of each component on this electrode. Based on the sensitivity values determined for the individual/ simultaneous detection of IBP and DCF it can be concluded that these pharmaceuticals did not interfere each other.

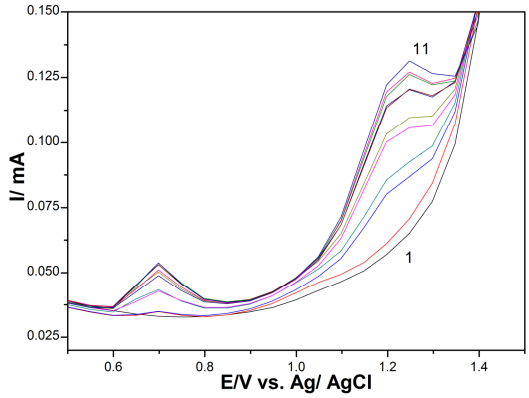


(a)

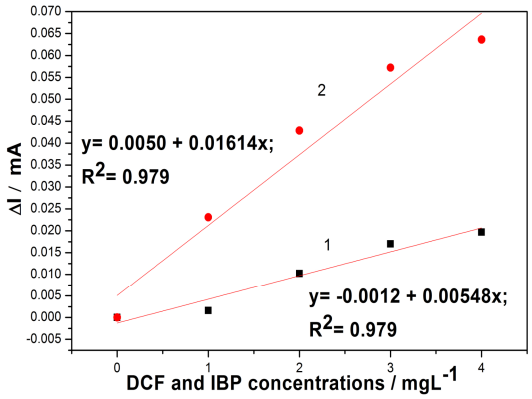


(b)

**Figure 10.8.** (a) DPV voltammograms recorded using the AgZGE electrode in 0.1 M $Na_2SO_4$ supporting electrolyte (curve 1) and in the presence of: 1 $mgL^{-1}$ DCF (curve 2), 1 $mgL^{-1}$ DCF + 1 $mgL^{-1}$ IBP (curve 3), 2 $mgL^{-1}$ DCF + 1 $mgL^{-1}$ IBP (curve 4), 2 $mgL^{-1}$ DCF + 2 $mgL^{-1}$ IBP (curve 5), 3 $mgL^{-1}$ DCF + 2 $mgL^{-1}$ IBP (curve 6), 3 $mgL^{-1}$ DCF + 3 $mgL^{-1}$ IBP (curve 7), 4 $mgL^{-1}$ DCF + 3 $mgL^{-1}$ IBP (curve 8), 4 $mgL^{-1}$ DCF + 4 $mgL^{-1}$ IBP (curve 9), 5 $mgL^{-1}$ DCF + 4 $mgL^{-1}$ IBP (curve 10), 5 $mgL^{-1}$ DCF + 5 $mgL^{-1}$ IBP (curve 11), conditions: Modulation amplitude (MT)= 0.1 V; Step potential (SP)= 0.05 V; Modulation time (MT)= 0.05 s, interval= 1 s; scan rate 0.05 $Vs^{-1}$. (b) Calibration plots of the peak current vs. pharmaceutical concentration: DCF (curve 1) and IBP (curve 2).

To improve the electroanalytical parameters, SWV was used for the simultaneous detection of IBP and DCF in the potential range of +0.5 to +1.5 V vs. Ag/ AgCl, which is comparable with DPV potential range. The operation parameters for SWV were the same prior established as optimum for IBP detection by SWV,

*e.g.*, 0.2 V modulation amplitude, 0.025 V step potential and 25 Hz frequency. Two peaks of the square wave voltammograms at about +0.7 and +1.25 V vs. Ag/ AgCl was observed corresponding to the presence of DCF and IBP. It is noticed that compared to DPV results, the peak corresponding to IBP oxidation is shifted to more positive potentials leading to larger peak separation (550 mV) (Figure 10.9). Compared with DPV, the sensitivities for the each component detection determined based on the slope of the linear dependence between useful currents corresponding to the oxidation peak are improved (see Table 10.2).

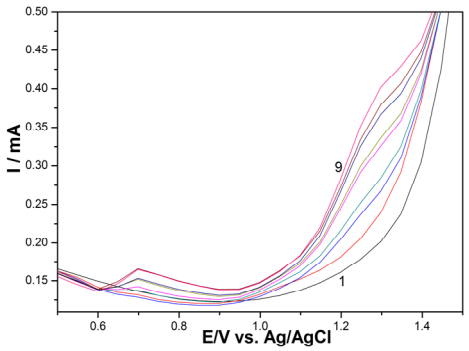


(a)

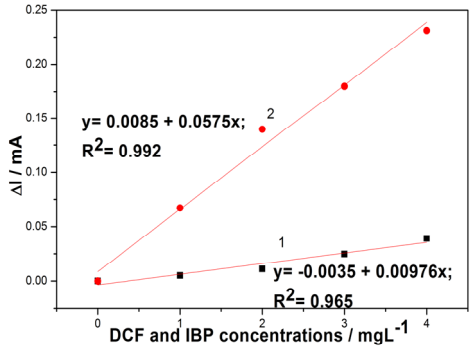


(b)

**Figure 10.9.** (a) SWV voltammograms recorded using the AgZGE electrode in 0.1 M $Na_2SO_4$ supporting electrolyte (curve 1) and in the presence of: 1 $mgL^{-1}$ DCF (curve 2), 1 $mgL^{-1}$ DCF + 1 $mgL^{-1}$ IBP (curve 3), 2 $mgL^{-1}$ DCF + 1 $mgL^{-1}$ IBP (curve 4), 2 $mgL^{-1}$ DCF + 2 $mgL^{-1}$ IBP (curve 5), 3 $mgL^{-1}$ DCF + 2 $mgL^{-1}$ IBP (curve 6), 3 $mgL^{-1}$ DCF + 3 $mgL^{-1}$ IBP (curve 7), 4 $mgL^{-1}$ DCF + 3 $mgL^{-1}$ IBP (curve 8), 4 $mgL^{-1}$ DCF + 4 $mgL^{-1}$ IBP (curve 9), conditions: frequency (f)= 10 Hz; Amplitude (A)= 0.1 V; Step potential (SP)= 0.05 V; scan rate 0.05 $Vs^{-1}$. (b) Calibration plots of the peak current vs. pharmaceutical concentration: DCF (curve 1) and IBP (curve 2).

The chronoamperometry as the easiest detection method envisaging the practical application was tested also, for the simultaneous detection of these components. Based on the cyclic voltammetry results as the reference for operating parameters, the chronoamperometry was tested for the two potential values of +0.75 and respective, +1.25 V vs. Ag/ AgCl, corresponding to the oxidation process of DCF and IBP. Fig. 10.10a shows chronoamperometric measurements of IBP and DCF with AgZEG electrode. This figure presents the current-time profiles obtained by setting the working electrode at both potential values for various concentrations of DCF and IBP. The useful net current signals recorded at 50 seconds for each potential value are linearly dependent on DCF and IBP concentration in the explored concentration range (Fig 10.10b).

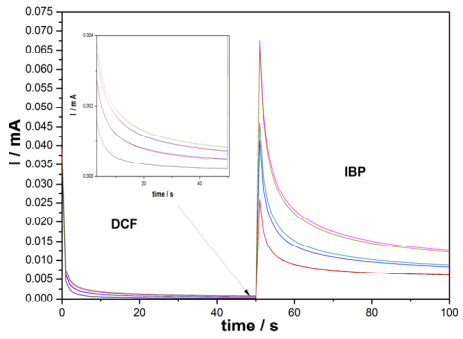


(a)

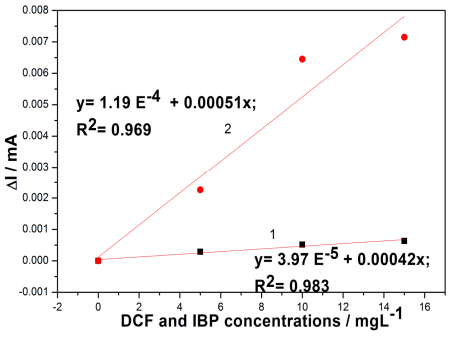


(b)

**Figure 10.10.** (a) CA recorded using the AgZEG electrode in 0.1 M $Na_2SO_4$ supporting electrolyte (curve 1) in the presence of 5 $mgL^{-1}$ DCF (curve 2), 5 $mgL^{-1}$ DCF + 5 $mgL^{-1}$ IBP (curve 3), 10 $mgL^{-1}$ DCF + 5 $mgL^{-1}$ IBP (curve 4), 10 $mgL^{-1}$ DCF + 10 $mgL^{-1}$ IBP (curve 5), 15 $mgL^{-1}$ DCF + 10 $mgL^{-1}$ IBP (curve 6), recorded at +0.75 V for DCF and +1.25 V for IBP vs. Ag/ AgCl. (b) Calibration plots of the peak current vs. pharmaceutical concentration: DCF (curve 1) and IBP (curve 2).

The amperometric response of the AgZEG electrode obtained for the successive and continuous addition of 2 $mgL^{-1}$ DCF in the presence of 2 $mgL^{-1}$ IBP recorded at +0.75 V vs. Ag/ AgCl for 400 seconds running time followed by the successive and continuous addition of 2 $mgL^{-1}$ IBP at applied potential of +1.25 V vs. Ag/ AgCl for the next running time of 400 seconds in 0.1 M $Na_2SO_4$ solution (batch system analysis- BSA), is shown in Figure 10.11a. The response of the electrode is linear both for DCF and IBP, and the similar sensitivities were achieved under both schemes of CA applying (CA and CA-BSA), the electroanalytical parameters are shown in Table 10.2.

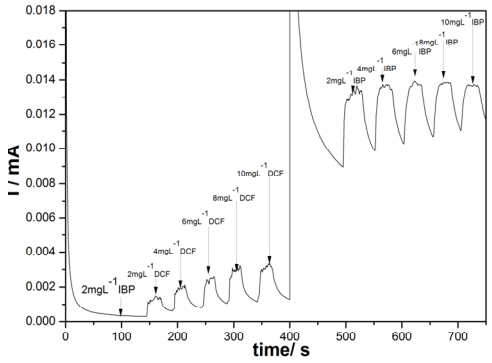


(a)

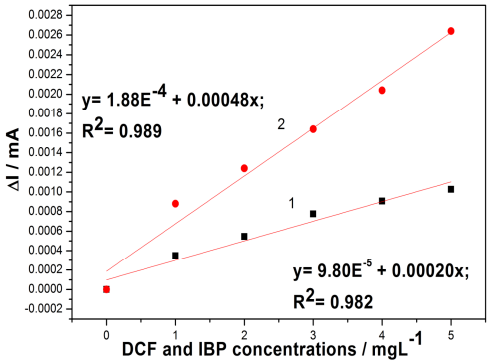


(b)

**Figure 10.11.** (a) Amperometric response (BSA) using the AgZEG electrode for the successive and continuous addition of 2 $mgL^{-1}$ DCF in the presence of 2 $mgL^{-1}$ IBP recorded at +0.75 V vs. Ag/ AgCl for 400 seconds running time followed by the successive and continuous addition of 2 $mgL^{-1}$ IBP at applied potential of +1.25 V vs. Ag/ AgCl for the next running time of 400 seconds. (b) Calibration plots of the peak current vs. pharmaceutical concentration: DCF (curve 1) and IBP (curve 2).

All electroanalytical parameters determined for the simultaneous detection of DCF and IBP at AgZEG electrode using CV, DPV, SWV, and CA are presented comparatively with the individual detection for each analyte in Table 10.2. Very promising results for the simultaneous detection of DCF and IBP were found, without main interferences of each other.

**Table 10.2.** Electroanalytical parameters for simultaneous DCF and IBP using AgZEG composite electrode.

| Electrode | Technique | Compound | E/V Individual | Sensitivity μA/ $mgL^{-1}$ Individual detection | E/V Simultaneously | Sensitivity μA/$mgL^{-1}$ simultaneous detection | Relative standard deviation RSD, % | Limit of detection, LOD, $mgL^{-1}$ | Limit of quantification, LQ, $mgL^{-1}$ |
|---|---|---|---|---|---|---|---|---|---|
| AgZEG | CV | IBP | +1.25 V | 6.83 | +1.25 V | 7.11 | 0.97 | 0.11 | 0.38 |
| | | DCF | +0.75 V | 0.69 | +0.75 V | 0.92 | 2.31 | 0.79 | 2.64 |
| | DPV | IBP | +1.17 V | 14.70 | +1.2 V | 16.14 | 1.17 | 0.12 | 0.41 |
| | | DCF | +0.70 V | 7.26 | +0.7 V | 5.48 | 1.55 | 0.27 | 0.91 |
| | SWV | IBP | +1.10 V | 47.5 | +1.25 V | 57.5 | 0.49 | 0.04 | 0.14 |
| | | DCF | -* | -* | +0.7 V | 9.76 | 1.56 | 0.64 | 2.13 |
| | CA | IBP | -* | -* | +1.25 V | 0.48 | 7.05 | 0.15 | 0.51 |
| | | DCF | -* | -* | +0.75 V | 0.20 | 0.18 | 0.24 | 0.81 |

* not determined

*AgZCNT composite electrode.*

This electrode was tested only for comparison to check if the presence of CNT improved the response for both components taking into account the results obtained for the individual detection of each analyte on AgZCNT. Two detection results obtained by using CV and DPV are presented in Figure 10.12 and 10.13.

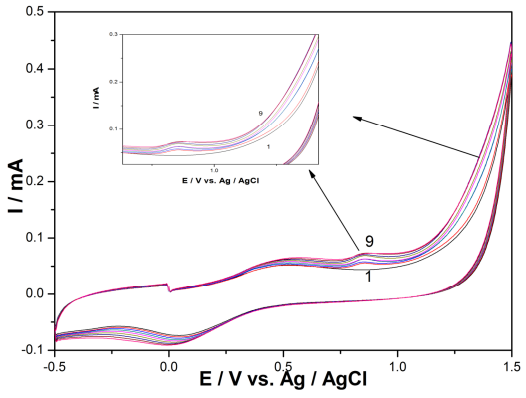


(a)

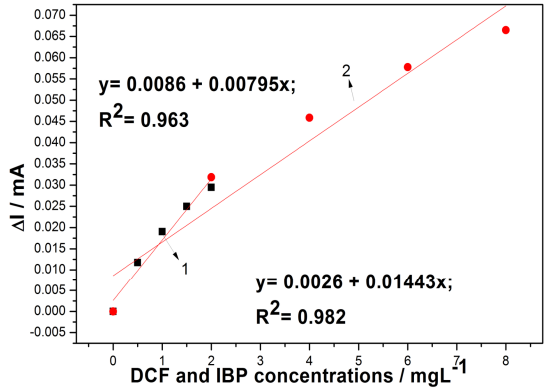


(b)

**Figure 10.12.** (a) Cyclic voltammograms recorded using the AgZCNT electrode in 0.1 M $Na_2SO_4$ supporting electrolyte (curve 1) and in the presence of: 0.05 $mgL^{-1}$ DCF (curve 2), 0.05 $mgL^{-1}$ DCF + 2 $mgL^{-1}$ IBP (curve 3), 1 $mgL^{-1}$ DCF + 2 $mgL^{-1}$ IBP (curve 4), 1 $mgL^{-1}$ DCF + 4 $mgL^{-1}$ IBP (curve 5), 1.5 $mgL^{-1}$ DCF + 4 $mgL^{-1}$ IBP (curve 6), 1.5 $mgL^{-1}$ DCF + 6 $mgL^{-1}$ IBP (curve 7), 2 $mgL^{-1}$ DCF + 6 $mgL^{-1}$ IBP (curve 8), 2 $mgL^{-1}$ DCF + 8 $mgL^{-1}$ IBP (curve 9); potential scan rate of 0.05 $Vs^{-1}$; potential range -0.5 to +1.5 V vs. Ag/ AgCl. (b) Calibration plots of the peak current vs. pharmaceutical concentration: DCF (curve 1) and IBP (curve 2).

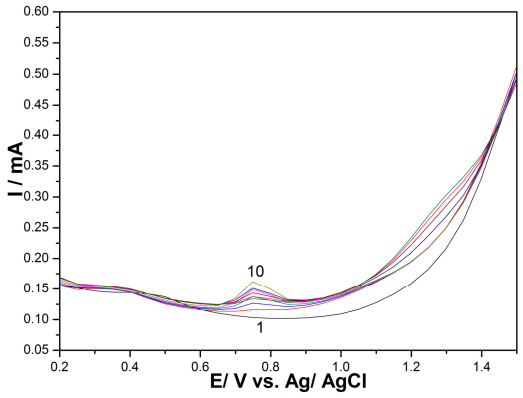


(a)

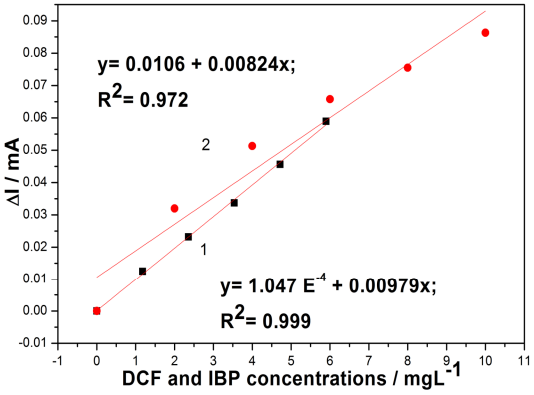


(b)

**Figure 10.13.** (a) DPV voltammograms recorded using the AgZCNT electrode in 0.1 M $Na_2SO_4$ supporting electrolyte (curve 1) and in the presence of: 1.18 $mgL^{-1}$ DCF (curve 2), 2.36 $mgL^{-1}$ DCF (curve 3), 3.54 $mgL^{-1}$ DCF (curve 4), 4.72 $mgL^{-1}$ DCF(curve 5), 5.9 $mgL^{-1}$ DCF (curve 6), 5.9 $mgL^{-1}$ DCF + 2 $mgL^{-1}$ IBP (curve 7), 5.9 $mgL^{-1}$ DCF + 4 $mgL^{-1}$ IBP (curve 8), 5.9 $mgL^{-1}$ DCF + 6 $mgL^{-1}$ IBP (curve 9), 5.9 $mgL^{-1}$ DCF + 8 $mgL^{-1}$ IBP (curve 10); conditions: Modulation amplitude (MA)= 0.2 V; Step potential (SP)= 0.025 V; (b) Calibration plots of the peak current vs. pharmaceutical concentration: DCF (curve 1) and IBP (curve 2).

The electroanalytical parameters achieved for the simultaneous detection of DCF and IBP using AgZCNT electrode are presented comparatively with those reached at AgZEG electrode in Table 10.3.

**Table 10.3.** Electroanalytical parameters for simultaneous DCF and IBP using CV and DPV on AgZEG and AgZCNT composite electrodes.

| Electrode | Technique | Compound | E/V Individual | Sensibility/ µA/ mgL$^{-1}$ Individual detection | E/V Simultaneously | Sensibility/ µA/mgL$^{-1}$ simultaneous detection | Relative standard deviation RSD, % | Limit of detection, LOD, mgL$^{-1}$ | Limit of quantification, LQ, mgL$^{-1}$ |
|---|---|---|---|---|---|---|---|---|---|
| AgZEG | CV | IBP | +1.25 V | 6.83 | +1.25 V | 7.11 | 0.97 | 0.11 | 0.38 |
| | | DCF | +0.75 V | 0.69 | +0.75 V | 0.92 | 2.31 | 0.79 | 2.64 |
| | DPV | IBP | +1.17 V | 14.70 | +1.20 V | 16.14 | 1.17 | 0.12 | 0.41 |
| | | DCF | +0.70 V | 7.26 | +0.70 V | 5.48 | 1.55 | 0.27 | 0.91 |
| AgZCNT | CV | IBP | +1.20 V | 10.88 | +1.20 V | 7.95 | 2.38 | 0.42 | 1.40 |
| | | DCF | +0.85 V | 12.15 | +0.85 V | 14.43 | 4.98 | 0.86 | 2.88 |
| | DPV | IBP | -* | -* | +1.20 V | 8.24 | 0.74 | 0.44 | 1.46 |
| | | DCF | -* | -* | +0.75 V | 9.79 | 0.83 | 0.27 | 1.46 |

* not determined

As we expected, CNT presence into electrode composition enhanced slightly the response for ibuprofen and more for DCF detection. This behaviour was expected taking into account that for IBP detection requires the presence of silver catalyst.

Based on the presented results, it may be concluded:

– Except GC electrode, all carbon based electrodes tested in this study, *i.e.*, CNT, AgZCNT, AgZEG and BDD exhibited useful peculiarities for the voltammetric detection of DCF in the aqueous solution. The electrooxidation of DCF occurred directly on the carbon surface, the silver catalyst presence did not enhance the electrode performance for DCF detection.

– However, to detect simultaneously DCF and IBP, silver catalyst is required and only silver-modified carbon electrodes are suitable for this type of application.

– Both AgZEG and AgZCNT composite electrodes exhibited the availability for the simultaneous direct anodic oxidation of diclofenac (DCF) and ibuprofen (IBP), without interfering each other, giving them a real potential for the simultaneous amperometric/ voltammetric detection of DCF and IBP.

– The exploitation of pulsed voltammetric techniques allowed enhancing the electroanalytical parameters for both DCF and IBP detection.

## 10.3. References

[1] X. Zhao, Y. Hou, H. Liu, Z. Qiang, Electrochim. Acta 54 (2009) 4172.
[2] A. Ambrosi, R. Antiochia, L. Campanella, R. Dragone, I. Lavagnini, J. Hazard. Mater. 122 (2005) 219.
[3] Z. Sun, W. Schussler, M. Sengl, R. Niessner, D. Knopp, Anal. Chim. Acta 620 (2008) 73.
[4] M. Tubino, R.L. De Souza, Talanta 68 (2006) 776.
[5] A. Chmielewska, L. Konieczna, A. Plenis, M. Bieniecki, H. Lamparczyk, Biomed. Chromatogr. 20 (2006) 119.
[6] F. Manea, M. Ihos, A. Remes, G. Burtica, J. Schoonman, Electroanal. 22 17-18 (2010) 2058.
[7] Z. Kormosh, I. Hunka, Y. Bazel, J. Anal. Chem. 64 (2009) 853.
[8] M. Jitaru, C. Cirtiu, C. Fillip, A. Katona, M. Schipu, JEPE 5 1 (2004) 171.
[9] M. Jitaru, R. Iacob, M. Popa, JEPE 5 1 (2004) 179.
[10] C. Radovan, F. Manea, Electroanal. 19 (2007) 91.
[11] M. Ihos, F. Manea, D. Botau, A. Iovi, Proceedings of the 16th Symposium on Analytical and Environmental Problems (2009) 264.
[12] L. Codognoto, S.A.S. Machado, L.A. Avaca, Diam. Relat. Mater. 11 9 (2002) 1670.
[13] D. Cinghita, C. Radovan, D. Dascalu, Sensors 8 (2008) 4560.
[14] A. Pop, F. Manea, C. Radovan, D. Dascalu, N. Vaszilcsin, J. Schoonman, Analyst 137 (2012) 641.
[15] C. Cofan, C. Radovan, Ind. Eng. Chem. (2011) in press.
[16] C. Cofan, C. Radovan, Sensors 8 (2008) 3952.
[17] M. Ihos, A. Remes, F. Manea, Environ. Eng. Manag. J. (2011), in press.
[18] C. Gonzalez-Barreiro, M. Lores, M.C. Casais, R. Cela, J. Chromatogr. A 993 1-2 (2003) 29.
[19] S. Weigel, R. Kallenborn, H. Huhnerfuss, J. Chromatogr. A 1023 (2004) 183.
[20] M.J. Gomez, M. Petrovic, A.R. Fernandez-Alba, D. Barcel, J. Chromatogr. A 1114 (2006) 224.
[21] J.L. Santos, I. Aparicio, E. Alonso, M. Callejon, Anal. Chim. Acta 550 (2005) 116.

# CHAPTER 11. GENERAL CONCLUSIONS

– The research and original contributions of the thesis are related to the elaboration, and manufacturing of several unmodified and silver-modified carbon-epoxy composite electrode materials, which involve both the detailed characterization of the electrode materials and their application, either the advanced degradation/ mineralization of ibuprofen (IBP) from water or its detection. Also, the electrode materials suitable for simultaneous detection of ibuprofen and sodium diclofenac (DCF) were investigated. Moreover, the dual character of the electrode material and the electrochemical technique was exploited for application of both ibuprofen degradation/ mineralization and its detection.

– Several unmodified and silver-modified carbon-epoxy composite electrodes were successfully obtained by a two-roll mill procedure: carbon nanotubes-epoxy composite (CNT), silver-doped zeolite-carbon nanotubes-epoxy composite, (AgZCNT), silver-doped zeolite-carbon nanofiber-epoxy composite (AgZCNF), silver-decorated carbon-nanofiber-epoxy composite (AgCNF), silver-doped zeolite-expanded-graphite-epoxy composite (AgZEG).

– The morphological, structural and electrical characterization results of the above presented compositions of the carbon-based composite electrode revealed:

- The conductive fillers, *i.e.*, expanded graphite, carbon nanotubes, and carbon nanofibers are well-distributed and dispersed within the epoxy matrix taking into account the specific preparation method involving a dispersion method in a suitable solvent by sonication;
- Silver presence in various forms, *i.e.*, silver-modified natural/ synthetic zeolite, chemically and decorated silver particles were evidenced by SEM images;
- Based on the results of the electrical conductivity measurements, it can be noticed that for the same content of the conductive filler (20 % wt.) the electrical conductivity decreased in the sequence: AgZEG> AgZCNT> AgZCNF> CNT> AgCNF. This should be in direct relation with the electrical properties of the conductive filler and also, in relation with dispersion and homogeneous degree of the conductive filler within the epoxy matrix;
- The presence of silver-modified natural/ synthetic zeolite within the composite composition improved the electrical properties due to the silver presence;
- All prepared carbon-based composite electrodes are characterized by their electrical conductivities to be suitable for the electrochemical applications.

– The electrochemical behaviour of the well-known ferri/ ferrocyanide standard redox system allowed determining the electroactive surface area of these electrodes. Based on the ratio between the electroactive and geometrical surface area, it can be concluded that CNT-based composite electrodes exhibited the best electroactive properties. Also, the good electroactive properties were found for CNF-based composite electrodes. In addition, some aspects related to the diffusion-control and adsorption processes on the electrode surface were discussed.

– The comparative study regarding the electrochemical behaviour of ibuprofen (IBP) on the carbon-based composite electrode tested in this study, *i.e.*, carbon nanotubes-epoxy composite (CNT), silver-doped zeolite-carbon nanotubes-epoxy composite, (AgZCNT), silver-doped zeolite-expanded-graphite-epoxy composite (AgZEG) allowed to select the operating conditions for its electrochemical degradation/ mineralization from aqueous solution. In addition, the electrochemical behaviour of IBP using the carbon-based composite electrodes was compared with the commercial glassy carbon (GC) and boron-doped diamond (BDD) electrode.

– Cyclic voltammetry (CV) results showed that the anodic current increased in the presence of IBP without the presence of the corresponding oxidation peak at the commercial GC and BDD electrodes, and also for the CNT composite electrode. Also, some information related to the direct electrochemical activity towards IBP electrooxidation was found, the best one being determined with the CNT electrode. The BDD electrode exhibited electrode fouling with the IBP concentrations ranging from 10 to 50 $mgL^{-1}$. Silver presence within the electrode composition led to a different behaviour of IBP using CV and the anodic peak corresponding to IBP oxidation was found for both AgZCNT and AgZEG composite electrodes, which informs about a possible diffusion-controlled oxidation process. The most evidenced oxidation peak was found for AgZEG, but the best electrochemical sensitivity for IBP oxidation was determined for the AgZCNT composite electrode.

– Chronoamperometry (CA) and multiple-pulsed amperometry (MPA) techniques were used to simulate the potentiostatic electrolysis envisaging also, the possibility of "*in-situ*" electrode reactivation by MPA. The selection of the operating conditions for CA and MPA were based on CV results as reference. No direct electrochemical oxidation of IBP with the tested electrode could be performed due to electrode fouling accompanied by the electrode activity loss. All electrolysis experiments were performed under the water decomposition potential range, where the hydroxyl radicals are generated leading to an advanced electrooxidation process, but with high energy consumption due to the secondary oxygen evolution occurring.

– The assessment of the electrode performance in terms of absorbance, organic load, and TOC reduction degrees and in terms of the electrochemical efficiencies, which take into account the charge passed during the electrochemical process showed that the BDD electrode exhibited the better performance for IBP degradation/ mineralization in comparison with the GC electrode. The practical utility of the BDD electrode for IBP degradation/ mineralization was proved by bulk electrolysis under optimum galvanostatic operating conditions using 10 $mA\ cm^{-2}$ current density.

– The influence of chloride presence in order to generate "*in-situ*" the oxidation agent (hypochlorite/ chlorine) did not improve significantly the process efficiency and moreover, the electrochemical efficiency was negatively influenced due to an excess of charge consumed for oxidant generation.

– MPA applying on the CNT composite electrode improved slightly the process efficiency, but the electrochemical efficiency decreased. Under these working conditions, based on the technical-economical criteria applying MPA is not suitable for IBP in comparison with applying CA.

– AgZCNT and AgZEG composite electrodes exhibited very good performance for the effective mineralization in comparison with CNT, boron-doped

diamond (BDD), and glassy carbon (GC) electrodes for which effective mineralization was not achieved.

– The AgZEG electrode features in relation with the diffusion-controlled electrooxidation of IBP were exploited for IBP detection, suggesting a dual exploitation of this electrode both in IBP degradation and its control by IBP monitoring using cyclic voltammetry.

– All tested electrodes, *i.e.*, AgZEG, AgZCNT, AgZCNF, and AgCNF composite electrodes exhibited the availability for the direct anodic oxidation of IBP, giving them a real potential for the amperometric/ voltammetric detection of IBP.

– Even if several characteristics regarding the direct electrooxidation of IBP are common for all silver-based composite electrodes, specific peculiarities linked to the carbon structures gave them different performances for IBP detection. Also, the silver content and form influenced the electrode performance for IBP detection.

– The electrode performance for IBP detection in relation with the sensitivities increased as: AgZCNT>AgZEG>AgZCNF>AgCNF. Also, the best limit of detection and quantification were achieved with the AgZCNT electrode. However, better reproducibility of AgZEG linked to the economic criteria makes this electrode to exhibit a great potential for practical application.

– The exploitation of pulsed voltammetric/ amperometric techniques allowed to enhance the electroanalytical parameters for IBP detection.

– The selection of the electrode type, the electrochemical technique, and the operating conditions will be selected taking into account the specific requirements imposed by the practical utility.

– To achieve the simultaneous detection of ibuprofen and sodium diclofenac, the preliminary studies for this stage were directed to the individual detection of sodium diclofenac, and it may be concluded that except for the GC electrode, all carbon-based electrodes tested in this study*, i.e.*, CNT, AgZCNT, AgZEG, and BDD exhibited useful properties for the voltammetric detection of DCF in the aqueous solution. The electrooxidation of DCF occurred directly on the carbon surface, while the silver catalyst presence did not enhance the electrode performance for DCF detection.

– However, to detect simultaneously DCF and IBP, a silver catalyst is required and only silver-modified carbon electrodes are suitable for this type of application, AgZEG and AgZCNT composite electrodes being selected for the simultaneous detection experiments.

– Both AgZEG and AgZCNT composite electrodes exhibited the right properties for the direct simultaneous anodic oxidation of DCF and IBP, without interfering each other, giving these electrodes a real potential for their simultaneous amperometric/ voltammetric detection.

– The exploitation of pulsed voltammetric techniques allowed to enhance the electroanalytical parameters for both sodium DCF and IBP detection.

– Due to the great complexity of the objectives proposed for this study, this study was conceived as a prerequisite stage to precede the development of a new nano-enhanced electrochemical green technology for advanced integrated water treatment and quality control. The electrode materials that reach the specific objectives in relation with the effective degradation/ mineralization of IBP and its detection are the AgZEG and AgZCNT composite electrodes. Also, these electrodes are able to detect simultaneously IBP and sodium DCF. Their practical application in

the degradation/ mineralization process of pharmaceuticals could be limited by the economic criteria in relation with the specific energy consumption. However, it must be kept in mind that the economic aspects will be improved by integration of the electrochemical process within the conventional treatment technological flow before or after the biological stage in accordance with the practical requirements, to improve the biodegradability of the refractory organics or to mineralize them.